

In situ and *in vitro* profiling of brain tumour initiating cells of high-grade gliomas



Dissertation
zur Erlangung des Doktorgrades
der Biomedizinischen Wissenschaften
(Dr. rer. physiol.)

der
Fakultät für Medizin
der Universität Regensburg

vorgelegt von
Verena Jeannine Leidgens
aus
Essen

im Jahr
2015

Die vorliegende Arbeit entstand im Zeitraum Mai 2011 bis Oktober 2015 unter Anleitung von Herrn Prof. Peter Hau am Zentrum für Hirntumoren sowie der Klinik und Poliklinik für Neurologie an der Fakultät für Medizin der Universität Regensburg.

Einreichung der Dissertation: November 2015

Tag der mündlichen Prüfung: 08. April.2016

Dekan: Prof. Dr. Dr. Torsten E. Reichert

Betreuer: Prof. Dr. Peter Hau

Prüfungskommission:

1. Gutachter: Prof. Dr. Peter Hau

2. Gutachter: Prof. Dr. Eugen Kerkhoff

3. Gutachterin: Prof. Dr. Dr. Ghazaleh Tabatabai

3.Prüfer: Prof. Dr. Markus Riemenschneider

Selbstständigkeitserklärung

Ich, Leidgens, Verena Jeannine; geb. Gawrisch geboren am 11.01.1986 in Essen, erkläre hiermit, dass ich die vorliegende Arbeit ohne unzulässige Hilfe Dritter und ohne Benutzung anderer als der angegebenen Hilfsmittel angefertigt habe.

Die aus anderen Quellen direkt oder indirekt übernommenen Daten und Konzepte sind unter Angabe der Quelle gekennzeichnet. Insbesondere habe ich nicht die entgeltliche Hilfe von Vermittlungs- bzw. Beratungsdiensten (Promotionsberater oder andere Personen) in Anspruch genommen.

Die Arbeit wurde bisher weder im In- noch im Ausland in gleicher oder ähnlicher Form einer anderen Prüfungsbehörde vorgelegt.

Ort, Datum

Verena Jeannine Leidgens

Table of contents

SELBSTSTÄNDIGKEITSERKLÄRUNG	V
------------------------------------	----------

TABLE OF CONTENTS	VII
--------------------------	------------

1. ABSTRACT	1
--------------------	----------

2. ZUSAMMENFASSUNG	3
---------------------------	----------

3. INTRODUCTION	7
------------------------	----------

3.1. GLIOBLASTOMA	8
-------------------	---

3.1.1. Molecular subclasses of glioblastoma	10
---	----

3.1.2. Intratumoural heterogeneity	12
------------------------------------	----

3.1.3. GBM origin – cancer stem cells	14
---------------------------------------	----

3.1.4. Brain tumour initiating cells	16
--------------------------------------	----

3.2. INFILTRATION AND MIGRATION	18
---------------------------------	----

3.2.1. Invasion infrastructure	18
--------------------------------	----

3.2.2. Principles of epithelial to mesenchymal transition	20
---	----

3.2.2.1. Migration modes required for infiltration	23
--	----

3.2.3. Modelling glioma cell migration	24
--	----

3.2.3.1. 3D <i>in situ</i> model of organotypic brain slice cultures	25
--	----

3.3. STAT3	26
------------	----

3.3.1. STAT3 regulation	26
-------------------------	----

3.3.2. Physiological function of STAT3	27
--	----

3.3.3. Role in oncogenesis	28
----------------------------	----

3.3.3.1. Role of STAT3 in GBM	29
-------------------------------	----

3.3.4. STAT3 and NSAIDs	30
-------------------------	----

3.4. AIMS OF THIS WORK	31
------------------------	----

4. RESULTS	33
4.1. MONITORING INVASIVENESS OF GLIOMA CELLS <i>IN SITU</i>	35
4.1.1. Brain slice cultures as an adequate model to monitor migration and invasion	35
4.1.1.1. Glioma cell line U87	35
4.1.1.2. Primary human glioma cells	39
4.1.2. Simultaneous implantation of proneural and mesenchymal BTICs	45
4.2. ANALYSIS OF GLIOMA CELL INVASIVENESS <i>IN SITU</i>	48
4.2.1. Formation of leader, follower, and stationary cells	48
4.2.2. Development of an isolation method to receive single cells from the OBSCs	49
4.2.3. Identification of distinct transcription profiles	52
4.2.4. Identification of a transcription factor signature defining leader cells	56
4.3. ANALYSIS AND MODULATION OF STAT3	58
4.3.1. Characterisation of primary human brain tumour initiating cells and glioma cell lines	58
4.3.1.1. Relative protein expression levels	59
4.3.1.2. Basic proliferation rates	67
4.3.1.3. Basic migration rates	73
4.3.2. Characteristics of primary human BTIC and GBM cell lines	78
4.3.3. STAT3 inhibition reduces GBM cell migration and proliferation	82
4.3.3.1. Effects of Diclofenac and Ibuprofen on glioma cell lines	82
4.3.3.2. Specific STAT3 inhibition to restrain glioma cells	88
4.3.4. Effects of STAT3 inhibition on glioma cells in the OBSC model	103

5. DISCUSSION	113
5.1. ORGANOTYPIC SLICE CULTURES AS MODEL FOR GLIOMA CELL INFILTRATION OF THE BRAIN	114
5.1.1. OBSC infiltration by U87 glioma cell line	114
5.1.2. OBSC infiltration by primary human brain tumour initiating cells	115
5.2. CELL SUBTYPE INDUCTION BY THE MICROENVIRONMENT: DEFINING LEADER, FOLLOWER, AND STATIONARY CELLS	121
5.2.1. Formation of leader, follower, and stationary cells in OBSCs	122
5.2.2. Directed invasion of glioma cells in OBSCs	124
5.2.3. Gene expression profiling of leader, follower and stationary GBM cells	128
5.2.4. The signature of leader cells	130
5.3. CLUSTERING PRONEURAL AND MESENCHYMAL BTICs AND TCs ACCORDING TO THEIR PROLIFERATION AND MIGRATION RATES	133
5.3.1. Deciphering transcription factor protein expression of BTIC and GBM cell lines	133
5.3.2. Correlation of proliferation and migration rates distinguished proneural and mesenchymal BTICs and TCs	137
5.4. DICLOFENAC AND IBUPROFEN RESTRICT GBM CELLS VIA MODULATION OF STAT3 SIGNALLING	141
5.5. SPECIFIC STAT3 INHIBITION VIA STAT3C RESTRICTS GLIOMA CELLS <i>IN VITRO</i> AND <i>IN SITU</i>	146
6. CONCLUDING REMARKS AND FUTURE PERSPECTIVES	151

7. MATERIALS AND METHODS	157
7.1. MATERIALS	157
7.1.1. Chemicals and Reagents	157
7.1.2. Disposable Materials	159
7.1.3. Equipment	160
7.1.4. Bioinformatic Analysis Software	161
7.1.5. Biological Materials	162
7.1.6. Antibodies	166
7.1.7. Oligonucleotides	167
7.1.8. Plasmid Vectors	168
7.1.9. Bacterial Cultivation	168
7.1.10. Enzymes and Enzyme Buffers	169
7.1.11. Kits	169
7.1.12. Molecular Weight Marker	170
7.1.13. Solution and Buffers	170
7.2. METHODS	173
7.2.1. Cell Culture methods	173
7.2.1.1. General Cell Culture	173
7.2.1.2. Transfection Methods	175
7.2.1.3. Inhibitor Treatment	178
7.2.1.4. Proliferation Assays	180
7.2.1.5. Migration assays	181
7.2.2. Organotypic Brain Slice Culture	184
7.2.2.1. Preparation	184
7.2.2.2. Culture	185
7.2.2.3. Implantation of Glioma Cells	186
7.2.2.4. Monitoring Migration and Invasion	186
7.2.2.5. Isolation of Single Cells	187
7.2.2.6. cDNA libraries, quality PCRs, and microarrays	188

7.2.3. Molecular Biological Analyses	190
7.2.3.1. Polymerase Chain Reaction (PCR)	190
7.2.3.2. Agarose Gel Electrophoresis	191
7.2.3.3. Quantitative real-time PCR	192
7.2.3.4. Plasmid Isolation	192
7.2.4. Protein Biochemical Analyses	195
8. BIBLIOGRAPHY	199
9. APPENDIX	215
9.1. LIST OF ABBREVIATIONS	216
9.2. LIST OF FIGURES	221
9.3. LIST OF TABLES	225
9.4. SUPPORTING MATERIAL	226
9.4.1. Detailed and Further Diagrams	226
9.4.2. Vector Charts	236
9.4.3. ImageJ Macros	237
9.5. CURRICULUM VITAE	239
9.5.1. Publications	240
9.5.2. Contributions to Conferences	240
9.5.3. Awards	242
9.6. ACKNOWLEDGEMENTS	244

1. Abstract

High-grade gliomas, especially glioblastomas, are highly complex and heterogeneous primary brain tumours. Glioblastoma (GBM) is one of the most aggressive cancers with poor overall survival prognosis. Fast and widespread invasion of the brain parenchyma by a subpopulation of progenitor tumour cells is a main pathophysiological feature of these tumours. Invasion renders localised therapies ineffective and is a primary cause of tumour recurrence as well as associated morbidity. Identification of factors related to invasion of brain tumour initiating cells (BTIC) into the surrounding parenchyma may provide strategic targets for early and sustained anti-invasion therapies. The dependency and interaction of infiltrative progeny cells with the tumour microenvironment as well as their adaptive development from the tumour cell fraction have not been adequately investigated.

Organotypic brain slice cultures (OBSC) were used as a valuable *in situ* model to analyse migration, as well as invasion, in conditions that simulate normal brain tissue and its respective microenvironmental influences. Unlike common animal models, this allowed monitoring of live tumour cell invasion in real time. Invasion of glioblastoma cells was induced by inoculation of fluorescence tagged human BTICs in the hippocampal region of OBSCs. During this analysis, morphologically distinct invasive cells emerged from the initial cell population, which drove invasion into the surrounding tissue. Differences in cell morphology and behaviour allowed categorisation of three populations of cells into leader, follower, and stationary which were otherwise not possible to observe in 2D migration assays.

To assess cellular expression markers specific for each group, a micromanipulator adapter was developed to isolate the separate cell subpopulations from OBSCs. After cDNA library generation and subsequent microarray analysis, a detailed comparison between stationary, follower, and leader cells was conducted. Invasive cells exhibited a markedly distinct expression pattern in comparison to follower and stationary cells, which allowed designation of a leader cell-specific gene expression signature. Unravelling the dynamics and complexity of leader cell invasion and induction by microenvironmental cues may provide new targets for future development of effective glioma treatments.

Deciphering the roles of leader, follower, and stationary cells in heterogeneous GBM is a long-term goal. However, an important short-term objective should be the improvement of existing standard therapy. Combined adjuvant therapies may prolong the currently very short median survival rate of patients with glioma. It was previously demonstrated that ibuprofen and diclofenac exhibit significant anti-tumourigenic effects on GBM cell lines *in vitro*. Although it was not conclusively proven here, restriction of signal transducer and activator of transcription number 3 (STAT3) phosphorylation and c-myc modulation could constitute mechanisms of their GBM restricting capacities.

In parallel, the unknown characteristics of primary BTICs and their differentiated pairs were analysed with regard to selected transcription factor expression as well as their motility and proliferation. Correlation of proliferation and migration allowed for clustering of the cells into separate subgroups. Subsequently, separate, well-characterised cell lines were analysed for sensitivity to STAT3-specific inhibition. This analysis revealed a remarkable restriction of both proliferation and migration in *in vitro* as well as *in situ* analyses.

The findings of the present study suggest that STAT3 is an important target for further therapy approaches of high-grade gliomas, and is supported by the identification of STAT3 as part of the leader cell gene expression signature in this work. The results presented here indicate that there may be value in the investigation of Stattic or other STAT3 specific inhibitors in clinical trials for glioma treatment.

2. Zusammenfassung

Höhergradige Gliome, im besonderen Glioblastome sind sehr komplexe, heterogene hirneigene Tumore. Glioblastome zählen zu den aggressivsten Krebsformen mit einer sehr schlechten Prognose. Ein pathophysiologisches Hauptmerkmal ist die schnelle und weit ausgedehnte Invasion des Hirnparenchyms durch eine Subpopulation von Tumovorläuferzellen. Diese infiltrierenden Tumorzellen stehen im Zusammenhang mit der Ineffektivität lokaler Therapien. Zugleich stellt die Infiltration die primäre Ursache für Rezidiventwicklung sowie die damit verbundenen Mortalität dar. Die Identifizierung von Faktoren, die wesentlich zur Invasion Hirntumor induzierenden Zellen (BTIC) in das umgebende Parenchym beitragen, kann entscheidende, strategische Ziele für frühe und nachhaltige invasionshemmende Therapien aufzeigen. Bislang ist die Abhängigkeit und Interaktion der infiltrierenden Vorläuferzellen mit dem sie umgebenden Mikromilieu wenig untersucht. Ebenso wenig ist die adaptive Entwicklung der Zellen an das Mikromilieu ergründet, die es den Zellen ermöglicht den Tumorherd zu verlassen.

Organotypische Hirnschnittkulturen (OBSC) wurden als nützliches *in situ* Model verwendet, um Migration sowie Invasion von Gliom-Zellen unter Konditionen, die das normale Hirngewebe reflektieren zu untersuchen. Im Gegensatz zu üblicherweise verwendeten Tiermodellen ermöglichen OBSCs die live Nachverfolgung der Invasion von Tumorzellen in das Gewebe. Diese Invasion wurde durch die Implantation von Fluoreszenz-markierten humanen BTICs in die Nähe der Hippocampusregion der OBSCs induziert. Durch diese

Analysemethode konnten invasive Zellen identifiziert werden, die sich aus der initialen Zellpopulation entwickelten und die Invasion in das umliegende Parenchym voran getrieben haben. Unterschiede in Zellmorphologie und –verhalten führten zur Differenzierung dreier Zellpopulationen: Leader, Follower und Stationary. Diese Unterscheidung war in 2D Migrationsanalysen nicht möglich. Um das spezifische Genexpressionsprofil der einzelnen Gruppen zu untersuchen, wurde ein Adapter für einen Mikromanipulator entwickelt, um die einzelnen Teilpopulationen getrennt von einander aus OBSCs isolieren zu können. Aus den isolierten Zellen wurden cDNA Bibliotheken generiert, sodass eine Microarray-Analyse erfolgen konnte, die einen detaillierten Vergleich zwischen Leader-, Follower- und Stationary-Zellen ermöglichte. Die invasiven Leader-Zellen wiesen ein von Follower- und Stationary-Zellen deutlich abweichendes Expressionsmuster auf, welches zur Identifizierung einer für Leader-Zellen spezifischen Gensignatur führte. Die Entschlüsselung der Leader-Zellinvasion unterliegenden Dynamik und Komplexität, sowie ihrer Induktion durch Einflüsse des Mikromilieus kann neue Angriffspunkte für die weitere Entwicklung effektiver Gliom-Therapien liefern.

Die Aufklärung relevanter Einflussfaktoren in der Beziehung von Leader-, Follower- und Stationary-Zellen zueinander und innerhalb heterogener Glioblastome ist ein langfristiges Ziel. Dahingegen stellt die Verbesserung existierender Standardtherapien eine wichtige kurzfristige Aufgabe dar. So könnten adjuvante Kombinationstherapien zur Verlängerung der momentan sehr kurzen medianen Überlebensrate führen oder die Lebensqualität von Patienten verbessern. Es wurde bereits gezeigt, dass Ibuprofen und Diclofenac *in vitro* signifikante anti-tumorigene Wirkung auf Glioblastom-Zelllinien haben. Diesen anti-tumorigenen Wirkmechanismen könnten eine Hemmung der Phosphorylierung des „signal transducer and activator of transcription number 3“ (STAT3) sowie eine Modulierung von c-myc zugrunde liegen, jedoch konnte dies in der vorliegenden Arbeit nicht eindeutig bewiesen werden.

Parallel dazu wurden die bisher unbekannten Eigenschaften primärer BTICs und der jeweiligen differenzierten Pendants bezüglich der Expression ausgesuchter Transkriptionsfaktoren sowie ihrer Migrations- und Proliferationsrate hin, untersucht. Durch Korrelation von Proliferations- und Migrationsraten war eine Gruppierung der Zellen in separate Untergruppen möglich. Diese gut charakterisierten Zellen wurden außerdem auf ihr Ansprechen auf eine STAT3-spezifische Hemmung hin untersucht, was eine beträchtliche Beeinträchtigung der Proliferation sowie Migration *in vitro* und *in situ* zur Folge hatte.

Die Ergebnisse der vorliegenden Arbeit weisen darauf hin, dass für zukünftige Therapieansätze höhergradiger Gliome, STAT3 ein wichtiges Angriffsziel darstellt. Dies wird durch die Tatsache gestützt, dass STAT3 in dieser Arbeit als Teil der Genexpressionssignatur der Leader-Zellen identifiziert wurde. Die hier präsentierten Daten deuten darauf hin, dass die Untersuchung von Stattic oder anderer spezifischer STAT3 Inhibitoren im Rahmen klinischer Studien für Gliom-Therapien von Nutzen sein könnte.

3. Introduction

Gliomas are the most common primary brain tumours in adults, accounting for about 30% of all tumours of the central nervous system and represent about 80% of all malignant gliomas in the US (Ostrom *et al.* 2014). Since 1979, the World Health Organisation (WHO) classifies different types of brain tumours and distinguishes between four malignancy based grades (WHO grade I – IV) in order to predict a response to therapy and outcome (Louis *et al.* 2007). The following introduction into gliomas refers to the currently still valid version of the WHO ‘Classification of Tumors of the Central Nervous System’ from 2007 (Louis *et al.* 2007). At present, the WHO classification is revised, mainly initiated by the report of a team of neuropathologists with expertise in molecular diagnosis (‘Guidelines for Nervous System Tumor Classification and Grading’ emerged from consensus meeting in 2014 in Haarlem, Netherlands; Louis *et al.* 2014).

Gliomas share histological features similar to the glia cells of the brain. Thus, they are mainly categorised on the basis of histologic features, such as morphology, genetic characterisations, mitotic activity, invasiveness, necrosis, and microvascular proliferation (Louis *et al.* 2007). Thereby most gliomas can be classified as astrocytic, oligodendroglial, mixed oligo-astrocytic or ependymal tumours according to the cell type they share histological features with (Riemenschneider *et al.* 2010). These classifications are not based on cell types tumours emanate from since the cell type(s) of origin are still uncertain (Phillips *et al.* 2006).

High-grade or malignant gliomas include anaplastic astrocytomas, oligodendrogliomas and oligoastrocytomas (WHO grade III), as well as the most malignant (WHO grade IV) glioblastomas (GBM) (Wen & Kesari, 2008) (see Figure 3-1). High-grade gliomas are nearly uniformly fatal with survival time between about 1 and 3.5 years (Phillips *et al.* 2006). Nearly all malignant gliomas are diffusely infiltrating tumours which infiltrate the adjacent brain parenchyma (Riemenschneider *et al.* 2010). This extensive infiltration is often clinically not evident and renders complete surgical resection impossible. Despite advances in medical imaging technologies, surgery, radiation, and chemotherapy, prognosis for glioma patients has hardly changed over the last decades. The emerged ‘Haarlem consensus guidelines’ of the ‘International Society of Neuropathology’ serve as a basis for the upcoming revision of the WHO classification of brain tumours by emphasising the importance to incorporate molecular characteristics of gliomas in their grading (Louis *et al.* 2014). They provide a direction towards explicit and stringently defined tumour entities that tailor current guidelines and therapy recommendations by integrating relevant molecular data, histologic features, and tumour grade in a layered fashion (Rushing & Wesseling, 2015). Although improved grading resulting in therapies tailored to individual tumour characteristics will improve patient survival, even advanced treatments often fail to improve patient survival, mainly due to the lack of therapies specifically targeting remaining tumour cells. Particularly in view of the overall poor outcome of current therapies, advanced treatment approaches are urgently sought.

3.1. Glioblastoma

GBM are the most prevalent and malignant primary brain tumours, with a mean incidence of about 3 cases 100.000 inhabitants each year and a mean overall survival of 14.6 months under standard care which combines resection, chemotherapy, and radiation (Stupp *et al.* 2005). Out of all brain tumour entities, GBM account for about 15% of all primary brain tumours and accounts for about 55% of all gliomas (Ostrom *et al.* 2014).

GBM are classified as astrocytoma by histological characterisation based on nuclear atypia, anaplasia, mitotic activity, microvascular proliferation, and/or necrosis (Van Meir *et al.* 2010). Predominantly, GBM arise *de novo* as primary tumours, while a fraction of about 5 to 10% has a clinical history of progression from pre-existing lower grade astrocytoma (Cloughesy *et al.* 2014; see Figure 3-1 for diagrammatic representation of progression). Secondary GBM are distinguished from primary by genetic heterogeneity.

For example, epidermal growth factor receptor (EGFR), as well as phosphatase and tensin homolog (PTEN), abnormalities are frequent in primary GBM, while isocitrate dehydrogenase (*IDH*) gene mutations appear frequently in secondary GBM (Riemenschneider *et al.* 2010). Worthy of note, is that the revised, forthcoming WHO classification will take *IDH* mutations and 1p19q loss into consideration for glioma grading (Louis *et al.* 2014). In general, *IDH* status can be an important distinguishing element of grading, since *IDH* wild type low-grade gliomas have clinical outcomes similar to GBM, while gliomas harbouring *IDH* mutation and 1p19p codeletion have the best prognosis (Cancer Genome Atlas Research Network *et al.* 2015).

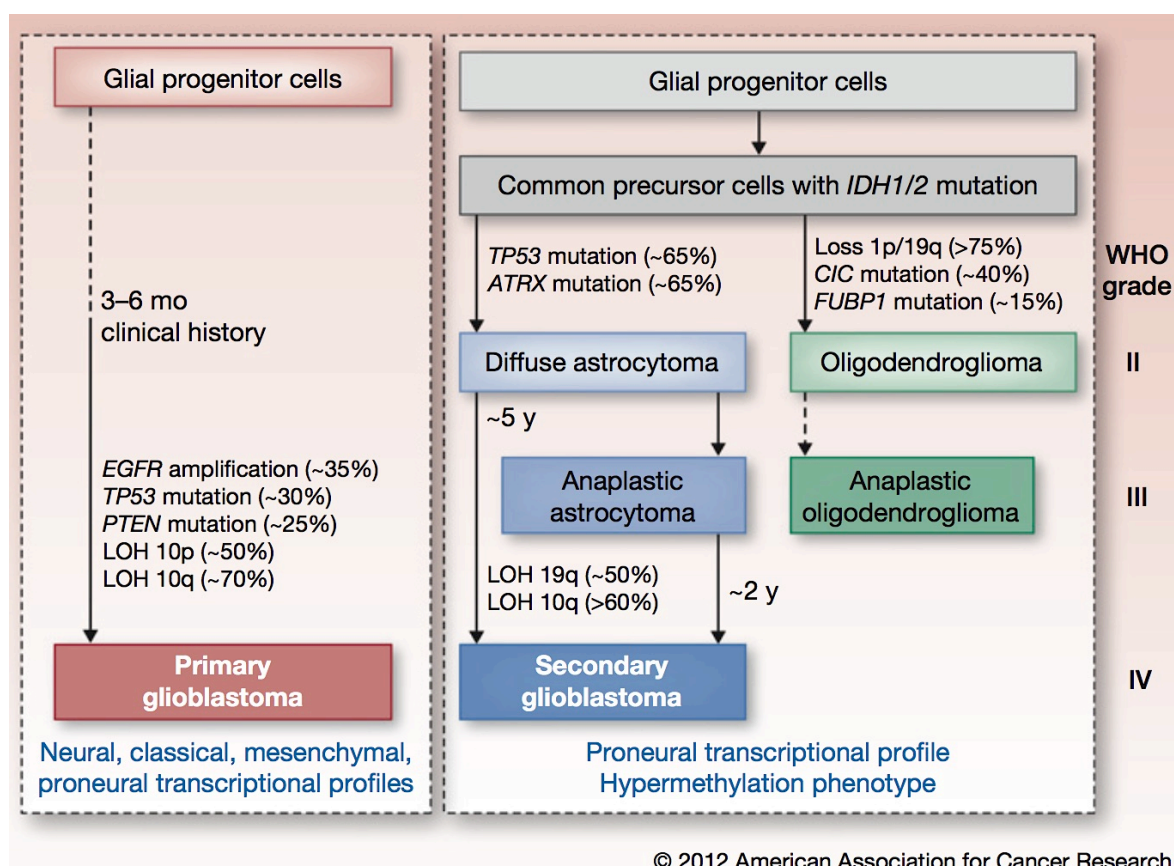


Figure 3-1: Proposed genetic pathways operative in the evolution of primary and secondary GBM

Loss of heterozygosity (LOH) on chromosome 10q is frequent in both primary and secondary GBM, whereas *TP53* genetic alterations are an early and frequent event on the way to secondary GBM. Note that in contrast to primary GBM, diffuse astrocytoma, oligodendroglioma, and later stages frequently carry mutations in *IDH1* or *IDH2*, indicative for a mutual, still to be identified cell of origin (Riemenschneider *et al.* 2010). Illustration adapted from Ohgaki & Kleihues (2013).

Fast and widespread invasion by a subpopulation of tumour cells is a main pathophysiological feature and the pivotal hallmark of GBM. The onset of invasion during tumour development has not yet been determined in the chronology of glioma-genesis, although this is a crucial milestone in its development. Although, even modern neuroimaging and resection techniques allow resection of $\geq 98\%$ of the tumour mass (Adamson *et al.* 2009), the remaining 2% are sufficient to induce local (about 90%; Wen & Kesari, 2008) or distal GBM recurrence. Recently Kim *et al.* (2015) indicated that distally recurred tumours share only a minority of initial tumour mutations (about 25%), indicative of branched evolution and genetic divergence. In contrast, the majority of initial tumour mutations was congruent with those of locally recurred GBM, consistent with linear evolution (Kim *et al.* 2015). This may indicate that tumour initiating cells reside in suitable niches near the tumour margin. Those may escape their dormant state to re-populate locally, causing GBM recurrence within a 2 to 3 cm perimeter of the initial tumour (Hou *et al.* 2006). Distant tumours may also arise from tumour cell clones which diffusely invade into the parenchyma at early stages of tumour development and accumulate various mutations leading to new distal tumour formation (Kim *et al.* 2015). Since the invasive cell fraction is the main reason for GBM relapse, this cell population constitutes a prime target for therapies.

3.1.1. Molecular subclasses of glioblastoma

It remains a challenge to decipher the molecular landscape that drives malignancy of GBM. However, this tumour entity has been selected as a pilot project by The Cancer Genome Atlas (TCGA) Research Network with the aim of assessing the molecular characteristics of GBM via large-scale multi-dimensional analysis (Cancer Genome Atlas Research Network 2008). GBM can be classified into four major subclasses based on molecular characteristics – proneural, mesenchymal, classical, and neural – classifications which have been established in recent years (Figure 3-2).

The classification was proposed by Verhaak *et al.* in 2010 using an integrated analysis which correlated results of unsupervised hierarchical clustering of the transcriptional GBM data from the TCGA with DNA copy number, and sequencing (Verhaak *et al.* 2010). Thus, the four specific molecular subclasses were revealed due to enrichment of distinct molecular alterations. In parallel, using the framework provided by TCGA, Noushmehr *et al.* (2010) performed unsupervised hierarchical clustering of DNA methylation profiles, revealing that approximately half of the GBM with a proneural signature are associated with the

glioma-CpG Island Methylator Phenotype (G-CIMP+). This G-CIMP+ signature correlates with secondary or recurrent tumours, and is tightly associated with *IDH1* mutations (Noushmehr *et al.* 2010).

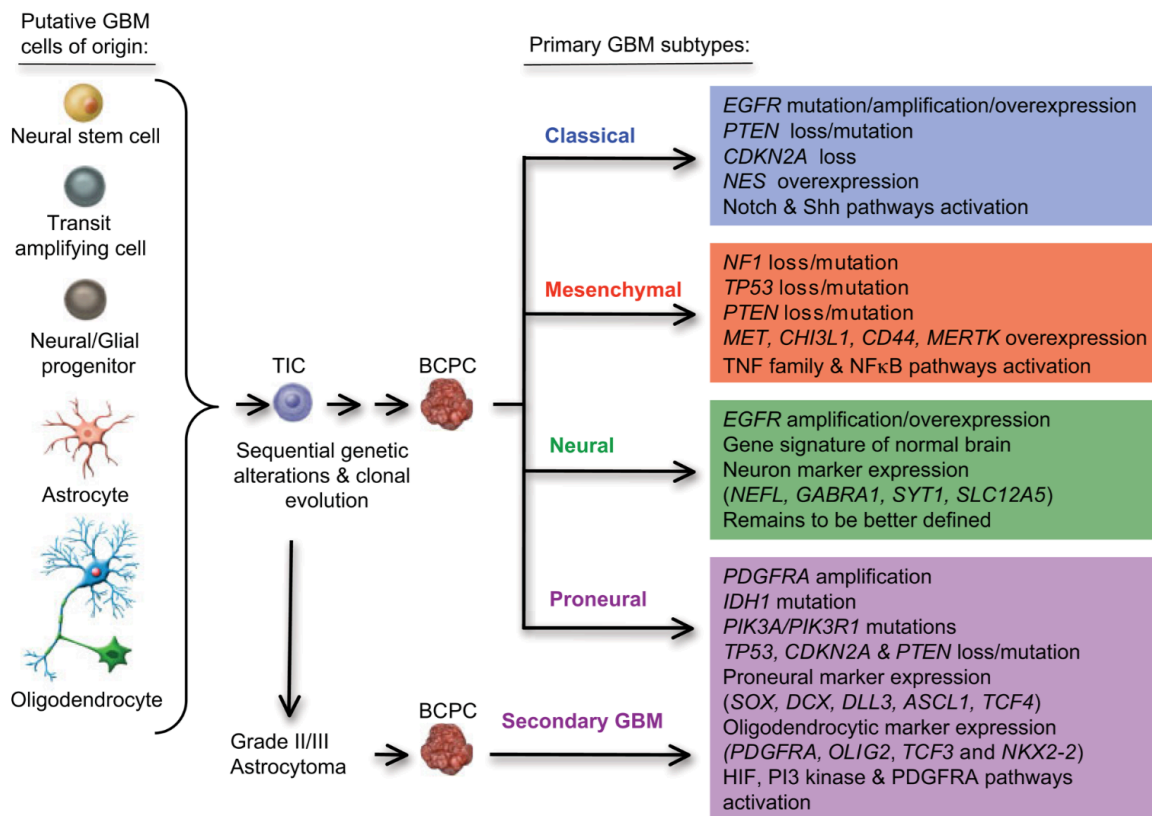


Figure 3-2: Sequential genetic changes define the molecular landscape of GBM subtypes

Molecular profiling of GBM tumours led to designation of four major subclasses bearing distinct genetic alterations. Those alterations can occur in normal brain cells and give rise to a population of tumour initiating cells (TIC). Further accumulation of genetic and epigenetic changes over time transforms these cells into brain cancer propagating cells (BCPC). BCPC are responsible for GBM formation and classified according to their genetic profile. Illustration and description adapted from Van Meir *et al.* 2010.

The subclass terminology originates from Phillips *et al.* (2006) who characterised distinct transcriptional subclasses of high-grade gliomas via DNA microarray profiling prior to availability of the TCGA framework. Their classification into proneural, mesenchymal, and proliferative subclasses is correlated to those identified by Verhaak *et al.*, (2010) although the proliferative class was substituted by the neural and classical subclasses. Phenotypes of the molecular subtypes were associated with stages in neurogenesis during normal brain development, astrocytic or oligodendroglial (Phillips *et al.* 2006). The proneural subtype was connected to low proliferation with concomitant expression of markers associated neuroblasts

and immature neurons. Whereas more differentiated transcription profiles applied to the mesenchymal subtype which share similarities with neural stem cells and/or transit-amplifying cells (Phillips *et al.* 2006). Finally, this study revealed a correlation of the mesenchymal subtype with shortest patient survival and a shift of recurrent GBM towards the mesenchymal category (Phillips *et al.* 2006). This provided first evidence that the mesenchymal subtype is the most aggressive and drug resistant of GBM molecular subclasses.

However, due to the anaplastic nature of GBM combined with constantly improving analysis techniques, newly emerging elegant studies reveal ever more detailed insights into cell phenotypes, which has enabled an even finer and more complex categorisation. For instance, Sturm *et al.* (2012) performed an analysis which integrated genetic, transcriptional, and epigenetic information of GBM specimen, defining a molecular architecture of six epigenetic and biologically distinct GBM subgroups. Although GBM is now one of the most molecularly profiled tumours due to the commitment of TCGA, clinical translation of the information gained from this initiative into therapies significantly contributing to overall patient survival and quality of life, has not yet been successful.

3.1.2. Intratumoural heterogeneity

The different GBM subtypes offer an explanation why GBMs effectively escape and evade therapy, but furthermore several groups have shown recently that GBM tumours are intrinsically heterogeneous (Sottoriva *et al.* 2013; Patel *et al.* 2014; Meyer *et al.* 2014). GBM share mutual histological features, but are also highly variable at the molecular level between patients and complex intrinsic GBM heterogeneity has been demonstrated. This intratumoural heterogeneity entails the biological diversity between cells descended from the same tumour, which seriously challenges the development of effective therapies for these tumours. In addition, it was recently determined that mainly the mesenchymal subtype bears an invasive behaviour (Sullivan *et al.* 2014; Ortensi *et al.* 2013).

Sottoriva *et al.* (2013) determined extensive intrinsic GBM heterogeneity in tumour evolution by integrated genomic analysis and demonstrated that most patients displayed different GBM subtypes within the same tumour (see Figure 3-3).

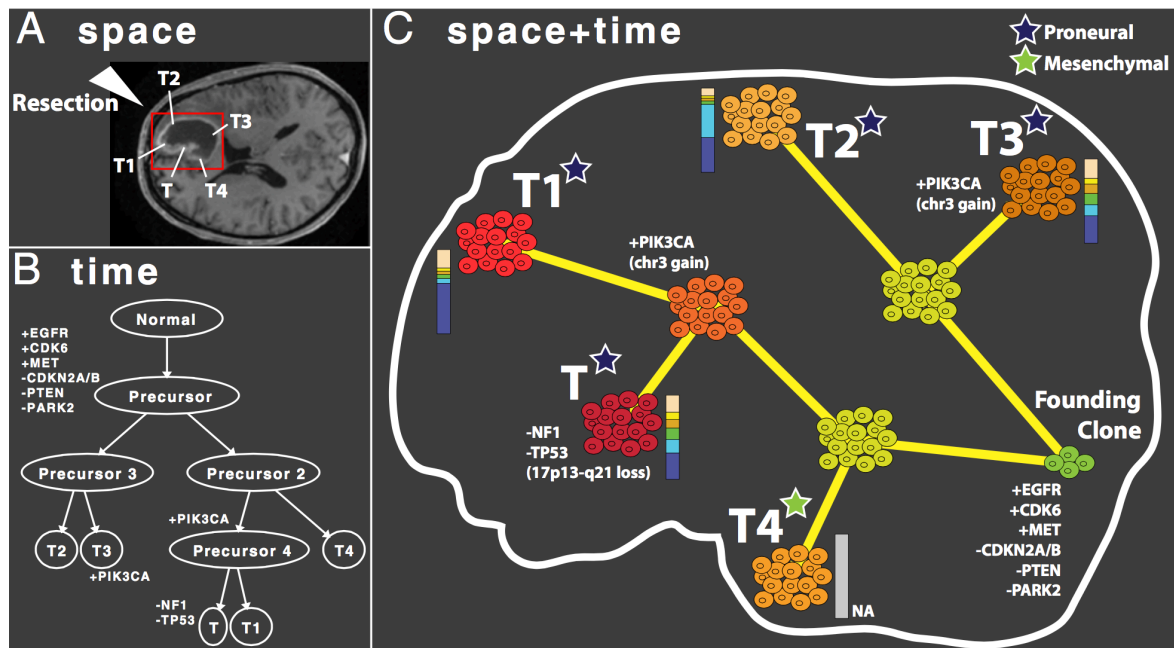


Figure 3-3: Reconstruction of evolution of intratumoural heterogeneity in GBM

Demonstration of intratumoural heterogeneity of a GBM by Sottoriva *et al.* (2013) (A) Sample collection (T – T4) from different tumour sites enabled (B) reconstruction of tumour phylogeny. (C) Analysis of gene expression profiles combined with molecular clock data resulted in temporal and spatial reconstruction of tumour evolution. Evolution of the malignancy is illustrated by accumulation of copy number alterations at different tumour sites. Correlation with respective gene expression profiles revealed that sample T4 was classified as mesenchymal subtype, while the remaining neoplasm appeared proneural. Illustration and description adapted from Sottoriva *et al.* 2013.

In addition, isolation, establishment, and functional profiling of single cell-derived clones from GBM specimen demonstrated distinct proliferation and differentiation capacities of these various clones (Meyer *et al.* 2014). This study unveiled a potential differential response and pre-existing resistance to conventional treatment, since clones derived before patient treatment included clones that were temozolomide resistant (Meyer *et al.* 2014).

Recently, Patel *et al.* (2014) compared single cell RNA sequencing data of 430 cells from five primary GBM with the dominant tumour bulk. They described variations in the transcriptional profiles of individual cells, indicating that GBMs contain cells expressing molecular classifiers of each subtype at once (Patel *et al.* 2014). However, it remained unclear if the genetic subgroups are predetermined or generated after tumour origin. Although, GBM development and evolution has been extensively investigated, relationships among different sources of intratumoural heterogeneity, underlying molecular pathways, and driver mutations remain to be deciphered.

3.1.3. GBM origin – cancer stem cells

Despite treatment, GBM recurrence is nearly inevitable, therefore, it is of great interest to determine how these tumours originate and are maintained. Combined with intratumoural heterogeneity, the pathogenesis of GBM may be based on a subset of cells possessing stem cell characteristics (Van Meir *et al.* 2010). Most importantly, cancer stem cells (CSC) are self-renewing and have tumour-initiating ability, but their origin is not yet known (Figure 3-2).

Generally two different concepts offer explanations for intrinsic GBM cellular heterogeneity (Figure 3-4). The model of clonal expansion, also referred to as the stochastic model (Vescovi *et al.* 2006), assumes that cancer cells within the tumour are heterogeneous, and tumour cells of many different phenotypes can proliferate extensively to generate new tumours (Reya *et al.* 2001). In contrast, the CSC hypothesis presumes a hierarchical organisation – despite aberrant growth – from where a tumour arises from, and is maintained by the stem cells. In this situation, a small subset of CSCs is the tumour seed which drives drug resistance and, as the less vulnerable population, also drives re-growth after treatment (Cloughesy *et al.* 2014). CSCs are solely responsible for tumourigenesis and proliferation, whereas most cells are depleted of this ability (Reya *et al.* 2001).

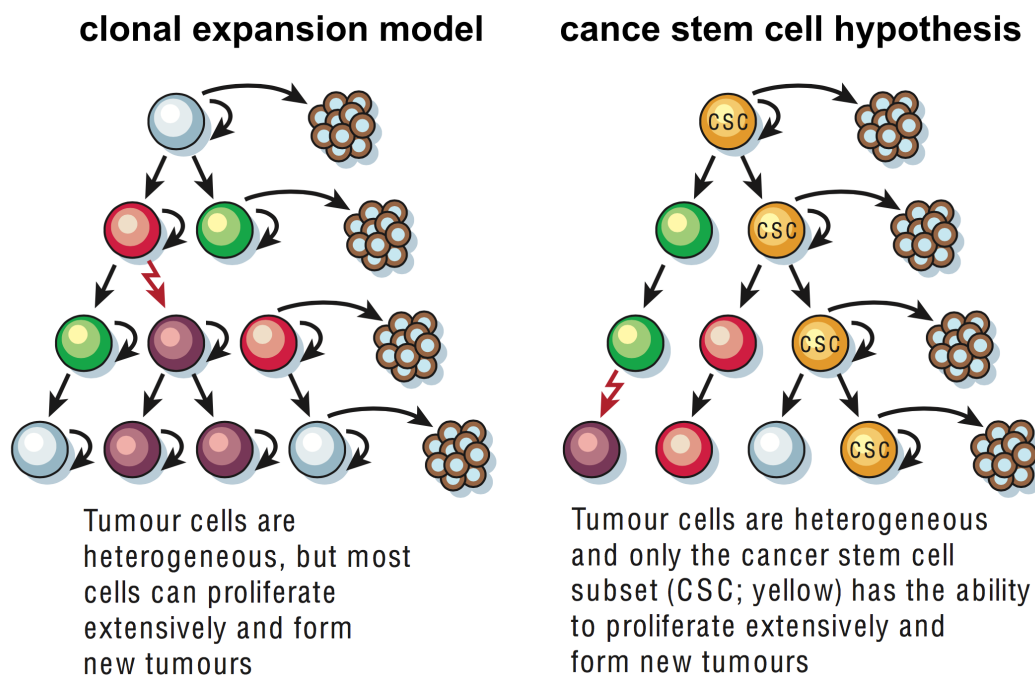


Figure 3-4: Hypothetical concepts of intrinsic GBM cellular heterogeneity

Illustration adapted from Reya *et al.* 2001.

Neither the CSC model nor the clonal expansion model is likely to exist alone, the truth behind the mechanism of tumourigenesis is likely a combination of these two scenarios (Reya *et al.* 2001). Recently, Tabassum and Polyak (2015) described the concept of clonal origin of tumours to be replaced as cancer is now commonly viewed and analysed akin to an evolving ecosystem. Considering the growing awareness of intratumoural heterogeneity, cells within a tumour may be subject to Darwinian forces – survival of the fittest – as a result of direct proximity of distinct clonal populations which may influence the fitness and survival of each other (Tabassum & Polyak, 2015). Thus, clonal evolution (Figure 3-5A), during tumour growth, appears to explain observed variances in drug sensitivity compared with tumours derived from a single clone (Marusyk & Polyak, 2013) and presence of more than one subtype in GBM (Sottoriva *et al.* 2013). In contrast to observations of clonal interference and competition, mutual and synergistic clonal cooperation by individual subpopulations of cancer cells substantially interacting with each other has also been described (Figure 3-5B). Thus, cancer cells may engage in heterotypic interactions with cells in their microenvironment and use the available resources to proliferate and survive (reviewed in Tabassum & Polyak, 2015). It has been hypothesised that CSCs and differentiated tumour cells are two phenotypically distinct states that may freely interconvert, a situation which implies that CSCs can be formed *de novo* from more differentiated tumour cells (Medema, 2013). This may also be due to microenvironmental factors, which could affect the conversion between states.

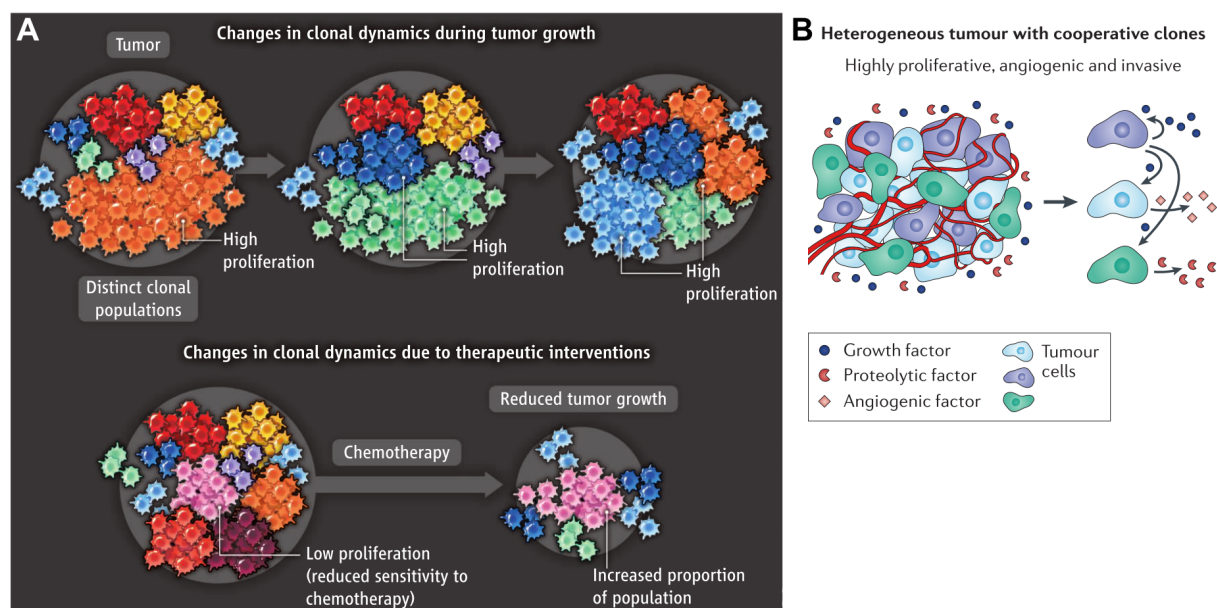


Figure 3-5: Clonal dynamic during tumour growth and clonal cooperation within heterogeneous tumours

(A) Treatment naïve tumours likely consist of clones with distinct phenotypes. In general, clones with high proliferation dominate a tumour. Dynamic and proportion of different clonal types can vary during progression. Therapeutic interventions may change the clonal landscape by increasing the proportion of slowly proliferating clones that reflect reduced sensitivity of slower-proliferating clones to chemotherapy. (B) Mutualistic relationship of different cancer cell populations cooperating with one another, which likely increases the whole tumour fitness as a result of survival enhancement of the heterogeneous sub clones. Illustrations and descriptions adapted from Marusyk & Polyak, 2013 (A) and Tabassum & Polyak, 2015 (B).

3.1.4. Brain tumour initiating cells

It seems reasonable to state that successful treatments of so-far incurable GBM depend on targeting and elimination of CSCs. The presence of brain tumour stem cells (BTSC) in GBM was described independently by two groups (Singh *et al.* 2003; Galli *et al.* 2004), who managed their isolation and cultivation. Although different methods were applied to identify BTSCs, the conclusion was drawn in both cases that the isolated fractions can be characterised by self-renewal, clonogenicity, pluripotency, and closely resemble the histopathological phenotype of parental tumours after implantation of these cells into athymic mice (reviewed in Das *et al.* 2008).

BTSC are derived from dissociated tumours after surgical resection and enriched in culture conditions, adapted from cultivation of adult neural stem cells, in specific serum-free neurobasal medium supplemented with appropriate growth factors, such as epidermal growth factor (EGF) and fibroblast growth factor (FGF) (Vescovi *et al.* 2006). In such *in vitro* conditions, BTSCs gained an immortal proliferative potential while maintaining the phenotype and genotype of primary tumours as well as their undifferentiated stem cell state (Ignatova *et al.* 2002). Like neural stem cells (NSC), BTSC were able to differentiate into the neuronal as well as glial lineages after withdrawal of the growth factors and addition of fetal calf serum (FCS) (Singh *et al.* 2003). Accordingly it was postulated that BTSCs derive from NSC or neural progenitors by escaping from the tight control of the spatially and temporally orchestrated sequence of differentiation, migration, and proliferation (Sanai *et al.* 2005), since BTSCs and NSCs share remarkable characteristics such as self-renewal and differentiation capabilities (Charles *et al.* 2011). Moreover, evidence has accumulated that NSCs and BTSCs are physically located in specialised microenvironmental niches, which regulate their self-renewal and differentiation (Li. *et al.* 2009). BTSCs are thought to occupy, among others,

perivascular, hypoxic, and necrotic niches (reviewed in Sundar *et al.* 2014), for instance, endothelial cells, which might influence stemness by secreted factors (Calabrese *et al.* 2007). However, targeting those niches is complex and tumour cells may escape. It has been determined that anti-angiogenic therapies that inhibit vascular endothelial growth factor (VEGF) signalling may promote an infiltrative tumour growth pattern (Van Meir *et al.* 2010). Besides niche factors, BTSC are constantly affected by microenvironmental factors, including stromal, immune, and non-stem tumour cells as well as factors secreted by those cells (Li. *et al.* 2009). Therefore, combination of anti-angiogenic therapies with anti-invasion therapy may delay disease progression (Van Meir *et al.* 2010).

BTSC are commonly propagated as neurospheres and identified by expression of markers, which include, among others, CD133, Nestin, SOX2, or Mushashi (Ignatova *et al.* 2002; Vescovi *et al.* 2006; Singh *et al.* 2003). Several studies have aimed to elucidate specific BTSC markers in order to develop innovative targeted therapies. However, BTSC markers are a controversial issue in literature (Venere *et al.* 2011; Medema, 2013), mainly due to varying extents in marker expression. For instance, CD133 was claimed to be a putative marker for BTSCs (Singh *et al.* 2003), but in contrast, Beier *et al.* (2007) postulated that CD133 negative BTSC are responsible for tumour progression. Tumour spheres derived from CD133 negative cells grew semi-adherent *in vitro* in contrast to CD133 positive BTSCs.

GBM are in all probability driven by a minority of cancer stem-like progenitor cells, but due to the limitations of CSC identification imposed by imperfect markers, the enriched cells in culture should rather be called brain tumour stem-like, or initiating cells (BTIC), preferentially, rather than CSCs. BTICs represent the minority of cancer stem-like progenitor cells which are not only implicated in tumour initiation, but also in recurrence and progression (Das *et al.* 2008).

BTICs are the best available model to investigate high-grade gliomas *in vitro* and *in vivo* so far (Moeckel *et al.* 2014), and provide tremendous insight into the genomic landscape as well as overall behaviour of GBM. However, drawing conclusions on *in vitro* cultures derived from a single biopsy specimen may be overly simplistic and inadequately reflect these heterogeneous and dynamic tumours. As indicated above, BTICs and non-stem tumour cells (TC) co-exists *in vivo* and likely change dynamically by the tumour microenvironment and cross talk between cell types. In depth profiling is, therefore, required to address the *in vivo* situation. It was shown that the phenotype of BTICs can be a product of their

microenvironment (Calabrese *et al.* 2007; Li. *et al.* 2009). This environment consists of their niche (for example, perivascular, necrotic, or hypoxic), the cellular context, and local soluble factors (Lane *et al.* 2014; Medema, 2013). Glioma cells, however, are known to actively modulate their environment to increase their invasive potential (for review see Cuddapah *et al.* 2014). The tumour microenvironment, BTIC niches, and GBM border regions, which may affect the invasive properties of tumour cells, are the focus of many current investigations (reviewed in Sundar *et al.* 2014).

3.2. Infiltration and migration

The almost inevitable recurrence of GBM, which is accompanied by minor improvement in likelihood of survival, is likely related to diffuse infiltration of the brain parenchyma – a major hallmark of high-grade gliomas. It is well known that infiltrating tumour cells lie well beyond the definable margin for maximal resections (Claes *et al.* 2007) and tumours recur predominantly within 2 to 3 cm of the resection cavity (Hou *et al.* 2006). BTICs find shelter in niches adjacent to the tumour bulk, endure first-line therapy and thus are able to induce local, but also distant and multi-focal relapse.

There is general agreement that invasion is an early event in glioblastoma progression (Louis, 2006). Since gliomas are usually not diagnosed at this stage, the exact appearance of this milestone is unknown, which may raise criticism on the value of anti-invasive therapies. Therefore, curative therapies specifically attacking infiltrative cells will have to be able to cross the highly selective blood–brain barrier and disperse within the entire brain, without affecting normal brain physiology and function (Adamson *et al.* 2009).

3.2.1. Invasion infrastructure

As one pioneer in glioma growth pattern study, in 1938, the neuropathologist Hans Joachim Scherer published that glioma cells preferentially migrate along existing brain structures (reviewed in Claes *et al.* 2007 and Cuddapah *et al.* 2014). This concept has been substantiated in recent years as it was shown that vascular co-option and migration along white matter tracts are important features of glioma cell invasion (Bellail *et al.* 2004; Demuth & Berens, 2004; Louis, 2006; see Figure 3-6).

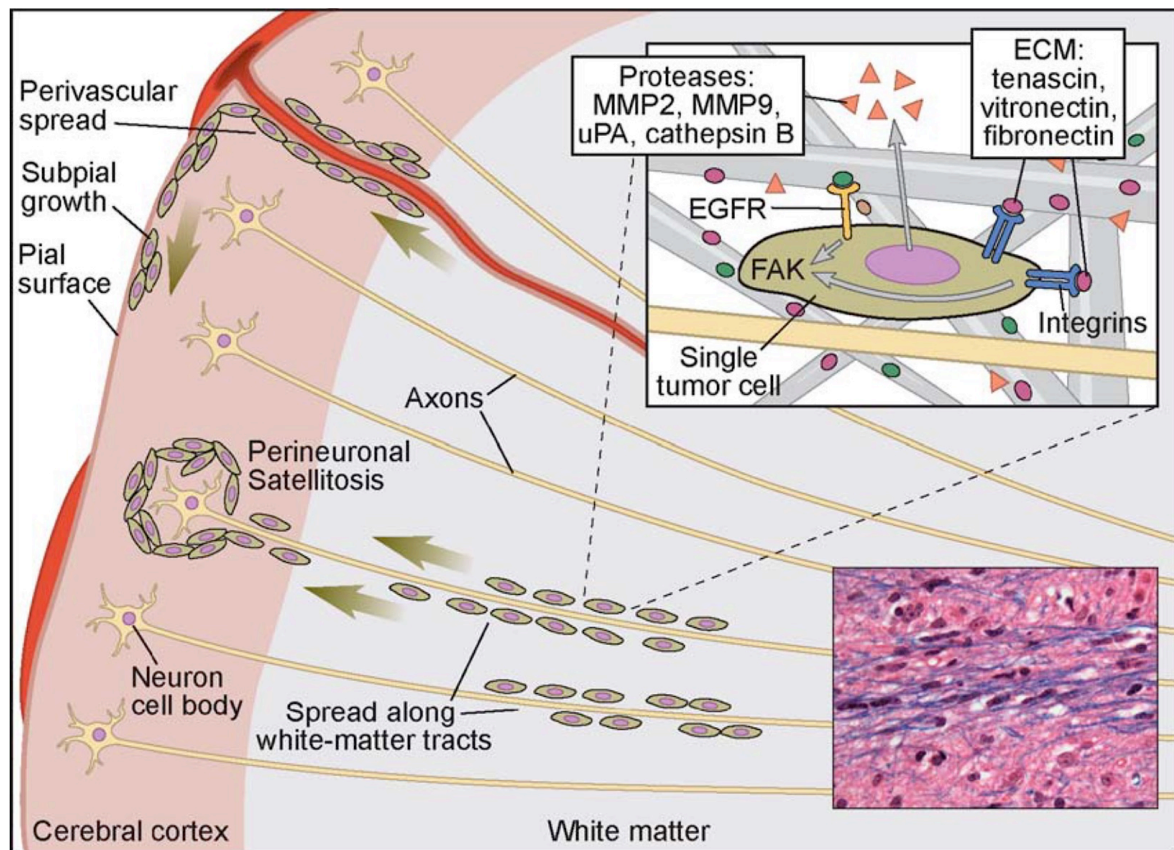


Figure 3-6: Infiltration of the brain by malignant glioma cells

White-matter tracts, around neurons and blood vessels are invasion routes along which glioma cells preferentially invade. Molecular requirements for single cell invasion are depicted at the upper right box and are characterised by, among other factors, release of proteases (matrix metalloproteinases (MMP) 2/9, urokinase-type plasminogen activator (uPA), cathepsin B), and expression of extra cellular matrix (ECM) interacting receptors such as integrins, which can activate focal adhesion kinase (FAK)-mediated cellular signalling. The Luxol fast blue H&E stain (400x) in the lower right depicts tumour cell nuclei aligned at myelinated axons (blue). Illustration and description adapted from Louis, 2006.

Several ‘active’ and ‘passive’ extracellular components are known to contribute to cancer invasion. Moreover, it was found that Scherer’s structures can actively attract glioma cells and provide a distinct advantage for their invasion (Louis, 2006; Bellail *et al.* 2004). Direction of infiltration can be coordinated by a wide range of chemoattractants (Cuddapah *et al.* 2014). ECM structures (for example, laminin, fibronectin, collagen) passively provide structural support and act as guiding scaffolds or barriers for cancer cells (Gritsenko *et al.* 2012). Soluble compounds such as growth factors, peptides, and chemokines (for further review see Louis, 2006; Cuddapah *et al.* 2014), provide an attractive microenvironment for invasion (Figure 3-6). Additionally, glioma cells are able to proteolytically cleave molecules blocking their way by altered protease expression and release (Gritsenko *et al.* 2012). Prevention of

glioma cell interaction with the ECM seems an attractive option. Foremost, integrins have been linked to glioma invasion (Demuth & Berens, 2004), but also other ECM components such as versicans (Onken *et al.* 2014). Inhibition of integrins had already been translated to clinical trials, but did not meet therapeutic expectations (Eisele *et al.* 2014). This indicates that a detailed understanding of mechanisms underlying glioma cell invasion is required.

3.2.2. Principles of epithelial to mesenchymal transition

Protease degradation of the ECM creates space into which infiltrative cells can migrate by an active mechanism that requires dissociation from neighbouring cells by disassembly of cell-cell junctions, detachment from previous matrix adhesion sites, cytoskeleton remodelling, as well as anchoring to ECM scaffold with the leading edge (Kong *et al.* 2011). The first apparent step towards an aberrant infiltration is the ability of single cells to detach from the primary tumour, which requires trans-differentiation from an epithelial-like to a more mesenchymal state (Zarkoob *et al.* 2013). This epithelial to mesenchymal transition (EMT) constitutes an apparently relevant mechanism by which glioma cells become invasive (Carro *et al.* 2010; Zarkoob *et al.* 2013).

In general, EMT is an essential and critical feature in embryogenesis as well as for inflammation, wound healing, and tissue regeneration (Kalluri, 2009). EMT is responsible for the formation of all the mesenchymal cells in early embryogenesis. The earliest EMT event is the formation of mesenchymal cells during gastrulation (reviewed by Polyak & Weinberg, 2009). For branching morphogenesis of multiple different organs during embryonic development, cells need to be very plastic and able to switch back from EMT when required, which occurs via mesenchymal to epithelial transition (MET) – the reversal of EMT (Polyak & Weinberg, 2009). Although, EMT is an essential key process during development, pathologically this mechanism is a hallmark of cancer (Hanahan & Weinberg, 2011). EMT can be aberrantly induced in tumour cells, enabling them to invade surrounding tissue, to promote, and ultimately lead to seeding of metastases (Scheel & Weinberg, 2012), since, at suitable niches, EM transformed cells may partially convert back (Claes *et al.* 2007).

Repression or relocation of epithelial markers such as E-cadherin, a glycoprotein responsible for cell-cell adhesion, is crucial for transformation into a mesenchymal state (Kong *et al.* 2011). In contrast, the motile invasive phenotype requires up-regulation of mesenchymal markers such as fibronectin, N-cadherin, or vimentin (Kong *et al.* 2011). Consequently, EMT

allows tumour cells to change into an infiltrative phenotype by loss of their epithelial shape and acquisition of a spindle-like phenotype which enables migration (Polyak & Weinberg, 2009). Several inducers of EMT are known in the tumour microenvironment. Paracrine influence of cytokines such as Notch, EGF, or ligands of transforming growth factor β (TGF β) (Scheel & Weinberg, 2012) have emerged as a major regulator of EMT (Singh & Settleman, 2010). Downstream signalling pathways involving pleiotropic transcription factors such as nuclear Factor κ -light-chain-enhancer of activated B cells (NF- κ B) (Dhruv *et al.* 2013), SNAI1, or Twist (Mani *et al.* 2008). Overall, up regulation of three major groups of transcription factors – SNAI, Twist, and Zinc-finger enhancer binding (ZEB) family members – are known to promote tumour invasiveness and to be associated with poor clinical prognosis (Ortensi *et al.* 2013).

In gliomas, SOX2, which is a critical transcriptional regulator of embryonic and neural stem cell function, directly contributes to an invasive phenotype of glioma cells (Alonso *et al.* 2011). In this work, gene amplification in 8.5% of GBM cases, overexpression in 86%, and promoter hypomethylation in 100% illustrate that genetic, transcriptional, and epigenetic events contribute to enhance invasion. Moreover, analysis of TCGA data revealed high expression of genes associated with mesenchyme-derived tissues (i) to be common in GBMs, (ii) to correlate with poor overall survival and treatment resistance and (iii) that mainly the mesenchymal signature contributes to invasion whereas cells of the proneural subtype display limited invasiveness, but high proliferation (reviewed in Ortensi *et al.* 2013). Carro *et al.* (2010) applied a bioinformatic reverse engineering algorithm to TCGA data of high-grade gliomas, which revealed a pivotal role for signal transducer and activator 3 (STAT3) and CAATT/enhancer binding protein β (C/EBP β). Those transcription factors appear to regulate the mesenchymal state as potential master regulators synergistic initiating EMT, as ectopic co-expression of STAT3 and C/EBP β reprogrammed NSCs along the aberrant mesenchymal lineage (Carro *et al.* 2010). Thus, their knockdown might be able to reverse the transition, which might bear therapeutic potential to restrict infiltration to convert gliomas into a focal disease. Figure 3-7 illustrates possible BTIC origin and involved mechanisms.

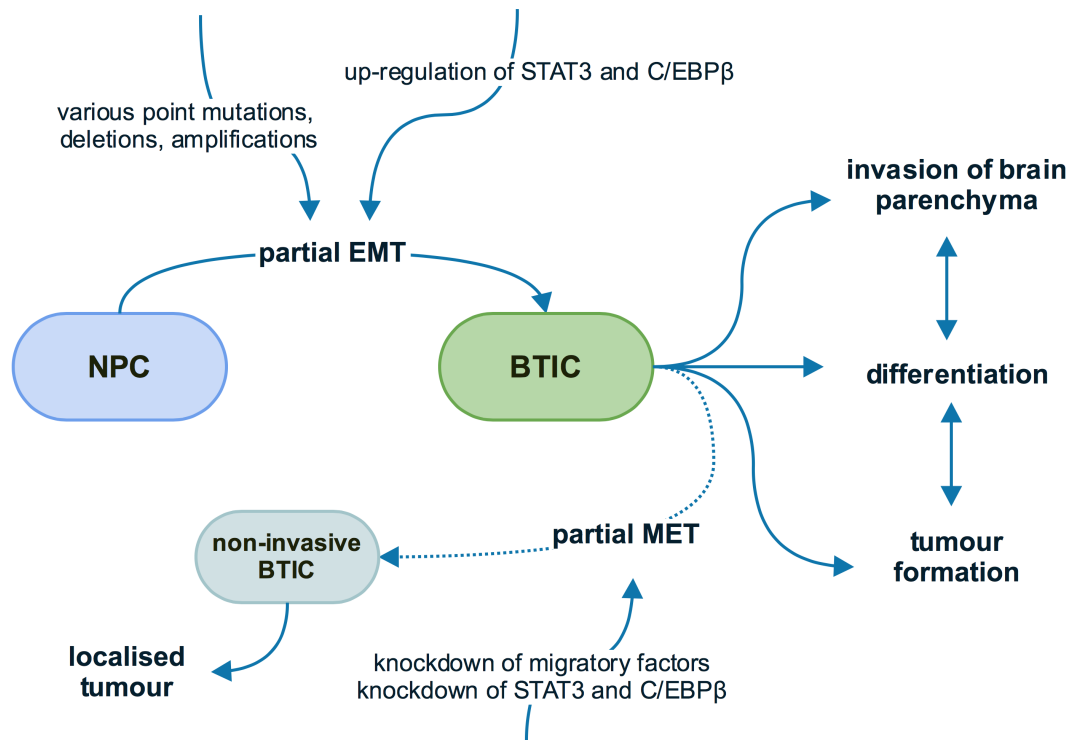


Figure 3-7: Possible origins of BTIC and their role in GBM formation

Knockdown of cell-cell contacts, release from cell cycle controls, accumulation of mutations, as well as an aberrant over-expression of transcription factors such as STAT3 and C/EBP β , may orchestrate conversion of neural progenitor or stem cells (NPC) into BTICs. Once released from control mechanisms, BTICs may cause tumour formation and a partial transition from an epithelial-like to more mesenchymal state favouring unrestricted infiltration of the brain parenchyma. Targeting EMT mechanisms of BTICs may render them non-motile leading to more localised tumours.

Overall, induction of EMT is a complex process which still remains to be unravelled in detail. Although increasing, knowledge of key factors orchestrating EMT and triggering invasion are often obtained in artificial glioma models which brings into question if the conclusions drawn from these analyses can be transferred to the patient situation. Therefore, a conclusive image of the invasive process in malignant gliomas is still not available, partly due to the lack of relevant models and an imbalance of the knowledge on cell intrinsic signals in contrast to microenvironmental triggers.

3.2.2.1. Migration modes required for infiltration

In general, and in malignant cancer situations, cell migration can be separated in two distinct forms (i) individual migration with absent cell-cell junctions, or (ii) collective migration when cells move as multicellular groups where cell-cell adhesions are retained (Friedl & Wolf, 2010; see Figure 3-8 for illustration).

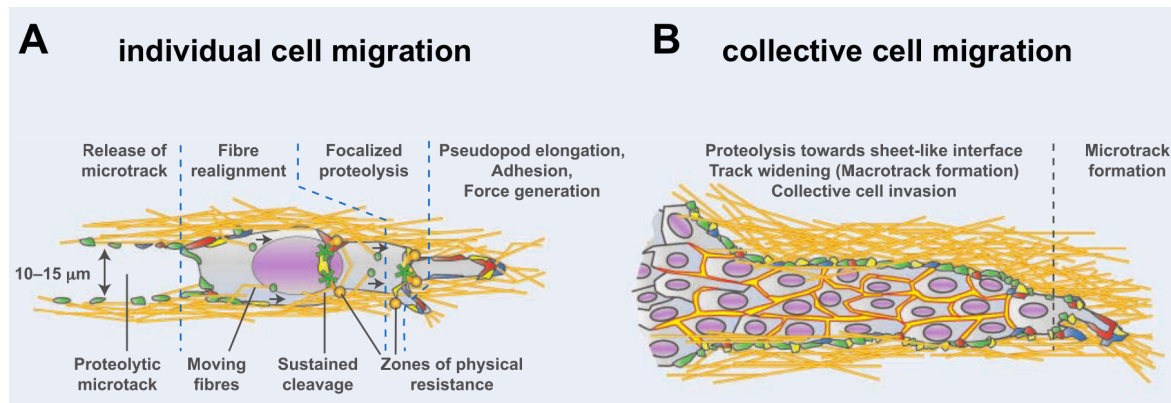


Figure 3-8: Two distinct forms of invasion

Invasion can occur by (A) individual or (B) collective cell migration. (A) Individual cell migration requires five different steps. Cells form protrusions in the direction of movement, use proteolysis to degrade surrounding ECM structures to make space for the cell body to track along. (B) Collective migration requires formation of two zones, where at least one leader cell generates a proteolytic microtrack to guide the cells at their rear, which then widen the track. Illustration and description adapted from Friedl & Wolf, 2010.

Cancer cell movement is similar to general cell migration, an orchestrated biological process that requires a coordinated sequence of adhesion of the leading edge of a migrating cell, anchoring to the ECM, and detachment of the trailing end (Friedl & Alexander, 2011). Basic prerequisites for individual cell migration are (i) cellular polarisation, (ii) massive cytoskeletal rearrangement which enables formation of a leading edge, (iii) anchoring, (iv) detachment, and (v) protease degradation of the ECM to generate space for invasion. Continuous actin polymerization at the leading edge is required to form and stabilise membrane protrusions in order to enable cell migration (Le Clainche & Carlier, 2008). Actin-myosin molecular motors have been shown to be a main contractile force in glioma cells (Beadle *et al.* 2008). In addition, other cytoskeletal components, such as the microtubule network, contribute to establish and maintain cellular polarity (Hall, 2009). Cell adhesion and its maintenance is a very complex and well-regulated process, which requires (i) synthesis of new adhesion proteins, (ii) their transport to target sites, (iii) adhesion complex formation and stabilization, and (iv) complex disassembly leading to cell detachment (Friedl & Wolf, 2010).

Collective migration requires at least one leader cell that paves the way for other cells to follow. Several mechanisms can polarise a cell cohort into leader cells that guide followers at their rear. Cells at the leading edge are often less ordered and mesenchyme-like, whereas cells at the rear tend to form more tightly packaged assemblies (reviewed in Friedl & Gilmour, 2009). This front–rear asymmetry can be predetermined from the onset or can result from a temporary, functional state like environmental influences and the presence of growth factors.

Although, cancer cell migration is reasonably well understood (for review, see Friedl & Wolf, 2003), the mechanisms underlying this movement are still poorly known for gliomas. It is of note that mechanisms of glioma cell invasion may differ from other metastasising tumours due to (i) cells are adapted to the brain parenchyma, which lacks many ECM elements found in other organs (Van Meir *et al.* 2010) and (ii) gliomas rarely – only 0.4 – 2% – metastasise outside the brain (Cuddapah *et al.* 2014).

3.2.3. Modelling glioma cell migration

Unfortunately, most current migration and invasion assays are highly artificial *in vitro* systems that do not resemble *in vivo* conditions (Valster *et al.* 2005). For example, such systems fail to incorporate topographical cues which guide cell movement (Figure 3-6). Standard 2D *in vitro* assays such as spheroid or wound healing provide plastic or glass surfaces for cell migration and thus can only provide first insight in candidate invasion mechanisms or demonstrate proof of principal (Valster *et al.* 2005). More advanced *in vitro* 3D assays use electro-spun nanofibre scaffolds to simulate white matter tract topography (Rao *et al.* 2013) or mimic ECM by crosslinking components in hydrogels. The latter are usually collagen-based matrices with Matrigel as well known representative, this does not resemble the unique composition of neural tissue ECM (Van Meir *et al.* 2010), both systems lack microenvironmental cues.

In contrast, *in vivo* analysis can simulate invasive growth patterns as observed in patients. Either spontaneous GBM mouse models (Shelton *et al.* 2010) or xenograft models of human glioma cells implanted in immune compromised mice are common. Implantation of BTICs into athymic mice generated tumours featuring histological characteristics similar to respective human GBMs (Beier, Röhl, *et al.* 2008; Beier, Wischhusen, *et al.* 2008). Although, these models appear attractive, they bear several obstacles: (i) use of immune compromised mouse hosts lacks immune-mediated responses, (ii) after initial *in vitro* culture,

glioma cells tend to lose their invasive properties (Galli *et al.* 2004), and (iii) evaluation of invasion at the end of the assay is time-consuming and online-monitoring is not possible.

3.2.3.1. 3D *in situ* model of organotypic brain slice cultures

The *in situ* model of hippocampal organotypic brain slice cultures (OBSC) may overcome some limitations of current brain tumour models. OBSC were developed to study tissue preservation and emerged in neurobiology and electrophysiology research involving neuronal growth and regeneration, synapse formation, as well as dendritic branching (reviewed in Gähwiler *et al.* 1997). OBSCs prepared from about 1 week-old rodents can be cultured for several weeks, and the interface technique has become general usage (Gogolla *et al.* 2006). Slices are placed on a porous membrane facing culture media on one side and controlled atmosphere on the other side.

Major features of OBSCs are preservation of (i) cryoarchitecture as well as ECM structure which conserves the organisation of structures similar to *in vivo* conditions, (ii) (Gogolla *et al.* 2006), (ii) microglial activity (Vinet *et al.* 2012), (iii) blood vessel structure preservation (Kovács *et al.* 2011; Bendfeldt *et al.* 2007), and (iv) 3D organisation via long-term thickness of 100 – 150 µm (Gogolla *et al.* 2006). In addition, slice cultures offer the convenience (i) to study brain regions of interest with their particular cellular and anatomical environments, (ii) of easy access for treatments including pharmacological stimulation or inhibition, (iii) OBSCs can be prepared from rodents of any genetic background, including those of poor postnatal viability, and (iv) allow microscopic monitoring during the entire experiment (Gogolla *et al.* 2006; Eyüpoglu *et al.* 2005; Gähwiler *et al.* 1997). Therefore, OBSC might be an innovative method to investigate glioma cell invasion, filling the gap between artificial 2D cell culture and *in vivo* animal studies. Reduction of *in vivo* models would reduce the amount of animals needed and limit the burden posed on these animals, and contribute to the 3Rs (reduce, refine, replace).

The OBSC model was previously used in glioma research, although mostly glioma cell line invasion was investigated. Eyüpoglu *et al.* (2005) implanted fluorescence-labelled rat, mouse, and human glioma cell lines on OBSCs and then documented their growth microscopically up to 20 days *in vitro*. This analysis revealed radial invasion already five days after implantation. Another application of OBSCs was demonstrated by Demuth *et al.* (2008) who validated a possible invasion driving gene via siRNA knockdown in glioma lines in OBSCs.

The candidate gene was identified by gene expression profiling transcriptional of migratory and stationary populations of human glioma cells. However, for this reasonable attempt the authors used mainly long-term glioma cell cultures and isolated migratory and stationary populations for microarray analysis from an *in vitro* assay; the relevance of this work in the patient situation is, therefore, questionable.

3.3. STAT3

STAT3 is a member of large family of transcription factors with a dual role as signal transduction and transcription activators. Zhong *et al.* first described STAT3 in 1994 as a DNA-binding protein activated by EGF and interleukin (IL) 6, in contrast to previously discovered interferon activated STAT members. Pleiotropic STAT3 is the most prominent family member, since it critically regulates an extensive spectrum of physiological processes (Levy & Lee, 2002).

3.3.1. STAT3 regulation

The classical mechanism which induces transcriptional activation of STAT3 occurs via sequential phosphorylation involving receptor-associated Janus kinases (JAK) (Levy & Lee, 2002). Canonical JAK-STAT activation is mediated by several different polypeptides via either cytokine or G-protein receptors (Bromberg, 2001). Upon cytokine or growth factor induced receptor dimerization, transphosphorylation and activation of JAKs occurs, followed by phosphorylation of receptor tails. Those recruit through Src-homology 2 domains (SH2) latent, cytosolic, and monomeric STAT3, which becomes activated by phosphorylation on the tyrosine residue 705 (Y705). STAT3 dimerization occurs by virtue of reciprocal interaction of SH2 and phosphorylated Y705, followed by nuclear entry and induction of target gene transcription (Bromberg, 2001; Xiong *et al.* 2014). Subsequent dephosphorylation causes nuclear export of inactive STAT3.

STAT3 can be activated via several mechanisms (Figure 3-9). The most prominent are: (i) receptor tyrosine kinases stimulated by EGF, PDGF, or FGF, (ii) cytokine (including ILs)-mediated activation of JAKs, (iii) G-protein mediated JAK activation, and (iv) non-receptor tyrosine kinases such as Src and Abl (Bromberg, 2001; Levy & Lee, 2002; Xiong *et al.* 2014).

Phosphorylation of STAT3 can also occur at serine 727 (S727). Both the function of this phosphorylation and the identity of the underlying serine kinase are controversially discussed (Xiong *et al.* 2014; Levy & Lee, 2002).

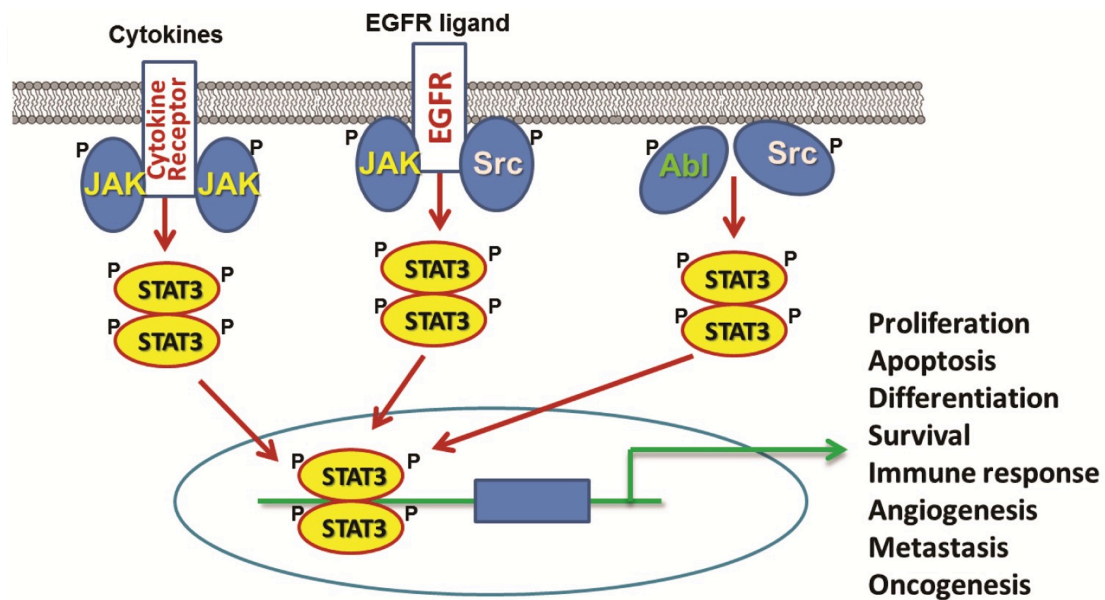


Figure 3-9: Simplified illustration of STAT3 signalling, adapted from Xiong *et al.* (2014)

3.3.2. Physiological function of STAT3

Miscellaneous functions of STAT3 orchestrate a wide variety of physiological processes, even seemingly contradictory ones, features of which have emerged in the last decades, and are constantly expanded (Levy & Lee, 2002; Xiong *et al.* 2014). The first indication of STAT3 importance was provided by loss of function experiments, which led to early embryonic lethality in mice as well as death of embryonic stem cells (reviewed by Levy & Lee, 2002).

The importance of STAT3 relates to transcriptional regulation of multiple key genes and modulation of signalling pathways. Among others, those that are involved in (i) proliferation, (ii) differentiation – including development and tissue repair processes, (iii) apoptosis, (iv) angiogenesis, (v) migration, (vi) immune response, (vii) survival, and (viii) maintenance of pluripotency (Hirano *et al.* 2000; Levy & Lee, 2002; Xiong *et al.* 2014). Due to its fundamental role, STAT3 is normally tightly regulated by suppressor of cytokine signalling (SOCS) family members which inhibit STAT3 on the transcriptional level. Additionally, protein inhibitor of activated STAT (PIAS) inhibits STAT3 via direct interaction (Xiong *et al.* 2014).

The question of how a universally expressed transcription factor can essentially regulate such diverse processes remains to be determined. Although, it seems likely that induction of distinct gene programs dependent on cell type and status, an even more important role may be played by microenvironmental cues.

3.3.3. Role in oncogenesis

The multifaceted regulatory processes controlled by STAT3, almost necessarily imply its contribution to tumourigenesis. Indeed, importance of STAT3 has been confirmed in tumour cells *in vivo* and *in vitro*. Persistent activation of STAT3 has been detected in many cancers (Bromberg, 2002), including gliomas, and is correlated with poor survival (Yu *et al.* 2014). STAT3 is often constitutively active in tumour derived cancer cell lines, which frequently become dependent on STAT3 activation to maintain their transformed phenotype (Bromberg, 2002). Thus, cells undergo growth arrest or apoptosis upon STAT3 inhibition. In contrast, molecular engineered constitutively active STAT3 can be sufficient to transform normal cells into tumourigenic ones. Bromberg *et al.* (1999) achieved spontaneous dimerization of STAT3 via C-terminal modification which led to cellular transformation and tumour formation. Therefore, STAT3 inhibition seems to be a promising candidate to reduce tumourigenesis, although, no naturally occurring mutations of STAT3 have been reported so far (Calò *et al.* 2003). Indeed, aberrant STAT3 signalling is rather the result of mutation in other members of the signalling pathway. However, STAT3 offers an ideal anticancer target, because of its central role in the aberrant signalling.

Overall, dysfunctional STAT3 signalling can promote tumourigenesis by aberrant expression of downstream genes involved in control of (i) proliferation, (ii) apoptosis, (iii) angiogenesis, (iv) metastasis, (v) immune surveillance, (vi) malignant transformation, and most importantly (vii) maintenance of CSCs. As a short overview, some relevant involved genes encode (i) Bcl2, Bcl-XL, and c-myc, that promote proliferation and survival while inhibiting apoptosis, (ii) VEGF, MMP, and FGF, which promote angiogenesis; (iii) NF- κ B and IL 6/JAK, involved in immune-surveillance; and (iv) Oct3/4, Nanog, and IL 6/JAK/STAT3, which maintain CSCs (for review see Xiong *et al.* 2014).

The most important targets to inhibit STAT3 functionality are (i) modification of the SH2 domain to prevent dimerization and/or phosphorylation, (ii) modification of the DNA binding domain to inhibit transcriptional activity, (iii) inhibition of nuclear shuttling and,

(iv) inhibition of upstream STAT3 activators such as JAK. Although, many STAT3 inhibitors were identified and proved to be effective *in vitro* and *in vivo*, none has successfully been clinically approved to date (Xiong *et al.* 2014).

3.3.3.1. Role of STAT3 in GBM

A series of elegant studies has convincingly demonstrated an important role of STAT3 in gliomas. As reviewed by Spitzner, Ebner *et al.* (2014), amplified expression of IL 6 accompanied by increased STAT3 activity in GBM specimen and cell lines implicated involvement of STAT3 in gliomas. This was confirmed by correlation of strong expression of phosphorylated STAT3 at Y705 in GBM specimen with decreased patient survival and a more aggressive subtype. In contrast to persistent activation of STAT3, malfunction of STAT3 inhibition was reported, by Brantley *et al.* (2008). STAT3 activation was assessed by Y705 and S727 phosphorylation, which was elevated in GBM compared to control tissue. In contrast, expression of PIAS3 was present in control tissue while significantly reduced in GBM samples. Contribution of PIAS loss to GBM was further sustained since inhibition enhanced GBM cell proliferation while overexpression led to decreased proliferation and transcriptional activity of STAT3 (Brantley *et al.* 2008). This is in contrast to high expression of the endogenous STAT3 inhibitor SOCS3 in primary GBM, which is a direct transcriptional target of STAT3, and might be reasonable considering SOCS3 expression was positively correlated with radioresistance in a GBM cell line (reviewed in Spitzner, Ebner, *et al.* 2014).

Evidence has emerged that STAT3 is further required by BTICs to maintain their stem-like characteristics. RNA interference of STAT3 sufficiently led to growth arrest, inhibited neurosphere-formation and could induce apoptosis of BTICs (Sherry *et al.* 2009). In addition, as pointed out above, STAT3 works in conjunction with C/EBP β to transform normal neural stem cells along the mesenchymal lineage causing loss of neuronal differentiation and manifestation of a fibroblast-like morphology (Carro *et al.* 2010). In accordance with these findings, STAT3 inhibition significantly reduced cell migration out of GBM-derived neurospheres, although topographical cues that affect cell adhesion and gene expression seem to be involved as well (Agudelo-Garcia & Jesus, 2011).

The seemingly important contribution of STAT3 to maintenance of BTICs and infiltration in gliomas, provides a rationale for therapeutic interventions in high-grade gliomas targeting STAT3.

3.3.4. STAT3 and NSAIDs

As indicated above, STAT3 is also involved in immune surveillance. The persistent activation of STAT3 can mediate tumour-promoting inflammation. Briefly, as reviewed by Yu *et al.* (2009), prostaglandins and cyclooxygenase 2 (COX), which is required for the production of prostaglandins, are important to induce and maintain a tumour-promoting inflammatory environment. In turn, STAT3 can participate in their expression regulation.

Traditional non-steroidal anti-inflammatory drugs (NSAIDs) are non-selective COX1 and 2 inhibitors. Those include aspirin, ibuprofen (Warner *et al.* 1999), and diclofenac, although diclofenac preferentially inhibits COX2 (Giuliano & Warner, 1999). Notably, NSAIDs have been associated with anti-tumourigenic effects in different tumour entities (Sørensen *et al.* 2003; Ulrich *et al.* 2006) such as breast (Harris *et al.* 2006) or prostate cancer (Andrews *et al.* 2002), and have been associated with growth delay of established tumours (Farrell *et al.* 1988; Johnsen *et al.* 2004). A key mechanism for NSAID efficacy is inhibition of COX inhibition which results in reduced production of prostaglandins. While COX1 is constitutively expressed in most tissues and relevant for homeostatic function of prostaglandins, COX2 is inducible and participates in many inflammatory and proliferative reactions (reviewed by Ulrich *et al.* 2006). Of note, prostaglandin E2 is inducible by COX1 and 2 (Ulrich *et al.* 2006) and was associated with tumour cell promotion (Marx, 2001).

Previous studies revealed that diclofenac inhibited STAT3 phosphorylation and lactate formation, induced cell cycle arrest at G2/M, and delayed tumour growth in an *in vivo* animal model (Chirasani *et al.* 2013). Moreover, diclofenac treatment of human and murine GBM cell lines caused c-myc inhibition followed by decreased gene expression of glucose transporter 1, as well as decreased lactate dehydrogenase A (LDH-A), and lactate secretion (Gottfried *et al.* 2013). This raises the question whether GBM patients might benefit from adjuvant NSAID treatment, a question which requires a detailed understanding of the yet undefined underlying mechanisms.

3.4. Aims of this work

This doctoral thesis research project emerged from the ‘Bundesministerium für Bildung und Forschung’ (BMBF)-funded *National Genome Research Network (NGFN^{plus}) Brain Tumour Network (BTN^{plus})*, which aimed to elucidate the cellular, genetic, and molecular mechanisms of the pathogenesis of GBM.

The propagation of malignant glioblastoma cells and their invasion into the healthy brain is a primary cause of tumour recurrence and associated morbidity. Identification of factors related to invasion of BTICs into the surrounding brain tissue from the initial tumour site – the transition from stationary into invading cells – was the aim of this doctoral research project. Here, the unknown characteristics of primary BTICs and their differentiated pairs were analysed with regard to their motility, proliferation, sensitivity to inhibitors, and marker transcription factor expression.

Invasion is an early event in glioblastoma progression (Louis, 2006), although glioblastomas are often not diagnosed at this stage. Screens based on conventional migration assays are highly artificial *in vitro* systems (Valster *et al.* 2005) and are limited, as they do not accurately reproduce native cell motility. *In vivo* screening systems such as nude mouse models using BTICs (Beier, Wischhusen, *et al.* 2008), or spontaneous mouse models (Shelton *et al.* 2010), may produce desired invasive growth patterns, however, exhibit periods of long latency, technical complexity, variable or low reproducibility, and the time-consuming evaluation of invasion at the end of such assays may prevent adequate online-monitoring of invasion.

Therefore, an OBSC model, mimicking the brain structure and microenvironment of the *in vivo* situation was established in the first phase of this project. Insights on invasive behaviour of tumour cells acquired in these investigations were compared to *in vitro* migration data obtained in the second project phase.

The study of Carro *et al.* (2010) published in *Nature* revealed two transcription factors, C/EBP β and STAT3, as synergistic initiators and master regulators of EMT, driving cells to the aberrant mesenchymal lineage. STAT3, a ubiquitous transcription factor, has previously been known as a central regulator of tumour progression and metastasis in cancer (Spitzner, Roesler, *et al.* 2014; Xiong *et al.* 2014).

Based on these insights, the section of this thesis work focused on STAT3 expression analysis as well as analysis of basal migration and proliferation rates of BTICs and GBM cell lines in the newly established *in vitro* assays developed in the first phase of this project. Proliferation rates were determined in order to address their correlation to those observed in migration assays. Since preceding work (Chirasani *et al.* 2013) revealed a decrease of STAT3 phosphorylation after diclofenac treatment, the NSAIDs ibuprofen and diclofenac were used as model substances for inhibition of migration and STAT3 regulation. As both agents inhibit STAT3 non-specifically, the effects of direct STAT3 knockdown were monitored by use of Stattic, a specific STAT3 inhibitor, and then verified in the more adequate OBSC model.

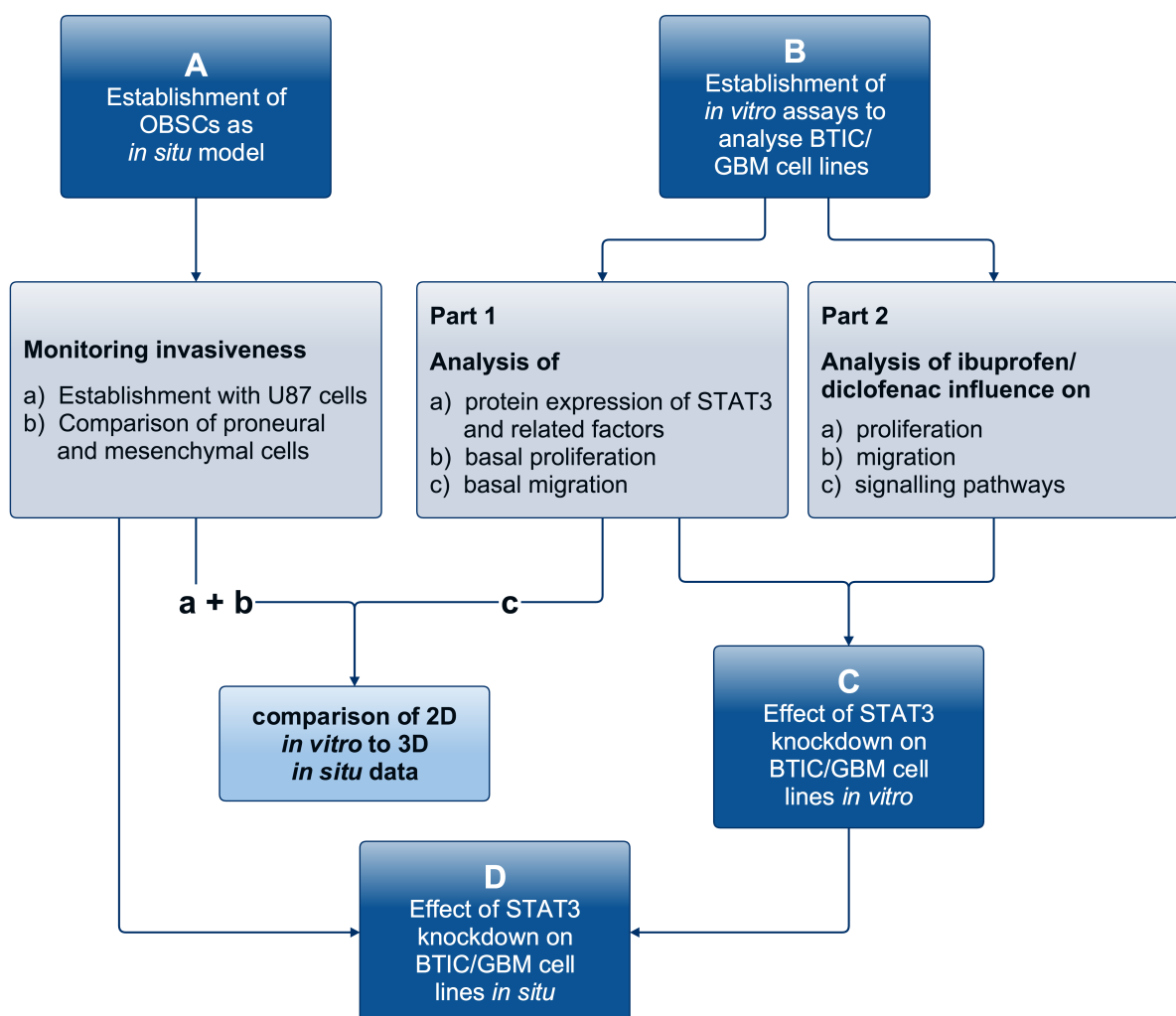


Figure 3-10: Work packages of the present PhD project

4. Results

To address the mechanisms underlying GBM cell invasion, an OBSC model was established during the first phase of this project and classic 2D assays were performed. The *in situ* model enabled live monitoring of invasion and direct access to implanted cells. Comparing the observations of OBSCs and 2D assays, separation of the initial cell population into three distinct subgroups – leader, follower, and stationary cells – could only be observed in the OBSC model. Most likely, these fractions only develop in the presence of microenvironmental influences, which are not present in the utilised 2D *in vitro* models. Consequently, the focus shifted from observing and comparing different patterns of invasion for BTICs and differentiated tumour cells (TC) to identifying responsible factors for the induction of the invasive subgroups. As formation of leader cells was proposed to be necessary for infiltration, inhibition of their development would be a major step towards glioma localisation. In order to characterise leader cells a micromanipulator tool was developed, to accurately dissect fragments containing cells of each subgroup. Combined with single cell analysis techniques – cDNA library generation and microarray analysis (Hartmann & Klein, 2006) – this permitted identification of a transcription factor signature specific to invasive cells. If these factors are indeed responsible for invasive behaviour of brain tumour cells, they may be targets for therapeutic agents, which can inhibit their expression and suppress the invasive tumourigenic phenotype. STAT3, for example, is one of the up-regulated transcription factors in leader cells and is known to promote oncogenesis when

constitutively active (Bromberg *et al.* 1999). Thus, it is likely that the observed expression of STAT3 is related to invasive behaviour.

In parallel, the second part of this project focussed on the expression and inhibition of the transcription factor STAT3. First, protein expression was analysed to identify unique patterns in different cell population subgroups of primary BTICs, as well as GBM cell lines. The analysed transcription factors are expressed in glioma cells during propagation and participate in signalling pathways that maintain their neoplastic nature. Specifically, STAT3 and C/EBP β , which function as initiators and master regulators of mesenchymal transformation, were chosen (Carro *et al.* 2010). Subsequently, analysis and correlation of proliferation and migration allowed for clustering of the cells into separate subgroups.

Non-steroidal anti-inflammatory drugs (NSAID) are known to possess anti-tumourogenic effects. Previous studies revealed that one of their effects is reduction of proliferation, resulting in containment of glioma cells (Chirasani *et al.* 2013; Gottfried *et al.* 2013). In the present study, proliferation and migration were decreased upon ibuprofen or diclofenac treatment (Leidgens *et al.* 2015). Reduced STAT3 phosphorylation caused by diclofenac was observed in accordance with previous studies (Chirasani *et al.* 2013). A similar effect was also detected with ibuprofen, suggesting a regulatory role of STAT3 in glioma cell migration and proliferation. With regard to possible adverse reactions of long-term high-dosage NSAID treatment, a more specific inhibition of STAT3 was desired. Therefore, specific inhibitor treatment by Stattic was investigated. Without exception, all tested cells were sensitive to the inhibitory effects of Stattic on migration and proliferation. However, each cell subgroup required different concentrations of Stattic.

In addition to the identification of STAT3 as part of the leader cell signature, the inhibitory effects observed with Stattic *in vitro*, led to verification of its inhibitory effect on cell motility in the OBSC model. Indeed, STAT3 inhibition led to a strong reduction in GBM cell propagation in the OBSC model.

4.1. Monitoring invasiveness of glioma cells *in situ*

4.1.1. Brain slice cultures as an adequate model to monitor migration and invasion

4.1.1.1. Glioma cell line U87

Organotypic brain slice cultures (OBSC) are a valuable tool to analyse migration as well as invasion in conditions simulating normal brain tissue, with features including ECM components and microenvironmental influences. To monitor migration and invasion of living glioma cells, the *in situ* OBSC model was established along published protocols for slice cultures (Eyüpoglu *et al.* 2005; Gähwiler *et al.* 1997; Gogolla *et al.* 2006) and adapted for this study. OBSCs at 350 μm thickness were derived from rats at postnatal day 8 to 12, see paragraph 7.2.2.

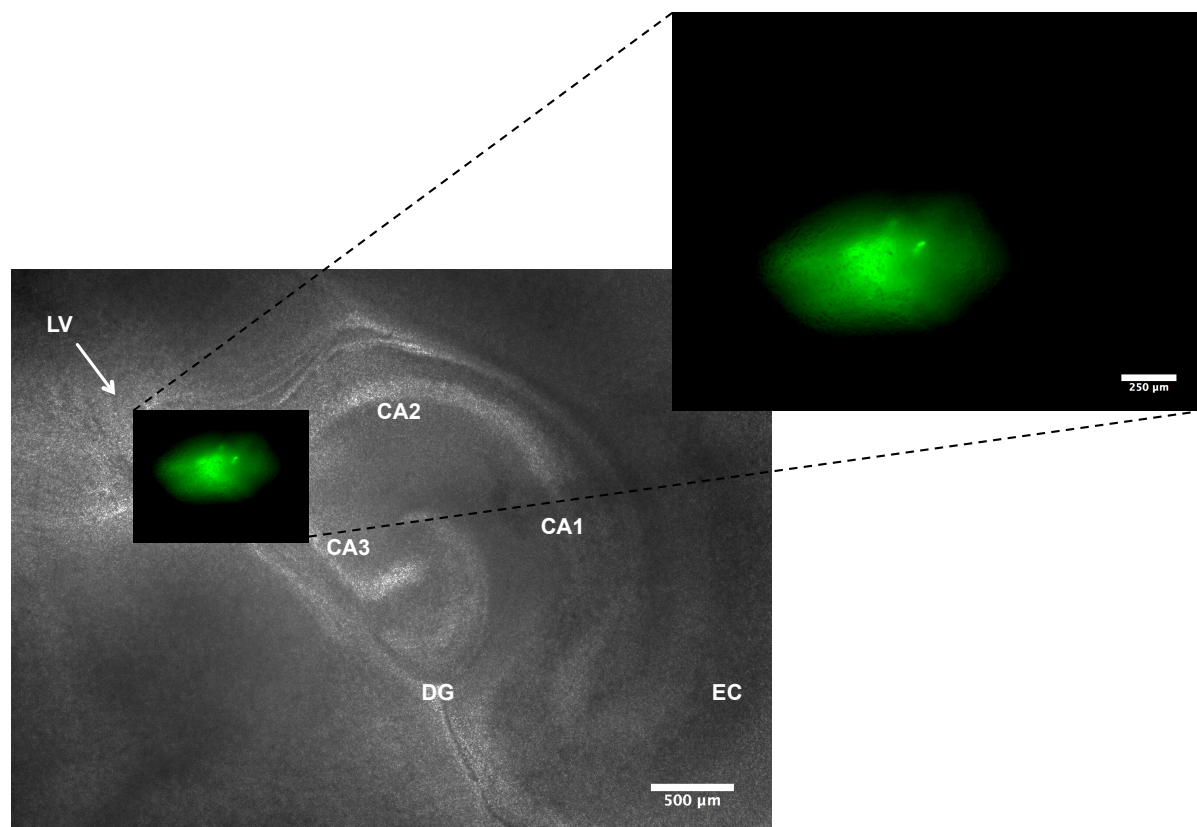


Figure 4-1: Implantation of U87-GFP cells on an organotypic brain slice

OBSCs were derived from new-born rats (P8). U87-GFP cells were implanted adjacent to the lateral ventricle one day after OBSC preparation. The bright field picture of the OBSC shows the hippocampal formation and the implantation site. The close-up view depicts the initial cell spot directly after implantation.

EC = entorhinal cortex, CA = *cornu ammonis*, DG = dentate gyrus, LV = lateral ventricle

In order to monitor invasive behaviour of glioma cells, cells were infected with a lentiviral vector to induce stable expression of a fluorescent protein. Invasion of glioma cells was induced by inoculation of fluorescence tagged cells in the hippocampal region of OBSCs (Figure 4-1). Unlike common animal models, this allowed live microscopic monitoring of tumour cell invasion in real time for up to 3 weeks (Figure 4-2) and gave direct access to the implanted cells.

An axial cutting of the brain into OBSCs led to reproducible results. Comparison of several implantation sites - lateral ventricle, hippocampus, and spots in the cortex region - revealed the lateral ventricle as the most suitable starting point from which cells invaded in distinct directions.

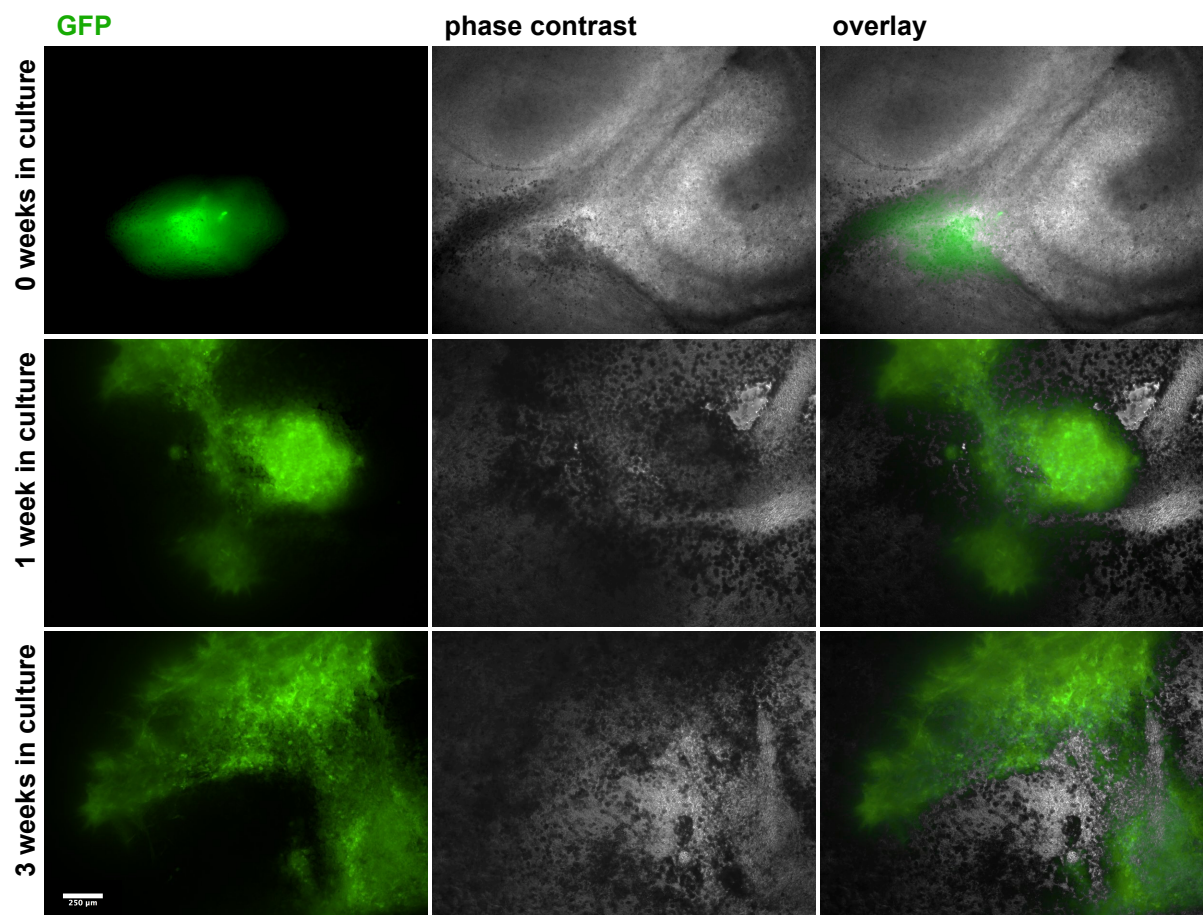


Figure 4-2: Periodic monitoring of U87-GFP invasiveness in OBSCs

Periodic monitoring of OBSC, corresponding to Figure 4-1. Fluorescence and phase contrast pictures display U87-GFP migration directly after implantation (upper panel), after one week (middle panel), and after 3 weeks (lower panel) in culture. Within 7 days, migration towards the CA2 region (middle panel) occurred. Scale bar = 250 μm .

During the culture period, invasive cells emerged from the initial cell population implanted adjacent to the lateral ventricle. Those cells drove invasion into the surrounding tissue and were able to cover long distances. Image analysis software was used to merge single recordings into one overall picture that depicts the entire area infiltrated by fluorescent tumour cells, allowing the area covered as well as the distance to be measured. For example, U87-GFP cells, as depicted in Figure 4-3, managed to travel a maximum distance of about 1950 μm , at approximately $100 \mu\text{m day}^{-1}$. Serial implantations were performed to average area expansion and maximum distances covered by the cells during the monitoring period (Figure 4-4). Measurements were performed on the first, 7th and 14th day *in vitro* (div). At later time points picture sizes were too large. On average, the area covered by U87-GFP cells increased 18-fold, 2 weeks after implantation, with a maximum distance of about 1917 μm travelled. This led to an estimated invasion rate of about $136.93 \mu\text{m day}^{-1}$, exceeding the rate estimated from the previous single measurement (Figure 4-3).

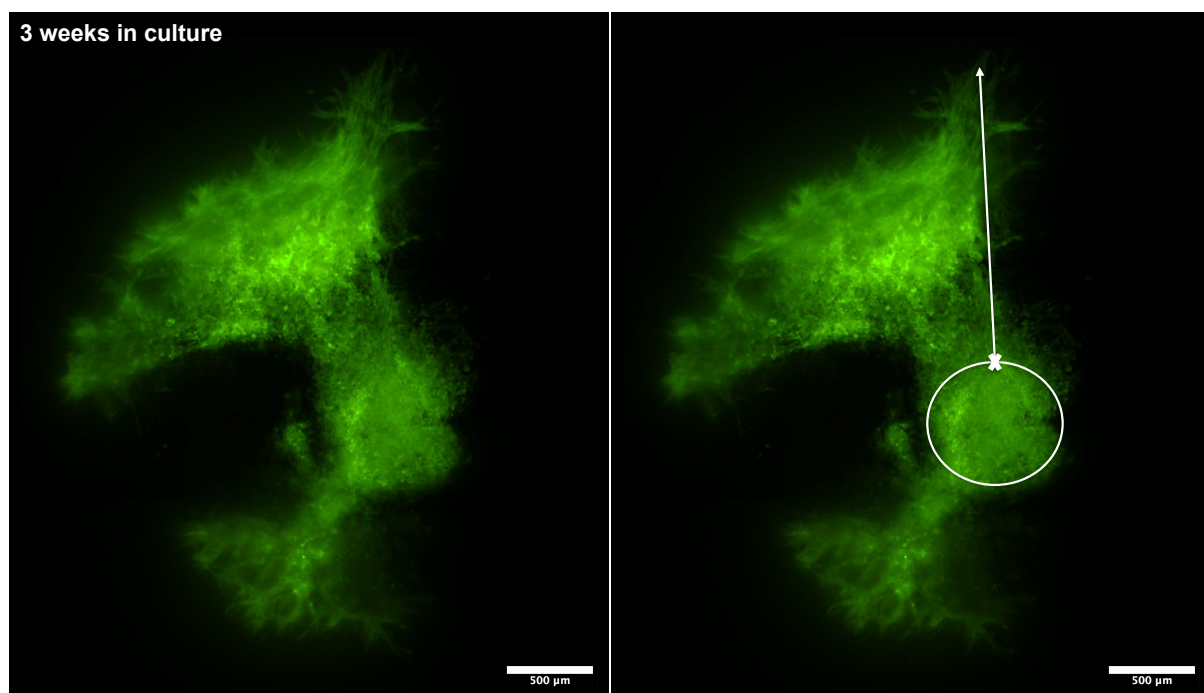


Figure 4-3: Composite image of U87-GFP invasiveness after 3 weeks in OBSC

Composite image corresponding to Figure 4-2 (lower panel). As shown in the merged pictures on the left, U87-GFP cells migrated in distinct directions originating from the initial implantation site at the lateral ventricle. On the right, the initial site is marked together with the maximum distance covered by U87-GFP cells within the 3 weeks in culture. The cells covered a distance of $\sim 1.950 \mu\text{m}$ from the initial edge to the tip of the invasive rim. Scale bars = 500 μm .

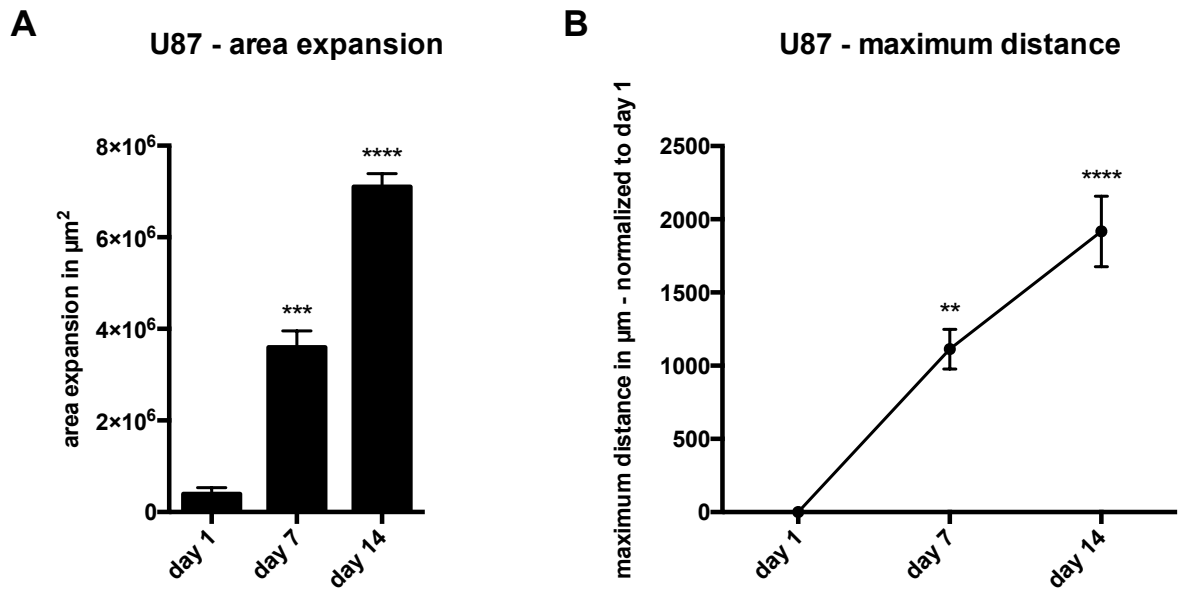


Figure 4-4: Evaluation of serial implantation of U87-GFP cells in OBSC

(A) Area expansion from implantation (day 1) increased ~9-fold after 7 days and ~18-fold after 14 days in culture. Values represent mean \pm SD. (B) Maximum distance covered by U87-GFP cells increased significantly. 1113 μm (SEM: \pm 234 μm) was the maximum distance after 7 days, which increased to 1917 μm (SEM: \pm 415 μm) after 14 days. The maximum distance was calculated by subtraction of the initial size at implantation. Values represent mean \pm SEM. All experiments were performed in triplicates; 1way ANOVA analysis with Dunnett's multiple comparisons test, **: $p \leq 0.01$, ***: $p \leq 0.001$, ****: $p \leq 0.0001$

4.1.1.2. Primary human glioma cells

After the system had been optimised by the investigation of the invasion of U87 cells, it was subsequently used to analyse primary human BTIC cultures. BTICs were derived from tumour tissue (Moeckel *et al.* 2014) and classified according to the Verhaak classification, which describes four genetically distinct GBM subgroups – proneural, neural, classical and mesenchymal (Verhaak *et al.* 2010). BTICs used in this work belonged to the proneural or mesenchymal subtype, which are the most frequent (Lin *et al.* 2014). The mesenchymal subtype is associated with higher aggressiveness (Carro *et al.* 2010), but tumours demonstrate response to a combination of aggressive chemo- and radiotherapy (Van Meir *et al.* 2010). In contrast, survival is slightly higher in patients with proneural GBM, although these tumours are the least responsive to aggressive classical therapies (Van Meir *et al.* 2010).

Generally, the mesenchymal BTIC lines RAV21, 26, and 27 revealed an invasive pattern similar to that of U87 cells (Figure 4-5 and Figure 4-6). RAV26 and 27 showed a strong invasive behaviour, whereas RAV21 was significantly less invasive within the first 2 weeks in the OBSCs compared to RAV27. However, increase of time in culture revealed a strong invasive potential of RAV21 after 3 weeks as depicted in Figure 4-6. During this time, a high proportion of elongated, spindle-shaped cells indicative of cell movement emerged similar to RAV26 and 27 cells (Figure 4-5).

Differentiation of mesenchymal BTICs into TCs (paragraph 7.2.1.1.1) caused significantly reduced invasive capacities of RAV21 and RAV27 TCs (Figure 4-7). RAV26, on the contrary, only revealed a tendency towards decreased infiltration after differentiation.

In contrast, proneural BTIC were not invasive (Figure 4-8 and Figure 4-9) and differentiation into TCs did not alter their invasive capacities (Figure 4-9). Small increases of the area and distance covered may have been the result of cell proliferation, since spindle-shaped cells indicative of movement were missing. However, at the rim of the initial spheroid of RAV57 BTIC, some spindle-shaped cells were detected after longer culture periods as can be seen in Figure 4-7 (lower panel).

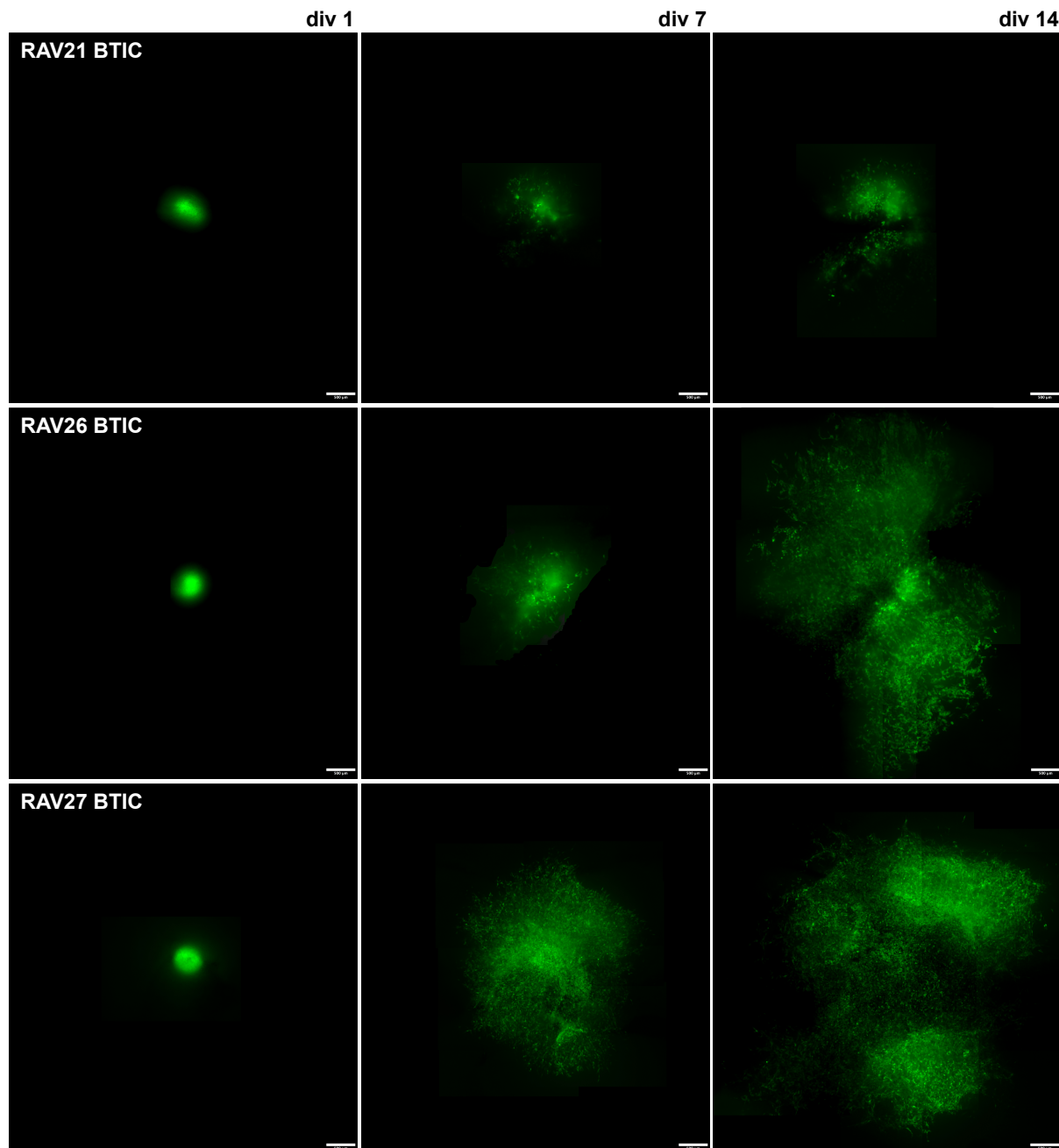


Figure 4-5: Periodic monitoring of mesenchymal BTICs RAV21, 26 and 27 in OBSCs

Invasive behaviour of each mesenchymal BTIC line in OBSCs revealed invasive behaviour by periodic monitoring after 1, 7, and 14 days *in vitro* (div). RAV26 (middle panel) and RAV27 (lower panel) were strongly invasive with a high proportion of spindle-shaped cells, indicative of moving cells. In contrast, RAV21 (upper panel) revealed a less distinctive invasion pattern after 14 days of culture in OBSCs. Scale bars = 500 μ m

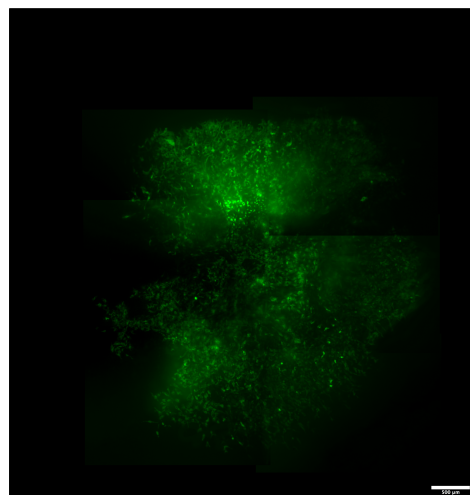


Figure 4-6: Invasion pattern of RAV21 in OBSCs after 3 weeks in culture

Corresponding to Figure 4-5 (upper panel) composite image of RAV21 invasion into brain slice tissue after 3 weeks in culture. Delayed RAV21 displayed similar invasive pattern to RAV26 and RAV27. Scale bar = 500 μm

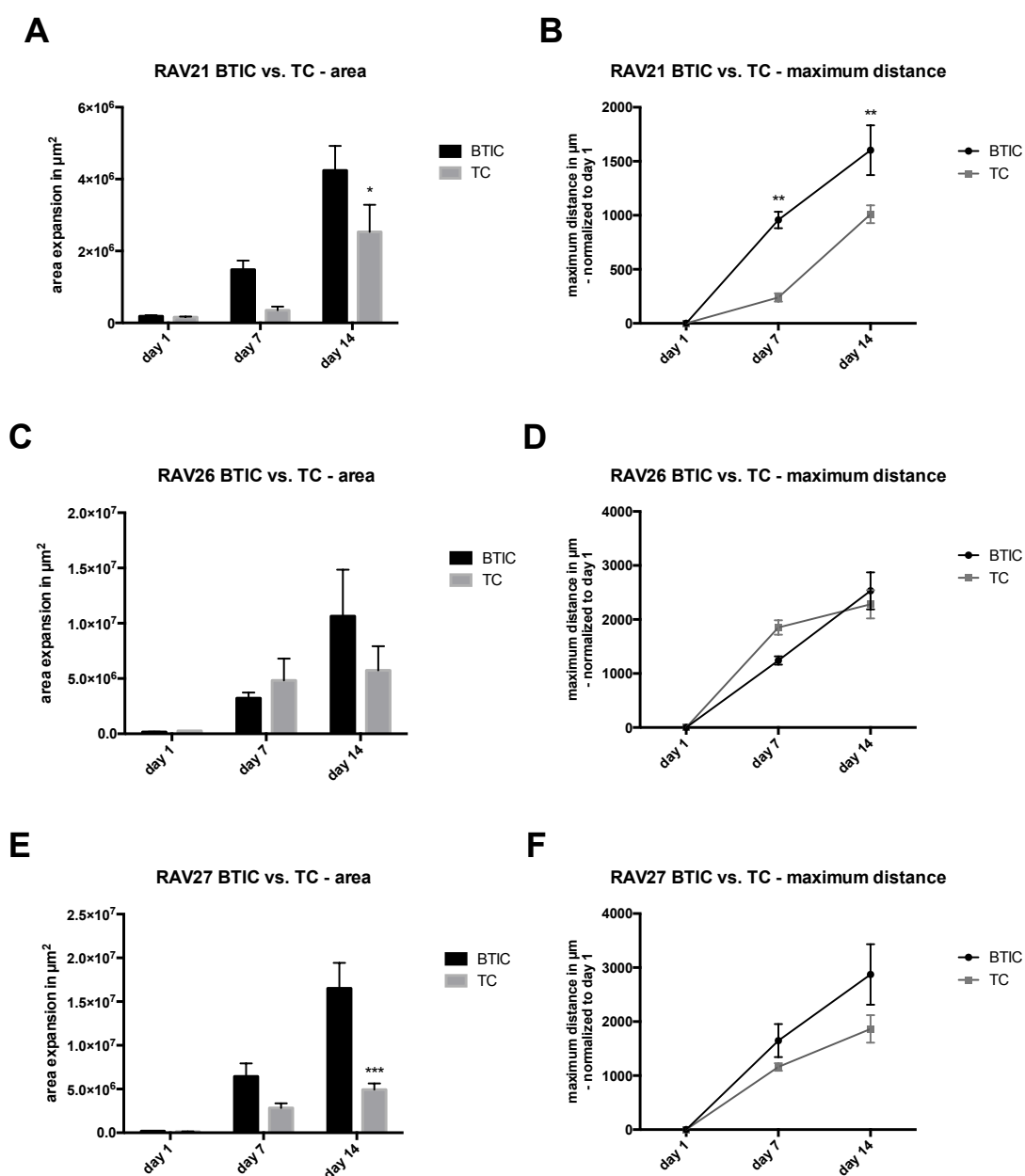


Figure 4-7: Area expansion and maximum distance covered by mesenchymal BTICs and TCs in OBSCs

(A, C, E) Area expansion is depicted from the initial spheroid implanted in OBSCs at day 1 until day 14 in culture. Values represent mean \pm SD. (B, D, F) The maximum distance (in μm) represents the distance covered from the initial spheroid rim to the outer edge of the invasive rim. Values represent mean \pm SEM. (A) The area covered by RAV21 BTICs increased ~ 23 -fold from implantation (day 1) to 14 days in culture. The increase was significantly higher compared to RAV21 TCs at 14 days with an area increase of ~ 16 -fold. (B) The maximum distance covered after 14 days in culture was significantly larger for RAV21 BTICs than TCs (BTICs: 1602.27 ± 230.14 , TCs: 1009.93 ± 82.51). (C) RAV26 BTIC and TC revealed a higher invasion potential than RAV21. The covered area by RAV26 BTICs increased ~ 64 -fold and ~ 21 -fold with TCs. (D) The maximum distance covered did not significantly differ between RAV26 BTICs (2530.24 ± 342.71) and TCs (2281.56 ± 262.65). (E) For RAV27 BTICs, increased invasion was observed compared to RAV21 and RAV26 as the area increased by ~ 88 -fold. Area expansion was significantly decreased in RAV27 TCs with an increase of only ~ 36 -fold. (F) However, the maximum distance covered did not significantly differ between RAV27 BTICs (2872.65 ± 561.04) and TCs (1864.93 ± 254.43). All experiments were performed in triplicates; 2way ANOVA analysis with Sidak's multiple comparisons test, ns: > 0.05 , *: $p \leq 0.05$, **: $p \leq 0.01$, ***: $p \leq 0.001$.

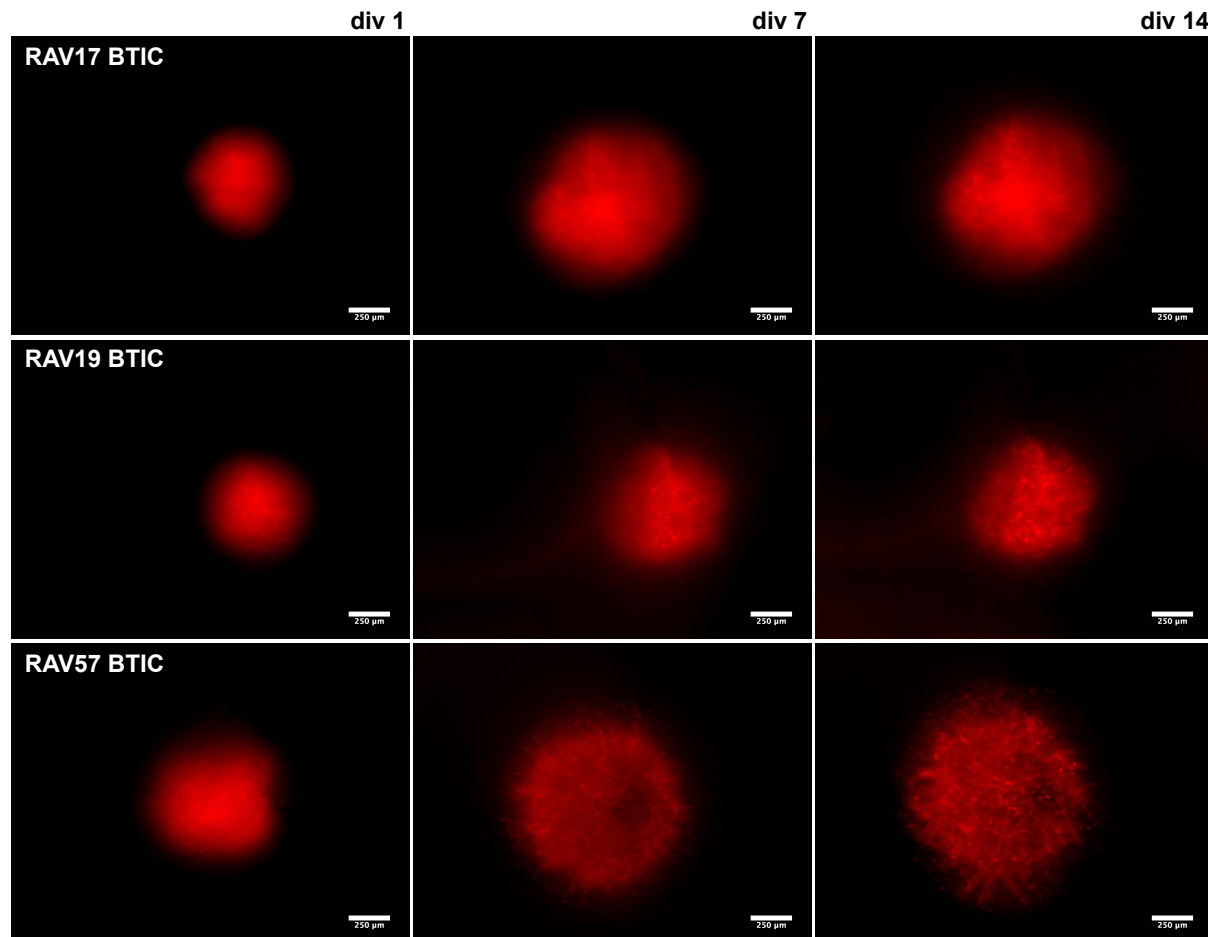


Figure 4-8: Periodic monitoring of proneural BTICs RAV17, RAV19, and RAV57 in OBSCs

Invasive behaviour of each proneural BTIC line in OBSCs was analysed by periodic monitoring after 1, 7, and 14 days *in vitro* (div). RAV17 (upper panel) and RAV19 (middle panel) did not invade the OBSC tissue. In contrast, from the initial spheroid of RAV57 (lower panel) some spindle-shaped cells, indicating the onset of invasion, emerged during the culture period. Scale bars = 500 μm

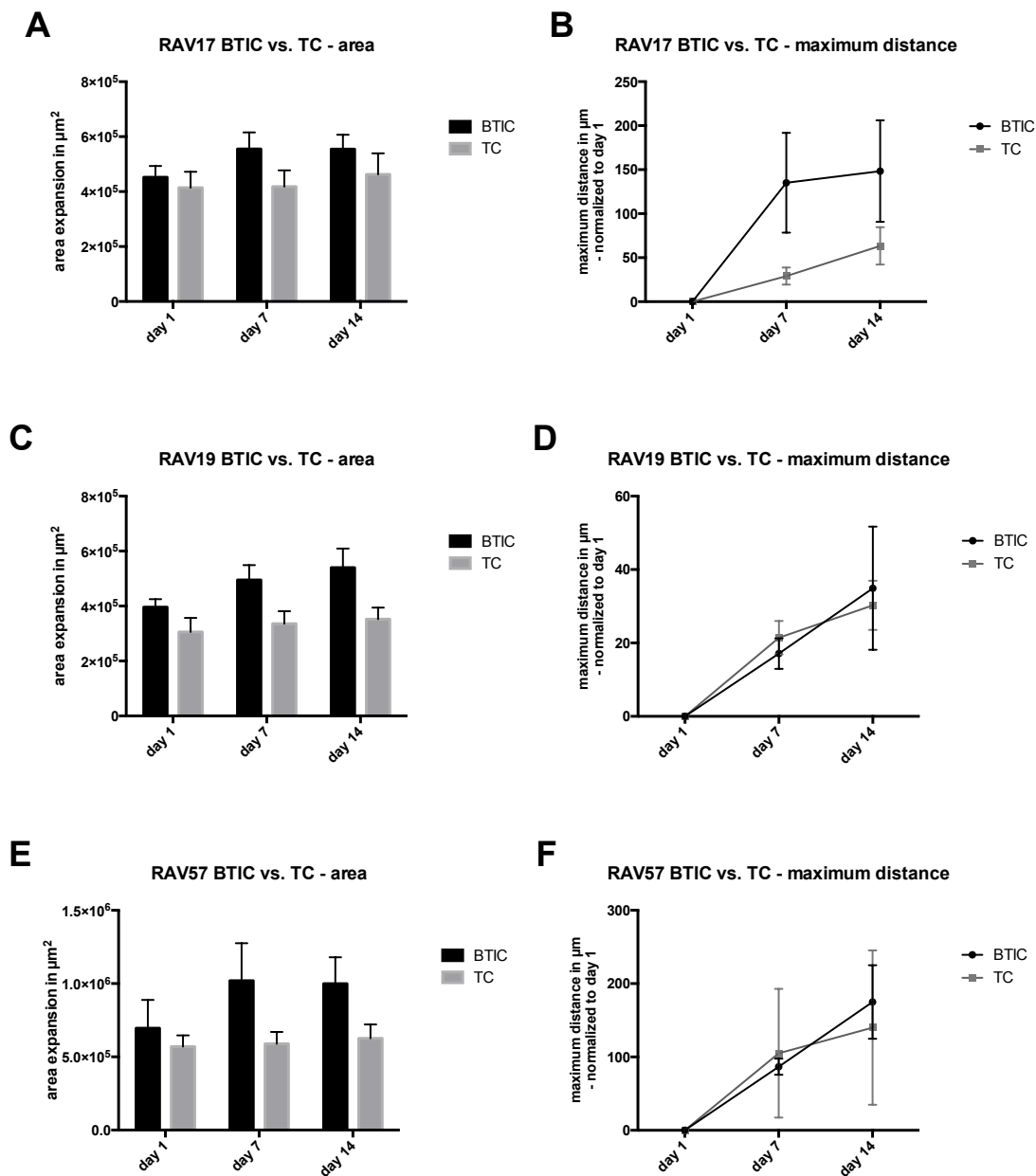


Figure 4-9: Area expansion and maximum distance covered by proneural BTICs and TCs in slice cultures

(A, C, E) Area expansion is depicted from the initial spheroid implanted in OBSCs at day 1 until day 14 in culture. Values represent mean \pm SD. (B, D, F) The maximum distance (in μm) represents the distance covered from the initial spheroid rim to the outer edge of the invasive rim. Values represent mean \pm SEM. (A) The area covered by RAV17 BTICs increased by ~ 1.23 -fold from implantation (day 1) to 14 days in culture. The increase was slightly higher than in RAV17 TCs (~ 1.12 -fold). (B) The maximum distance covered after 14 days in culture was larger for RAV17 BTICs than TCs (BTICs: 148.36 ± 57.72 , TCs: 63.42 ± 21.16). (C) RAV19 BTIC and TC were similar to RAV17. The covered area by RAV19 BTICs increased by ~ 1.36 -fold and by ~ 1.15 -fold with TCs. (D) The maximum distance covered was alike for RAV19 BTICs (34.92 ± 16.77) and TCs (30.26 ± 6.70). (E). The area covered by RAV57 BTICs increased slightly, ~ 1.44 -fold, and a smaller increase of ~ 1.10 -fold was detected in RAV57 TCs. (F) The maximum distance covered did not significantly differ between RAV57 BTICs (174.99 ± 50.13) and TCs (140.05 ± 105.24). All experiments were performed in triplicates.

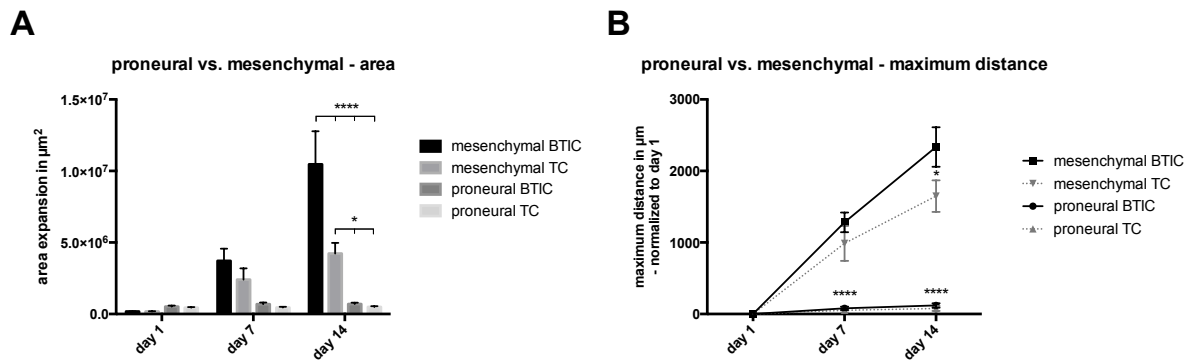


Figure 4-10: Average area expansion and maximum distance covered by proneural and mesenchymal glioma cells in slice cultures

(A) Area expansion is depicted from the initial spheroid implanted in OBSCs at day 1 until day 14 in culture. Values represent mean \pm SD. (A) Proneural BTICs and TCs revealed a significantly decreased invasive capacity compared to mesenchymal BTICs and TCs. Additionally, mesenchymal BTICs covered significantly more of the OBSC tissue than their differentiated pairs. (B) The maximum distance (in μm) represents the span covered from the initial spheroid rim to the outer edge of the invasive rim. Values represent mean \pm SEM. The difference of maximum distance coverage did not differ significantly among proneural BTICs and TCs. In contrast, mesenchymal BTICs and TCs moved significantly longer distances than proneural lines. In addition, mesenchymal BTICs covered significantly longer distances than their differentiated counterparts. All experiments were performed in triplicates; 2way ANOVA analysis with Sidak's multiple comparisons test, ns: $p > 0.05$, *: $p \leq 0.05$, ****: $p \leq 0.0001$

The OBSC model revealed significant differences among proneural and mesenchymal cells, the results of these investigations are summarised in Figure 4-10 and Table 4-1. Average invasion rates of U87 cells and BTICs RAV17, 19, 21, 26, 27, 57, and their differentiated counter parts were determined by use of the OBSC model. Rates were calculated by measuring the maximum distance covered by the cells after 7 and 14 days both *in vitro* and in OBSCs, the values obtained were normalised by subtraction of initial spheroid sizes at the day of implantation. Cells of each subtype cluster within the same range of invasion rates, as visualised in Table 4-1. It was clearly visible that proneural BTIC moved significantly less in the OBSC tissue than mesenchymal cells. Both the area of expansion (Figure 4-10A) as well as maximum covered distance were significantly different for these two groups (Figure 4-10B). The differentiated counterparts covered similar distances (Table 4-1), except for RAV21. Upon differentiation, TC area increase and invasion was significantly reduced compared to BTICs (Table 4-1, Figure 4-7A, B). This was the main cause of the significant decrease of overall area expansion and maximal distance coverage (Figure 4-7). Average invasion rates of U87 cells corresponded to mesenchymal BTIC and TC rates.

Category	Invasion day ⁻¹ in μm	Range ($\pm\text{SD}$)
GBM lines		
U87	147.99	117.21 – 178.77
BTIC		
RAV17	14.95	3.92 – 25.98
RAV19	2.47	1.00 – 3.93
RAV57	12.45	8.16 – 16.74
average proneural BTIC	9.96	1.43 – 18.48
RAV21	125.56	100.76 – 150.37
RAV26	179.0	149.57 – 208.42
RAV27	220.30	153.27 – 287.32
average mesenchymal BTIC	174.95	117.08 – 232.82
TC		
RAV17	4.34	2.09 – 6.60
RAV19	2.61	1.60 – 3.62
RAV57	12.51	0.0 – 28.75
average proneural TC	6.49	0.0 – 16.44
RAV21	53.16	30.58 – 75.74
RAV26	213.75	151.78 – 276.32
RAV27	149.48	120.60 – 178.35
average mesenchymal TC	121.82	42.76 – 200.87

Table 4-1: Overview of average invasion day⁻¹ of U87, primary BTICs, and TCs in the OBSC model

4.1.2. Simultaneous implantation of proneural and mesenchymal BTICs

GBMs are characterised by intratumoural heterogeneity (Sottoriva *et al.* 2013) and glioblastoma cells have the ability to transdifferentiate from an epithelial-like to a more mesenchymal state (EMT) (Tso *et al.* 2006; Zarkoob *et al.* 2013). By transforming, cells become invasive (Carro *et al.* 2010). To simulate intratumoural heterogeneity, proneural (RAV57) and mesenchymal (RAV26 or RAV27) BTICs were implanted in OBSCs simultaneously (Figure 4-11 and Figure 4-12). Here, 2,500 cells of each mesenchymal

(green fluorescence) and proneural cells (red fluorescence) were mixed and inoculated to cause spheroid formation (see paragraph 7.2.1.5.1) two days prior to implantation in OBSCs. This experimental model resembled intratumoural heterogeneity with proneural cells remaining and at the implantation site, whereas mesenchymal cells massively infiltrated the slice culture tissue over 14 days *in vitro* as can be seen in Figure 4-11 and Figure 4-12, which might be competitive growth or cooperative. Simultaneous implantation of RAV27 and RAV57 (Figure 4-12) suggested that the proneural RAV57 fills the space between implantation centre and infiltration zone comprised of RAV27.

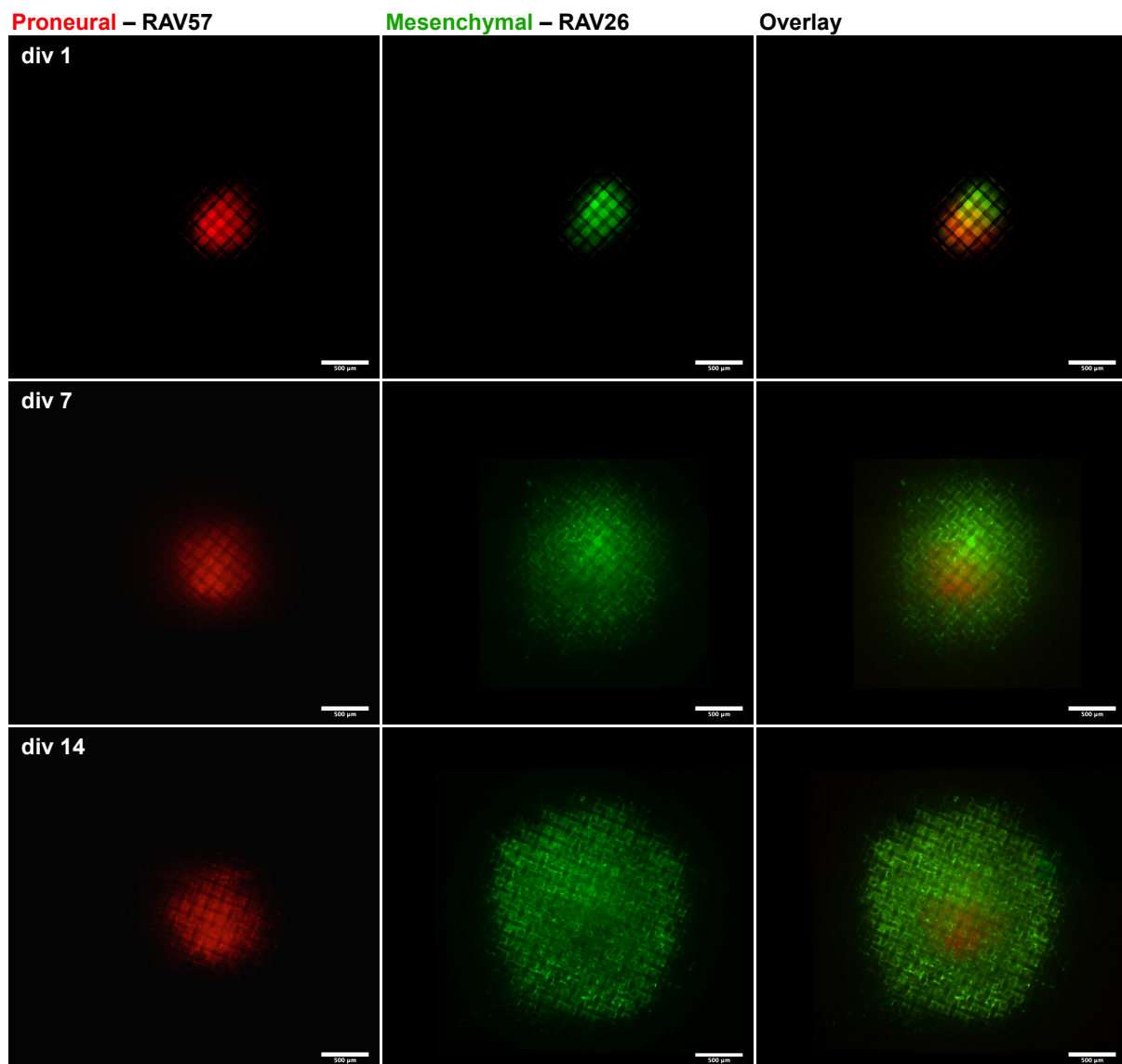


Figure 4-11: Simultaneous implantation of proneural (RAV57) and mesenchymal (RAV26) in OBSC

Mesenchymal RAV26 (GFP) and proneural RAV57 (RFP) BTICs were seeded simultaneously to form one spheroid that was subsequently implanted on OBSCs. Periodic monitoring revealed distinctly increased invasion of OBSC tissue by mesenchymal compared to proneural BTICs during 14 days *in vitro* (div). Scale = 500 µm

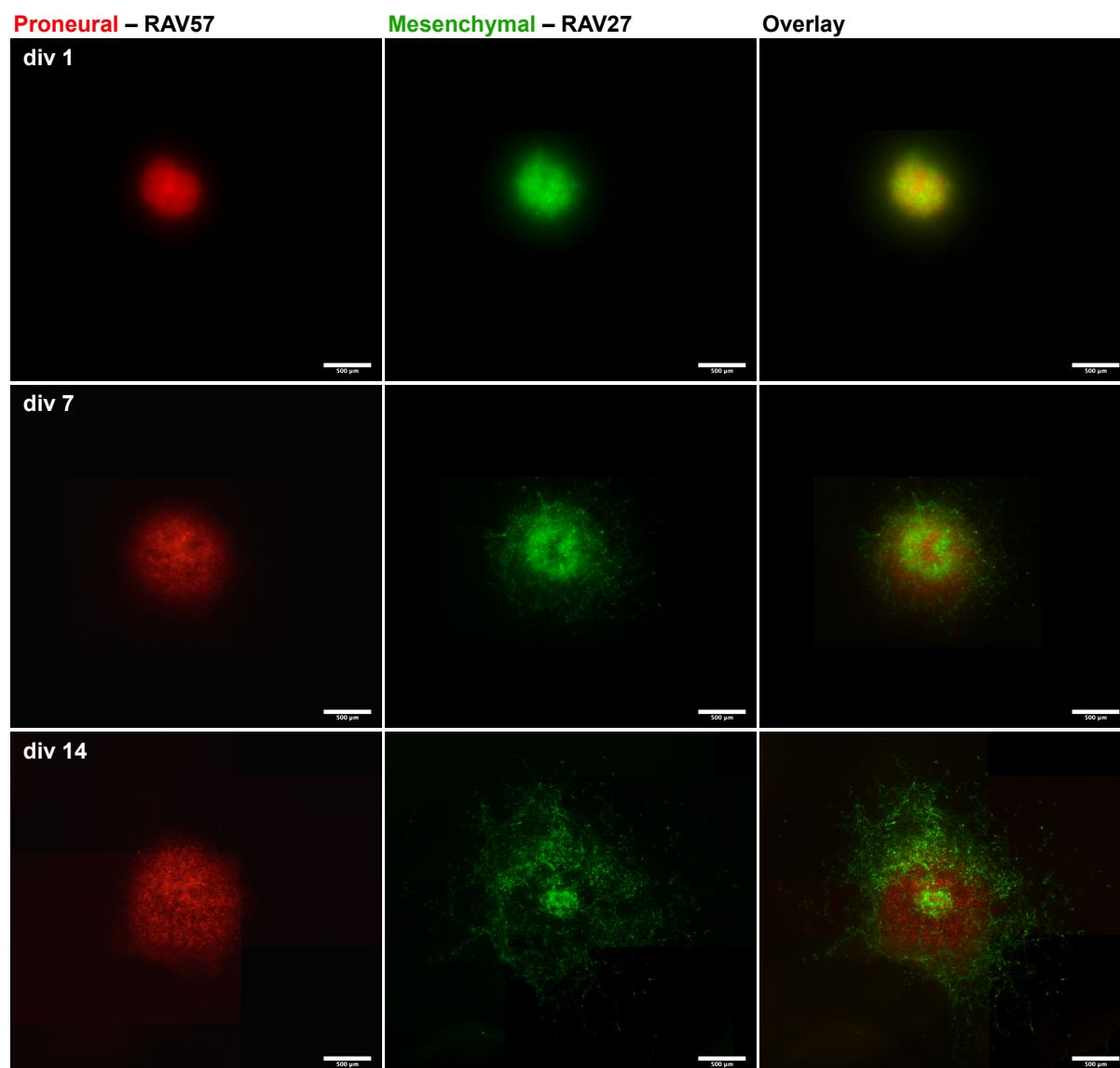


Figure 4-12: Simultaneous implantation of proneural (RAV57) and mesenchymal (RAV27) in OBSC

Mesenchymal RAV27 (GFP) BTICs showed significant increased invasion of OBSC tissue compared to proneural RAV57 (RFP) BTICs during 14 days *in vitro* (div). Scale bars = 500 µm.

4.2. Analysis of glioma cell invasiveness *in situ*

4.2.1. Formation of leader, follower, and stationary cells

Cell movement is an orchestrated biological process requiring a coordinated sequence of adhesion at the leading edge of a migrating cell to anchor in the ECM and detachment at the trailing end (Ridley *et al.* 2003). The loss or cessation of normally inhibitory controls may cause the reappearance of a motile phenotype in cancer cells (Demuth & Berens, 2004).

From the initially homogeneous cell population implanted on OBSC models, subpopulations emerged, differing in morphology and invasive behaviour. After implantation, a subpopulation of U87 cells switched to a spindle-shaped phenotype, indicating motility, and invaded the tissue surrounding the implantation site, as shown in Figure 4-2. After one week of incubation, tube-like cell formations migrating in distinct directions were detected. Another population remained at the implantation site as shown in Figure 4-12. Between the most invasive cells at the tip of the invasive rim and the non-invasive cells at the implantation site, a third intermediate population was distinguished. These three fractions were stably observed over several assays and were hence termed leader, follower, and stationary cells (Figure 4-13). The terms leader and follower were chosen according to Haeger *et al.* (2014) describing a leader – follower pattern in collective invasion of mesenchymal tumour cells, while the term stationary derived from a study comparing migratory and stationary populations of human glioma cells (Demuth *et al.* 2001).

Invasive strands led by leader cells were consistently observed after implantation of mesenchymal BTICs in the OBSC model. For U87, RAV21, RAV26, and RAV27, the initial homogenous cell population subdivided into three distinct subgroups during 3 weeks of monitoring: (i) leader, (ii) follower, and (iii) stationary cells. The latter remain at the initial implantation site and appear round-shaped, which might be due to proliferation. Leader cells are located at the outer edges of the invasive rim. Leader cells seem to initiate invasion and guide follower cells, which trace the track of leader cells. Leader and follower cells can be distinguished from stationary cells by a spindle-shaped morphology. To enable analysis of emerged leader, follower, and stationary cells separately, an isolation method was sought.

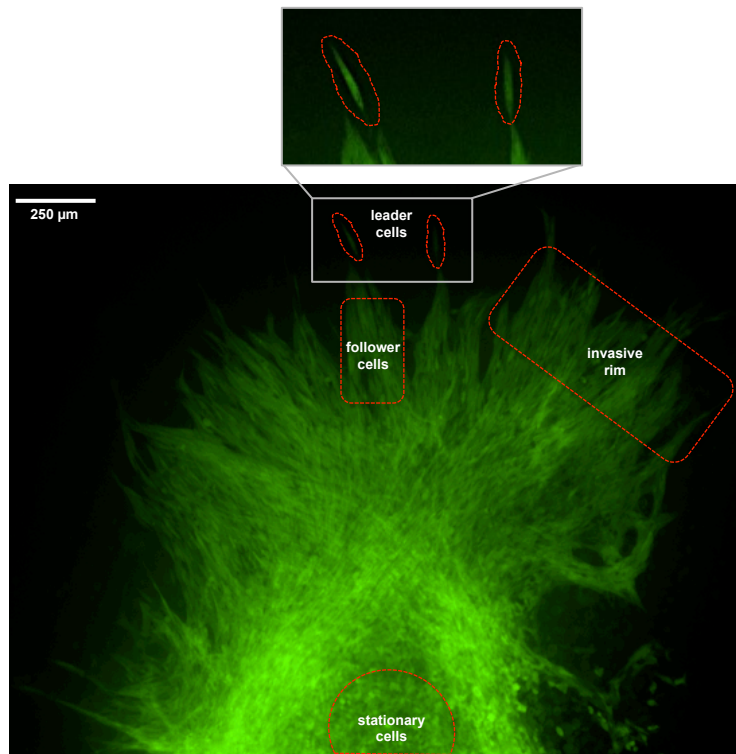


Figure 4-13: Formation of distinct U87 cell populations in the OBSC model

The invasion pattern of U87 cells is shown after 9 div. Migrating cells could be easily distinguished from stationary cells by their spindle-shape (mesenchymal-like). The invading cells divided into leader cells - located at the outer edges of the invasive rim - and follower cells which are positioned in the track of leader cells. For better visualization the close-up shows two leader cells at higher magnification. In contrast, the stationary cells remained at the implantation site and appeared round-shaped. Scale bar = 250 μm .

4.2.2. Development of an isolation method to receive single cells from the OBSCs

The BTIC hypothesis (Singh *et al.* 2003) indicates the importance of non-genetic changes in tumour development that may trigger some cells to develop an invasive – leader cell – phenotype. The detailed underlying mechanisms, relevant for formation of the three different subpopulations under physiological conditions, are poorly investigated in gliomas. An isolation method was developed in this work to investigate if the phenotypes are a product of the microenvironmental characteristics of the cell niche: perivascular or hypoxic, as ECM components, white matter tracks, microglia cells, or soluble factors such as the presence of growth factors. Here, the specific gene expression profiles that may be responsible for leader cell formation were investigated.

In this work, the development of a new micromanipulator adapter permitted the isolation of the three subpopulations of leader, follower, and stationary cells from OBSC, allowing individual assessment of their respective expression profiles. As described in section 7.2.2.5, the adapter was manufactured from a cannula to fit to a finely controllable micromanipulator (Figure 4-14). The adapter was mounted at the position where the capillary would normally

be located. The cannula was cut off at front and end site to generate a 2.5 cm tube with clean straight edges. One side was designed with a screw thread to fit the micromanipulator cannula holder. The other side was bent 0.8 mm from the edge in a 135° angle as depicted in Figure 4-14A – C.

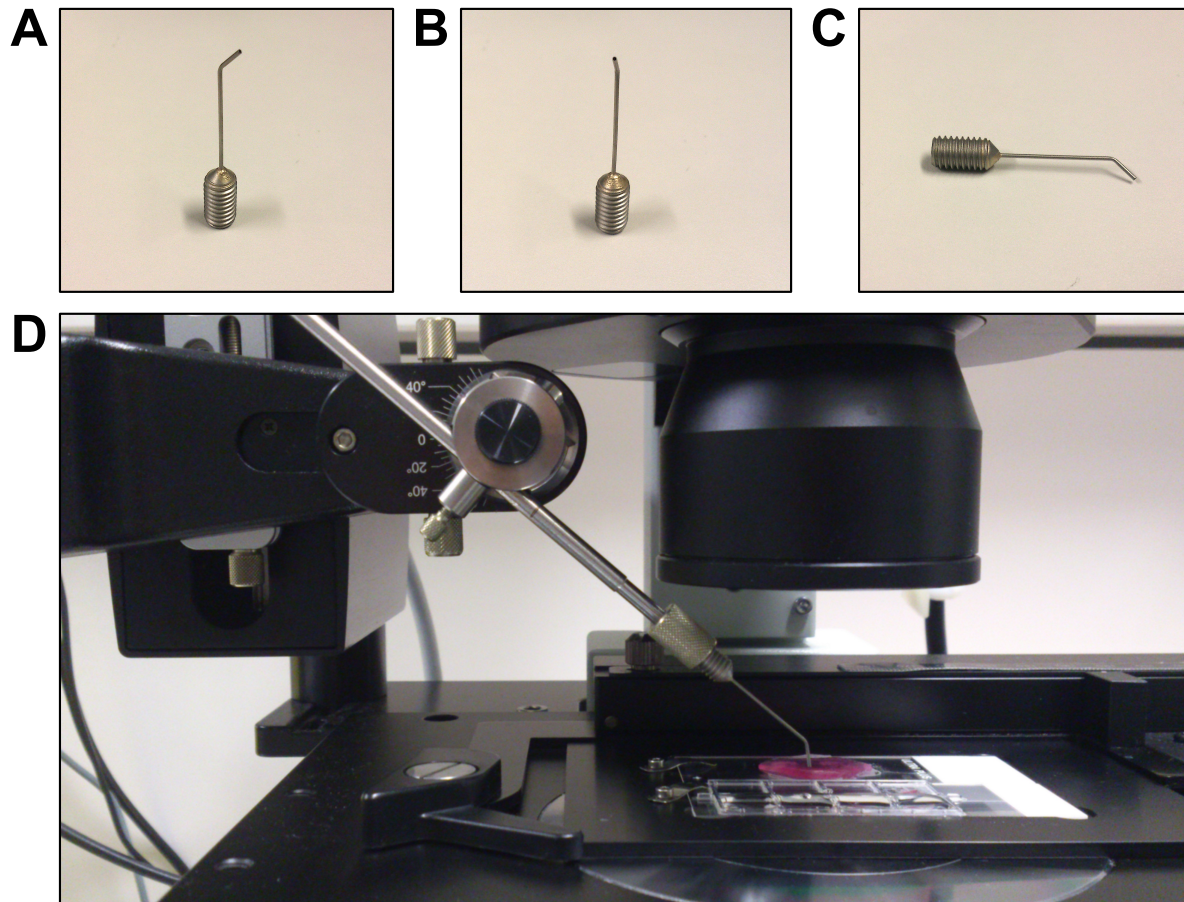


Figure 4-14: Equipment setup of the micromanipulator with the newly developed adapter

(A – C) Exemplary adapter manufactured from a cannula (0.6×30 23 G 1 ¼) and equipped with a thread fitting to the micromanipulator. (D) Full setup with an adapter attached to the micromanipulator and a prepared OBSC sample covered with culture media. The 8-chamber slide served to gather isolated tissue samples, separate, and isolate single cells.

This new method achieved precise cutting of respective regions and enabled isolation of viable small tissue fractions containing the fluorescent-labelled cells of interest (Figure 4-15A and B). The adapter permitted absorption and transfer of the separated tissue fragments into a fresh well. Transfer plus additional absorption of isolated tissue caused release and separation of single cells without further need of enzymatic dissociation. Intact fluorescent-tagged cells were harvested with a capillary (Figure 4-15C). Single cells or pools of up to 20 cells were immediately transferred for further analysis.

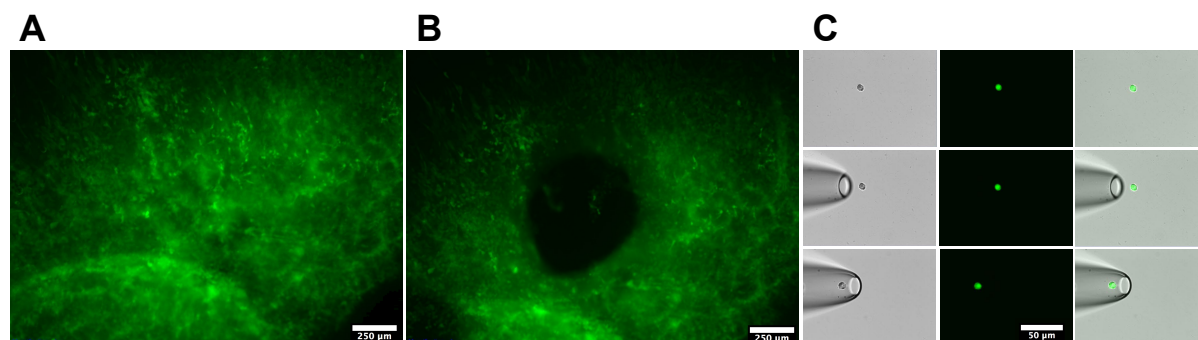


Figure 4-15: Isolation of single cells from the OBSC model

(A) OBSC infiltrated by U87-GFP cells before isolation. (B) OBSC after precise cutting of a respective region. The tissue fragment was gathered into the adapter and transferred into a fresh well. Scale bars = 250 μ m (C) Single cell collection for further processing. Scale bar = 50 μ m

Collected cells were immediately processed and either transferred into fresh 96-well plates for re-cultivation or into cell lysis buffer to proceed with mRNA isolation followed by cDNA library preparation from single cells or small pools of up to 20 cells (Hartmann & Klein, 2006). Quality PCRs with human specific primers for the three housekeeping genes β -Actin, EF1 α and GAPDH were performed on every cDNA library obtained from isolated cells to

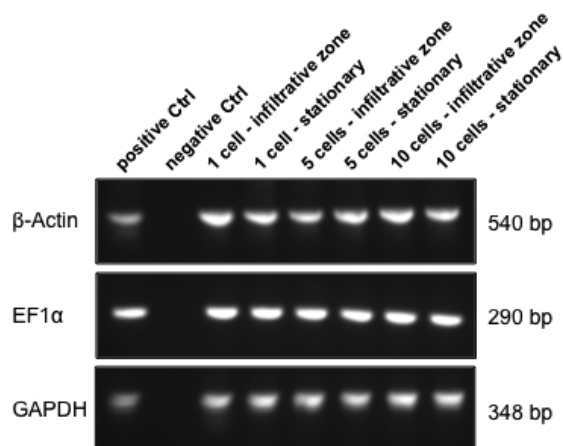


Figure 4-16: Representative quality PCRs on cDNA libraries

Successful cDNA library generation from one to ten U87 cells, previously isolated from OBSCs, was confirmed by quality PCRs. All libraries, either generated from single cells or pools of cells, were positive for all three housekeeping genes: β -Actin, EF1 α , and GAPDH.

verify the human progeny of cells as well as cDNA library functionality prior to microarray hybridization. Functional cDNA libraries could be obtained even from one cell extracted from OBSCs (Figure 4-16). However, to increase the credibility and to generate reliable data, 20 single cells were pooled prior to cDNA library generation. Eight libraries of every group that were positive for all three markers were hybridised to *Agilent whole human genome* microarray chips (4 x 44k). Despite their fluorescence labelling, quality PCRs verified the human origin of the glioma cells by human specific primers.

Therefore, the newly developed isolation method combined with mRNA isolation and amplification methods for single cells (Hartmann & Klein, 2006) enabled the characterisation of emerging cell subtypes of leader, follower, and stationary cells.

4.2.3. Identification of distinct transcription profiles

Transcription profiles of the three subpopulations of leader, follower, and stationary cells were analysed. They emerged from a cell population that after implantation on OBSCs had initially appeared homogenous. The aim of isolation and analysis was to identify a leader cell specific signature, based on increased transcription factor activity.

Here, the glioma cell line U87-GFP served as model. After 3 weeks *in situ*, 20 single cells were isolated of every subpopulation. A total of eight such pools per subgroup were isolated, transcribed, and amplified. During cDNA library generation, the samples were hybridised to microarray chips and the read-out analysed. The sample size decreased to 23 as one leader cell sample did not meet the quality requirements. Thus, 7 leader, 8 follower, and 8 stationary samples were gathered. The following examines briefly the results obtained during bioinformatics analysis performed by Xin Lu, in the Department of Experimental Medicine and Therapy Research, Faculty of Medicine, University of Regensburg.

Differentially expressed genes (DEG) were identified using Linear Models, part of the Limma software package (Ritchie *et al.* 2015), see paragraph 7.2.2.6. This statistical methodology uses pairwise comparison to separate input data in two groups, if significant differences exist. Here, the samples with highest variance were clustered in two groups at the first hierarchical stage. The first group consisted of leader cell samples, whereas the second group was composed of follower and stationary cells, which did not cluster separately in the following stage. The heat-map after hierarchical clustering in Figure 4-17 depicts that leader cells were separated from follower and stationary cells, consequently designated as non-leader when referring to both groups. Leader cell samples differed significantly from follower and stationary cells by 506 DEGs. In leader cells, 272 genes were significantly up-regulated, whereas 234 genes were repressed compared to non-leader cells. Specific comparison between the three subtypes revealed 96 significant genes (56 up- and 40 down-regulated in leader samples) that distinguished leader cells from follower cells. In contrast, 637 significant genes (313 induced, 324 repressed in leader samples) distinguished leader cells from stationary cells, while only 8 genes were differentially expressed between follower and

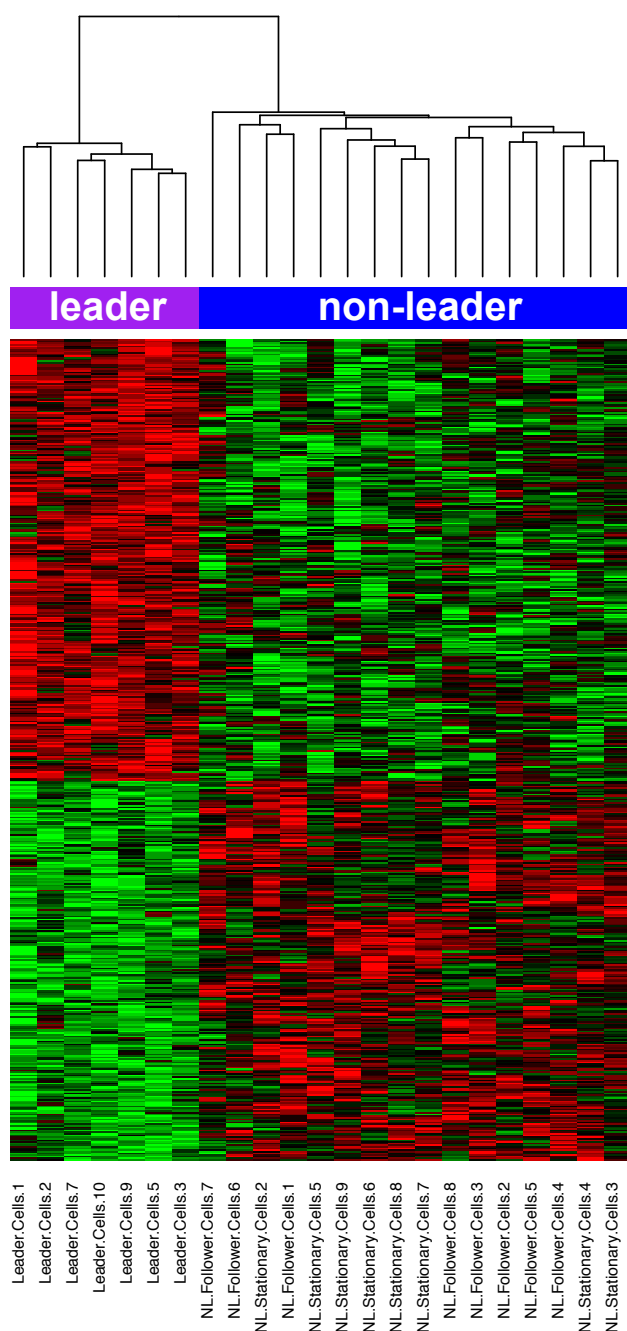


Figure 4-17: Hierarchic cluster analysis of differentially expressed genes of leader versus non-leader U87 cells

The x-axis lists the cell pools by name, the y-axis indicates the differentially expressed genes. Leader cell samples ($n = 7$) cluster together according to their gene expression pattern, whereas stationary ($n = 8$) and follower ($n = 8$) cells are inhomogeneous and do not cluster in their subgroups. False discovery rate (FDR) = 0.05

stationary cells (2 up-, 6 down-regulated in follower compared to stationary), indicative of high similarity. For instance, several matrix metalloproteinases (MMP) and associated factors were enriched in leader cells compared to non-leader cells. Note that the follower sample 7 clustered not directly with any other sample, indicating a high divergence to the other non-leader samples.

To verify that the three cell populations had truly differentiated expression patterns, DEGs among the three groups were detected by combining three pair-wise comparisons into one Fisher's exact-test. In contrast to the DEG analysis described above, this analysis took advantage of given information on the pre-defined subgroups to determine if the groups possessed pronounced differences as expected. Indeed, they were truly distinguishable by 462 significantly up-regulated DEGs ($q\text{-value} \leq 0.05$), as depicted in the heat-map in Figure 5-18A. The Venn diagram (B) shows different regulations between all subgroups. Notably, leader cells revealed hardly any overlap with stationary and follower samples.

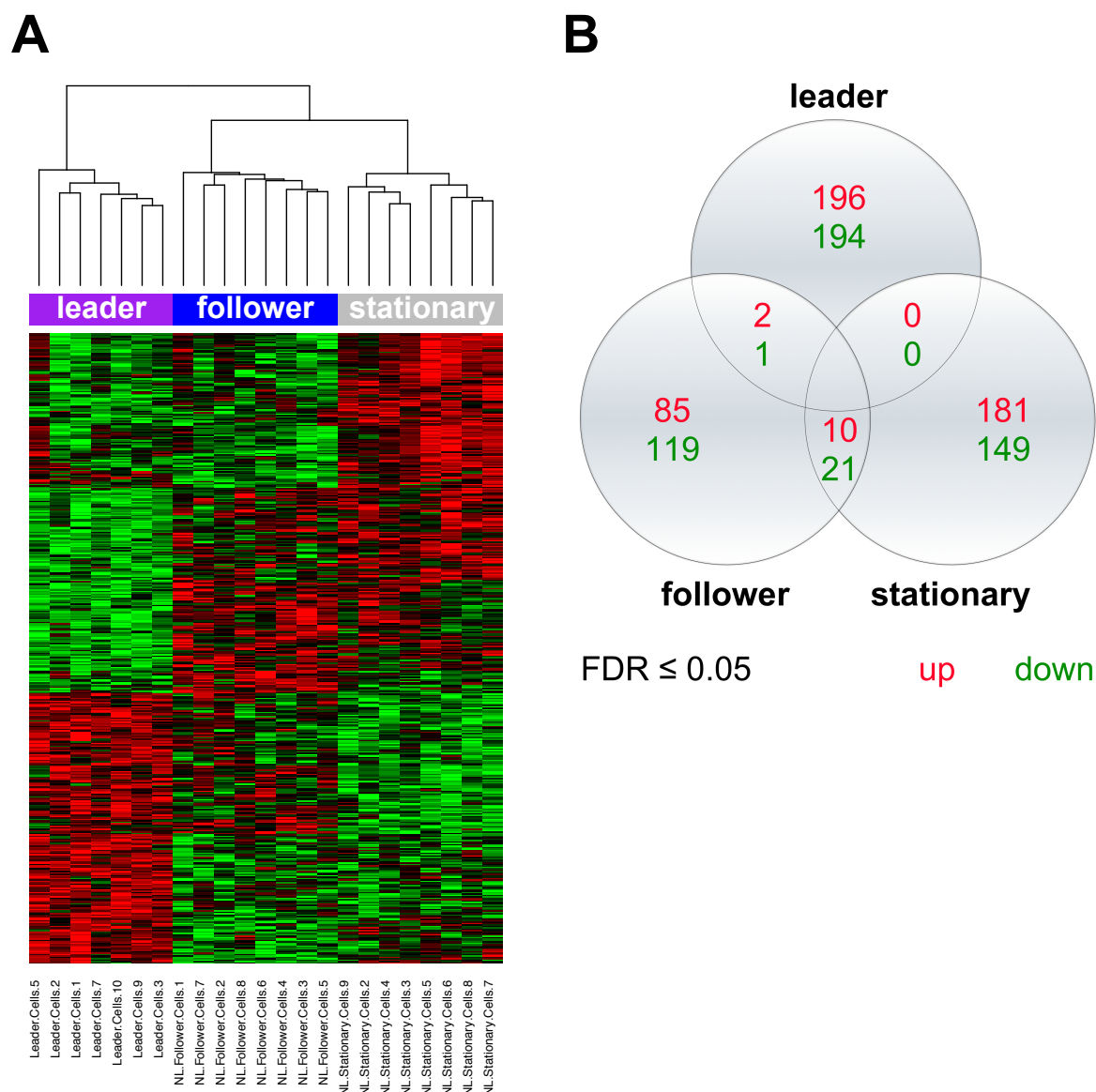


Figure 4-18: Three pair wise comparison of differentially expressed genes of leader, follower, and stationary U87 cells

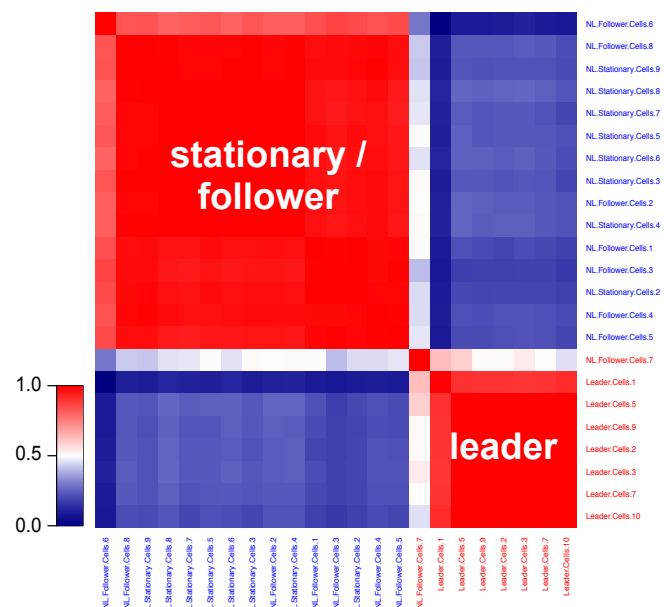
(A) Hierarchical clustering analysis. Leader, follower and stationary gene expression were clustered separately, using three pair-wise comparisons within one Fisher's exact-test. Significant differences in gene expression were revealed between leader and stationary cells, whereas follower cells showed an intermediate expression pattern (FDR q-value = 0.05). Note that the hierarchical clustering at first and second stage was pre-defined by the information to which subgroups the samples belong. (B) Venn diagram depicting differentially expressed genes identified within the three pair wise comparison. 196 genes were found to be up-, and 194 to be down-regulated in leader cells. In follower cells, 85 genes were induced and 119 repressed, while in stationary cells, 181 genes were up-, and 149 down-regulated. Leader cells had only minor similarities with follower cells as 2 genes were induced and one repressed in both compared to stationary cells.

The previously shown result of the initial DEG analysis – the natural difference between leader and non-leader cells – was verified by unsupervised clustering (nearest neighbour analysis, see paragraph 7.2.2.6). Clustering was performed with $k = 2$ and $k = 3$ clusters. Subsequent statistic analysis with SigClust (Liu *et al.* 2008) revealed $k = 2$ cluster to be significantly different. The received consensus matrix is shown as a heat map in Figure 4-19. Samples of the same cell type were more likely to cluster, which revealed a grouping of the three cell types in two clusters as most significant. The significance of the association with the distinct sample types was calculated by Fisher's test ($p < 3.3 \times 10^{-5}$). Leader samples clustered, separately from non-leader samples. An exception was found, as the follower sample 7 was not similar to either group and clustered only with itself. This sample clustered separately from all other non-leader samples before in DEG analysis (Figure 4-17), probably due to contamination with leader cells.

The specific regulation of individual genes will not be described further at this point, as the principal aim was to reveal a leader cell specific transcription factor signature.

Figure 4-19: Heat-map of leader, follower and stationary subpopulation clustering after k -means clustering

The subgroup samples cluster into two parts ($k = 2$) in which the variances were minimised. The first group, lower right, consisted of leader samples, whereas the second group, upper left, was composed of both, stationary and follower samples. An exception was found for one follower cell sample, which exhibited no similarity with either the leader cell or the stationary cell subgroup. High likelihood is indicated by red, low by blue colour and intermediate in white. Blue labels indicate non-leader; red labels indicate leader cell samples.



4.2.4. Identification of a transcription factor signature defining leader cells

Invasive leader cells revealed a distinct expression pattern in comparison to follower and stationary cells. These findings were utilised to identify a signature of active transcription factors characteristic for leader cells. This signature allows the reliable identification of leader cells within a cell cohort and may lead to identification of factors causing their induction.

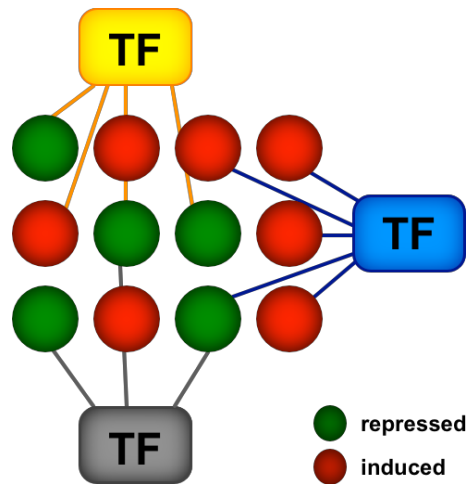


Figure 4-20: Schematic view of transcription factor identification based on DEGs

Transcription factors (TF) are identified on basis of information on gene (dots) induction and repression.

Two approaches were used to identify relevant transcription factors. Both offer the possibility to detect differentially regulated transcription factors on the basis of the annotated differentially expressed genes received from DEG analysis, see Figure 4-20.

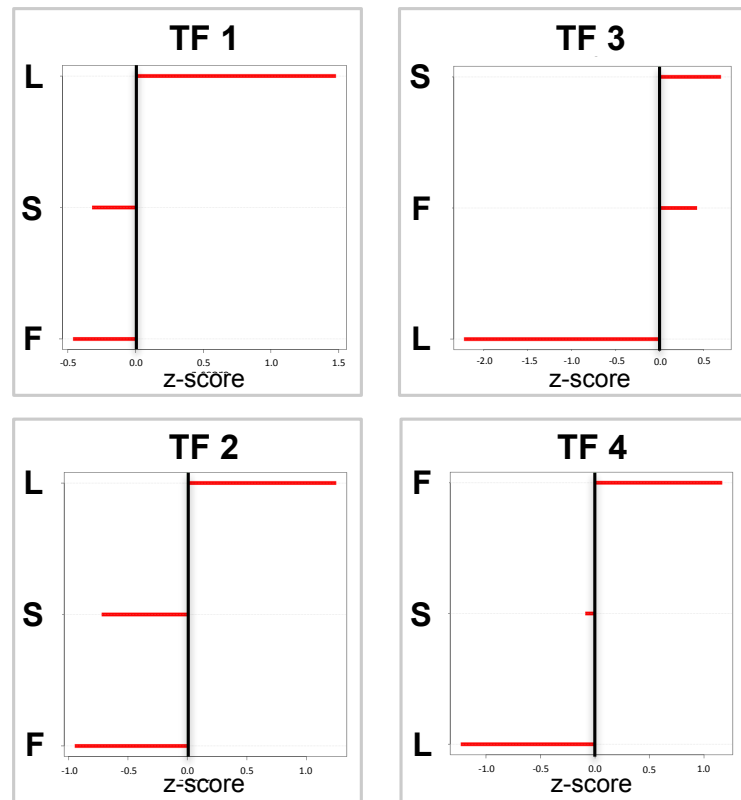
First, the Integrated System for Motif Activity Response Analysis (ISMARA) (Balwierz *et al.* 2014) was applied to the dataset. From the obtained set of gene expression data, ISMARA used motif activity response analysis to identify the key transcription factors driving gene expression and their activity profiles. Nine most significant regulatory motifs were revealed, distinguishing leader cells from follower and stationary cells. The motifs of four transcription

factors were found to be significantly enriched, while another five were down-regulated in leader cells compared to non-leader cells. Figure 4-21 depicts representative output data of ISMARA. Often, transcription factor activities in both stationary and follower cells were regulated in the same direction (in six cases), contrary to leader cells, although to different extents. For three transcription factors, activities were increased in follower samples only, but slightly decreased in stationary samples ($|z\text{-score}| < 0.2$). In contrast, activities were distinctly decreased in leader samples ($|z\text{-score}| > 1.1$). However, this was not considered further, since only increased activity was considered to be important for the leader cell phenotype.

The transcription factors whose activities were induced were related to cancer progression in general and represent promising candidates for anti-tumourigenic treatment, as they have known functions in gliomas as well. For example, one of the identified transcription factors is known to function as an oncogene in glioma driving proliferation.

Figure 4-21: Exemplary ISMARA transcription factor binding motifs

ISMARA analysis revealed the activities of the transcription factors (TF) 1 and 2 to be induced in leader compared to non-leader cells (left hand), whereas the activities of TF 3 and 4 were down-regulated (right hand side). Activity of TF 1 – 3 appeared to be similarly regulated in follower and stationary cells, and contrary to leader cells. Only TF 4 was induced in follower cells, while slightly down-regulated in stationary cells. The x-axes indicate the significance (by z-score). Positive values indicate high and negative low expression. L = leader, F = follower, S = stationary



The panel of transcription factors that characterises leader cells was expanded with second analysis utilising ConsensusPathDB (Kamburov *et al.* 2013). ConsensusPathDB is a database for interaction network analysis via integration of interactions provided by public resources and curated from pertinent literature. Based on information included in the database, the uploaded gene list was analysed for interaction network modules. Some of these modules included transcription factors that were not present in the supplied list, but had significant connections within the network (Kamburov *et al.* 2013). These transcription factors were not detected during DEG analysis and ISMARA, because they were not regulated at the transcriptional level and thus did not appear on the initial list, but were drawn from documented interactions. The top 78 DEGs ($p < 0.01$) between leader and non-leader samples were included in the interaction network analysis. 67 transcription factors were identified by significant connections to members of the gene list. 31 transcription factors were included in the annotated gene list, but were not significantly regulated during previous analysis. Those transcription factors might not necessarily be regulated themselves, but may regulate the leader cell phenotype by enhancing or repressing their target genes' expression. It could be concluded from the interaction network analysis that the activities of 12 transcription factors

were induced, whereas 20 were repressed. Among them, previously known candidates regulating invasion of glioma cells like STAT3 and C/EBP β (Carro *et al.* 2010) appeared. Two of those factors corresponded to ones already known from ISMARA. Again, only transcription factors with increased activity were considered as candidates comprising the leader cell specific signature.

In summary, evaluation of the microarray data indicates differential gene expression between leader, follower and stationary cells. However, leader cells were found to be distinctly different from non-leader cells, while less variance was seen between follower and stationary cells. Using two approaches – ISMARA and ConsensusPathDB – 16 transcription factors were identified in total to possess increased activity in leader cells.

4.3. Analysis and modulation of STAT3

The second section of this project focussed on STAT3 expression and modulation *in vitro*. Basal transcription factor expression at the protein level was analysed. In addition, proliferation and migration rates of BTICs and GBM cell lines were determined, followed by determination of the impact of STAT3 inhibition on these lines. Non-specific STAT3 inhibition by treatment with NSAIDs resulted in a decrease of proliferation as well as migration of BTICs and GBM cell lines with high dosages of these compounds. After specific STAT3 inhibition via Stattic, an even greater reduction in proliferation and migration was observed for BTICs and GBM cell lines.

4.3.1. Characterisation of primary human brain tumour initiating cells and glioma cell lines

In the attempt to reveal unifying patterns according to which primary BTICs can be clustered, the cells were characterised by expression profiles of transcription factors which regulate critical signalling pathways. In addition, the proliferation and migration capacities of these cells were determined. Among the BTIC lines analysed *in vitro*, four were classified as proneural: RAV17, 19, 39, and 57; and five as mesenchymal: RAV1, 21, 26, 27, and 28; which were compared to three established GBM cell lines: A172, HTZ349, and U87.

4.3.1.1. Relative protein expression levels

Western blot analysis was used to characterise the initial basal expression levels of transcription factors relevant for signalling pathways associated with proliferation and/or migration. The data obtained for transcription factor expression in both BTIC and GBM lines was compared, in order to determine relative quantifications in relation to the housekeeping gene GAPDH. Protein samples were generated from three sequential passages of each cell line, in order to determine expression levels accounting for passaging effects. Representative Western blot pictures are shown in Figure 4-22.

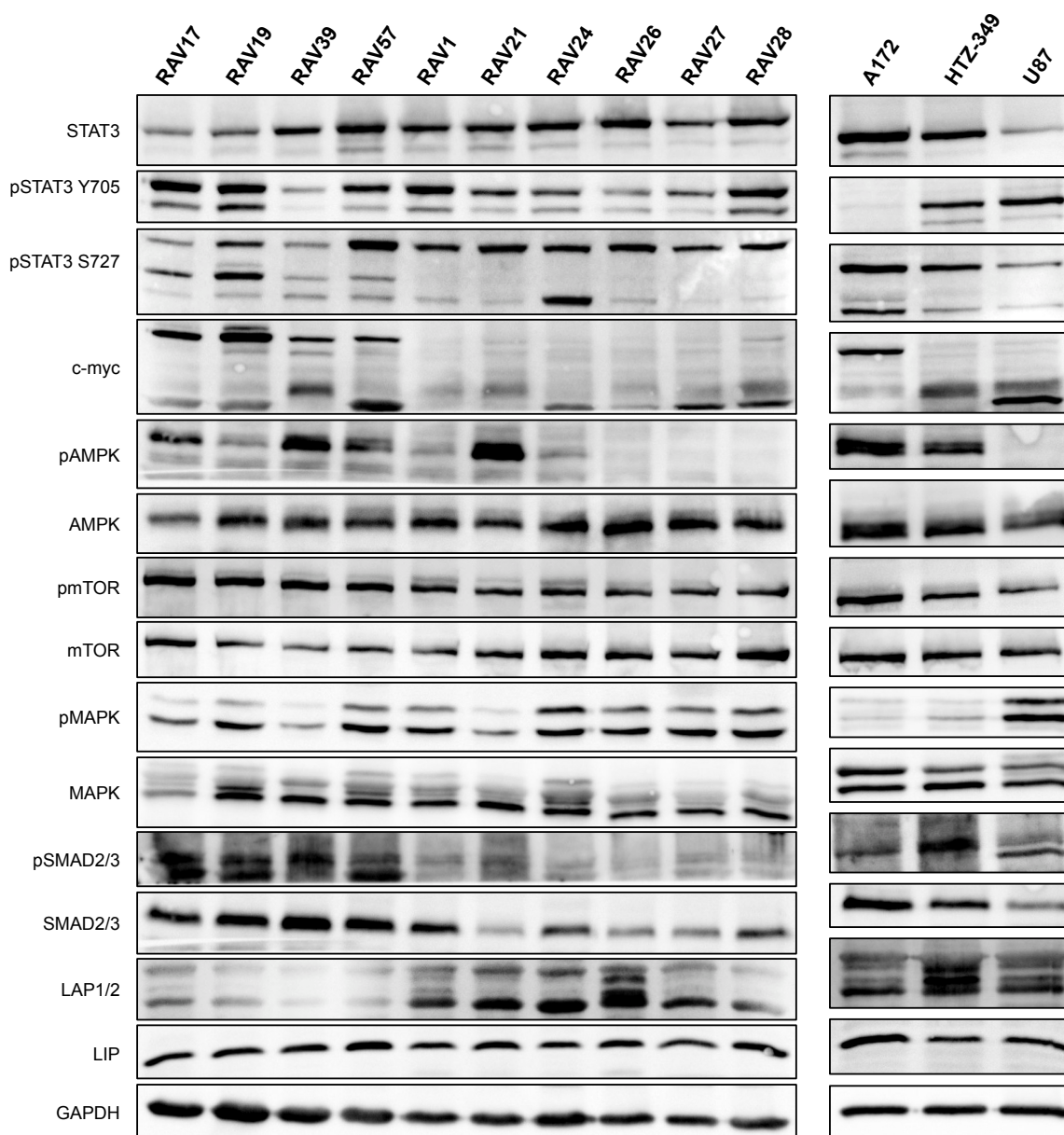


Figure 4-22: Representative Western blots depicting basal expression levels of transcription factors in BTIC and GBM cell lines

As outlined in the introduction, STAT3 is known, together with C/EBP β , as a master regulator in the transcriptional network which induces EMT in BTSC (Carro *et al.* 2010), and is, therefore, related to BTSC migration and invasion. STAT3 is activated by phosphorylation at Y705 which induces its dimerization, nuclear translocation and DNA binding (Darnell *et al.* 1994). Figure 4-23A illustrates that all groups exhibited moderate expression of pSTAT3 Y705. A detailed analysis of different cell lines included in each group revealed phosphorylated pSTAT3 Y705 expression is moderate in most lines (Figure 4-24A). Low expression was observed in RAV39 cells, whereas HTZ349 displayed increased expression. STAT3 contains a second phosphorylation site, S727, which was observed to be expressed to equal amounts as pSTAT3 Y705, although often at elevated levels in proneural and mesenchymal BTIC, as well as GBM lines (Figure 4-23A and Figure 4-24B). A172 displayed elevated pSTAT3 S727 compared to pSTAT3 Y705 (3-fold). Total STAT3 expression was increased in mesenchymal compared to proneural BTIC and GBM lines (Figure 4-23A). Proneural BTIC exhibited low total STAT3 expression, with the exception of RAV57. Mesenchymal BTIC displayed higher expression (Figure 4-23A), which confirmed the expectation of Carro *et al.* (2010) that STAT3 expression is characteristic for mesenchymal GBM cells.

Before C/EBP β was identified as a master regulator in BTSCs, in addition to STAT3 (Carro *et al.* 2010), it was already known as an essential transcription factor for cellular differentiation and proliferation. C/EBP β has been described as stimulator for GBM stem cell maintenance and proliferation (Aguilar-Morante *et al.* 2011) and its expression correlates with tumour aggressiveness (Homma *et al.* 2006). Figure 4-23B reports the basal expression levels of C/EBP β splice variants LIP, LAP1 and 2. They were equal for LIP in BTICs. In GBM cell lines, increased protein amounts were observed. Particularly, A172 was observed to express twice as much of the C/EBP β isoforms as other cell lines. LAP1/2 were expressed to a higher extent than LIP (~3-fold). LAP1 and 2 levels were raised from proneural over mesenchymal BTIC (~1.8-fold) in comparison to GBM lines (~2.5-fold). Single cell line expression levels (see Figure 4-24B) revealed the same trend, except that RAV28 and U87 exhibited decreased LIP1 and 2 compared to the other group members.

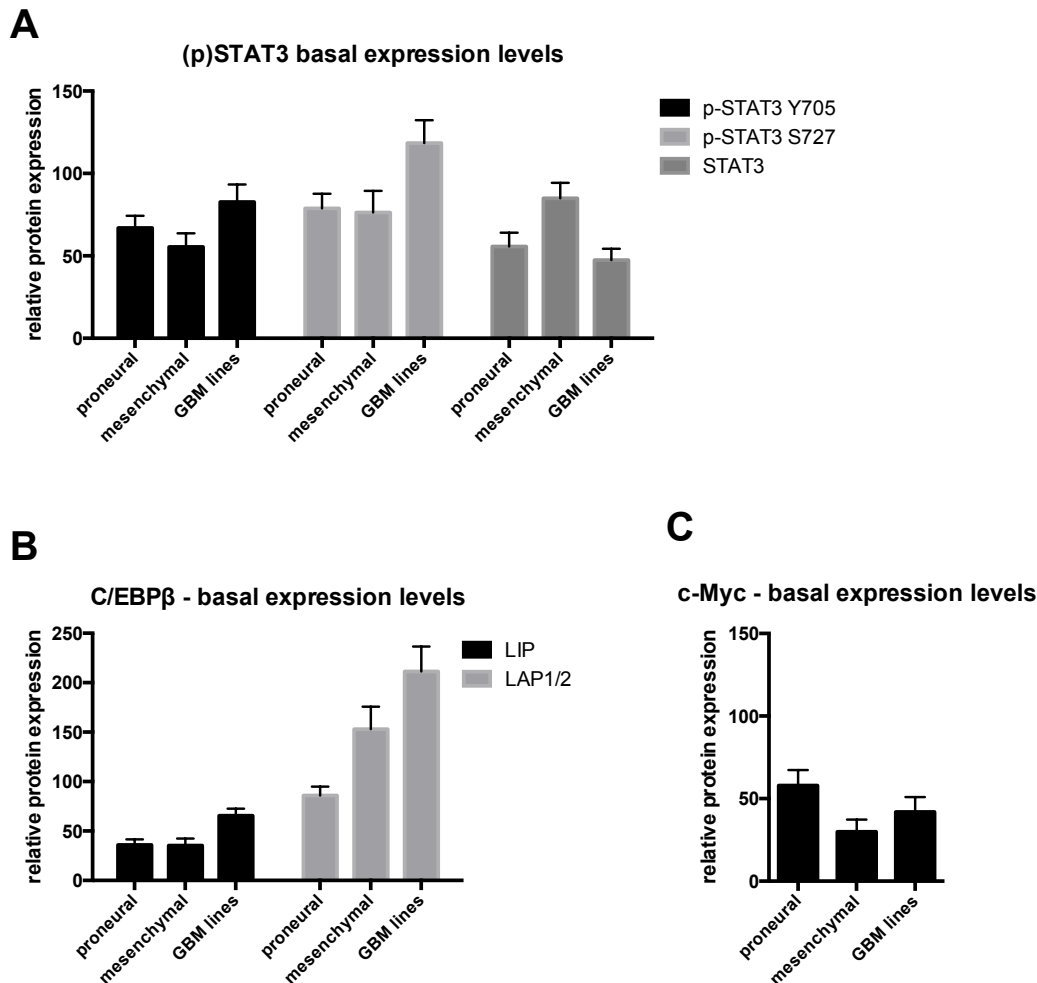


Figure 4-23: Basal protein expression of (p)STAT3, C/EBP β , and c-myc in proneural, mesenchymal BTIC, and GBM lines

(A) All groups show moderate expression of phosphorylated pSTAT3 Y705, with the highest level observed in GBM cell lines. Equal amounts of pSTAT3 S727 were detected in both proneural and mesenchymal BTICs. GBM lines displayed ~1.6-fold increase. STAT3 expression was increased in mesenchymal BTICs (~1.8-fold) compared to both proneural BTICs and GBM cell lines (~1.2-fold). (B) C/EBP β expression was reviewed separately for the different splice variants LIP, as well as LAP1 and 2. The small variant LIP (20 kDa) displayed moderate expression in all groups with proneural and mesenchymal BTICs, which exhibited similar expression rates. GBM had an increased expression of LIP (~1.8-fold). The larger splice variants LAP1 (44 kDa) and LAP2 (42 kDa) were expressed to greater amounts than LIP. Proneural BTICs expressed a 2.3-fold higher amount of LAP1 and 2 than LIP, which was observed at higher expression levels in mesenchymal BTICs (~4.2-fold) and GBM cell lines (~3.2-fold). (C) c-myc was observed to have moderate expression in proneural, mesenchymal and GBM cells. Proneural BTICs expressed twice the amount of c-myc than mesenchymal BTICs. Each group consisted of three representative cell lines (n=9); proneural: RAV17, 19, 57; mesenchymal: RAV21, 26, 27; GBM lines: A172, HTZ349, U87; values represent mean \pm SEM; relative protein expression was normalised to GAPDH expression.

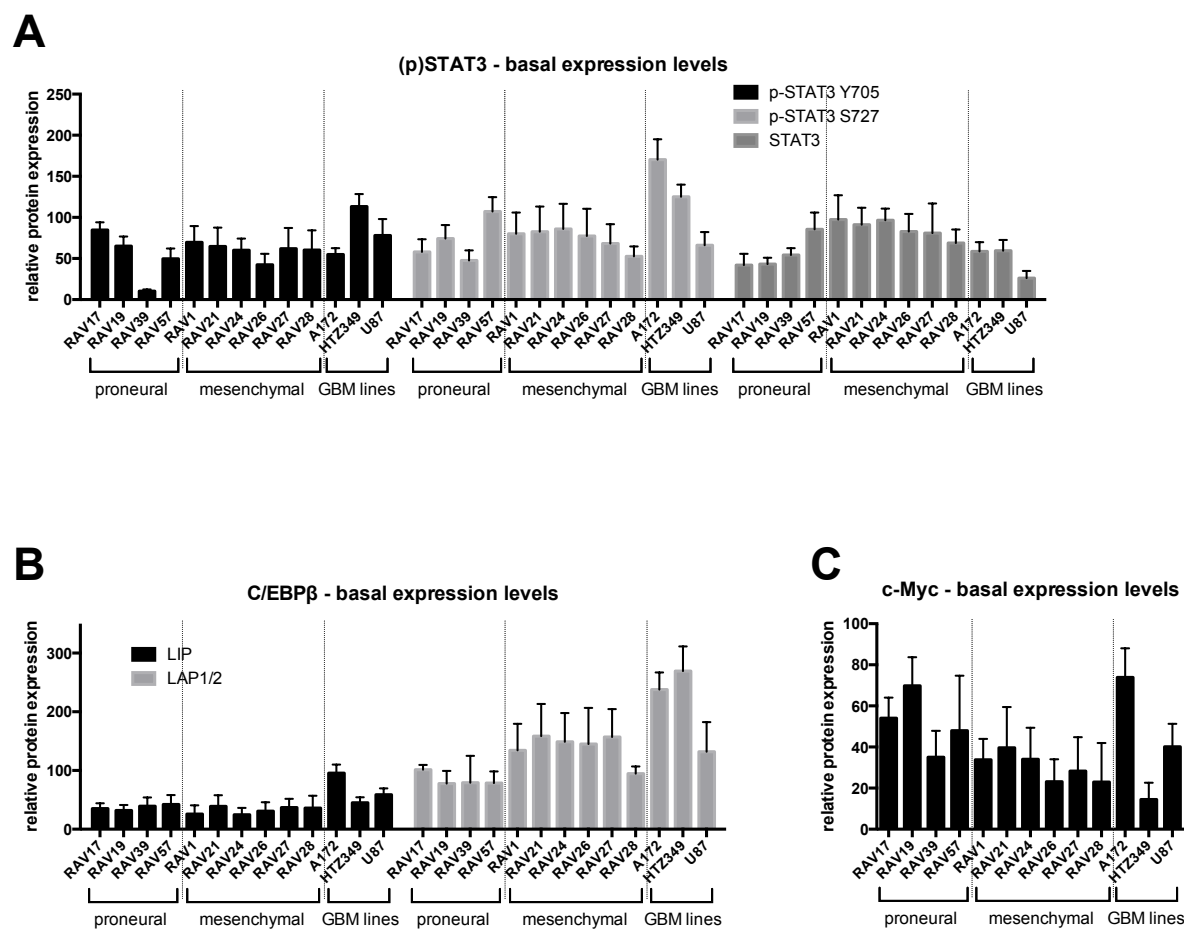


Figure 4-24: Basal protein expression of (p)STAT3, C/EBPβ, and c-myc in single BTIC and GBM lines

(A) Expression of phosphorylated pSTAT3 Y705 was moderate in most lines. Lowest expression was observed in RAV39 cells. HTZ349 displayed high expression titres. In most cases, expression of pSTAT3 S727 was increased compared to pSTAT3 Y705. Of note, A172 displayed a ~3-fold increase in pSTAT3 S727. Low STAT3 expression was observed in proneural BTICs RAV17, 19, 39 and in U87. Mesenchymal BTICs revealed increased expression up to ~3.3-fold compared to proneural BTICs. STAT3 expression was moderate in A172 and HTZ349. (B) C/EBPβ splicing variant LIP was equally expressed among all specimens, except A172 with up to ~3.7-fold increase. The larger variants LAP1/2 were expressed to higher extent. Proneural BTICs expressed up to ~2.8-fold (RAV17) more LAP1/2 than LIP. Compared to proneural cell lines, mesenchymal BTICs expressed approximately twice the amount of LAP1/2. The same was observed for U87. In A172 and HTZ349, levels were more than doubled. (C) Basal c-myc expression varied between all specimens. Mesenchymal BTICs expressed less c-myc than proneural BTICs. A high degree of variability was observed across the GBM lines. All experiments were performed in triplicates; values represent mean \pm SD; relative protein expression is normalised to GAPDH expression.

A downstream target of STAT3 is c-myc, which is a critical regulator of cell growth and proliferation, and is especially important for the G1 to S phase cell-cycle transition, as it drives the expression of cell cycle promoters such as cyclins (Hirano *et al.* 2000). The basal expression level of c-myc was increased in GBM (~1.4-fold). It was increased even more in proneural BTICs (~2-fold). Mesenchymal BTICs expressed c-myc at a lower level (Figure 4-23C). Considered in detail in Figure 4-24C, c-myc protein levels varied in-between BTICs, but a trend towards higher protein levels in proneural BTICs was observed. The commercially available GBM line A172 showed fairly high c-myc expression. The expression was elevated in U87 as well, whereas line HTZ349 displayed the lowest expression rate.

In glioma cell propagation, several other pathways are involved in addition to the transcription factors STAT3 and C/EBP β . These include PI3K, adenosine monophosphate-activated protein kinase (AMPK), TGF β , and mitogen-activated protein kinase (p44/42 MAPK; Erk1/2) signalling cascades, which were analysed for basic expression in this work as well. As a key component of PI3K signalling pathway, mTOR controls cell growth by regulating mRNA translation, metabolism, and autophagy, it has also been shown to be important in gliomagenesis (Akhavan *et al.* 2010). Mammalian target of rapamycin (mTOR) can act either indirectly via SOCS3 or directly on STAT3 downstream of IL-6 (Howie *et al.* 2014). It is also able to interact with the pSTAT3 S727 site. Phosphorylated mTOR was observed to be at equal protein levels in proneural and mesenchymal BTICs (summarised in Figure 4-25A). GBM line A172 displayed approximately twice as much phosphorylated mTOR than HTZ349 and U87 (Figure 4-26A, Figure 9-1F). This observation was similar for total mTOR, despite an overall increased expression in all GBM lines.

A controversial issue is the role of the metabolic master switch AMPK in GBM, whether its role is either as a tumour suppressor or contextual promoter (Liang & Mills, 2013). Located upstream of mTOR, AMPK likely acts as a tumour suppressor, because it inhibits mTOR. However, AMPK was shown to promote cancer cell survival in presence of certain stress factors and may be required for oncogenic transformation (Liang & Mills, 2013). Twice as much pAMPK and AMPK protein were detected in GBM lines than in proneural BTICs, (Figure 4-25B). However, the pAMPK increase is based on fairly high levels in cell line A172, whereas total AMPK was high in all GBM lines (Figure 4-26B, Figure 9-1G). In general, lower pAMPK levels correlated with higher phosphorylation of mTOR (Figure 4-26A and B) in mesenchymal BTICs, but not in proneural BTICs or GBM cell lines.

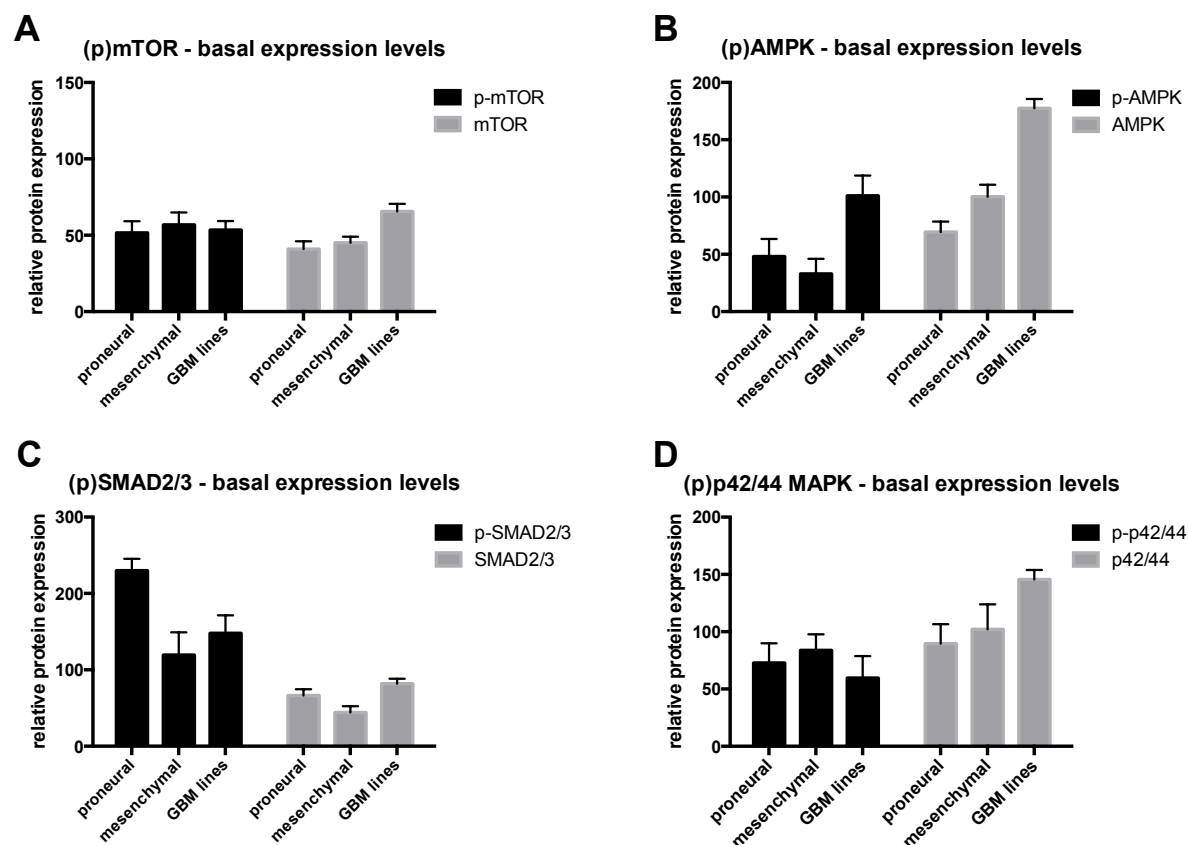


Figure 4-25: Basal protein expression of (p)mTOR, (p)AMPK, (p)SMAD, and (p)p42/44 MAPK in proneural, mesenchymal BTIC and GBM lines

(A) Active, phosphorylated mTOR protein levels were similar across BTICs and GBM lines, whereas mTOR was ~1.4-fold increased in GBM lines compared to BTICs. (B) pAMPK expression was higher in GBM lines: twice that of proneural BTICs. Mesenchymal BTICs displayed ~0.7-fold reduced pAMPK in relation to proneural BTICs. In contrast, AMPK protein levels increased from proneural over mesenchymal BTICs (~1.3-fold) and were highest in GBM lines (~1.7-fold). (C) SMAD2/3 expression titres were considerably lower compared to pSMAD2/3. Proneural BTICs expressed ~1.6-fold more and mesenchymal BTICs expressed less (~0.8-fold reduction) pSMAD2/3 than GBM lines. Non-phosphorylated SMAD2/3 was expressed to a far lesser extent in all groups, but almost twice as much in GBM lines than in mesenchymal BTICs. (D) Phosphorylated p42/44 MAP kinase expression titres were comparable across all groups. p42/44 MAPK increased from proneural to mesenchymal BTICs (~1.1-fold) increase, to ~1.7-fold higher in GBM lines. Each group consisted of three representative cell lines (n=9); proneural: RAV17, 19, 57; mesenchymal: RAV21, 26, 27; GBM lines: A172, HTZ349, U87; values represent mean \pm SD; relative protein expression was normalised to GAPDH expression.

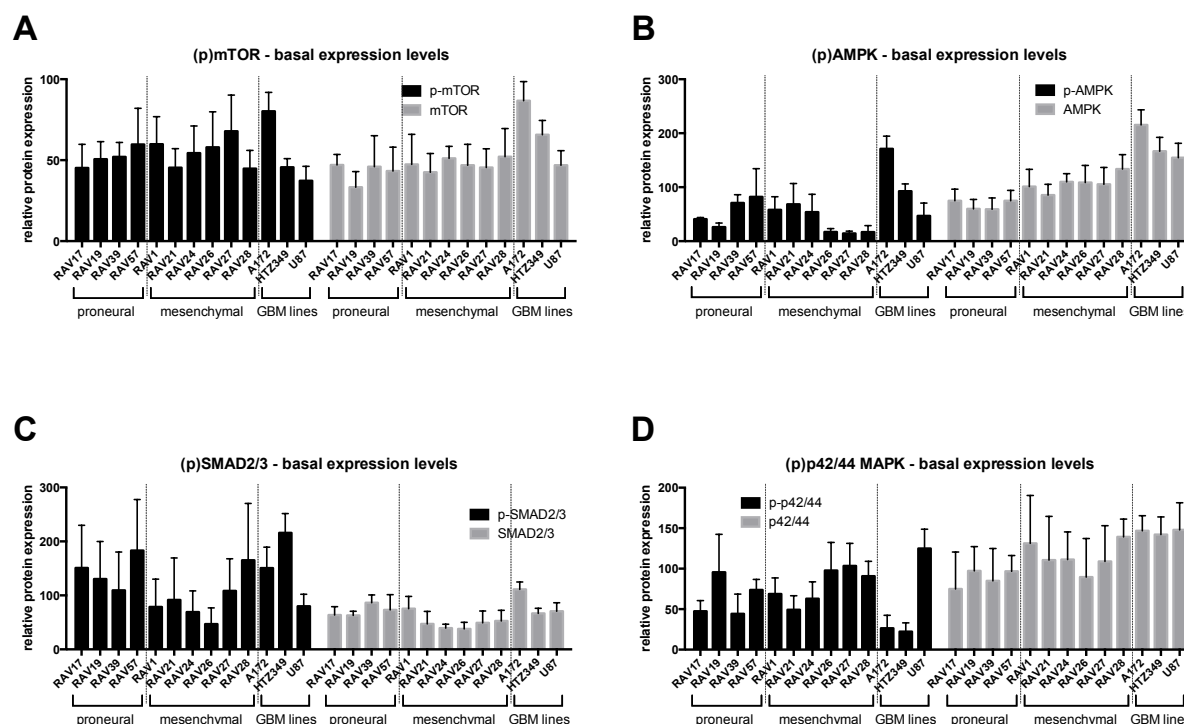


Figure 4-26: Basal protein expression of (p)mTOR, (p)AMPK, (p)SMAD, and (p)p42/44 MAPK in single BTIC and GBM lines

(A) (p)mTOR levels were moderately different between all specimens. Except, A172 displayed elevated expression of pmTOR and mTOR. (B) Remarkable variances in pAMPK protein expression were seen in BTICs. In A172 pAMPK expression was ~1.7-fold increased compared to HTZ349 and U87. AMPK expression titres were distinct between the groups. Proneural BTICs displayed lower AMPK expression (~0.6 – 0.75-fold), while expression was elevated (~1.5 – 2.2-fold) in GBM cell lines compared to mesenchymal BTICs. GBM lines. (C) Large differences in pSMAD2/3 levels were found in all specimens. On average, pSMAD2/3 expression titres were decreased in mesenchymal BTICs. SMAD2/3 titres were low in all specimen compared to pSMAD2/3. Again, lowest levels were observed in mesenchymal BTICs. (D) Phosphorylated p42/44 MAPK protein titres differed between the cell lines. Remarkably, phosphorylated p42/44 MAPK was decreased ~5-fold in A172 and HTZ349 compared to U87. In contrast, p42/44 MAPK was expressed to high levels and to similar extent in all GBM lines. Proneural BTICs displayed a trend towards reduced p42/44 MAPK expression, compared to mesenchymal BTICs. All experiments were performed in triplicates; values represent mean \pm SD; relative protein expression is normalised to GAPDH expression.

SMAD2/3 basal expression was also determined due to its role as key regulator mediating TGF β , which regulates multiple cellular processes including proliferation, differentiation, and apoptosis. The TGF- β /Smad2/3 signal pathway is activated in human brain glioma cells (Zhao *et al.* 2015) and is associated with glioma cell motility (Grzmil *et al.* 2011), it also promotes GBM proliferation (Bruna *et al.* 2007). pSMAD2/3 protein was highly expressed in proneural BTICs and considerably low in mesenchymal BTICs, except in RAV28 (Figure 4-25C and Figure 4-26C). Protein expression levels were approximately 2.2-fold higher in A172 and HTZ349 than in U87. SMAD2/3 protein was lower compared to its phosphorylated form.

The p44/42 MAPK (Erk1/2) signalling pathway is involved in regulation of cell growth, differentiation and motility (Roberts & Der, 2007). It is part of the Ras-Raf-MEK-ERK pathway, which is a key downstream effector of the Ras small GTPase, the most frequently mutated oncogene in human cancers and is, itself, a key downstream effector of the EGF receptor (Roberts & Der, 2007), which is commonly altered in GBM (Roth & Weller, 2014). Here, phosphorylated p42/44 MAPK was roughly constant across proneural BTICs, mesenchymal BTICs, and GBM cell lines (Figure 4-25D), although inter-line diversity was observed upon single specimen analysis, as shown in Figure 4-26D. Notably, U87 displayed remarkably higher p42/44 MAPK expression. Non-phosphorylated p42/44 MAPK levels rose from proneural to mesenchymal BTICs (grouped and individually) and were quite high (~1.7-fold) in GBM lines (Figure 4-25D).

A high degree of variability in protein expression levels was observed across all proneural, mesenchymal and GBM cell lines. For instance, pAMPK expression was highly elevated in A172, but virtually non-existent in RAV26 – 28. Such inhomogeneous distributions were observed in most cases, thus the present data did not depict distinct patterns for the analysed groups.

In light of these findings, further analyses of the proliferation and migration rates were performed with a reduced panel of cell lines, including three of each subcategory: RAV17, 19, and 57 proneural, RAV21, 26, and 27 mesenchymal BTIC lines, as well as A172, HTZ349, and U87 as GBM cell lines.

4.3.1.2. Basic proliferation rates

To reveal whether proliferation, one of the known key characteristics of glioma pathogenesis, is distinct between proneural, mesenchymal, and GBM cell lines, their proliferation rates were compared. Basic proliferation rates of GBM cell lines A172, HTZ349, U87 as well as BTICs RAV17, 19, 21, 26, 27, 57, and their differentiated TC counterparts were determined. To rule out alterations caused by DMSO, which was used as solvent at later stage, proliferation was assessed at control (media) and after DMSO treatment conditions. To determine proliferation, the CyQuant assay was used, in contrast to other common assays, this assay specifically detects nucleic acids rather than analysing enzymatic reactions or growth media components. This allows quantification of proliferation independent of changes in cellular metabolism. Fluorescence emission of the CyQuant dye–nucleic acid complexes correlates linearly with cell number (Jones *et al.* 2001).

GBM cell lines displayed high proliferation rates as cell numbers were more than doubled within 48 h (Figure 4-26). Minor alterations of proliferation were observed upon DMSO treatment compared to control, but not significantly Figure 4-27A – C. Thus, possible side effects due to DMSO were considered negligible for further experiments. Between 48 and 96 h, a plateau in cell proliferation was observed as the cell amount did not increase exponentially in A172 and HTZ349, whereas U87 proliferated exponentially. Comparison of proliferation at control conditions (Figure 4-27D) demonstrated similar rates of all GBM lines since deviations were not significant.

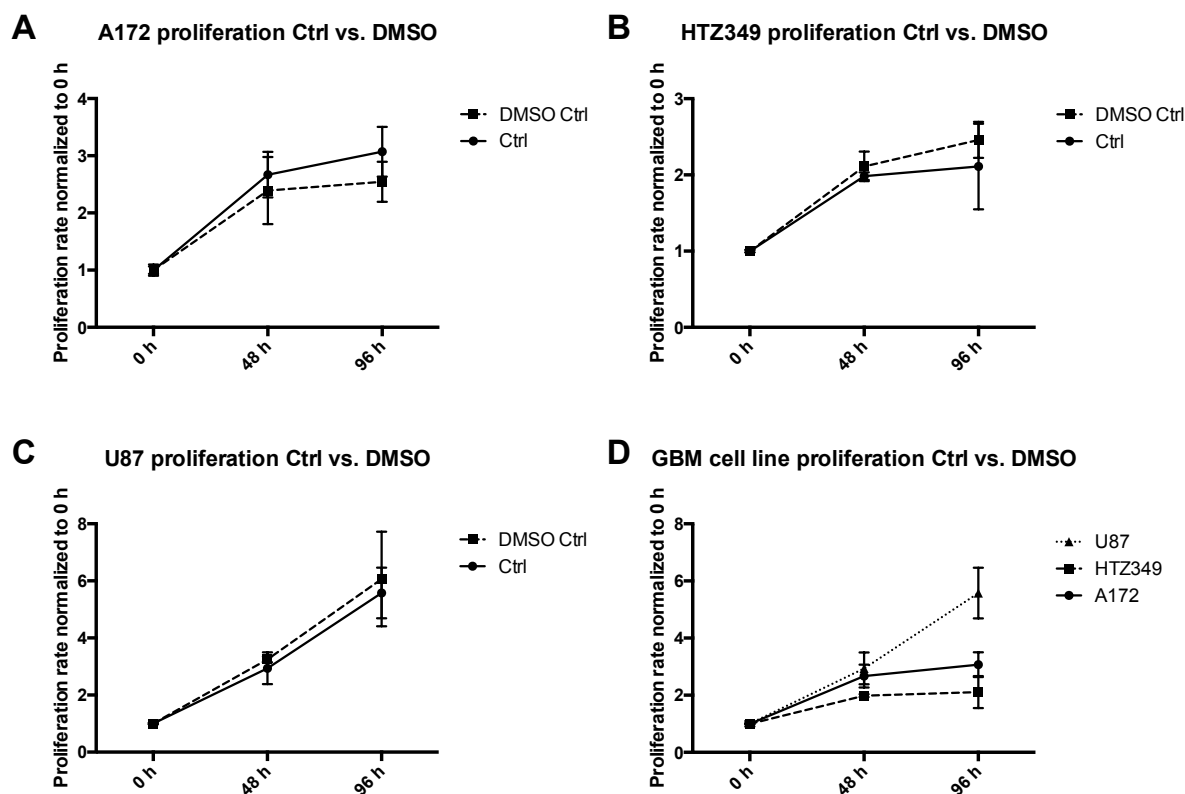


Figure 4-27: Basic proliferation rates for GBM cell lines A172, HTZ349, and U87

Basic proliferation is depicted as proliferation rate normalised to the initial cell amount at 0 h. Control (media) was compared to DMSO treatment (DMSO amount in 20 μ M Stattic treatment). (A) Proliferation of A172 was reduced upon DMSO treatment compared to control, but not significantly. From 0 to 48 h, cell number increased by ≥ 2.5 -fold (control: 2.67 ± 0.4 , DMSO: 2.49 ± 0.61). Between 48 and 96 h, cell proliferation reached a plateau. (B) In HTZ349, proliferation increased minimally with DMSO compared to control treatment. Cell number increased ≥ 2 -fold (control: 1.98 ± 0.05 , DMSO: 2.11 ± 0.19), from 0 to 48 h and a plateau was reached between 48 and 96 h. (C) U87 cell proliferation was almost identical at both conditions with exponential growth leading to an increase of ≥ 5.5 -fold (control: 5.58 ± 0.89 , DMSO: 6.06 ± 1.66) after 4 days compared to the initial cell number. (D) Summarised data of the three lines (at control treatment) indicated similar proliferation rates as differences were not significant. All experiments were performed in two independent measurements with 3 measurements/assay; values represent mean \pm SD; 2way ANOVA analysis with Sidak's multiple comparisons test, ns: $p > 0.05$, *: $p \leq 0.05$, **: $p \leq 0.01$, ***: $p \leq 0.001$, ****: $p \leq 0.0001$.

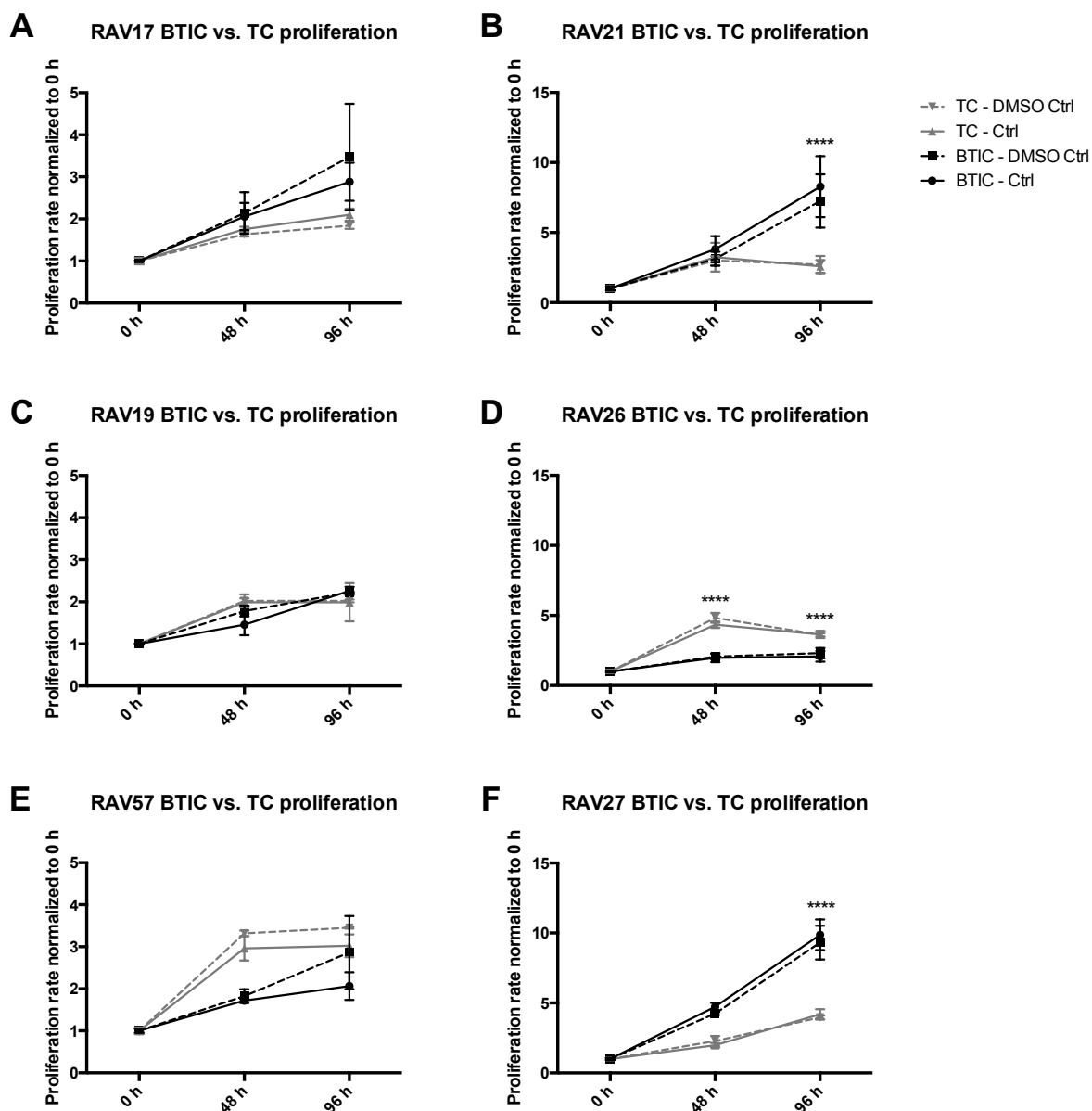


Figure 4-28: Basic proliferation rates of BTICs compared to their differentiated pair of TCs

Basic proliferation is depicted at control (media) or DMSO treatment conditions. Data was normalised to the initial cell amount at 0 h. BTICs are compared to respective TCs. (A) RAV17 BTICs displayed higher proliferation (0 – 48 h: control: 2.14 ± 0.99 , DMSO: 2.01 ± 0.58) than TCs. TC number increased ~ 1.7 -fold after 48 h (control: 1.76 ± 0.1 , DMSO: 1.78 ± 0.25) and remained stable until 96 h. (B) RAV21 BTIC and TC proliferation rates were similar between 0 and 48 h with ~ 3 -fold increase (BTIC: control: 4.13 ± 1.01 , DMSO: 3.39 ± 0.54 ; TC: control: 3.02 ± 0.32 , DMSO: 3.26 ± 1.03). RAV21 BTIC proliferation had a further increase at 96 h (~ 8 -fold) indicating exponential growth. Corresponding RAV21 TC number was decreased between 48 and 98 h. (C) RAV19 BTIC and TC had similar proliferation rates, although BTIC proliferation increased ~ 1.4 -fold from 0 to 48 h (control: 1.46 ± 0.62 , DMSO: 1.78 ± 0.23) and ~ 2.2 -fold from 0 to 96 h (control: 2.26 ± 0.19 , DMSO: 2.23 ± 0.03), whereas TC proliferation increased ~ 2 -fold until 48 h (control: 1.99 ± 0.19 , DMSO: 2.02 ± 0.27) and remained stable until 96 h. (D) In RAV26 the proliferation rate was observed to be significantly elevated in BTICs (~ 2 -fold: control: 2.02 ± 0.32 , DMSO: 2.1 ± 0.2) compared to TCs (~ 4 -fold: control:

4.35 ± 0.22 , DMSO: 4.83 ± 0.35) at 48 h. (E) RAV57 TC proliferation increased by ~3-fold (control: 3.52 ± 0.12 , DMSO: 2.96 ± 0.5) by 48 h compared to BTICs (0 – 48 h: control: 1.72 ± 0.06 , DMSO: 1.83 ± 0.27 ; 48 – 96 h: control: 2.07-fold ± 0.66 , DMSO: 2.86-fold ± 1.4). (F) RAV27 proliferation differed significantly between BTICs and TCs. Cell number of BTICs increased by ~4-fold from 0 and 48 h (control: 4.29 ± 0.51 , DMSO: 3.84 ± 0.2) and ~8.7-fold from 48 to 96 h (control: 8.94 ± 1.98 , DMSO: 8.44 ± 2.45) and for corresponding TCs only ~2-fold from 0 to 48 h (control: 1.98 ± 0.29 , DMSO: 2.28 ± 0.63) and ~4-fold from 48 to 96 h (control: 4.19 ± 0.64 , DMSO: 3.96 ± 0.24). All experiments were performed in two independent measurements with 3 measurements/assay; values represent mean \pm SD; 2way ANOVA analysis with Sidak's multiple comparisons test, ns: $p > 0.05$, *: $p \leq 0.05$, **: $p \leq 0.01$, ***: $p \leq 0.001$, ****: $p \leq 0.0001$.

Inter-line diversity was observed for proliferation rates between all specimens. In all cases proliferation upon DMSO treatment did not deviate significantly from the control measurements (Figure 4-28). In contrast, considerable proliferation variances were determined between BTICs and TCs. RAV17, 21, and 27 BTICs (Figure 4-28A, B, F) displayed increased proliferation compared to their respective TCs. Similar proliferation was revealed for RAV19 BTICs and TCs (Figure 4-28C). In RAV26 and 57 increased proliferation of TCs compared to BTICs was observed (Figure 4-28E, F). In general, proneural cells proliferated less (1.5 – 2.8-fold increase of cell number from 0 to 48 h) than mesenchymal cells (2 – 4-fold), summarised in Figure 4-29. A high degree of variability was observed across all cell lines regarding proliferation rates, which often differed significantly between BTICs and their respective TCs.

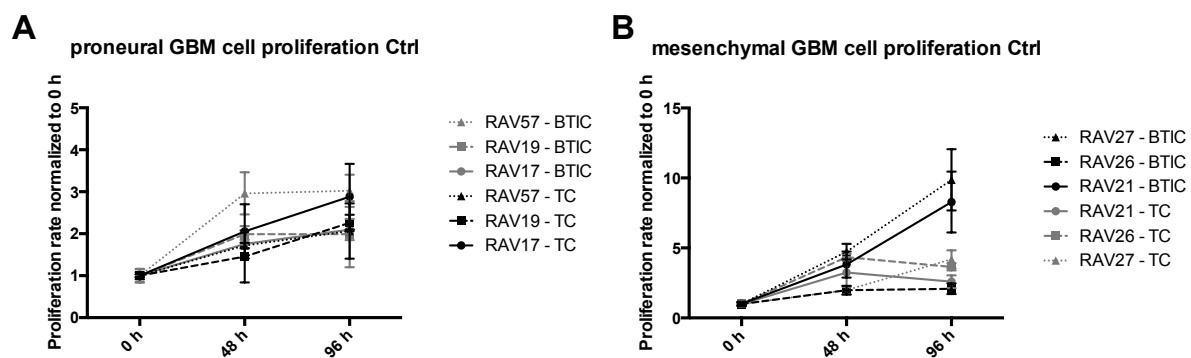


Figure 4-29: Basic proliferation rates of proneural compared to mesenchymal lines

The basic proliferation rate is shown for BTICs and TCs under control (media) conditions. Proneural lines (A) revealed decreased proliferation rates compared to mesenchymal lines (B). (A) Mean increase of cell number from 0 – 48 h: for BTICs: 1.8-fold ± 0.44 , for TCs: 2.2-fold ± 0.58 . (B) Mean increase of cell number from 0 – 48 h: for BTICs: 3.4-fold ± 1.26 , for TCs: 3.7-fold ± 1.0 . Notably, proliferation of RAV26 BTICs was distinctly lower than that of the other mesenchymal BTICs. All experiments were performed in two independent measurements with 3 measurements/assay; values represent mean \pm SD.

Based on the cell number measured by fluorescence, the growth constant λ was calculated between 0 to 48 h and 0 to 96 h. Normally, the mean of both λ was considered or λ_{0-48h} in case cell growth had reached a plateau between 48 and 96 h. Using λ , the doubling time and percentage proliferation day⁻¹ were calculated for each specimen. Analysis of the proliferation variables, as shown in Table 4-2, revealed that proliferation rates were not unique for the subgroups of (i) GBM cell lines, (ii) proneural BTICs, (iii) proneural TCs, (iv) mesenchymal BTICs, and (v) mesenchymal TCs. A clustering between proneural BTICs and TCs from all other values became apparent as those proliferated distinctly slower. GBM lines revealed an intermediate growth with doubling times ranging between 30 and 48 h, which is represented by an increase of cells of about 55% within one day. Proneural BTICs had considerably low proliferation, with an increased average doubling time of 64 h, which lead to 30% increase of cells per day. Remarkably higher proliferation was observed for BTICs and TCs of the mesenchymal subtype. Mesenchymal BTICs and TCs proliferated twice as fast as the proneural cells on average. Altogether, a significant segregation of all the subgroups according to their proliferation rates was impossible.

Category	Growth constant λ	Doubling time (h)	Proliferation day ⁻¹ (%)
GBM lines			
A172	0.491	33.883	63.390
HTZ349	0.343	48.562	40.855
U87	0.539	30.859	71.442
average GBM lines	0.440	37.810	55.267
BTIC			
RAV17	0.261	63.635	29.877
RAV19	0.204	81.607	22.611
RAV57	0.271	61.417	31.109
average proneural BTIC	0.259	64.336	29.574
RAV21	0.599	27.770	82.493
RAV26	0.343	48.479	40.938
RAV27	0.675	24.649	97.418
average mesenchymal BTIC	0.527	31.563	69.716
TC			
RAV17	0.233	71.258	26.441
RAV19	0.258	64.523	29.887
RAV57	0.277	60.160	31.853
average proneural TC	0.243	68.556	27.463
RAV21	0.589	28.267	80.133
RAV26	0.529	31.436	73.353
RAV27	0.358	46.458	40.549
average mesenchymal TC	0.476	34.929	63.480

Table 4-2: Overview of growth constant, doubling time, and proliferation day⁻¹ for GBM and primary cell lines

4.3.1.3. Basic migration rates

Similar to proliferation measurements, basic migration rates were estimated. Migration rates of the GBM cell lines A172, HTZ349, and U87 as well as of the BTICs RAV17, 19, 21, 26, 27, 57, and respective TCs were determined by spheroid assays. Migration out of spheroids of 2,500 cells was monitored photographically at 0, 16, 24, 40, and 48 h. The area covered by cells at each time point was measured and normalised by division to the initial spheroid size at 0 h to calculate average migration rates. Similar to proliferation measurements, the influence of DMSO was simultaneously analysed.

Similar basic migration rates were observed for all GBM lines in the control or DMSO treatment (Figure 4-30A – C). All cell lines displayed high migration rates, the area covered by cells increased in 48 h between ~15-fold (A172) and ~25-fold (HTZ349) (Figure 4-30D).

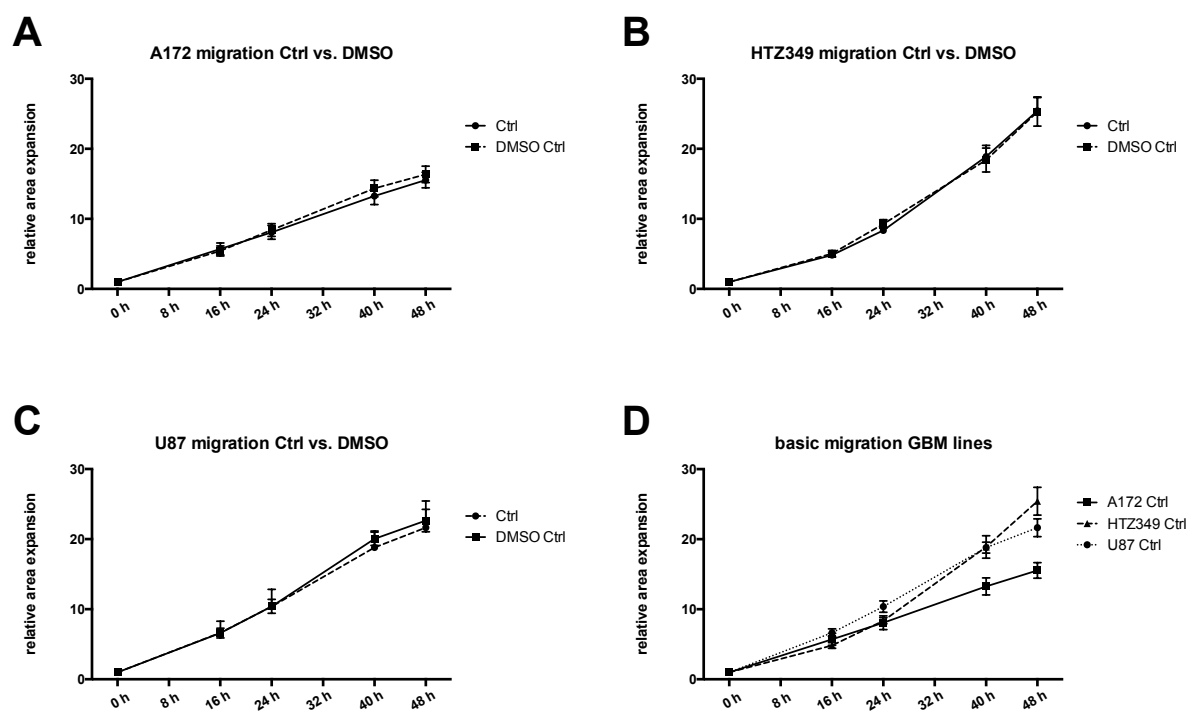


Figure 4-30: Basic migration rates for GBM cell lines A172, HTZ349, and U87

Basic migration rates are shown as relative area expansion normalised to initial spheroid sizes at 0 h. (A) A172 exhibited similar migration since the area covered by cells after 48 h was observed to increase by ~15-fold (control: 15.55 ± 3.32 , DMSO: 16.35 ± 3.52). (B) Migration rates were similar between control and DMSO treated HTZ349. Cells displayed an increase of ~25-fold of covered area after 48 h (control: 25.42 ± 5.97 , DMSO: 25.28 ± 6.1). (C) U87 cells also exhibited similar expansion of ~22-fold in both conditions after 2 days (control: 21.65 ± 3.81 , DMSO: 22.65 ± 4.79). (D) Alignment of migration rates in control conditions between all GBM lines revealed no significant differences. All experiments were performed in triplicates (3 repetitions with 3 spheroids/assay); values represent mean \pm SD; relative area expression was normalised to spheroid size at 0 h.

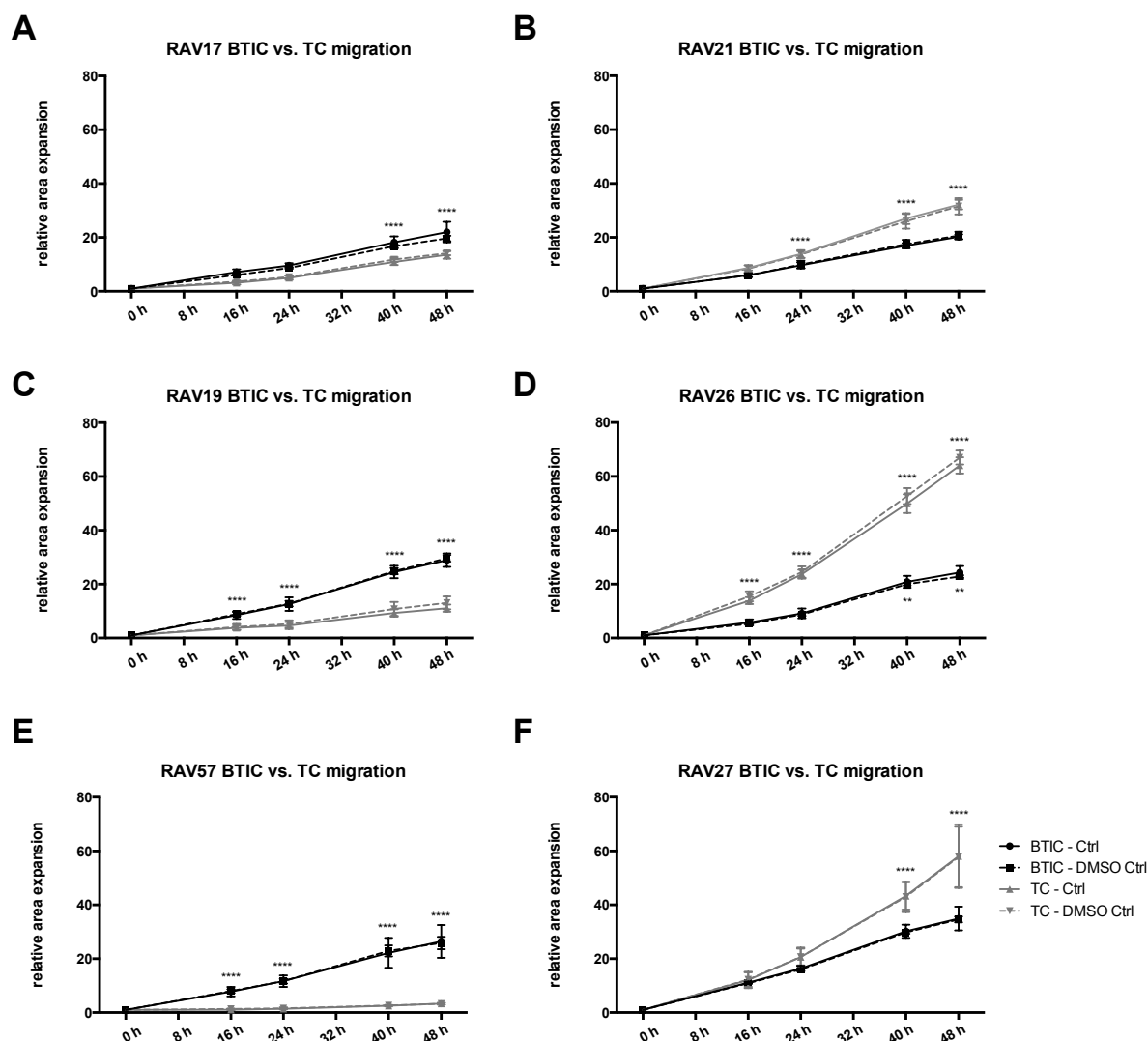


Figure 4-31: Basic migration capacities of BTICs compared to respective TCs

Basic migration rates in control (media) or DMSO treatment are shown for BTICs compared to respective TCs. (A) After 48 h, the area covered by RAV17 BTICs was expanded by ~21-fold (control: 21.01 ± 3.8 , DMSO: 19.65 ± 2.96) compared to the initial spheroid size. Corresponding RAV17 TCs migrated significantly slower (control: 13.57 ± 1.5 , DMSO: 14.12 ± 2.24). (B) RAV21 TCs showed significantly increased (control: 32.19 ± 1.77 , DMSO: 31.54 ± 3.01), almost doubled, migration compared to respective BTICs (control: 20.21 ± 0.9 , DMSO: 20.7 ± 1.4). (C) RAV19 BTICs displayed higher migration (control: 28.93 ± 2.51 , DMSO: 29.6 ± 3.74) compared to RAV17 BTICs. Compared to RAV19 BTICs, respective TCs migrated significantly slower (control: 11.08 ± 1.34 , DMSO: 13.08 ± 2.38). (D) In RAV26 the migration rate was significantly different between BTICs (control: 24.32 ± 2.41 , DMSO: 22.87 ± 1.21) and TCs (control: 64.08 ± 3.01 , DMSO: 67.02 ± 2.58). (E) The migration rate of RAV57 TCs was significant decreased (control: 3.3 ± 0.29 , DMSO: 3.27 ± 0.33) compared to RAV57 BTICs (control: 26.42 ± 6.08 , DMSO: 25.85 ± 6.89). (F) Migration of RAV27 increased from BTICs (control: 34.92 ± 4.41 , DMSO: 34.58 ± 3.22) to TCs (control: 58.01 ± 11.81 , DMSO: 57.81 ± 11.23). All experiments were performed in triplicates (3 repetitions with 3 spheroids/assay); values represent mean \pm SD; relative area expression was normalised to spheroid size at 0 h.; 2way ANOVA analysis with Tukey's multiple comparisons test, ns: $p > 0.05$, *: $p \leq 0.05$, **: $p \leq 0.01$, ***: $p \leq 0.001$, ****: $p \leq 0.0001$.

Analysis of the relative migration rate in each line revealed differences between BTICs and their differentiated counterparts, as well as between proneural and mesenchymal subgroups. Proneural BTICs (Figure 4-31A, C, E) migrated distinctly slower than mesenchymal BTICs and TCs (Figure 4-31B, D, F). Consistently all proneural TCs exhibited decreased migratory capacity, ranging from about 3–14-fold increase of the area covered by cells at 48 h compared to their respective BTIC counterparts (~20–30-fold increase). In contrast, mesenchymal TCs revealed strongly increased migration rates. Those extended from the initial area on average by about 50-fold after 48 h. In comparison, the respective mesenchymal BTICs migrated significantly slower with an average area increase of about 26-fold.

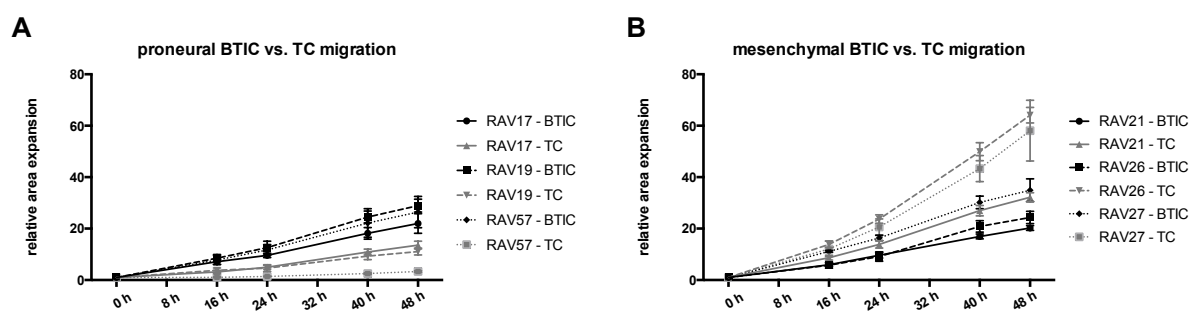


Figure 4-32: Basic migration capacities of proneural compared to mesenchymal lines

Migration rates are depicted for each subtype of BTICs and TCs (shown as relative area expansion normalised to the initial spheroid size at 0 h) at control conditions. (A) All proneural BTICs revealed increased migration compared to their respective TCs. Expansion of the area covered by cells BTIC or TC specimen. (B) Mesenchymal TCs migrated distinctly faster than the respective BTICs. Migration rates did not deviate significantly within individual BTICs, whereas RAV21 TCs migrate distinctly slower than RAV26 and 27 TCs.

Specimen of each subgroup revealed migration rates within the same range, as visualised in Figure 4-32. Proneural BTICs and TCs exhibited distinctly reduced migratory capacity than mesenchymal ones. Upon differentiation, proneural TC migration capacity was significantly reduced compared to their corresponding BTICs. In contrast, mesenchymal TCs showed a significant increase of migratory potential compared to respective BTICs.

No significant differences in migration were observed between DMSO and control media treated cells. Therefore, no further media controls were conducted for experiments using substances dissolved in DMSO.

The mean migration velocity of the cells was calculated in order to estimate the mean migration within spheroid assays (Table 4-3). The covered area after 24 h was assumed as an ideal circle surface area since radial and non-directed migration was expected, the radius was calculated by: $radius = \sqrt{area/\pi}$

Both, BTIC and GBM lines revealed high migration rates ranging from 514.27 μm (HTZ349) to 731.19 μm (RAV27) per day. On average, BTIC migration rates resembled each other (proneural: 626.31 $\mu\text{m day}^{-1}$; mesenchymal: 642.39 $\mu\text{m day}^{-1}$) and exceed those of GBM lines (564.64 $\mu\text{m day}^{-1}$). However, it has to be noted that proneural BTIC were transferred in laminin coated wells to analyse migration. Otherwise proneural BTIC did not show any migration (data not shown). Differentiated proneural TCs displayed reduced migration, only half as fast as BTICs (proneural BTICs: 626.31 $\mu\text{m day}^{-1}$; proneural TCs: 305.96 $\mu\text{m day}^{-1}$). Mesenchymal TCs, however, showed increased migration velocity after proliferation, roughly 1.5-fold elevated (mesenchymal BTICs: 642.39 $\mu\text{m day}^{-1}$; mesenchymal TCs: 947.72 $\mu\text{m day}^{-1}$). Reviewing these results, a clustering becomes apparent, proneural TCs possess decreased migration capacities and mesenchymal TCs exhibit increased migration capacities (Table 4-3).

Category	Mean of migration day ⁻¹ (μm)	Range (± SD)
GBM lines		
A172	559.86	486.76 – 632.96
HTZ349	514.27	465.61 – 562.93
U87	619.78	590.40 – 649.15
GBM lines	564.64	496.98 – 632.29
BTIC		
RAV17	584.72	534.11 – 632.33
RAV19	695.91	666.05 – 725.78
RAV57	598.29	570.59 – 625.98
proneural BTIC	626.31	564.29 – 688.33
RAV21	538.35	530.61 – 546.1
RAV26	656.41	627.11 – 685.72
RAV27	731.19	623.88 – 838.51
mesenchymal BTIC	641.99	540.15 – 743.82
TC		
RAV17	275.08	258.84 – 291.32
RAV19	344.99	309.55 – 380.43
RAV57	297.81	251.76 – 343.86
proneural TC	305.96	261.24 – 350.69
RAV21	803.98	763.16 – 844.80
RAV26	1033.35	1006.28 – 1060.42
RAV27	1005.83	939.64 – 1072.02
mesenchymal TC	947.72	833.94 – 1061.49

Table 4-3: Overview of average migration day⁻¹ of GBM and primary cell lines

4.3.2. Characteristics of primary human BTIC and GBM cell lines

Comprehensive phenotypic characterisation of 3 GBM cell lines and 6 GBM patient-derived BTIC lines revealed certain subgroup clustering (GBM cell lines: Table 4-4, BTIC: Table 4-5). This analysis focused on basal cellular growth and migration capacity, as well as on the protein expression of key factors of essential cellular signalling pathways associated with proliferation, migration, and metabolism. Analysis of protein expression alone failed to cluster the cells according to their subtype as a high degree of variability was observed across the lines. Significant inter-line differences were found during the analysis of proliferation and migration. Proneural BTICs were characterised by moderate migration, slow proliferation, and preferential spheroidal growth *in vitro*. When differentiated, cell growth behaviour changed to adherent growth in monolayers of spindle-shaped cells, often with long protrusions, already separating proneural TCs from BTICs phenotypically (Figure 4-33). Mesenchymal BTICs often grew in an adherent state, similar to respective differentiated cells, which rendered mesenchymal BTICs and TCs phenotypically indistinguishable. Reduced proliferation and migration capacity of proneural compared to mesenchymal TCs was also observed. Moreover, mesenchymal TCs displayed increased migration rates than their corresponding BTICs, while proliferation rates remained similar.

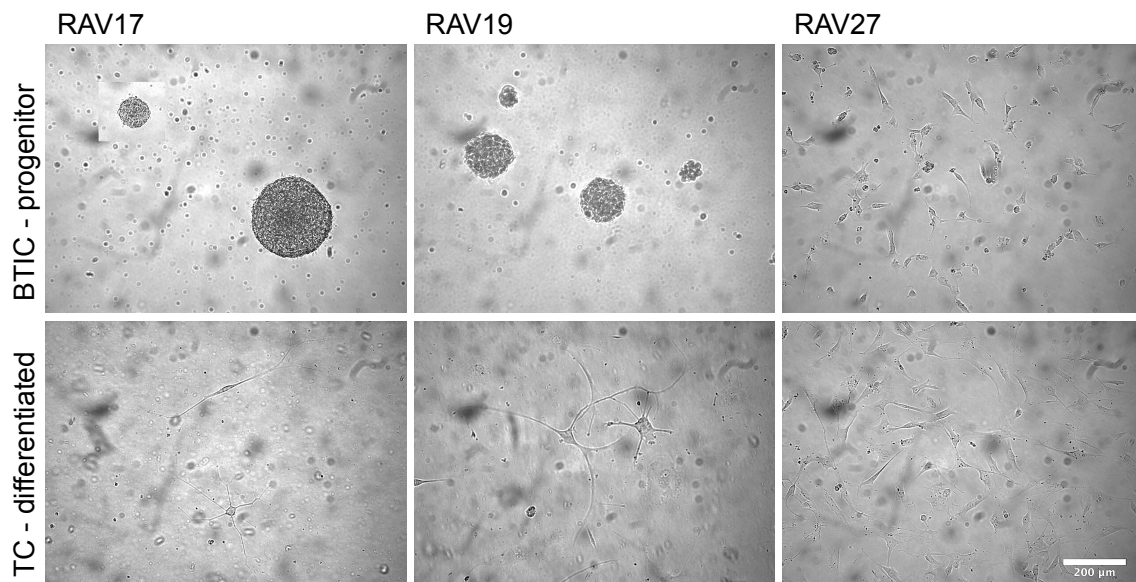


Figure 4-33: Representative BTICs compared to their differentiated TCs

Upper panel: Proneural and mesenchymal BTICs are phenotypically different *in vitro*. Proneural cells (RAV17 and 19) grow in spheres, whereas mesenchymal BTICs (RAV27) grow adherently. Lower panel: Upon differentiation by exposure to FBS, proneural BTICs undergo massive phenotypic change into adherent and spindle shaped cells.

GBM line	Parental tumour		Cell line									
	Histology	WHO grade	Growth <i>in vitro</i>	Proliferation day ⁻¹ (%)	Migration day ⁻¹ (µm)	STAT3 expression	C/EBPβ expression	c-myc expression	mTOR expression	AMPK expression	SMAD2/3 expression	p42/44 MAPK expression
A172	prim. GBM	IV	adherent	63.390	559.86	++	+++	+++	+++	+++	+++	++
HTZ349	prim. GBM	IV	adherent	40.855	514.27	+++	+++	o	++	++	+++	++
U87	Anaplastic astrocytoma	III	adherent	71.442	619.78	+	+	+	+	+	+	+++

Table 4-4: Summarised characteristics of GBM cell lines

General background information of each GBM cell line combined with the data gained in the present work.

Determination of proliferation and migration rates independently revealed incomplete separation of the subgroups of (i) GBM cell lines, (ii) proneural BTICs, (iii) proneural TCs, (iv) mesenchymal BTICs, and (v) mesenchymal TCs as summarised by scatter plots in Figure 4-34A and B. Averaged values of each group revealed significantly distinct separation of mesenchymal TCs from all other groups considering proliferation (Figure 4-34A). Looking at migration rates, specimen of each subgroup clustered together and the groups were set apart, except for proneural and mesenchymal BTICs which overlapped with each other (Figure 4-34B). Correlation of both analyses provided evidence for a unifying pattern that defined each subgroup on the basis of their respective proliferation and migration rate (Figure 4-34C). Proneural BTICs were observed to be characterised by low proliferation and moderate migration, whereas their differentiated counterparts were set apart because of their decreased migration capacity. Mesenchymal BTICs were distinguished by higher proliferation rates, whereas corresponding TCs may be identified by their increased migration. In turn, the GBM cell lines differ by high proliferation and intermediate migration, locating them in the centre of the scatter plot (Figure 4-34C).

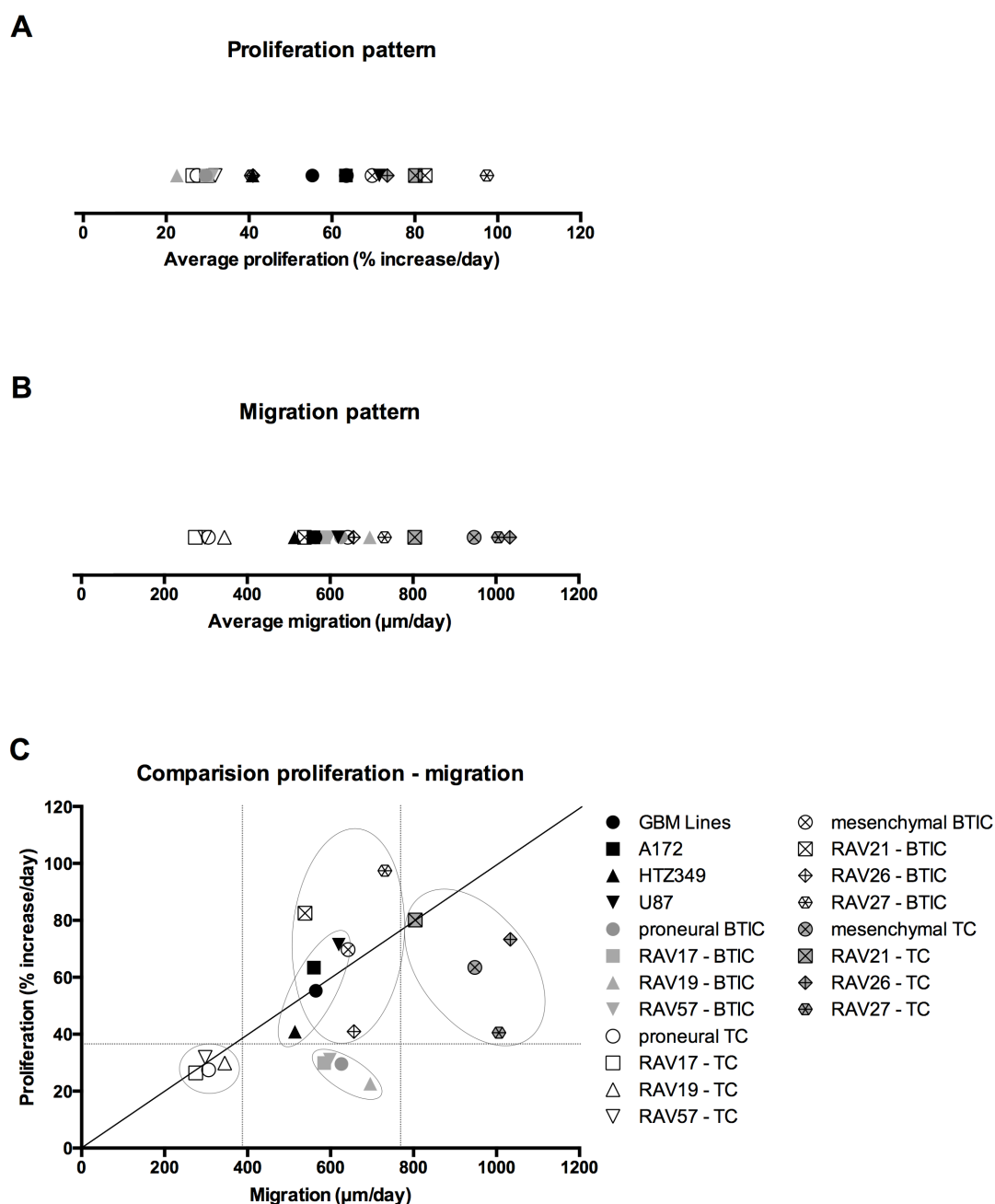


Figure 4-34: Scatter plots comparing proliferation and migration of BTICs, TCs, and GBM cell lines

(A) Percentage proliferation day⁻¹ for each cell line. Proneural BTICs and TCs created separate clusters. Mesenchymal BTICs and TCs, as well as GBM lines, scattered diffusely, rendering segregation of the subgroups according to their proliferation rates impossible. (B) Average migration day⁻¹ for each line. A separate clustering of proneural TCs (decreased migration) and mesenchymal TCs (increased migration) away from all other values was observed. Interjacent GBM lines, proneural, and mesenchymal BTIC overlapped with each other. Thus, segregation of all subgroups according to their migration rates was not possible. (C) Correlation of proliferation and migration rates. Proneural TCs clustered separately due to their slow proliferation and migration. As proneural BTICs possessed a higher migration capacity, they were set apart from their corresponding TCs. Due to slow proliferation of proneural BTICs, they were also separated from the other groups. GBM cell lines were located in the centre. Mesenchymal BTICs were separated from GBM lines by increased proliferation, with exception of RAV26. Mesenchymal TCs were separated from the other groups by increased migration.

BTIC		RAV17	RAV19	RAV39	RAV57	RAV01	RAV21	RAV24	RAV26	RAV27	RAV28
Parental tumour	Histology	prim. GBM	prim. GBM	prim. GBM	prim. GBM	prim. GBM	prim. GBM	prim. GBM	prim. GBM	sec. GBM	prim. GBM
	WHO grade	IV	IV	IV	IV	IV	IV	IV	IV	IV	IV
	Age	52	52	72	49	44	46	55	69	42	78
	Survival (weeks)	65	16	55	82	75	75	70	66	34	58
	MGMT-methylation (%)	0	0	4	0	n.a.	19	17	100	0	100
	IDH1 (wt/mut.)	wt	wt	wt	wt	n.a.	n.a.	wt	wt	p.R132H	wt
Primary cells	Growth <i>in vitro</i>	spheres	sphere	sphere	semi-adherent	adherent	adherent	semi-adherent	adherent	adherent	adherent
	MGMT-methylation (%)	1	2	8	0	19	100	12	100	32	13
	IDH1 (wt/mut.)	wt	wt	n.a.	n.a.	n.a.	wt	n.a.	n.a.	wt	wt
	CD133+ (%)	1	3	6	0	0	1	6	29	62	0
	Proliferation day ⁻¹ (%)	29.88	22.61	n.a.	31.11	n.a.	82.49	n.a.	40.94	97.42	n.a.
	Migration day ⁻¹ (µm)	584.72	695.91	n.a.	598.29	n.a.	538.35	n.a.	656.41	731.19	n.a.
	STAT3 expression	++	++	+	++	+++	+++	+++	++	++	++
	C/EBPβ expression	+	+	+	+	+	++	+	+	++	+
	c-myc expression	++	++	+	++	+	+	+	o	+	o
	mTOR expression	+	+	+	++	++	+	++	++	++	+
	AMPK expression	+	o	+	++	+	+	+	+	+	+
	SMAD2/3 expression	++	++	++	+++	++	+	+	+	+	++
	p42/44 MAPK expression	+	++	+	++	++	++	++	++	++	+++

Table 4-5: Summarised characteristics of BTIC lines

Characteristics of each BTIC line combined with the data gained in the present work. RAV17, 19, 39 and 57 were defined as proneural and match the Verhaak criteria (Verhaak *et al.* 2010; Moeckel *et al.* 2014), whereas RAV1, 21, 24, 26, 27 and 28 were classified as mesenchymal.

4.3.3. STAT3 inhibition reduces GBM cell migration and proliferation

4.3.3.1. Effects of Diclofenac and Ibuprofen on glioma cell lines

Since NSAIDs have been found to have anti-tumourigenic effects (Sørensen *et al.* 2003; Ulrich *et al.* 2006), the NSAIDs ibuprofen and diclofenac were applied to GBM cell lines. Both agents proved to restrain proliferation and migration. Diclofenac is known to have impact on LDH-A (Gottfried *et al.* 2013; Chirasani *et al.* 2013), which is in turn a direct target of c-myc (Shim *et al.* 1997). c-myc can be a down stream target of STAT3 (Bromberg, 2001), therefore, STAT3 and c-myc levels were investigated as possible modulators of the observed functional effects. Both, diclofenac and ibuprofen were found to modulate STAT3-associated glioma invasion in a non-specific manner (Leidgens *et al.* 2015).

First, proliferation and migration of the GBM cell lines A172, HTZ349, and U87 were investigated after treatment with ibuprofen or diclofenac. IC₅₀ was determined prior to these assays (Leidgens *et al.* 2015). Effect of the NSAIDs on proliferation was investigated by cultivation of the cell lines in the presence of increasing diclofenac (0.05 – 0.2 mM) or ibuprofen (0.5 – 2 mM) concentrations and appropriate controls, over a 120 h period. Daily measurements revealed that proliferation was significantly impaired depending on increasing dosages of diclofenac (Figure 4-35A, C, E) or ibuprofen (Figure 4-35B, D, F). Starting at either 72 or 96 h, all dosages demonstrated significant anti-proliferative effects ($p \leq 0.0001$) on all cell lines. Both agents were most effective on cell line HTZ349, followed by A172 and then U87.

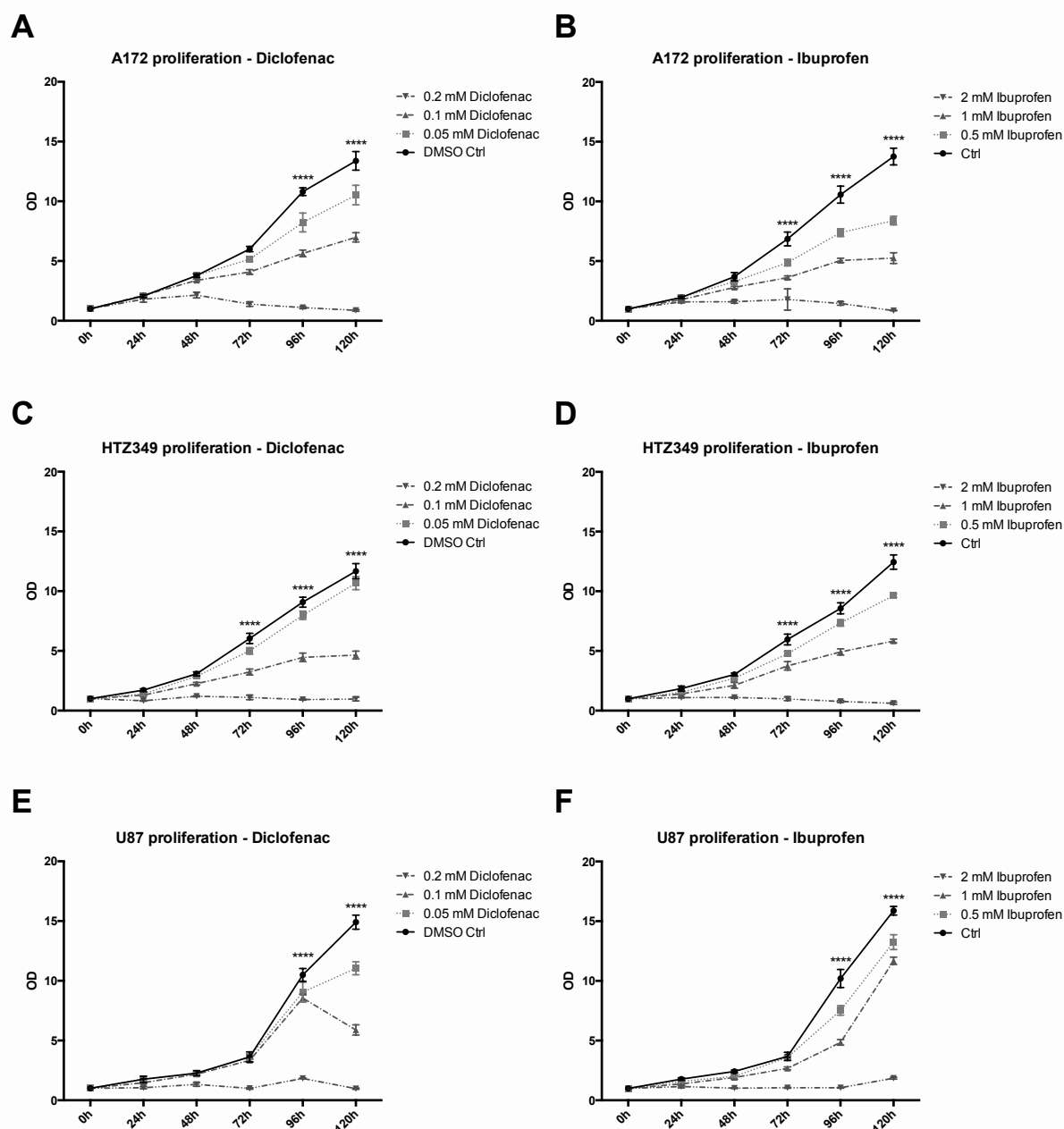


Figure 4-35: GBM cell line proliferation after diclofenac or ibuprofen treatment

(A) At 96 h and 120 h, all diclofenac concentrations exhibited significant reduction of A172 proliferation (compared to DMSO control) (B) Ibuprofen demonstrated significant proliferation decrease at all concentrations used, starting at 72 h (in comparison to non-treated media control). (C) At 72 h, all diclofenac concentrations showed a significant reduction of HTZ349 proliferation. (D) Similar effects were obtained with ibuprofen at respective concentrations in HTZ349. (E) U87 proliferation was demonstrated to be significantly decreased by all diclofenac concentrations applied from 96 h onwards. (F) Ibuprofen effectively reduced proliferation of U87 at all concentrations from 96 h onward. All experiments were performed in triplicates (3 measurements/assay); values represent mean \pm SD; 2way ANOVA analysis, 95% CI, ns: $p > 0.05$, *: $p \leq 0.05$, **: $p \leq 0.01$, ***: $p \leq 0.001$, ****: $p \leq 0.0001$.

To further investigate the restricting effects of diclofenac and ibuprofen on glioma cells, their influence on migration was investigated by spheroid assays. Here, spheroids of GBM cells were cultured in the presence of increasing diclofenac or ibuprofen concentrations, and cells were given 30 h to migrate away from the initial spheroid. Strong inhibitory effects on migration were noticeable with all diclofenac concentrations in A172 and HTZ349 (Figure 4-36A and C). Starting 24 h after treatment, concentration- and time-dependent migration-inhibiting effects were observed. In contrast, U87 were resistant to diclofenac until 30 h of treatment, after this time 0.1 and 0.2 mM demonstrated significant restriction of migration (Figure 4-36E).

Ibuprofen demonstrated a significantly greater reduction of migration effect in all GBM cell lines (Figure 4-36B, D, F) than diclofenac. Most prominent effects were observed in HTZ349. 30 h after exposure to 2 mM ibuprofen, spheroid diameters were only 45% that of the respective control spheroids. Diclofenac treated (0.2 mM) cells covered 68% of the area respective to that covered by control cells. A highly significant restriction of migration for U87 cells was observed from ibuprofen, whereas diclofenac had only minor effects. Exposure to 2 mM ibuprofen resulted in significantly decreased migration starting at 6 h after treatment (Figure 4-36F).

The observed reduction of migration is likely independent of proliferation, since significant reduction of proliferation was measurable only from 72 h on, as shown in Figure 4-36.

As outlined above, STAT3 and c-myc were investigated as possible modulators of the observed anti-proliferative and -migratory effects. Analysis of the relative protein expression of c-myc, pSTAT3, STAT3, and LDH-A in GBM cell lines after 24 h exposure to diclofenac or ibuprofen treatment revealed that increasing concentrations of both NSAIDs led to reduced STAT3 phosphorylation without affecting total STAT3 expression (Figure 4-37). Expression of c-myc was enhanced significantly after treatment with ibuprofen, whereas diclofenac reduced c-myc protein expression. The c-myc inducing effect of ibuprofen was consistently observed to varying extents in all cell lines, while diclofenac acted contrastingly in A172 and HTZ349 (Figure 4-37). Pictures of exemplary Western blots and further analysis can be found in (Leidgens *et al.* 2015).

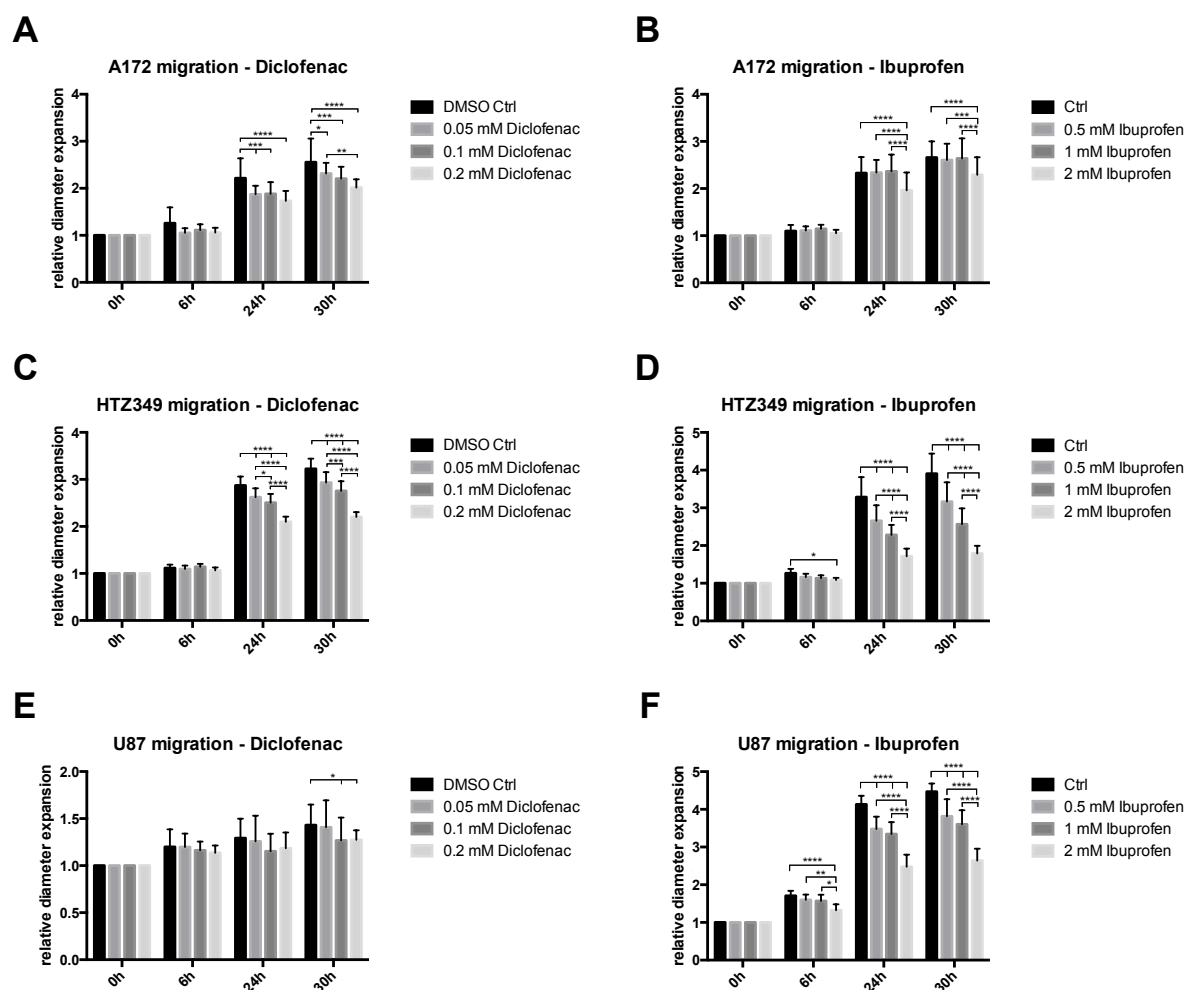


Figure 4-36: GBM cell line migration after diclofenac or ibuprofen treatment

A migration decrease caused by diclofenac or ibuprofen treatment was measured in all three GBM lines. (A) Diclofenac caused decreased migration in a time- and concentration-dependent manner for A172 starting at 24 h after treatment. (B) Ibuprofen exposure resulted in similar, but less pronounced, effects than diclofenac. (C) HTZ349 migration was shown to be reduced by diclofenac from 24 h on. (D) In HTZ349, 2 mM ibuprofen resulted in a noticeable and significant migration restriction already at 6 h. (E) U87 cells exhibited resistance to all diclofenac concentrations until 30 h of exposure. (F) In contrast, response was increased in U87 cells after ibuprofen treatment and 2 mM achieved significant inhibition of migration already after 6 h. All experiments were performed in triplicates; values represent mean \pm SD; relative area expression were normalised to spheroid size at 0 h; 2way ANOVA analysis with Tukey's multiple comparisons test, 95% CI, ns: $p > 0.05$, *: $p \leq 0.05$, **: $p \leq 0.01$, ***: $p \leq 0.001$, ****: $p \leq 0.0001$.

Category	Doubling time (h)	Migration day ⁻¹ (μm)	Doubling time (h)	Migration day ⁻¹ (μm)	Doubling time (h)	Migration day ⁻¹ (μm)	Doubling time (h)	Migration day ⁻¹ (μm)
Diclofenac in mM	none		0.05		0.1		0.2	
A172	27.958	527.938	31.580	431.438	38.468	456.688	81.611	368.250
HTZ349	30.161	785.375	32.040	687.438	44.501	645.750	178.310	477.375
U87	28.304	152.688	32.957	118.063	42.117	74.687	117.863	94.063
average GBM lines	28.808	488.667	32.192	412.313	41.695	392.375	125.928	313.229
Ibuprofen in mM	none		0.5		1.0		2.0	
A172	27.958	613.547	33.284	605.757	41.061	619.485	180.269	439.382
HTZ349	30.161	1003.462	33.353	721.900	41.776	555.918	-	309.984
U87	28.304	1591.345	32.957	1238.461	42.117	1162.158	-	739.453
average GBM lines	28.808	1069.451	33.198	855.373	41.651	779.187	60.090	496.273

Table 4-6: Summary of doubling times and migration rates of GBM cell lines after NSAID treatment

Treatment of GBM cell lines with either diclofenac or ibuprofen resulted in increased doubling times, and concentration dependent decreased migration rates. In both cases, the highest dosages were most effective, although only 2 mM ibuprofen blocked proliferation completely in A172 and HTZ349. For more details, see appendix Table 9-1 and Table 9-2.

In summary, the NSAIDs diclofenac and ibuprofen were able to demonstrate a homogeneous response in restriction of proliferation and migration of GBM cells (Table 4-6) with stronger effects observed from ibuprofen treatment. Remarkable diversity in the mechanisms of action between the drugs was found via protein expression analysis, see Figure 4-37. In agreement with (Chirasani *et al.* 2013), STAT3 phosphorylation at Y705 was non-specifically prevented by both agents. However, different down-stream effects were detected as diclofenac reduced c-myc expression, while ibuprofen induced it.

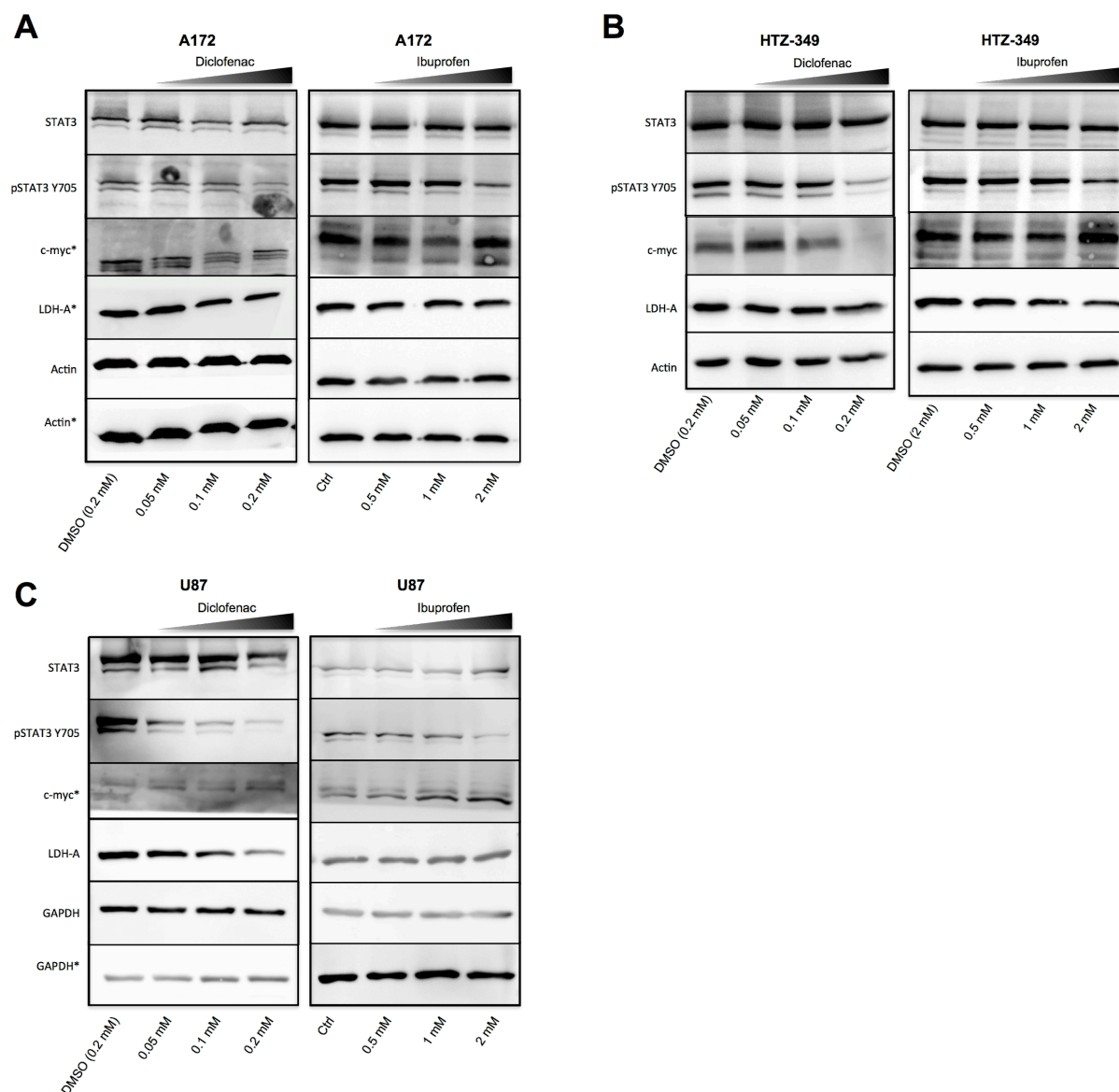


Figure 4-37: Protein expression in GBM cell lines after diclofenac or ibuprofen treatment

(A) Depending on concentration, diclofenac or ibuprofen reduced STAT3 phosphorylation significantly without affecting total STAT3 levels. c-myc was observed to be significantly down-regulated by diclofenac, whereas ibuprofen treatment resulted in the tendency of increased protein expression. LDH-A tended to be reduced, but not to significant extent. (B) Distinct effects were exhibited with diclofenac in HTZ349, as pSTAT3 and c-myc were observed to be reduced in a concentration-dependent way and LDH-A exhibited a tendency towards decreased expression. In contrast, after ibuprofen treatment, expression of c-myc was shown to be significantly increased in a concentration-dependent manner. Additionally, a trend towards reduced pSTAT3 expression was observed. (C) Depending on ibuprofen and diclofenac concentrations, a significantly reduced pSTAT3 was observed, without affecting total STAT3. Expression titres of c-myc was not affected by diclofenac, whereas ibuprofen caused significant expression increase. A concentration dependent significant decrease, was observed for LDH-A when cells were exposed to diclofenac, while ibuprofen did not affect protein amounts. All Western blots were performed in triplicates, quantifications are detailed in the appendix Figure 9-3.

4.3.3.2. Specific STAT3 inhibition to restrain glioma cells

To further assess the importance of STAT3 in glioma cell migration and proliferation, STAT3 was directly modulated through Stattic. Approaches like transient siRNA transfection and stable lentiviral transduction are difficult to transfer to the OBSC model as well as to patient treatment. Therefore, the small molecule inhibitor Stattic (Schust *et al.* 2006) presents an effective alternative. Stattic binds specifically to the STAT3 phosphorylation site at Y705 and prevents its phosphorylation, as verified by protein expression (Figure 4-38). After application of Stattic, decreased cell proliferation and migration were detected. Stattic was used in concentrations ranging from 0.625 to 20 μM , since some studies (Villalva *et al.* 2011) revealed high cytotoxicity rates *in vitro* even with low Stattic concentrations ($\leq 2.5 \mu\text{M}$), whereas others administered 17.75 μM Stattic (3.75 mg kg^{-1}) (Scuto *et al.* 2011), or 47.35 μM (10 mg kg^{-1}) (Spitzner, Roesler *et al.* 2014) without side effects in their animal models.

4.3.3.2.1. Targeting STAT3 directly – effects on molecular level

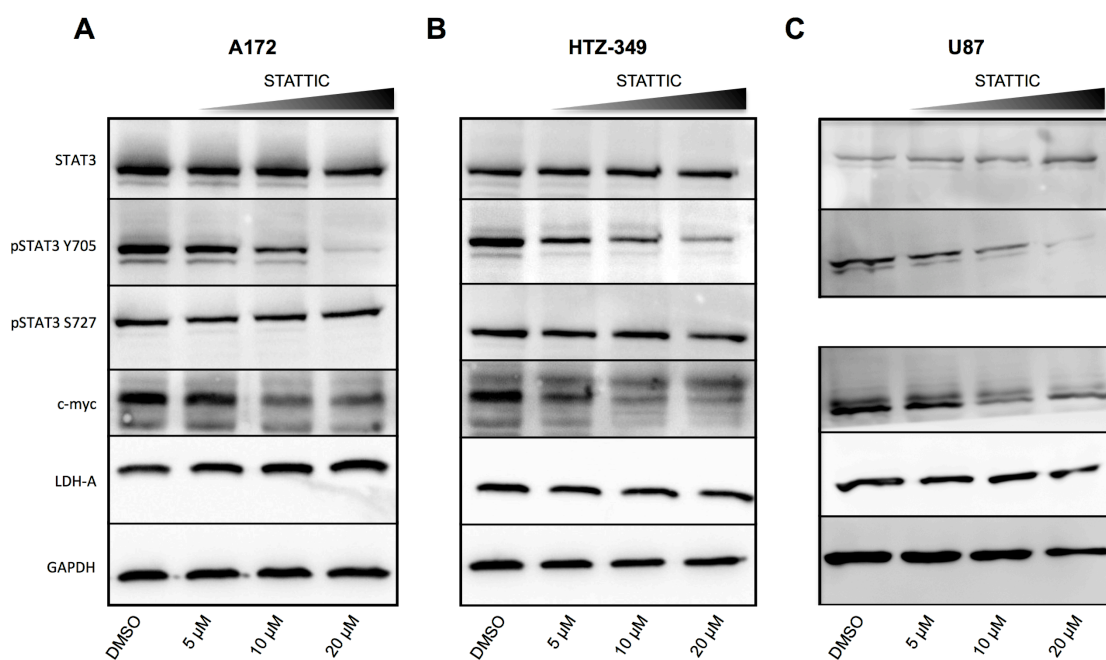


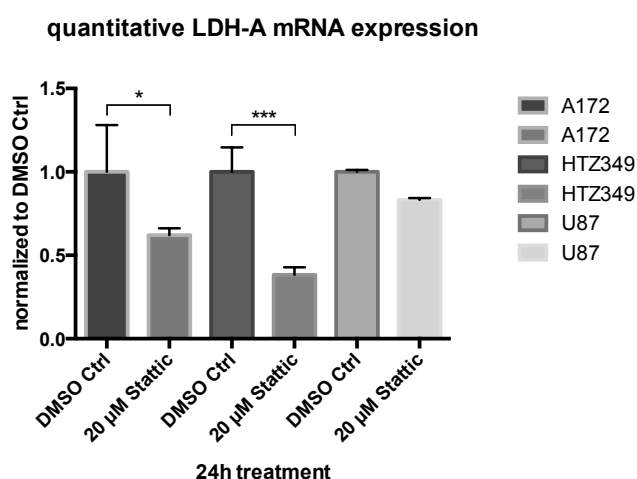
Figure 4-38: Exemplary Western blots of protein expression in GBM lines after Stattic treatment

Cells were treated with increasing concentrations of Stattic: 5, 10, and 20 μM for 24 h prior to protein isolation. (A) A172 displayed pSTAT3 Y705 expression decrease with increasing Stattic concentrations, 10 μM treatment led to moderate and 20 μM to almost complete inhibition. Changes in STAT3 levels were not observed. c-myc expression was decreased at 10 and 20 μM Stattic, while LDH-A levels remained constant. (B) In HTZ349, pSTAT3 Y705 and c-myc levels were decreased at 5 μM , already. STAT3, pSTAT3 S727, and LDH-A levels remained stable. (C) In U87, pSTAT Y705 and c-myc titres were decreased concentration dependently, whereas STAT3 and LDH-A were not altered. pSTAT3 S727 was not analysed as levels were not altered in the other lines. For quantification, see appendix Figure 9-4.

Western blot analyses were performed with GBM cell lines to ensure that Stattic targeted and diminished pSTAT3 Y705 levels, illustrated in Figure 4-38. A172, HTZ349, and U87 revealed a visible response to Stattic as down regulation of pSTAT3 Y705 was seen with increasing Stattic concentrations. Total STAT3 and pSTAT3 S727 were not, or only slightly, modulated. Along with pSTAT3 Y705, levels of the STAT3 target, c-myc, decreased. Protein levels of the c-myc target LDH-A were not affected by Stattic treatment. As LDH-A persists with a long protein half-life (Parra-Bonilla *et al.* 2013), mRNA expression was assessed to detect altered gene expression, via qRT-PCR after 24 h exposure of the cells either to diclofenac or ibuprofen (Figure 4-39). For A172 and HTZ349, a significant decrease of LDH-A was confirmed after exposure to Stattic, while for U87, a negative trend was observed.

Figure 4-39: Quantitative real-time PCR of GBM cell lines after Stattic treatment

Quantitative RT-PCR revealed inter-line diversity. LDH-A protein expression was not decreased within 24 h of exposure to Stattic. mRNA levels were shown to be significantly decreased in A172 and HTZ349 compared to DMSO control. Stattic had a small effect on LDH-A mRNA expression in U87 cells. qRT-PCR were performed in triplicates; values represent mean \pm SD; one-way ANOVA analysis with Tukey's multiple comparisons test, 95% CI, ns: $p > 0.05$, *: $p \leq 0.05$, ***: $p \leq 0.001$.



4.3.3.2.2. Targeting STAT3 directly – effects on proliferation

The influence of targeted prevention of STAT3 phosphorylation at Y705 by Stattic on proliferation of BTIC, TC, and GBM cell lines was assessed by CyQuant analyses. Figure 4-40 – Figure 4-42, and Table 4-7, show that proliferation was decreased Stattic concentration dependently.

Comparison of the three GBM cell lines A172, HTZ349, and U87, revealed inter-line variances (Figure 4-40) as A172 and HTZ349 were observed to remain mostly unaffected by Stattic treatment – except at highest concentrations. In contrast, U87 has shown to respond with decreased proliferation even at lowest concentrations. Summarised data revealed proliferation-reducing effects to be more pronounced with increasing Stattic concentrations.

Proneural BTICs and respective TCs responded in a time- and concentration-dependent manner to Stattic treatment (Figure 4-41). All BTICs had earlier responses to Stattic treatment than TCs, as proliferation was decreased with lower Stattic concentrations. As evident from Figure 4-41, RAV19 BTICs (C) and the corresponding RAV19 TCs (D) represent the best example of high sensitivity to Stattic in BTICs, while TCs were more resistant. High Stattic concentrations ($\geq 10 \mu\text{M}$), and the lowest concentration of $0.625 \mu\text{M}$, caused a significant decline of proliferation in RAV57 TC (F), which was also visible in aggregated data of all proneural TCs (H). Intermediate concentrations of $1.25 - 5 \mu\text{M}$ failed to reduce proliferation. Cell doubling times, depicted in the appendix (Table 9-3), reflected these findings. It should, however, be noted that higher Stattic concentrations may cause growth arrest or cell death as proliferation rates dropped below the initial value. It can be seen from the percentage growth rates of all analysed cell lines that proneural BTIC proliferation was affected earlier by lower Stattic concentrations (RAV19: $2.5 \mu\text{M}$, RAV57: $5 \mu\text{M}$, RAV17: $10 \mu\text{M}$) than TC proliferation (RAV17: $10 \mu\text{M}$, RAV19: $15 \mu\text{M}$, RAV57: $20 \mu\text{M}$).

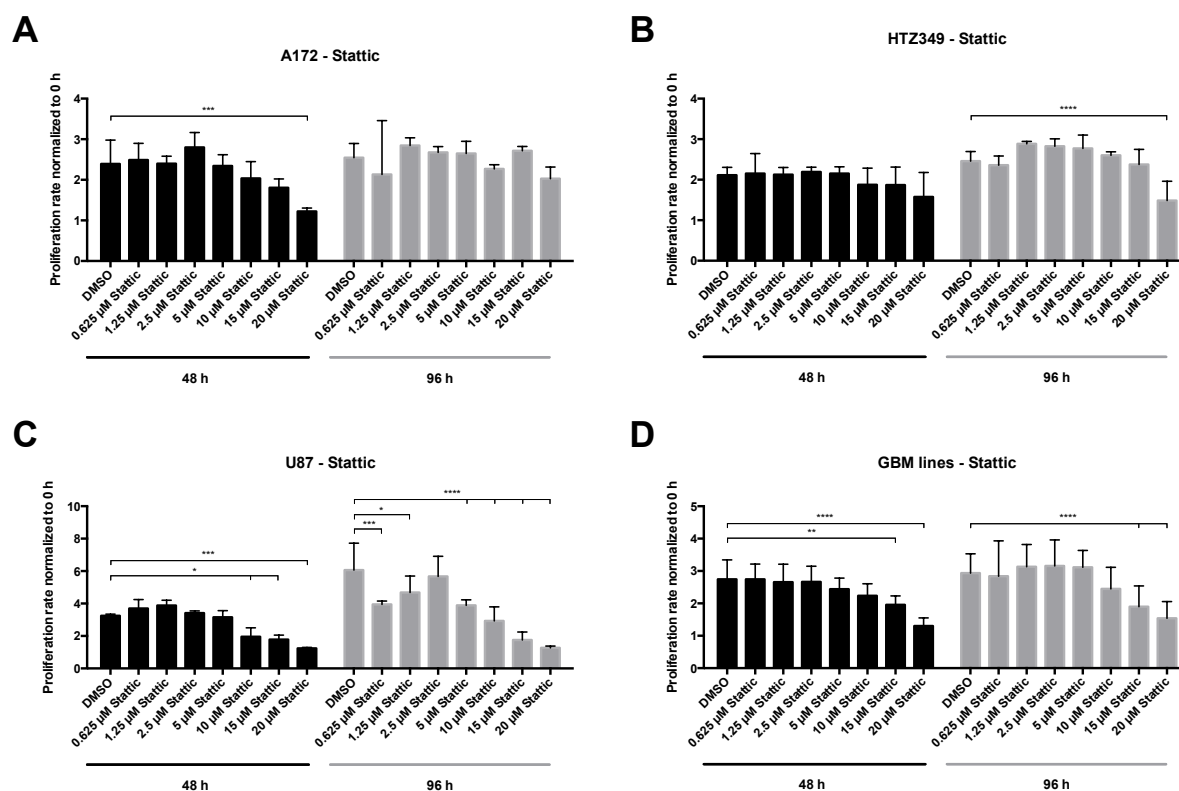


Figure 4-40: Proliferation of GBM cell lines after Stattic treatment

Proliferation rates were normalised to the initial fluorescence at 0 h. (A) A172 were observed to remain unaffected by treatment with low Stattic concentrations, which declined with increasing concentrations (10 – 20 μM). At 48 h proliferation was significantly reduced by 20 μM of Stattic, while the effect was compensated at 96 h. (B) HTZ349 remained unchanged by Stattic, only 20 μM slowed proliferation down significantly after 96 h. (C) Proliferation dropped significantly in concentration-dependent over time for U87. At 48 h, higher concentrations, 10 – 20 μM of Stattic, reduced proliferation significantly, whereas after 96 h, even low concentrations reached significance, with the exception of 2.5 μM. (D) Aggregate data of all GBM lines verified the observation of decreased proliferation at high Stattic concentrations. All experiments were performed twice each with 3 measurements/assay; values were normalised to 0 h control and represent mean \pm SD. 2way ANOVA analysis with Tukey's multiple comparisons test, ns: $p > 0.05$, *: $p \leq 0.05$, **: $p \leq 0.01$, ***: $p \leq 0.001$, ****: $p \leq 0.0001$. Significances between every condition are detailed in the statistics on the enclosed CD.

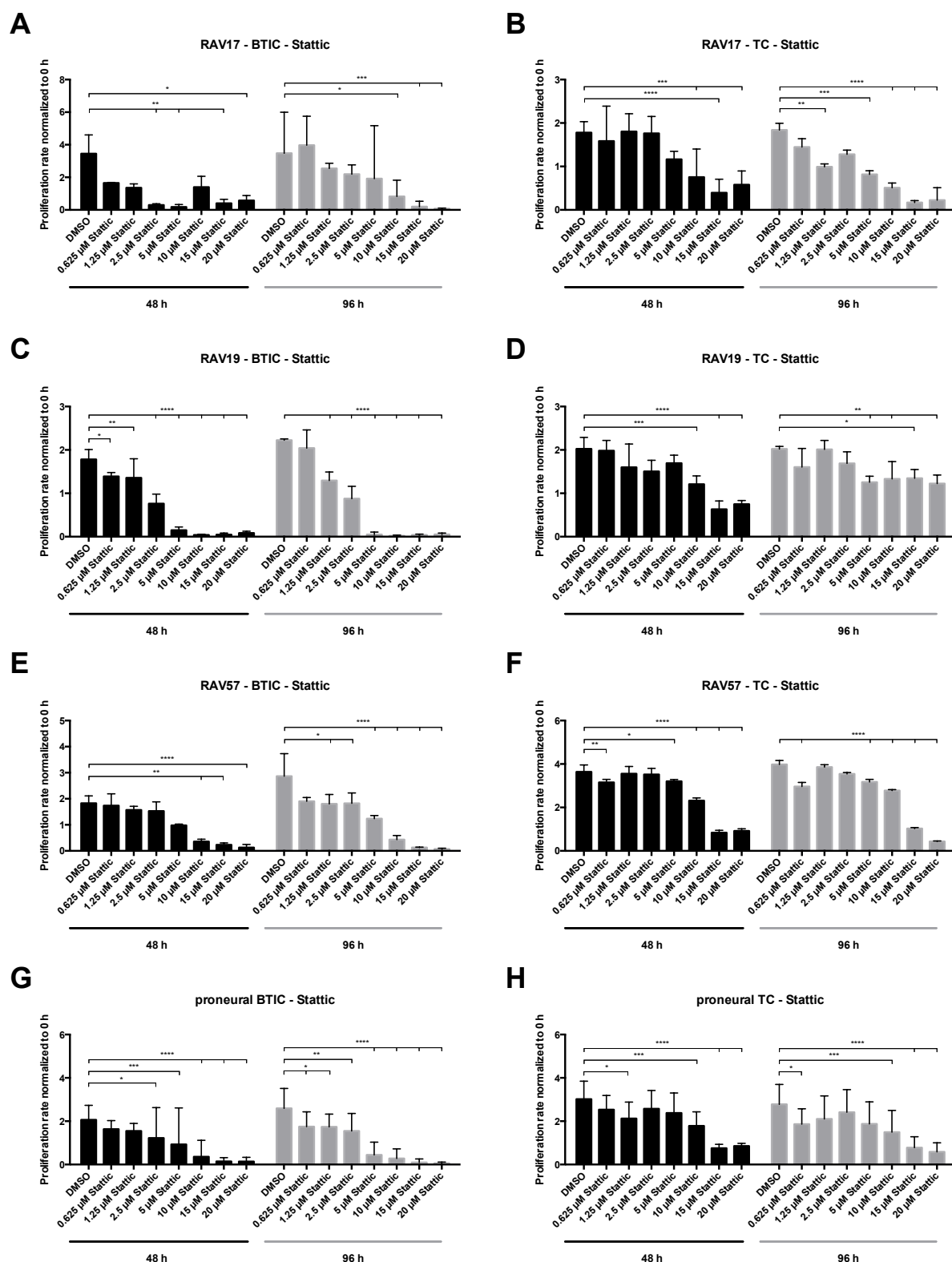


Figure 4-41: Proliferation of proneural BTICs and corresponding TCs after Stattic treatment

Proliferation rates were normalised to the initial fluorescence at 0 h. (A) RAV17 BTIC proliferation was observed to be decreased by most concentrations of Stattic. Even at lowest concentrations, proliferation dropped remarkably at 48 h. (B) Proliferation of RAV17 TCs was decreased in a time- and concentration-dependent

manner. Even low concentrations ($\geq 1.25 \mu\text{M}$) resulted in significant decreases of proliferation rates after 96 h. (C) Proliferation of RAV19 BTICs was found to be decreased depending on concentration and time, with response to even the lowest dosage used ($0.625 \mu\text{M}$, 48 h). (D) RAV19 TCs responded similarly to Stattic as was observed for RAV19 BTICs, although with delayed effects. (E) RAV57 BTICs exhibited a time- and concentration-dependent decrease in proliferation, which was significant at the highest concentrations ($\geq 10 \mu\text{M}$) after 48 h, whereas lower concentrations ($\geq 1.25 \mu\text{M}$) were only effective after 96 h. (F) RAV57 TCs responded to higher Stattic concentrations ($\geq 5 \mu\text{M}$) at 48 and 96 h with proliferation decrease, where $0.625 \mu\text{M}$ also caused a significant decline of proliferation. (G) Aggregated data confirmed time- and concentration-dependent proliferation reducing effect of Stattic in proneural BTICs. (H) In contrast, aggregated data of proneural TCs revealed response to the lowest and high Stattic concentrations, while intermediate concentrations failed to reduce proliferation. All experiments were performed twice with each 3 measurements/assay, values were normalised to 0 h control and represent mean \pm SD. 2way ANOVA analysis with Tukey's multiple comparisons test, ns: $p > 0.05$, *: $p \leq 0.05$, **: $p \leq 0.01$, ***: $p \leq 0.001$, ****: $p \leq 0.0001$. Significances between every condition are detailed in the statistics on the enclosed CD.

Comparing Figure 4-41 and Figure 4-42 (each A, C, E, G), restriction of proliferation required, on average, higher Stattic concentrations in mesenchymal BTICs than in proneural BTICs. All BTIC lines remained unaffected upon low dosage ($0.625 - 2.5 \mu\text{M}$) treatment, but responded remarkably starting at $2.5 \mu\text{M}$ (48 h) or $5 \mu\text{M}$ (96 h). Whereas in proneural BTICs proliferation was observed to be reduced in a time- and concentration-dependent manner, in mesenchymal BTICs proliferation was unchanged at first, however, a sudden decline from the initial value was observed with Stattic concentrations $\geq 5 \mu\text{M}$. In general, mesenchymal TC proliferation rates declined in a concentration-dependent manner, but required higher Stattic concentrations to reach significance. Inter-line variance was also observed, RAV21 TCs responded with significantly reduced proliferation to $0.625 \mu\text{M}$ and high concentrations of Stattic, whereas intermediate dosages were not effective. RAV27 TCs (Figure 4-42F) were resistant to Stattic, only $20 \mu\text{M}$ decreased proliferation significantly after 96 h of treatment.

Effects of Stattic on proliferation corresponded to observed doubling times (Table 4-7, appendix Table 9-3). A striking difference in the concentrations required to decrease proliferation by half (IC_{50}) was revealed. Mesenchymal BTIC proliferation dropped below the initial value with concentrations ranging from 2.5 to $10 \mu\text{M}$ Stattic (RAV26: $2.5 \mu\text{M}$, RAV27: $5 \mu\text{M}$, RAV21: $10 \mu\text{M}$), whereas mesenchymal TCs required concentrations between 15 and $20 \mu\text{M}$ Stattic (RAV21, RAV26: $15 \mu\text{M}$, RAV27: $20 \mu\text{M}$).

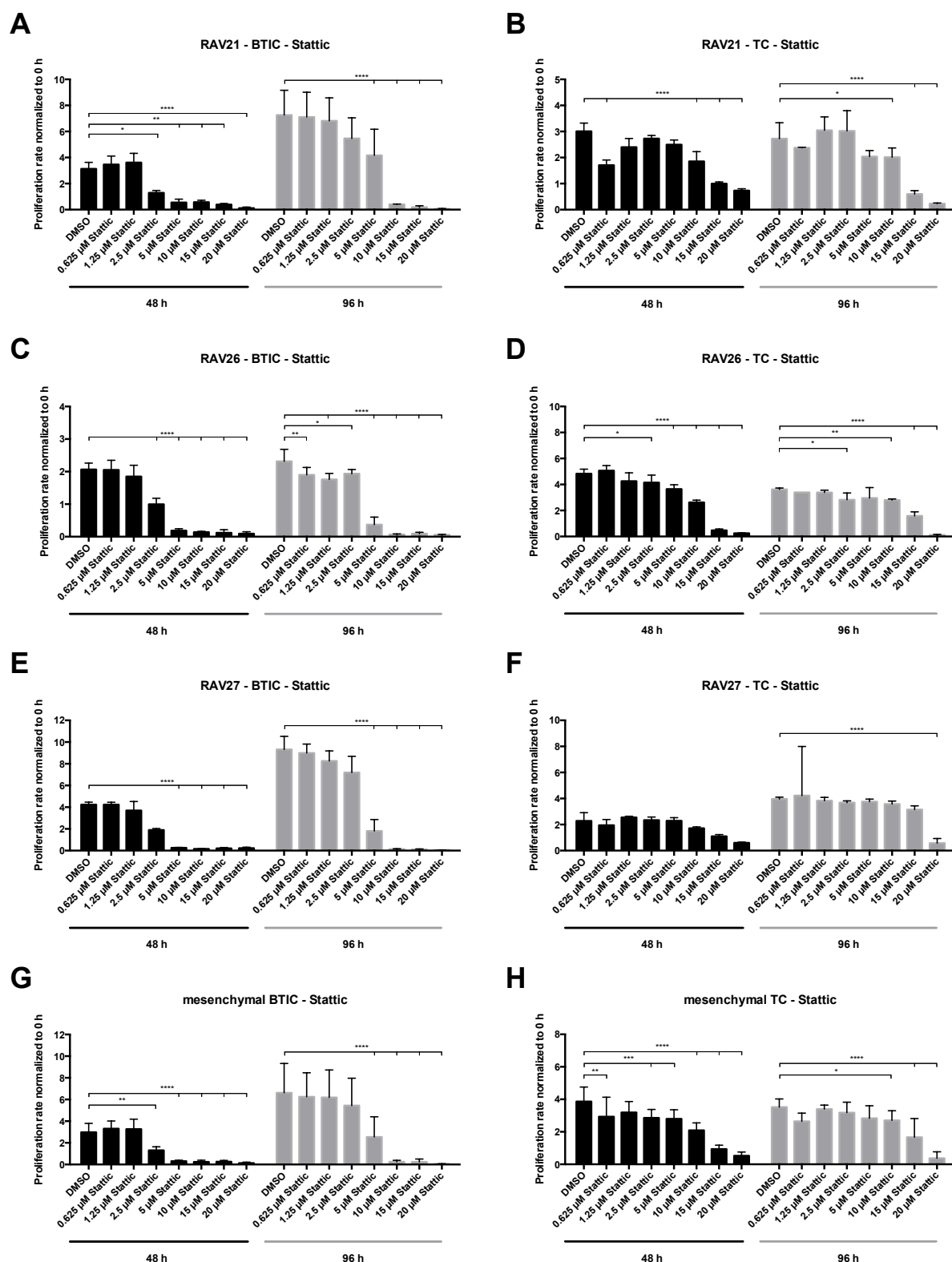


Figure 4-42: Proliferation of mesenchymal BTICs and corresponding TCs after Stattic treatment

Proliferation rates were normalised to the initial fluorescence at 0 h. (A) RAV21 BTIC proliferation was decreased, marked by a sudden drop of proliferation with $\geq 2.5 \mu\text{M}$ Stattic at 48 h and $\geq 10 \mu\text{M}$ at 96 h. (B) In general, corresponding RAV21 TCs were observed to be less sensitive than RAV21 BTICs,

but proliferation was decreased with low concentrations of Stattic as well, while it remained unchanged at intermediate concentrations. (C) Proliferation of RAV26 BTICs was found to decrease similarly to RAV21 BTICs. (D) RAV26 TCs were observed to respond in a concentration-dependent manner at 48 h with strong effects at highest concentrations (15, 20 μ M). At 96 h, effects were less prominent, but significant beginning at 10 μ M. (E) RAV27 BTICs remained unchanged by low dosages (0.625, 1.25 μ M), but proliferation declined suddenly with concentrations ≥ 2.5 μ M (48 h) or 5 μ M (96 h). (F) RAV27 TC proliferation remained constant at most conditions, but a trend towards reduction can be seen at 48 h starting with 10 μ M Stattic. At 96 h proliferation was uniform, only 20 μ M Stattic treatment resulted in a significant decline. (G) Aggregated data of mesenchymal BTICs confirmed the indicated resistance to low Stattic dosages, but remarkable decline of proliferation rates at ≥ 2.5 μ M (48 h) or ≥ 5 μ M (96 h). (H) In contrast, aggregated data of mesenchymal TCs revealed a strong concentration-dependent reduction in proliferation upon Stattic treatment at 48 h, which was partially compensated after 96 h. Therefore, mesenchymal TC proliferation required higher Stattic concentrations to be effectively reduced than BTIC proliferation. All experiments were performed twice with each 3 measurements/assay, values were normalised to 0 h control and represent mean \pm SD. 2way ANOVA analysis with Tukey's multiple comparisons test, ns: $p > 0.05$, *: $p \leq 0.05$, **: $p \leq 0.01$, ***: $p \leq 0.001$, ****: $p \leq 0.0001$. Significances between every condition are detailed in the statistics on the enclosed CD.

In summary, it can be stated that prevention of STAT3 phosphorylation at Y705 caused concentration-dependent decline of proliferation. Effects were consistent in proneural and mesenchymal BTICs, as their proliferation was reduced upon treatment with about 5 μ M Stattic. TCs differed in their response to treatment. The results indicated that for reduction of TC proliferation higher Stattic concentrations are required as for BTICs. Of note, proliferation of the GBM cell lines A172 and HTZ349 was found to be almost independent of STAT3, only U87 seemed reliant on phosphorylated STAT3.

4.3.3.2.3. Targeting STAT3 directly – effects on migration

A proliferation-restricting effect mediated by targeted prevention of STAT3 phosphorylation at Y705 via Stattic treatment was observed. Therefore, an influence on migration was predicted for cells treated with Stattic. As previously described, migration was analysed by spheroid assays. Exemplary pictures of the respective GBM cell lines are depicted in Figure 4-43, which reveal a concentration-dependent inhibitory effect of Stattic on migration.

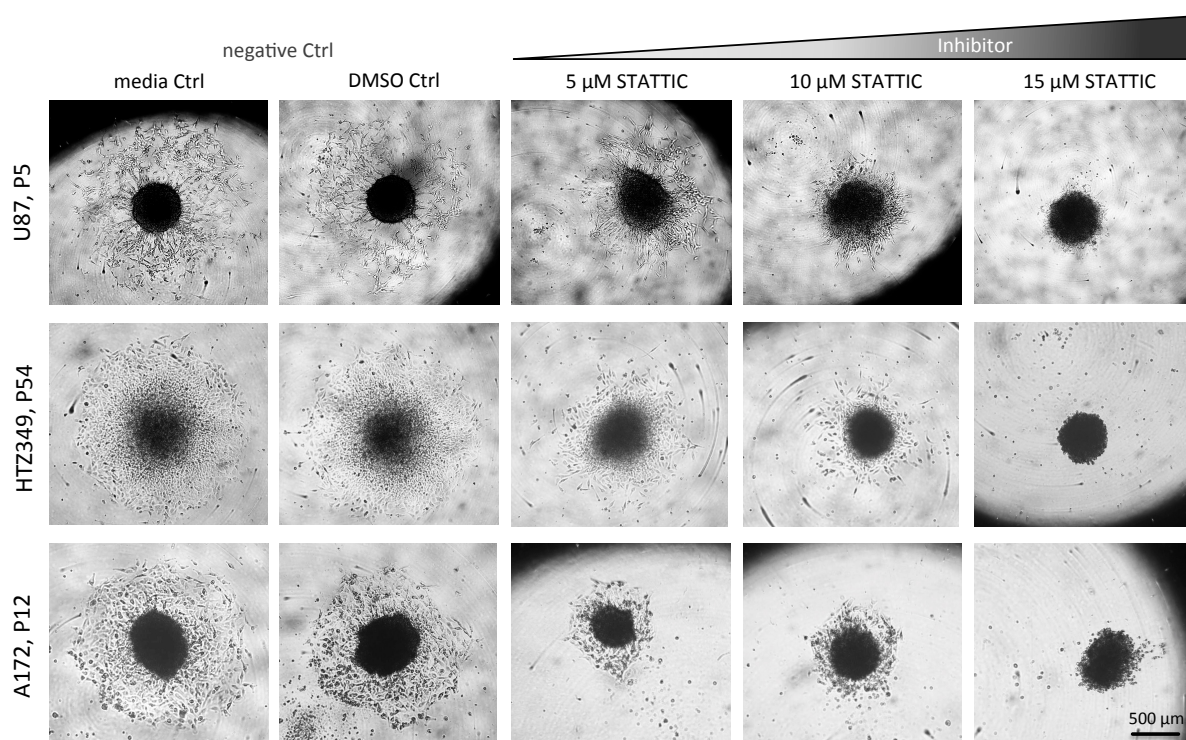


Figure 4-43: Spheroid assay with Stattic treatment of GBM lines A172, HTZ349, and U87

Representative spheroids are depicted after 40 h of Stattic treatment. Increasing concentrations of Stattic reduced cell migration away from the initial spheroid, whereas DMSO treatment had no influence on observed migration compared to control.

The migration rates of BTIC, TC, and GBM cell lines were shown to be reduced (Figure 4-44 to Figure 4-46), in line with the previously described proliferation decrease induced by Stattic treatment. Comparison of Figure 4-44A to C indicates that even the three GBM lines responded in a time- and concentration dependent manner. A172 migration was significantly reduced upon treatment with high Stattic concentrations after 16 h. In HTZ349 and U87, significant reduction was not observed before 24 h. After 40 h, even 0.625 μM of Stattic was sufficient to significantly reduce migration. In general, low Stattic dosages had only minor decreasing effects on migration. Only highest Stattic concentrations decreased migration by half (IC_{50}) (Table 4-7). These observations correlated to average migration rates (appendix in Table 9-2), since the covered distance day^{-1} decreased in a concentration-dependent manner.

Wound healing assays with A172 and HTZ349 upon Stattic treatment were performed to verify the data obtained from spheroid migration assays. As evident from Figure 9-5 in the appendix, wound healing experiments were consistent with the results obtained in spheroid assays. Spheroid assays were preferred for activity analysis, because more assays could be performed in parallel than wound healing assays.

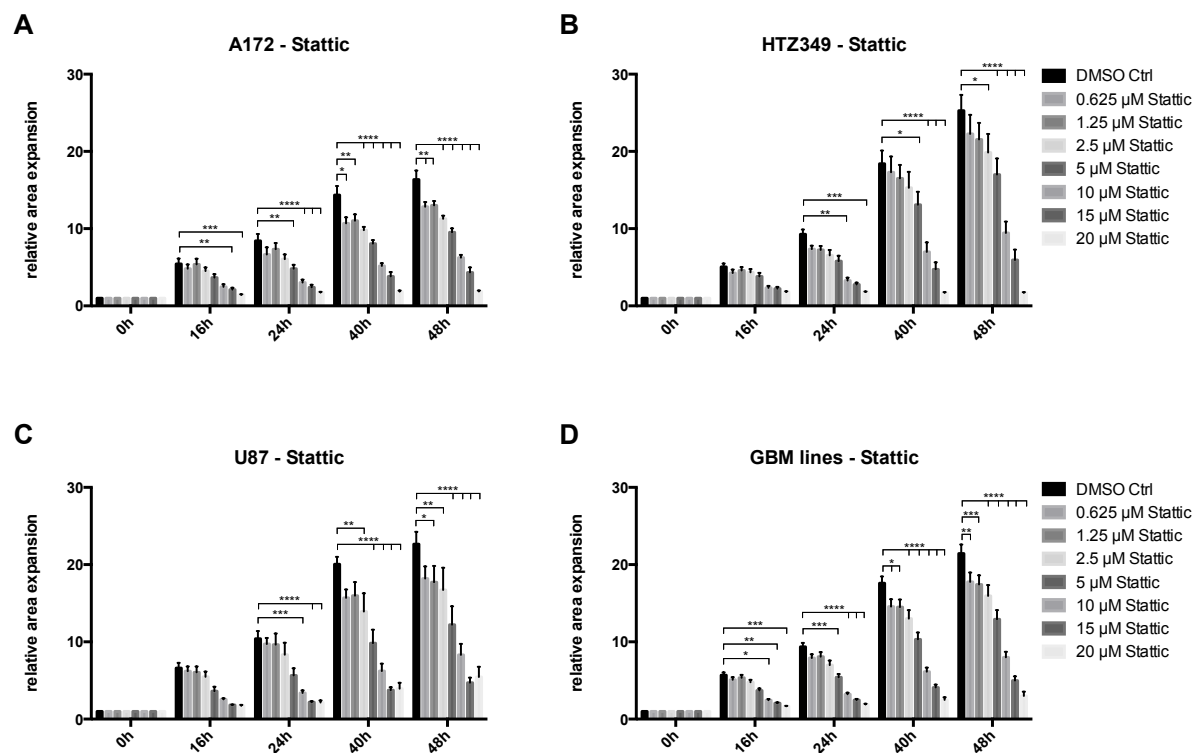


Figure 4-44: Migration of GBM cell lines after Stattic treatment

(A) Starting 16 h after treatment, significantly decreased migration was observed for A172, which increased in time- and concentration-dependent manner. Even 0.625 µM achieved a significantly reduced migration after 48 h. (B) HTZ349 cells migrated significantly slower after 24 h of treatment with increasing effects in time- and concentration-dependent manner. (C) A significant decrease of U87 cell migration was observed starting at 24 h with ≥ 10 µM of Stattic. After 48 h, even low concentration of Stattic (≥ 1.25 µM) had significant reducing effects on migration. (D) Aggregated data revealed that 0.62 µM of Stattic was sufficient to reach a significant decrease of migration after 40 h. All experiments were performed in triplicates with 9 spheroids/assay; values represent mean \pm SD; relative area expression were normalised to spheroid size at 0 h; 2way ANOVA analysis with Tukey's multiple comparisons test, ns: $p > 0.05$, *: $p \leq 0.05$, **: $p \leq 0.01$, ***: $p \leq 0.001$, ****: $p \leq 0.0001$. Significances between every condition are detailed in the statistics on the enclosed CD.

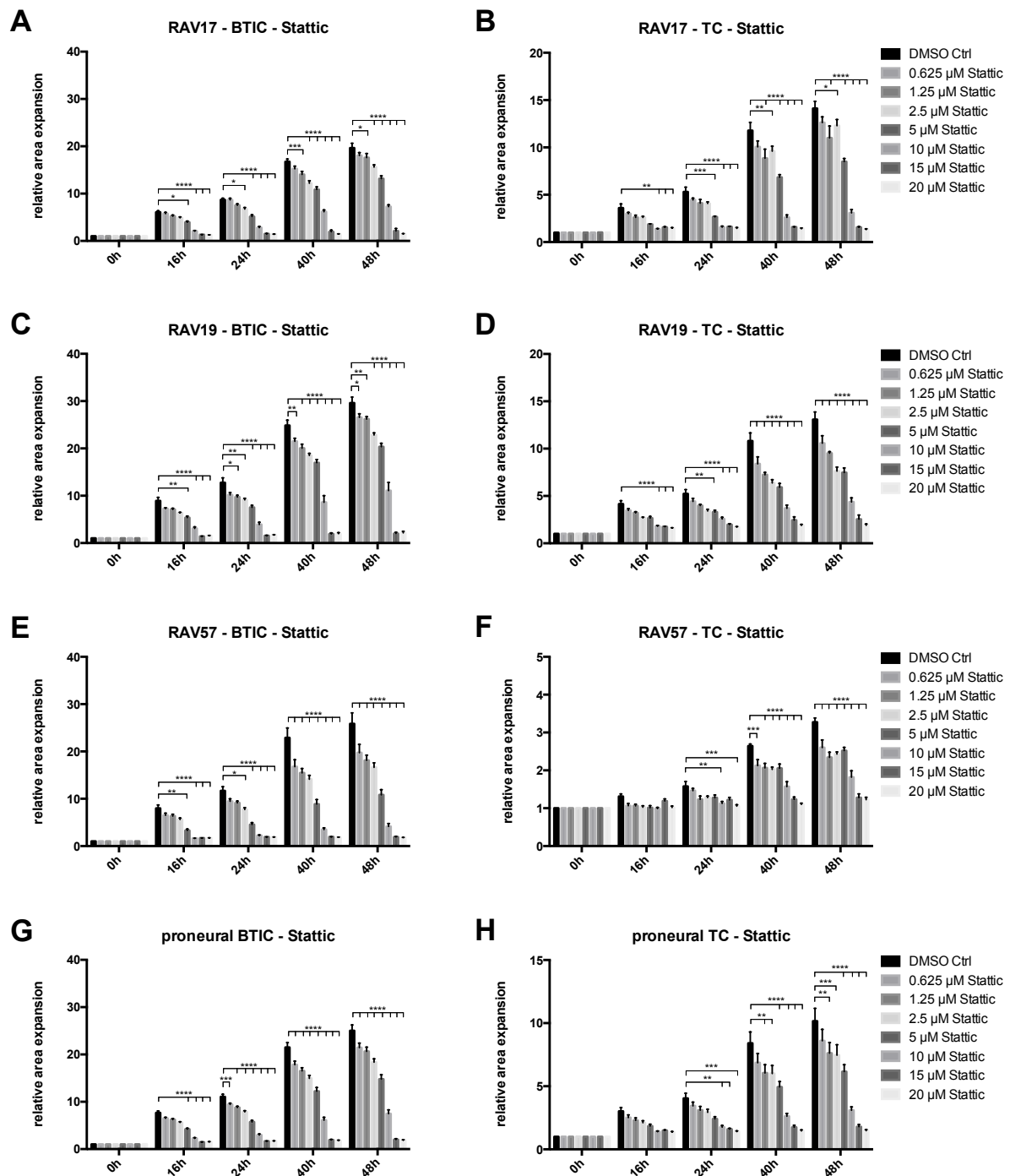


Figure 4-45: Migration of proneural BTICs and corresponding TCs after Stattic treatment

(A) A significant decrease of migration was measured in RAV17 BTICs, 16 h after treatment with Stattic concentrations $\geq 5 \mu$ M. This effect intensified in time- and concentration-dependent manner. At 48 h, even 1.25 μ M resulted in a significant decrease of migration. (B) For RAV17, only the highest concentrations were sufficient to significantly reduce migration rates after 16 h, lower concentrations were sufficient at later time points (40 h, 48 h). (C) RAV19 BTICs were highly sensitive to Stattic, which can be seen in significantly reduced migration at all concentrations by 48 h. (D) RAV19 TCs were even more sensitive to Stattic, as all concentrations slowed migration significantly at 40 and 48 h. (E) RAV57 BTICs were most sensitive, all Stattic concentrations significantly decreased migration after 40 and 48 h. (F) RAV57 TCs migration rates were also

decreased efficiently upon Stattic treatment. (G) Aggregated data of proneural BTICs revealed that 0.625 μ M of Stattic was sufficient to significantly slow migration after 40 h. (H) Aggregated data of proneural TCs indicated a lower sensitivity to Stattic compared to BTICs, as migration was decreased only at later time points. All experiments were performed in triplicates with 9 spheroids/assay; values represent mean \pm SD; relative area expression were normalised to spheroid size at 0 h; 2way ANOVA analysis with Tukey's multiple comparisons test, ns: $p > 0.05$, *: $p \leq 0.05$, **: $p \leq 0.01$, ***: $p \leq 0.001$, ****: $p \leq 0.0001$. Significances between every condition are detailed in the statistics on the enclosed CD.

It became evident that proneural BTIC and TC migration rates declined time- and concentration-dependently upon Stattic treatment (Figure 4-41). In general, proneural BTIC responded earlier, with significant effects detectable after 16 h, compared to other TCs. Overall, proneural TCs displayed a decreased migratory potential compared to BTICs. BTICs treated with 20 μ M of Stattic travelled only about 15% of the distance that control-treated cells covered. In contrast, under the same conditions, TCs still covered about 25% of the reference distance (migrated by control-treated TCs). Based on this observation, Stattic may be considered as more efficient for decreasing proneural BTIC, than TC migration.

Comparing proneural (Figure 4-45) and mesenchymal (Figure 4-46) BTICs and TCs, it became apparent that proneural BTICs and TCs were more sensitive to Stattic treatment than mesenchymal BTICs and TCs. Decline of migration rates of mesenchymal cells implied that both BTICs and TCs respond in a concentration-dependent manner to Stattic treatment. On average, BTICs were more sensitive to Stattic than TCs. Often, even the lowest dosage of Stattic (0.625 μ M) was sufficient to significantly decelerate migration of BTICs after 48 h, whereas higher dosages were required in TCs, but migration was only prevented at the highest concentrations ($\geq 20 \mu$ M) in both – BTICs and TCs. The migration rates of each cell line (as listed in Table 4-7 and detailed in the appendix Table 9-3) revealed that effects of Stattic treatment were higher in mesenchymal TCs due to their initial higher migration rates. For example, after treatment with 20 μ M Stattic, BTICs were still able to cover about 15% of the distance control-treated cells covered, whereas TCs covered only about 0.5%. It should, however, be noted, that RAV21 constituted an exception, as the Stattic treatment had minor effect on RAV21 TCs, which were still able to cover about 30% of the distance which control-treated cells migrated. In contrast, corresponding BTICs managed to travel only about 16% of the distance covered by control-treated cells. The data indicates that mesenchymal BTICs responded earlier to all Stattic concentrations used than other TCs. However, to inhibit migration, high concentrations of Stattic are necessary for both mesenchymal subtypes.

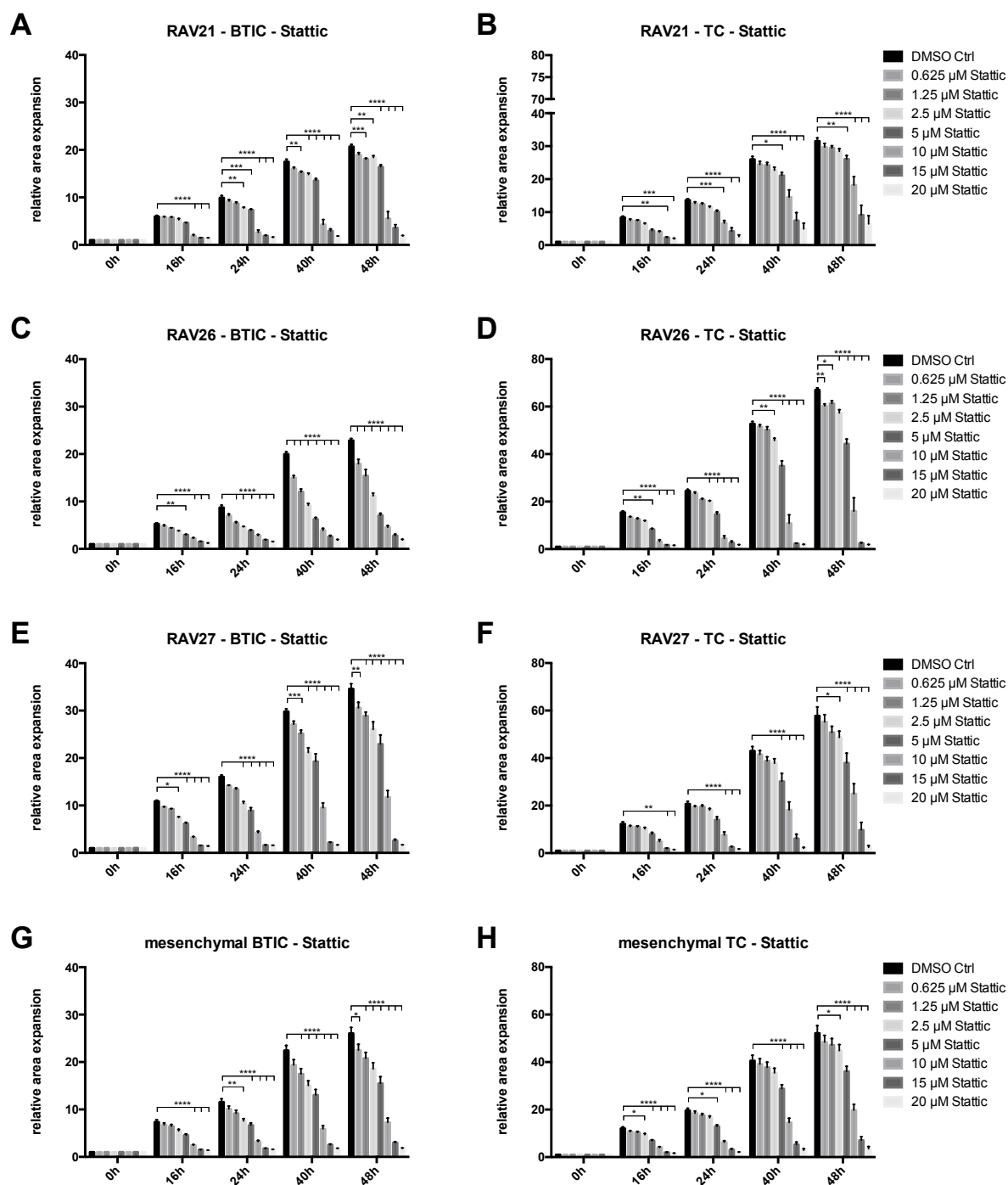


Figure 4-46: Migration of mesenchymal BTICs and corresponding TCs after Stattic treatment

(A) RAV21 BTICs demonstrated significantly decelerated migration at Stattic concentrations $\geq 5 \mu\text{M}$ after 16 h of treatment. After 40 and 48 h, even with $1.25 \mu\text{M}$, a significant reduction of migration was observed, but only highest concentrations, $\geq 10 \mu\text{M}$, prevented migration almost completely. (B) RAV21 TC migration was decreased over time at concentrations $\geq 5 \mu\text{M}$. (C) RAV26 BTICs were observed to have a high sensitivity to Stattic, as at 40 and 48 h all concentrations significantly decreased migration. (D) All concentrations of Stattic achieved a significant migration reduction over time, but only 15 and $20 \mu\text{M}$ prevented migration of RAV26 TCs. (E) For RAV27 BTICs, $0.625 \mu\text{M}$ was sufficient to significantly reduce migration rates at 40 and 48 h,

but migration was prevented only at the highest concentrations ($\geq 15 \mu\text{M}$). (F) RAV27 TCs displayed decreased sensitivity to Stattic as only the highest concentration ($20 \mu\text{M}$) was sufficient to prevent migration. Concentrations of $\geq 2.5 \mu\text{M}$ were sufficient to achieve a significant decrease of migration. (G) Aggregation of all mesenchymal BTIC datasets revealed that $0.625 \mu\text{M}$ of Stattic were sufficient to significantly decrease migration after 48 h, higher concentrations of Stattic $\geq 10 \mu\text{M}$ were already efficient after 16 h. (H) Aggregated data of all mesenchymal TCs confirmed increased migration of mesenchymal TCs compared to respective BTICs, along with decreased sensitivity to Stattic. All experiments were performed in triplicates with 9 spheroids/assay; values represent mean \pm SD; relative area expression were normalised to spheroid size at 0 h; 2way ANOVA analysis with Tukey's multiple comparisons test, ns: $p > 0.05$, *: $p \leq 0.05$, **: $p \leq 0.01$, ***: $p \leq 0.001$, ****: $p \leq 0.0001$. Significances between every condition are detailed in the statistics on the enclosed CD.

It was evident that preventing STAT3 phosphorylation at Y705 caused a concentration-dependent restriction of migration in all lines, but to different extents. GBM cell lines proved to be most resistant to Stattic treatment, compared to BTICs and TCs. Proneural TCs migration was less affected by Stattic treatment than migration rates of proneural BTICs, although this is difficult to identify due to overall low migration of proneural TCs. The observed effects were quite similar between mesenchymal BTICs and TCs, which were more sensitive to Stattic treatment than GBM cell lines, but nevertheless required the highest Stattic concentrations to prevent their migration.

Comparison of data obtained from proliferation (4.3.3.2.2) and migration (4.3.3.2.3) assays revealed a time- and concentration-dependent response to Stattic treatment which resulted in decreased rates of proliferation and migration. GBM cell lines were in both cases most resistant to Stattic treatment compared to BTICs and TCs (Table 4-7). In mesenchymal and proneural BTICs, distinctly lower Stattic concentrations were observed to reduce their proliferation rates by half, but higher concentrations were required to reduce migration rates. In contrast, to decelerate mesenchymal TC proliferation and migration by half, equal Stattic concentrations were necessary. Likewise, IC_{50} concentrations of Stattic were similar for both proliferation and migration rates in proneural TCs.

Based on these results, STAT3 was considered as one factor which modulates proliferation and invasion. Since, BTICs are considered as the cell population which is most resistant to standard therapy and generally leads to re-growth of GBM, the inhibitory effect of Stattic on BTICs and TCs was further investigated in the established OBSC model.

Category	IC ₅₀ Stattic	
GBM lines	Proliferation	Migration
A172	15 – 20 µM	≥ 15 µM
HTZ349	≥ 20 µM	≥ 15 µM
U87	≥ 15 µM	10 – 15 µM
GBM lines	15 – 20 µM	10 – 15 µM
BTIC	Proliferation	Migration
RAV17	≥ 5 µM	10 – 15 µM
RAV19	0.625 – 1.25 µM	10 – 15 µM
RAV57	2.5 – 5 µM	5 – 10 µM
proneural BTIC	1.25 – 2.5 µM	≥ 10 µM
RAV21	≥ 2.5 µM	5 – 10 µM
RAV26	1.25 – 2.5 µM	5 – 10 µM
RAV27	2.5 – 5 µM	10 – 15 µM
mesenchymal BTIC	≥ 2.5 µM	≥ 5 µM
TC	Proliferation	Migration
RAV17	2.5 – 5 µM	5 – 10 µM
RAV19	5 – 10 µM	10 – 15 µM
RAV57	5 – 10 µM	5 – 10 µM
proneural TC	5 – 10 µM	5 – 10 µM
RAV21	≥ 1.25 µM	10 – 15 µM
RAV26	10 – 15 µM	5 – 10 µM
RAV27	15 – 20 µM	≥ 10 µM
mesenchymal TC	10 – 15 µM	≥ 10 µM

Table 4-7: Proliferation and migration inhibitory effects of Stattic on BTIC and TC

Half the inhibitory concentrations (IC₅₀) of Stattic are summarised for each GBM cell, BTIC, and TC line. Differentiated cells are more resistant to Stattic as they require higher concentrations to reduce proliferation by half, in comparison to BTICs. Doubling times and migration rates for each Stattic concentration in each cell line are detailed in the appendix Table 9-3 and Table 9-4.

4.3.4. Effects of STAT3 inhibition on glioma cells in the OBSC model

To verify the potential of Stattic to inhibit GBM cell migration, the established OBSC model from project section 1 was combined with the findings of project section 2. Here, cells were implanted in OBSCs and the culture media was supplemented with 15 μ M Stattic. This concentration was chosen according to the determined IC_{50} (Table 4-7) which sufficiently reduced migration of all analysed specimen *in vitro*. Infiltrated areas were measured on implantation day (1) as well as after 7 and 14 days.

As evident from Figure 4-47, Stattic treatment led to decreased infiltration of brain slice tissue by U87 cells. Significant decrease was measured for the area covered by cells (Figure 4-47A). After 14 days of Stattic treatment, the area infiltrated by U87 cells was only about 23% the size of control areas (Table 4-8). Since, spatial expansion of cells in OBSCs was not radial (see paragraph 4.1) as in *in vitro* spheroid assays, the maximum distance travelled by cells was assessed and was decreased, also (Figure 4-47B). The maximum distance travelled by U87 cells was only about 32% in treatment conditions compared to control (Table 4-9).

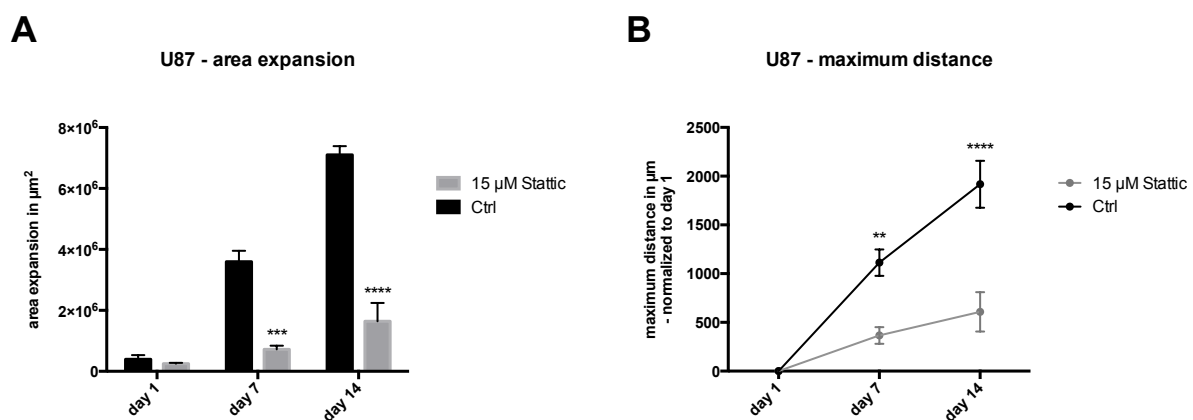


Figure 4-47: Decreased OBSC infiltration by U87 glioma cells with Stattic treatment

Spheroids formed of 5,000 GFP-expressing U87 glioma cells implanted in OBSCs. The culture media was supplemented with 15 μ M Stattic or respective DMSO concentration (Ctrl). (A) Infiltration of tissue by U87 cells was significantly reduced, after 7 days of Stattic treatment, the covered area was ~80% less than in control treatment (after 14 days: ~77%). (B) Reduced OBSC infiltration was sustained as the maximum distance covered by U87 cells was significantly decreased. After 7 days, the maximum distance covered upon Stattic treatment was 365.82 $\mu m \pm 148.90$ compared to control 1113.29 $\mu m \pm 234.23$ (14 days: Stattic = 608.38 $\mu m \pm 350.57$; control = 1917.11 $\mu m \pm 415.87$). An overview of measurements is listed in the appendix, Table 9-5 and Table 9-6. All experiments were performed in triplicates; values represent mean \pm SEM; 2way ANOVA analysis with Sidak's multiple comparisons test, ns: $p > 0.05$, **: $p \leq 0.01$, ***: $p \leq 0.001$, ****: $p \leq 0.0001$.

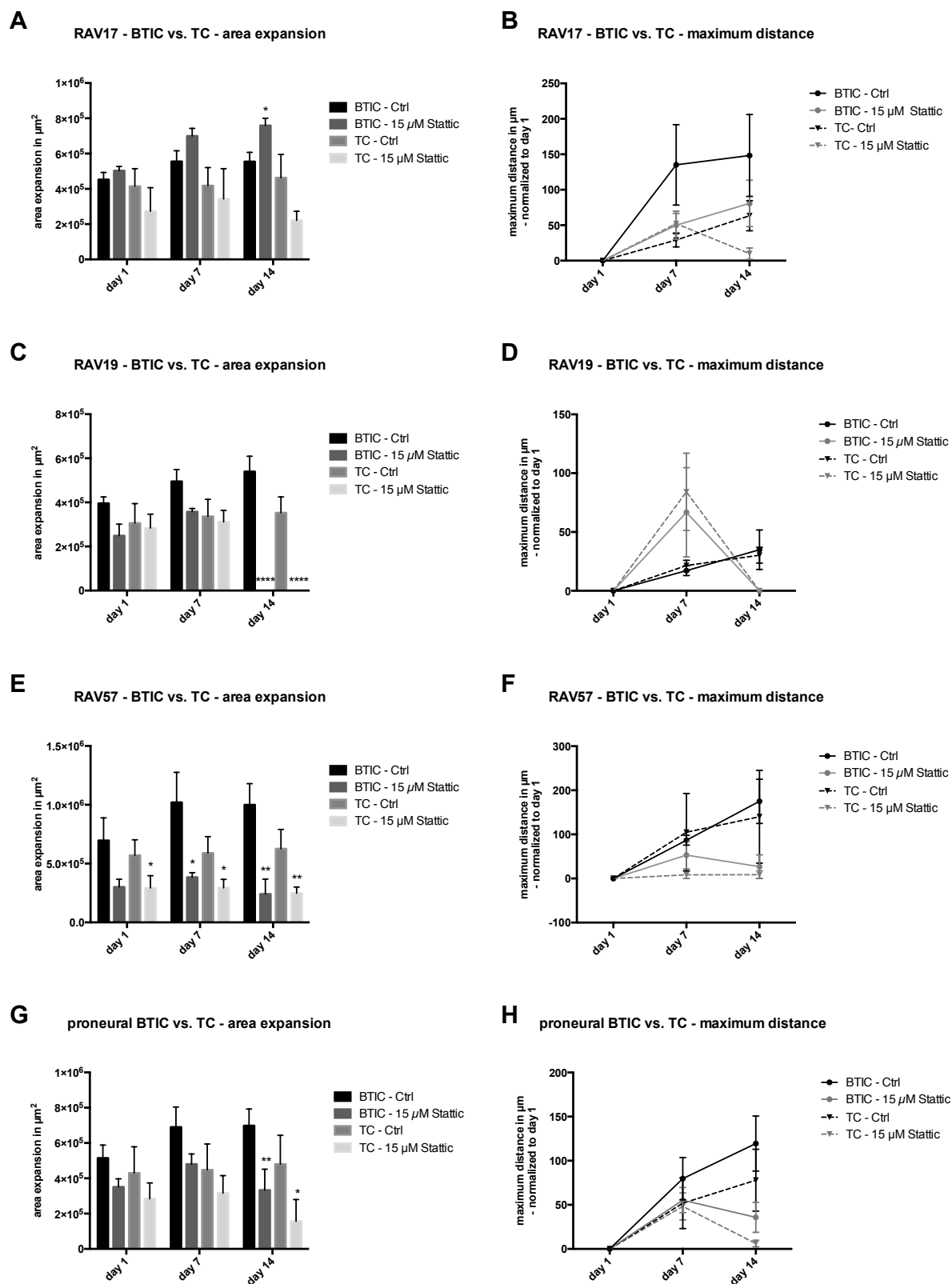


Figure 4-48: Decreased OBSC infiltration by proneural BTIC and TC lines with Stattic treatment

Comparisons refer always to Stattic compared to control treatment at the same time point. (A) RAV17 BTIC infiltration of brain slice tissue was determined to be increased by ~37% after 14 days of Stattic (7 days: ~26%) compared to control treatment. RAV17 TC exhibited significantly decreased infiltration upon Stattic treatment,

cells covered ~18% of the area control cells covered after 7 days (14 days: ~52%). (B) Decrease of maximum distance travelled by RAV17 BTICs and TCs was determined; BTICs: 7 days: Stattic = $49.98 \mu\text{m} \pm 34.39$; control = $135.11 \mu\text{m} \pm 56.65$; 14 days: Stattic = $80.76 \mu\text{m} \pm 56.59$; control = $148.36 \mu\text{m} \pm 57.72$; TCs: 7 days: Stattic = $52.17 \mu\text{m} \pm 25.24$; control = $29.11 \mu\text{m} \pm 9.72$; 14 days: Stattic = $9.88 \mu\text{m} \pm 13.78$; control = $63.42 \mu\text{m} \pm 21.16$. (C) In RAV19 BTICs and TCs, Stattic led to a complete inhibition of infiltration after 14 days. (D) The maximum distance covered was increased for RAV19 BTICs (Stattic = $52.17 \mu\text{m} \pm 25.24$; control = $17.10 \mu\text{m} \pm 4.15$) and RAV19 TCs (Stattic = $84.16 \mu\text{m} \pm 56.88$; control = $21.44 \mu\text{m} \pm 4.54$) 7 days after implantation. (E) RAV57 BTIC infiltration was decreased by ~62% after 7 days and ~76% after 14 days. Much the same applied to RAV57 TC with a decrease of ~50% after 7 days and of ~60% after 14 days. (F) A decrease of maximum distance covered after Stattic treatment was observed for RAV57 BTICs (7 days: Stattic = $53.06 \mu\text{m} \pm 53.86$; control = $86.78 \mu\text{m} \pm 11.08$; 14 days: Stattic = $26.76 \mu\text{m} \pm 46.35$; control = $174.99 \mu\text{m} \pm 50.13$) and TCs (7 days: Stattic = $8.32 \mu\text{m} \pm 14.42$; control = $105.06 \mu\text{m} \pm 8.72$; 14 days: Stattic = $8.67 \mu\text{m} \pm 15.02$; control = $140.42 \mu\text{m} \pm 105.23$). (G) Aggregated data indicate that infiltration of OBSCs by proneural BTICs and TCs was distinctly decreased upon Stattic treatment. After 14 days, the area covered by glioma cells was significantly smaller in Stattic treated OBSC compared to control treatment: BTICs: ~52%; TCs: ~67%. (H) Aggregated data revealed decreased infiltration 7 days after implantation for proneural BTICs: Stattic = $55.33 \mu\text{m} \pm 14.27$; control = $79.66 \mu\text{m} \pm 23.93$, but not for TCs: Stattic = $48.22 \mu\text{m} \pm 15.30$; control = $51.87 \mu\text{m} \pm 28.79$. After 14 days invasion, measured through the maximum distance covered, was significantly reduced in both proneural BTICs ($p > 0.05$: Stattic = $35.84 \mu\text{m} \pm 17.02$; control = $119.42 \mu\text{m} \pm 31.17$) and TCs (Stattic = $6.18 \mu\text{m} \pm 3.73$; control = $77.91 \mu\text{m} \pm 35.05$). A tabular overview of measurements is listed in the appendix, Table 9-5 and Table 9-6. All experiments were performed in triplicates; values represent mean \pm SEM; 2way ANOVA analysis with Sidak's multiple comparisons test, ns: $p > 0.05$, *: $p \leq 0.05$, **: $p \leq 0.01$, ****: $p \leq 0.0001$.

Proneural cells responded with decreased infiltration to Stattic treatment (Figure 4-48), with the exception of RAV17 BTICs (A). Upon differentiation, the cells were more sensitive to Stattic treatment than as BTICs. The maximum distances travelled by cells upon Stattic treatment was distinctly decreased in all cases, although often not significantly due to small values with high standard deviations. Of note, RAV17 BTICs were observed to exhibit significantly increased infiltration of OBSC tissue upon treatment (Figure 4-48A), while the maximum distance travelled was still smaller for Stattic treated compared to control treated cells (B). The area covered increased upon treatment compared to control (Table 4-8), while the covered maximum distance day^{-1} was only 43% of the distance covered by cells at control treatment (Table 4-9). Stattic treatment was observed to be cytotoxic for RAV19 cells in the long-term, the spatial expansion declined to 0% after 14 days of treatment. However, the average maximum distance travelled increased (Table 4-9) as both RAV19 BTICs (154%) and TCs (230%) responded to Stattic treatment with increased invasion, determined after 7 days (Figure 4-48D). RAV57 BTICs and TCs responded to Stattic with decreased infiltration on OBSCs as measured by covered area and maximum distance (Figure 4-48E, F). However, it has to be noted that the size of RAV57 spheroids treated with Stattic was initially smaller. However, spatial expansion declined by 76% (RAV57 BTICs) and 61% (RAV57 TCs) corresponded to the general trend of decreased infiltration upon Stattic treatment (Table 4-8). This was accentuated by the decline of maximum distance covered to 38% (RAV57 BTICs) and 7% (RAV57 TCs) with Stattic treatment compared to control (Table 4-9).

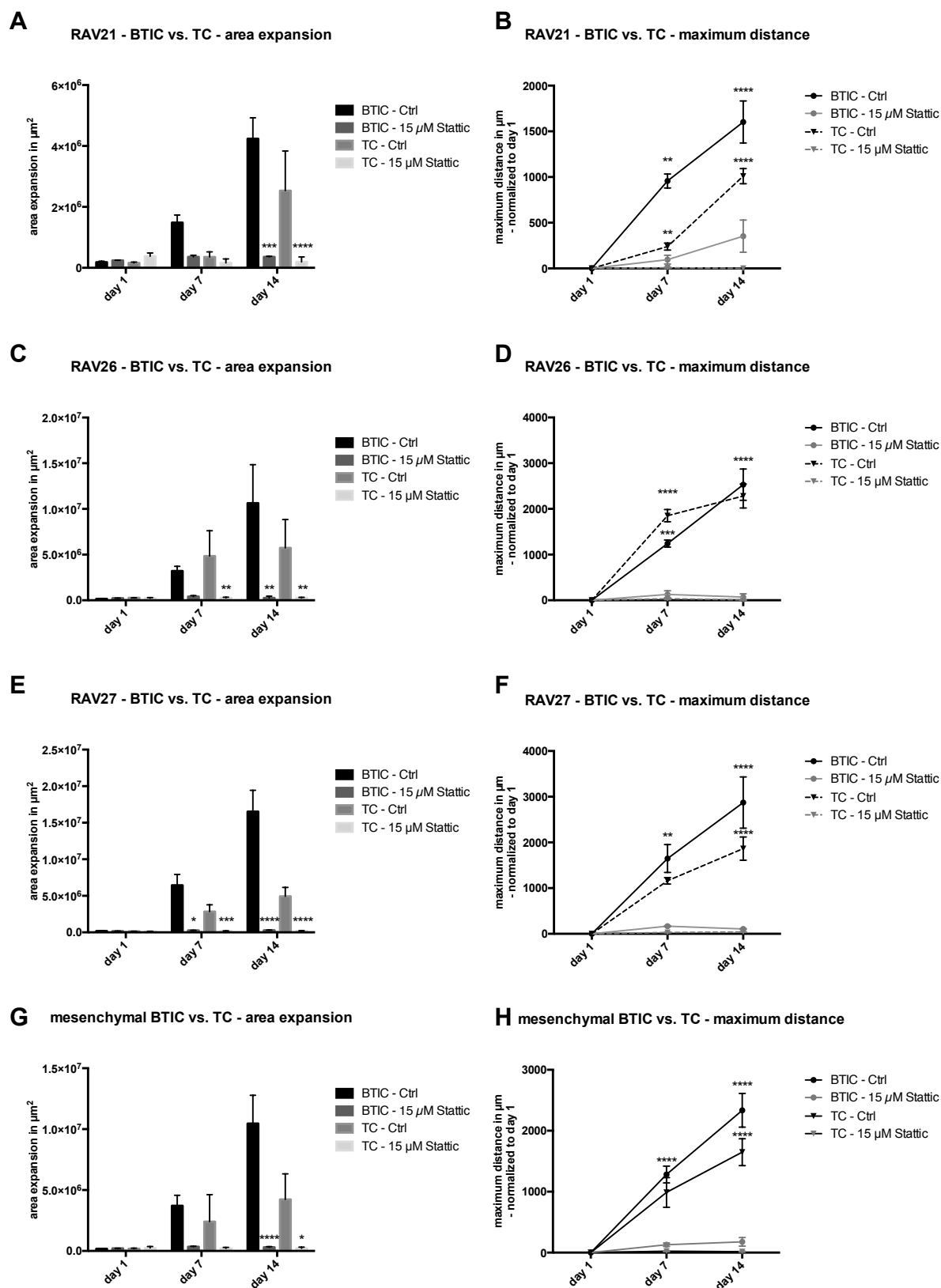


Figure 4-49: Decreased OBSC infiltration by mesenchymal BTIC and TC lines with Stattic treatment

Comparisons refer always to Stattic compared to control treatment at the same time point. (A) RAV21 BTIC infiltration of brain slice tissue was significantly decreased by ~92% after 14 days of Stattic treatment,

~76% after 7 days. The area covered by RAV17 TC was significantly smaller upon Stattic treatment after 14 days: ~93%; 7 days: ~56%. (B) Invasion in OBSC were observed to be significantly decreased upon Stattic treatment for RAV21 BTICs at 7 days: Stattic = $96.09 \mu\text{m} \pm 82.46$; control = $956.76 \mu\text{m} \pm 76.31$ and at 14 days: Stattic = $352.81 \mu\text{m} \pm 304.57$; control = $1602.27 \mu\text{m} \pm 230.14$, likewise for RAV21 TCs at 7 days: Stattic = $7.74 \mu\text{m} \pm 13.41$; control = $239.27 \mu\text{m} \pm 38.27$ and at 14 days: Stattic = $0.00 \mu\text{m} \pm 0.00$; control = $1009.93 \mu\text{m} \pm 38.27$. (C) Infiltration of RAV26 BTICs and TCs was significantly reduced by Stattic. After 14 days, the area covered was ~96% smaller for RAV26 BTICs and ~95% for TCs; after 7 days: BTICs ~87%; TCs ~94%. (D) Maximum distance covered during Stattic treatment was significantly ($p \leq 0.0001$) shorter for both RAV26 BTICs 14 days after implantation (Stattic = $70.82 \mu\text{m} \pm 122.66$; control = $2530.24 \mu\text{m} \pm 342.71$) and TCs (Stattic = $8.97 \mu\text{m} \pm 15.54$; control = $2281.76 \mu\text{m} \pm 342.71$) as well as after 7 days: BTICs: Stattic = $127.34 \mu\text{m} \pm 140.15$; control = $1240.81 \mu\text{m} \pm 76.45$; TCs: Stattic = $35.78 \mu\text{m} \pm 36.47$; control = $1851.78 \mu\text{m} \pm 133.21$. (E) The area covered in OBSCs by RAV27 BTICs was observed to be significantly decreased. Only ~2% of the area was covered by cells after 14 days of Stattic treatment compared to control (7 days: ~96%). For RAV27 TC, the area covered was significantly decreased by ~96% after 14 days (7 days: ~93%) compared to control. (F) A significantly shorter maximum distance covered after Stattic treatment was observed for RAV27 BTICs (7 days: Stattic = $165.73 \mu\text{m} \pm 53.86$; control = $1647.81 \mu\text{m} \pm 305.87$; 14 days: Stattic = $105.69 \mu\text{m} \pm 14.12$; control = $2876.65 \mu\text{m} \pm 561.04$) and TCs (7 days: Stattic = $29.73 \mu\text{m} \pm 16.26$; control = $1160.23 \mu\text{m} \pm 69.96$; 14 days: Stattic = $40.65 \mu\text{m} \pm 15.65$; control = $1864.93 \mu\text{m} \pm 254.43$). (G) Covered area by mesenchymal BTICs and TCs was determined to be significantly decreased after 14 days of Stattic treatment. (H) Compiled data reveal that infiltration of both mesenchymal BTICs and TCs was significantly ($p \leq 0.0001$) decreased by Stattic 7 days after implantation (BTICs: Stattic = $129.65 \mu\text{m} \pm 29.13$; control = $1281.79 \mu\text{m} \pm 137.20$; TCs: Stattic = $24.42 \mu\text{m} \pm 8.21$; control = $987.76 \mu\text{m} \pm 244.09$) as well as after 14 days (BTICs: Stattic = $176.44 \mu\text{m} \pm 70.50$; control = $2335.05 \mu\text{m} \pm 276.47$; TCs: Stattic = $16.54 \mu\text{m} \pm 7.18$; control = $1648.47 \mu\text{m} \pm 220.90$). A tabular overview of measurements is listed in the appendix, Table 9-5 and Table 9-6. All experiments were performed in triplicates; values represent mean \pm SEM; 2way ANOVA analysis with Sidak's multiple comparisons test, ns: $p > 0.05$, *: $p \leq 0.05$, **: $p \leq 0.01$, ***: $p \leq 0.001$, ****: $p \leq 0.000$.

In contrast to proneural cells, a uniform pattern was observed for mesenchymal cells, which responded with a very noticeable decline of infiltration to Stattic treatment (Figure 4-49). Infiltration of OBSCs was determined to be significantly inhibited already at first measurement of the maximum distance covered by cells after 7 days (Figure 4-49B, D, F, H). On average, upon Stattic treatment, mesenchymal BTICs travelled at maximum only about 9% of the distance control treated cells covered, TCs only 2% (Table 4-9). The compiled data revealed that the area covered by mesenchymal BTICs was only 3% (5% for TCs) upon Stattic treatment compared to control (Table 4-8). Overall, mesenchymal cell infiltration of OBSCs reached only a fractional amount upon Stattic treatment compared to control.

In summary, Stattic treatment of glioma cells proved to be a promising approach in this context. Mesenchymal BTICs and TCs infiltration of OBSCs was reduced to greatest extent. Their infiltration upon Stattic treatment reached only a fractional amount of that reached at control conditions. Proneural BTICs and TCs responded to Stattic treatment with decreased infiltration, although effects were distinctly less, which is attributed to overall limited invasion. The observed increase of area and maximum distance covered by proneural BTICs 17 and 19 may be attributable to low values and a high degree of variability between the measurements. Overall, a distinct decline of glioma cell invasion upon Stattic treatment was observed after 14 days of Stattic treatment.

Category	Covered area – Percentage increase		Percentage of area covered with Stattic treatment
GBM lines	Ctrl	15 μ M Stattic	
U87	1807.371	646.354	23.10
BTIC			
RAV17	122.677	150.969	136.76
RAV19	136.349	0.000	0.00
RAV57	143.577	80.151	24.11
average proneural BTIC	135.604	95.020	47.74
RAV21	2286.962	149.327	8.47
RAV26	6477.487	112.404	2.45
RAV27	8842.317	183.365	1.77
average mesenchymal BTIC	5852.507	144.333	2.91
TC			
RAV17	111.717	81.156	52.14
RAV19	115.373	0.000	0.00
RAV57	109.824	84.725	39.61
average proneural TC	111.746	55.284	32.58
RAV21	1592.585	50.057	7.40
RAV26	2171.891	118.646	4.65
RAV27	3558.679	149.847	4.09
average mesenchymal TC	2383.450	89.393	5.16

Table 4-8: Percentage spatial expansion of glioma cells on OBSCs was decreased by 15 μ M Stattic

Area covered by cells was measured at the implantation day and 14 days later. Spatial expansions were calculated in comparison to the initial sizes and are depicted as percentage increase or decrease. Stattic treatment led to decreased infiltration, except for RAV17 BTICs. Mesenchymal cells were more sensitive to Stattic than proneural ones. The last column depicts the proportion of the area that was infiltrated by Stattic treated cells expressed as percentage with the area covered by respective control treated cells set to 100% after 14 days.

Category	Maximum distance day ⁻¹ (μm, ± SD)		Percentage of distance travelled with Stattic treatment
GBM lines	Ctrl	15 μM Stattic	
U87	147.99 (± 30.78)	47.86 (± 21.33)	32.34
BTIC			
RAV17	14.95 (± 11.03)	6.45 (± 4.09)	43.17
RAV19	2.47 (± 1.46)	3.82 (± 6.478)	154.54
RAV57	12.45 (± 4.29)	4.75 (± 6.14)	38.13
average proneural BTIC	9.96 (± 8.52)	5.08 (± 5.36)	50.98
RAV21	125.56 (± 24.80)	19.46 (± 16.86)	15.50
RAV26	178.99 (± 29.43)	11.61 (± 15.58)	6.49
RAV27	220.30 (± 67.02)	15.61 (± 9.06)	7.09
average mesenchymal BTIC	174.95 (± 57.87)	15.56 (± 13.79)	8.90
TC			
RAV17	4.34 (± 2.26)	4.14 (± 4.31)	95.36
RAV19	2.61 (± 1.01)	6.01 (± 8.35)	230.15
RAV57	12.51 (± 16.24)	0.90 (± 1.50)	7.23
average proneural TC	6.49 (± 9.95)	3.69 (± 5.60)	56.82
RAV21	53.16 (± 22.58)	0.55 (± 1.36)	1.04
RAV26	213.75 (± 62.57)	2.88 (± 4.17)	1.35
RAV27	149.48 (± 28.88)	3.58 (± 1.79)	2.39
average mesenchymal TC	121.81 (± 79.05)	2.34 (± 2.89)	1.92

Table 4-9: Maximum distance covered by glioma cells on OBSCs was decreased upon 15 μM of Stattic treatment

The maximum distance covered by cells was measured 7 and 14 days after implantation. Average maximum distances covered per day (in μm) were calculated based on both values. Stattic treatment led to decreased invasion, except for RAV19 BTICs and TCs. Mesenchymal cells were more sensitive to Stattic than proneural ones. The last column depicts the percentage distance covered by Stattic treated cells, with the distance covered by respective control treated cells set to 100% after 14 days.

5. Discussion

Glioblastomas (GBM) represent the most common primary and aggressive brain tumours (Bleeker *et al.* 2012). GBM are associated with one of the worst survival rates among all cancers, approximately 14.6 months after diagnosis (Stupp *et al.* 2005). The primary cause and main pathophysiological feature of these highly aggressive neoplasms is diffuse infiltration of the brain by progenitor and tumour cells (Sanai *et al.* 2005; Nevo *et al.* 2014). Infiltration into the parenchyma constitutes an early (Louis, 2006), but still largely unexplored event in the progression of the disease strongly contributing to treatment difficulties. Currently, there are no specific therapies that target invasive cells left behind after local therapy. Neoplastic transformation is attributed to a subset of cancer stem-like brain tumour initiating cells (BTIC) (Singh *et al.* 2004), which are not only implicated in tumour initiation, but also in recurrence and progression (Das *et al.* 2008). The ability to transdifferentiate from an epithelial-like to a more mesenchymal state (EMT) (Tso *et al.* 2006; Zarkoob *et al.* 2013), constitutes an apparently relevant mechanism by which glioma cells become invasive (Carro *et al.* 2010) as introduced in (Figure 3-7). Extracellular matrix (ECM) components and the tumour microenvironment can orchestrate EMT and induce infiltration. To provide insight in detailed underlying mechanisms that are relevant under physiological conditions for brain infiltration by BTICs, proneural and mesenchymal BTIC invasiveness was analysed in an organotypic brain slice culture (OBSC) model.

5.1. Organotypic slice cultures as model for glioma cell infiltration of the brain

5.1.1. OBSC infiltration by U87 glioma cell line

The *in situ* OBSC model that was established for this study according to Eyüpoglu *et al.* (2005) has demonstrated its value as a tool to visualise and analyse tumour cell migration as well as invasion with *in vivo* like simulated conditions. Slice cultures allow several aspects of structural and synaptic organization of the original tissue to be preserved, including ECM components and microenvironmental influences (reviewed in Humpel, 2015). Unlike common animal models which employ luciferase to provide a rough estimate of tumour volume increase (Shelton *et al.* 2010), or the review of established tumours at the end of experiments (Beier, Wischhusen, *et al.* 2008), the OBSC models allowed detailed monitoring of live tumour cell invasion in real time (see section 4.1). Although, the aim was to analyse primary BTIC locomotion with OBSCs, the already fluorescence tagged glioma cell line U87 was employed for OBSC establishment. U87 are known for a high migratory capacity *in vitro* (Glassmann *et al.* 2011), which was in agreement with the massive tissue infiltration observed in this work with the OBSC model. However, in mice, U87 cells are known to give rise to tumours that did not resemble the typical GBM characteristics, which especially lack infiltration capacity (Galli *et al.* 2004). This divergence may be due to clonal or phenotypic evolution, a common phenomenon in cell culture (Choi *et al.* 2014) and *in vivo* (Sottoriva *et al.* 2013). This hypothesis is reinforced by the observation that while the determined average invasion rate of U87 in the OBSCs ($147.99 \pm 30.78 \mu\text{m day}^{-1}$, see Table 4-1) corresponds well to a previously published single cell migration study ($179 \pm 91 \mu\text{m day}^{-1}$; Glassmann *et al.* 2011). This indicates that U87 cells might have similar locomotion velocity in artificial 2D assays and complex 3D surroundings such as the OBSC model.

In the OBSC model, cells were observed to invade into the brain slice rather than simply migrating along the surface. This was confirmed by focussing through the slices during microscopy, although, this should be visualised and quantified by enhanced techniques, for example, by in-depth measurement of infiltration as described by Valster *et al.* (2005). Other techniques, such as the window model used by Kienast *et al.* (2010) to reveal steps of brain metastasis formation, also allow real-time imaging and 3D visualization of invasion. However, OBSCs are more advantageous concerning cost and time efficiency. Most importantly, several slices can be obtained from one brain, and therefore, promote the

3Rs (reduce, refine, replace) by markedly reducing the number of animal experiments and limiting the burden posed on individual animals (Humpel, 2015).

Comparison of several implantation sites (data not shown) – lateral ventricle, hippocampus, and spots in the cortex region - revealed the lateral ventricle as the most suitable starting point from which the cells invade in distinct directions. It became evident that the cells migrate in a directed manner, and monitoring their exact direction of movement was possible in the OBSC model. These results indicated that a close proximity to the lateral ventricle is important for directed infiltration. The presence of ECM structures as white matter tracks and blood vessels are known to attract and trigger GBM cell movement (reviewed in Cuddapah *et al.* 2014). Both structures are present at the site of the lateral ventricle and thus may cause directed infiltration. Coordinates for implantation of intracranial tumour models in mice are usually chosen to be relative to the lateral ventricle (Patel *et al.* 2014). Moreover, subventricular zone (SVZ) derived stem cells populate a complex niche adjacent to the lateral ventricles (Vescovi *et al.* 2006) and are known to migrate directed to distant sites in the brain, for example, after neuronal injury and stroke (Santra *et al.* 2006). The same factors influencing migration of stem cells from the SVZ may influence induction of glioma cell invasion as well. Using the isolation method developed in this work, enabled analysis of differential gene expression of tumour cells in different OBSC regions, and will be valuable in elucidating mechanisms which trigger tumour cell infiltration.

5.1.2. OBSC infiltration by primary human brain tumour initiating cells

BTICs are characterised by self-renewal, clonogenicity, pluripotency, and invasive behaviour in animal models (Galli *et al.* 2004; Beier *et al.* 2007). Therefore, they are the most relevant and best available model to investigate high-grade gliomas *in vitro* and *in vivo* (Moeckel *et al.* 2014). BTICs represent a minority of cancer stem-like progenitor cells that are responsible for tumour recurrence and resemble closely the parental tumour (Singh *et al.* 2003). Based on this knowledge, it seems reasonable that successful treatments depend on targeting and elimination of BTICs. According to the cultivation method published by Singh *et al.* (2004), brain tumour initiating cells were enriched in serum-free culture conditions with growth factor – EGF and bFGF – supplementation. As previously described, stem-like properties of BTICs were verified by analysis of stem cell marker expression (Nestin, SOX2, and CD133), clonogenicity, and differentiation ability (Moeckel *et al.* 2014). Due to varying extents

in marker expression and the limitations of cancer stem cell identification imposed by imperfect markers (Medema, 2013), the enriched cells are preferentially termed ‘brain tumour initiating cells’, rather than ‘cancer stem cells’. It remains unknown if *in vitro* culture conditions cause selective pressure, however, solely proneural and mesenchymal BTICs are found in culture, while classical and neural subtypes might require different conditions. This culture phenomenon, may, however, correspond partially to subtype frequencies as it has been previously observed that proneural and mesenchymal tumours make up the majority (65%) of GBMs (Lin *et al.* 2014). The selection of proneural and mesenchymal BTIC cultures investigated here, represent typical GBM based on their molecular and genetic characteristics as well as corresponding patient data (see Table 4-5).

BTICs were assumed to be the driving force for diffuse infiltration characterising GBMs, see Figure 5-1. Based on the observation of induced infiltration of U87 in the OBSC model, the *in situ* assay served as model to monitor subtype specific invasive behaviour of primary BTICs. As known so far, BTICs have not been previously analysed with such an *in situ* assay. During analysis in the OBSC model, high invasive potential of mesenchymal BTICs was revealed, contributing to evolving evidence that mainly the mesenchymal subtype bears an

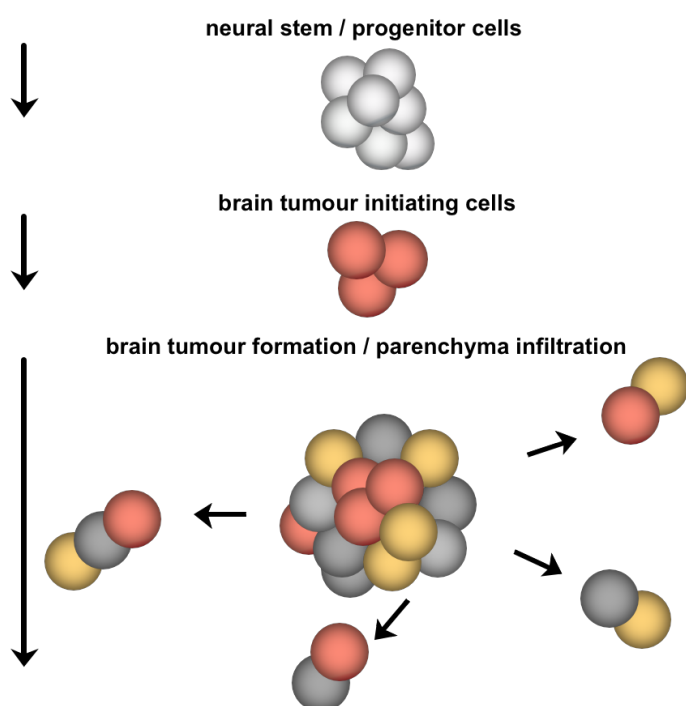


Figure 5-1: GBM formation and diffuse infiltration driven by BTICs

increased invasive behaviour (Sullivan *et al.* 2014; Ortensi *et al.* 2013). Interestingly, two of three BTIC lines even exceeded U87 infiltration in both expansion of area covered and maximum distances travelled. However, on average, U87 corresponded best to mesenchymal BTICs consistent with observations of Tso *et al.* (2006) that U87 exhibited mesenchymal expression characteristics similar to those of primary glioblastoma samples.

After differentiation, mesenchymal TCs revealed a trend towards decreased infiltration capacity

compared to corresponding BTICs. This observation indicates BTICs as driving force for invasion of the brain parenchyma, a characteristic which should be addressed primarily in therapeutic approaches. In contradiction, however, *in vitro* spheroid assays revealed migration rates of mesenchymal TCs that exceeded those of the corresponding BTICs, indicating differentiation as beneficial for migration in 2D settings, but rather disadvantageous in an *in vivo* like situation.

Additionally, migration rates determined for mesenchymal BTICs *in vitro* ($641.99 \pm 101.84 \mu\text{m day}^{-1}$) consistently exceeded those obtained in OBSCs ($174.95 \pm 57.87 \mu\text{m day}^{-1}$). This divergence may seem surprising at first, but bearing in mind that spheroid assays were performed on flat plastic surfaces free from obstacles, in contrast to OBSCs in which the entire brain ECM structure was present, it seems likely that cells require more time for migration. A point worthy of note, however, is the variation in the data obtained from OBSC experiments occurring in the different cell lines, is likely due to the different age of animals used for OBSCs, and different cell passages during repetitive experiments. These issues could be overcome with a larger sample set and enable verification of the hypothesis that mesenchymal BTICs are more infiltrative than differentiated tumour cells.

Extensive infiltration of the tumour surrounding parenchyma is a pivotal hallmark of GBM (Claes *et al.* 2007) likely regardless of GBM subtype. It was, therefore, surprising that proneural cells virtually lacked invasive capacities in contrast to mesenchymal BTICs and TCs (Figure 4-8). Although still under evaluation, tumours of the proneural subtype were reported to have prognostic benefit compared to the three other GBM subtypes (Verhaak *et al.* 2010; Phillips *et al.* 2006). For instance, a study of high-grade gliomas even described dramatically increased survival of patients diagnosed with a proneural subtype (median survival 174.5 weeks) compared those with mesenchymal subtype (65 weeks) (Phillips *et al.* 2006). The worse prognosis of preferentially *de novo* originating mesenchymal GBMs compared to proneural ones may result from a subset of proneural tumours displaying mutation as *IDH1* and a G-CIMP+ phenotype, which is known to provide survival benefit (Cloughesy *et al.* 2014). The present BTIC subset and corresponding parental tumours displayed wild-type *IDH1*, with the exception of one line (Table 4-5). The G-CIMP status was not analysed for the present BTIC set, which should be investigated to provide further insight into genetic divergences that may influence invasiveness. It is, therefore, not feasible to draw conclusions regarding the role of *IDH1* mutation or G-CIMP in the reduced invasion

observed here. It is not yet known if poor prognosis is connected to enhanced invasion. Correlation of the infiltrative zones of respective parental tumours to infiltration in OBSCs would be beneficial to reveal if different invasion patterns were already present.

Parallel *in vitro* migration assays with proneural BTIC conducted in this work revealed migration rates corresponding to mesenchymal cells, although with the important difference that proneural BTIC migration was dependent on laminin coating. Coating was necessary since adherent cells were required for analysis in the spheroid assay setups and proneural BTICs grow usually in spheres. The major brain ECM component laminin is well preserved in OBSCs and present in high abundance in vascular brain structures (Humpel, 2015). Laminin is cross-linked to other components of cell membranes or ECM such as hyaluronan, proteoglycans, or tenascins (Gritsenko *et al.* 2012). Most likely, as this inter ECM cross-linking cannot be given by coating, observed migration is likely an artificial effect induced by the laminin chains. Glioma cells are known for increased expression of adhesion molecules, which were most likely laminin receptors (Gritsenko *et al.* 2012), thus proneural BTICs may be triggered by laminin coating to migrate. Future work should validate if laminin receptor expression is increased in proneural compared to mesenchymal BTICs. The DEG analysis (Figure 4-17) revealed MMPs and associated factors to be enriched in leader compared to non-leader cells. This poses an important question, do proneural cells lack expression of MMPs or other ECM interaction factors which hinder invasiveness through the complex ECM structure of OBSCs, even though they have the genetic capacity to invade. This may be elucidated using the isolation and analysis method conducted in this work, by comparing gene expression profiles of re-isolated proneural cells from the implantation centre and the rim.

In contrast, it was shown that the BTIC phenotype is a product of their microenvironment (Calabrese *et al.* 2007; Hjelmeland *et al.* 2011; Li *et al.* 2009), which consists of a perivascular or hypoxic niche (Vlashi and Pajonk, 2014), the cellular context and soluble factors (Medema, 2013; Lane *et al.* 2014). In contrast, glioma cells actively modulate their environment to increase their invasive potential (Tabassum and Polyak, 2015). These observations provide other explanations for the missing infiltration of proneural BTICs, which may respond differently to the immediate micro-anatomical niche than mesenchymal BTICs. Dhruv *et al.* (2013) proposed the hypotheses of ‘go versus grow’ indicating that invasive, dispersive glioma cells can be distinguished from cognate, stationary ones in terms of phenotype – invasive versus proliferative. The authors further imply that the – growing to going – phenotypic shift of glioma cells may underlie the reciprocal and coordinated

suppression or activation of transcription factors, such as c-myc and NF- κ B, depending on micro-anatomical niche stimuli (Dhruv *et al.* 2013). The authors based their hypothesis on *in vitro* studies with established cell lines and a direct transcription factor presence in the nuclear fraction isolated at migration-activated (sparse cell seeding) or migration-restricted (dense cell seeding) conditions on an artificial ECM monolayer (Dhruv *et al.* 2013). The methodology presented here provides the framework for future studies to assess the differential regulation of transcription factors with four major advantages: (i) use of primary BTICs, (ii) primary BTICs can be analysed according to proneural and mesenchymal GBM subgroups, (iii) this *in situ* setup closely resembles the *in vivo* situation, (iv) identification of a transcription factor signature based on underlying differentially expressed gene expression at the level of single cells. Individual signatures for both GBM subgroups may be identified in this manner which could reveal the distinct behaviour of proneural and mesenchymal BTICs on OBSCs.

In contrast to EMT induction in tumour cells via TGF β (Joseph *et al.* 2014), EMT is also known to be caused by aberrant expression of the transcription factors C/EBP β and STAT3 (Carro *et al.* 2010). Both were identified as important regulators of the mesenchymal phenotype in GBM thereby promoting aggressive infiltration. Indeed, lower protein expression of C/EBP β and STAT3 was revealed in the panel of proneural BTICs compared to the mesenchymal panel. It should be noted that phosphorylation of STAT3 was alike in proneural and mesenchymal cells and the divergence in C/EBP β expression resulted from increased levels of LAP1 and 2 isoforms rather than of the LIP isoform. This corresponds to a recent study reporting LAP isoforms, but not LIP to promote breast cancer cell migration (Xia *et al.* 2015). Tumour necrosis factor α (TNF α) induced expression and stabilization of C/EBP β dependent on p38 MAPK activation, while C/EBP β in turn mediated TNF α -induced migration via induction of MMP1/3 expression (Xia *et al.* 2015). The authors further suggest an interaction of C/EBP β and NF- κ B, also known to be activated by TNF α . In conclusion, this indicates the need to perform comparative analysis as described in the present study to reveal the complex interplay of transcription factors upon induction of an invasive phenotype.

Recently there is growing awareness of intratumoural heterogeneity (Phillips *et al.* 2006), indicating blurred boundaries between GBM subtypes. Correspondingly, the presence of multiple coexisting cell lineages and expression subtypes coexisting in a time- and space-dependent manner in individual GBMs has been shown (Sottoriva *et al.* 2013). Moreover, the authors concluded that the population of malignant cells escaping initial treatment may not derive from a single resistant clone, but rather consist of a heterogeneous population with genetic aberrations thus providing a survival benefit (Sottoriva *et al.* 2013). Hence, the approach of simultaneous implantation of proneural and mesenchymal BTICs on OBSCs may provide deeper insight into the interplay of the subtypes. It may be possible that proneural cells somehow interact with mesenchymal cells upon invasion. In this work, initial experiments suggested that proneural BTICs drove mesenchymal cells away from the implantation spot and filled the gap to the invasive rim comprised of mesenchymal cells (Figure 4-12). It is worth noting that some mesenchymal cells remained together with proneural ones at the implantation site and appeared rather proliferative, round-shaped, rather than invasive, spindle-shaped as the cells at the invasive rim were. This observation is encouraged by the hypothesis of mutualistic or synergistic subtype cooperation (Tabassum and Polyak, 2015) and a possible dependency. The conclusion of higher proliferation of cells remaining at the implantation site drawn upon phenotypical differences, must be validated in future studies with label-retention assays, for example carboxyfluorescein succinimidyl ester (CFSE). Additionally, further studies are required in order to determine whether the lack of invasion of proneural BTICs may result from clonal selection or the absence of inducing triggers and if simulating intratumoural heterogeneity may restore it.

The data generated in this work is the first comparative analysis of primary proneural and mesenchymal BTICs and TCs infiltration via real time monitoring of invasion in an *in vivo* simulated setting. Organotypic brain slice cultures provided the framework to track the invasion of human glioma BTIC and tumour cells in an online, time- and space-disseminated manner. High infiltrative potential of mesenchymal GBM cells was confirmed, while cells of proneural subtype were barely invasive. The findings emphasise the importance of further investigation and understanding the dynamics and complexity of glioma cell invasion and its induction by microenvironmental cues for the future development of effective glioma treatments.

5.2. Cell subtype induction by the microenvironment: Defining leader, follower, and stationary cells

The ability of cancer cells to invade surrounding tissue is a major hallmark of cancer (Hanahan and Weinberg, 2011). Cancer cell invasion is not restricted to a single cell process (Friedl *et al.* 2012). Indeed, the majority of solid tumours exhibit characteristics of collective invasion or multicellular streaming (Polyak and Weinberg, 2009). There is general agreement that invasion is an early event in glioblastoma progression (Louis, 2006), although the exact appearance of this milestone is unknown. In regards to diffuse infiltration during glioma progression, it remains challenging, if not impossible, to find curative treatments. The motivation to develop anti-migratory therapeutic agents for glioma is to restrict them to their primary site, by arresting invasive tumour cells.

Prior studies often describe single glioma cells invading widely anywhere within the brain (Bellail *et al.* 2004), this concept is currently reconsidered towards a less rigid system where cells switch between single cell and collective invasion (Friedl and Wolf, 2003; Nevo *et al.* 2014). The detailed underlying molecular mechanisms and microenvironmental prerequisites that are relevant under physiological conditions for collective invasion as well as interdependence or contribution of other invasion modes, such as EMT and the ‘go versus grow’ hypothesis, are still under investigation. To gain deeper insight into the cues underlying glioma cell invasion, it was investigated whether cells invade in a radial or directed manner. It was investigated whether these cells interact during invasion or move separately and if they are attracted by certain structures.

OBSCs proved to be an advisable model to investigate direction and mechanisms of invasion as well as evolving phenotypic variability. The present data provided the first evidence for leader cell formation, cells which were assumed to be required for invasion as has been previously shown for breast cancer cells (Cheung *et al.* 2013). It was revealed that three distinct subpopulations – leader, follower, and stationary – emerged from the initial homogeneous cell population during OBSC infiltration (see paragraph 4.2.1). These cell subgroups exhibited distinct phenotypes. Utilising a newly developed single cell isolation method, the subgroups were isolated and defined according to their gene expression profiles. Although follower and stationary cells had some similarities, the clear distinction of leader cells at the level of gene expression was observed. The transcription factor signature of leader cells determined here offers the opportunity to identify and target their formation.

5.2.1. Formation of leader, follower, and stationary cells in OBSCs

Mesenchymal BTICs possess enhanced ability to infiltrate OBSC tissue compared to differentiated tumour cells, indicating that targeting this therapeutically resistant population of self-renewing cells might be the key to successfully treat GBM. Based on the present data, it seems likely that glioma cells assigned to the mesenchymal subtype develop specialised cells for multicellular invasion (Polyak and Weinberg, 2009) that are essential for glioma progression despite the commonly assumed concept of single cell infiltration (Bellail *et al.* 2004; Friedl and Wolf, 2010). Discrimination of different cell subtypes was, at first, an unexpected discovery, which was not described in context of OBSCs before. Encouragingly, Cheung *et al.* (2013) discovered that leader cell formation occurred depending on the microenvironment and was required for invasion of breast cancer cells. Additionally, a recently published report on melanoma and fibrosarcoma invasion in a 3D collagen matrix model elegantly revealed matrix porosity, but not rigidity, as the determinant of leader cell invasion (Haeger *et al.* 2014). The authors concluded that mesenchymal cells with constitutively weak cell-cell adhesion capacity, respond to ECM density by adjusting their cell-cell interactions in conjunction with aggregation and protease dependence, which results in a transition from single cell to collective invasion strategy, and vice versa. They postulate that this flexible response likely depends on signals received from local cues. In line with these findings, the observation of invasive strand formation of mesenchymal BTICs, TCs, and U87 on OBSCs, which was not seen in *in vitro* spheroid assays, suggests that there is a switch between migration patterns. This is further substantiated by measured differences in locomotion, as Friedl *et al.* (2012) described rates of $\leq 0.1 - 1 \mu\text{m min}^{-1}$ for collective invasion with maintained cell-cell contacts, whereas for multicellular or individual cells, streaming rates of about $1 \mu\text{m min}^{-1}$ were observed. Although, a fluent transition between both exists, rendering a clear demarcation difficult, locomotion of approximately $0.12 \mu\text{m min}^{-1}$ was observed for mesenchymal BTICs *in situ*, which supports an organised collective invasion form, whereas the distinctly faster migration of about $0.45 \mu\text{m min}^{-1}$ *in vitro* indicates a less rigid form of locomotion.

The present data indicate a model such as the OBSCs as being highly relevant, as it enables the investigation and dissociation of events within the infiltrative and non-infiltrative GBM cells. In addition, the microenvironment induces leader cells. Despite the advantages, the model is complex, thus to ensure reproducibility the development of a defined 3D matrix

similar to that used for breast cancer (Cheung *et al.* 2013), melanoma and fibrosarcoma (Haeger *et al.* 2014) invasions, would improve further glioma invasion studies. A defined matrix assay mimicking the tumour microenvironment present in the brain would enable reproducible high-throughput screening to target the onset of invasion.

Differences between cells from the periphery and the core have often been described in tumours (Nevo *et al.* 2014) or *in vitro* (Dhruv *et al.* 2013). The cell population in the tumour bulk is described as non-invasive, stationary and proliferative with intercellular connections (Nevo *et al.* 2014). In contrast, those are reduced or absent in invasive cells at the periphery (Hoelzinger *et al.* 2005). In the OBSC model, the observation of stationary cells that remained at the implantation site and of infiltrative cells leaving the implantation point matched predicted expectations. However, invasive strands were detected. It was possible to distinguish between leader cells at the migratory tip that may guide follower cells through the surrounding tissue (Haeger *et al.* 2014).

Although 2D single cell approaches *in vitro* provide insight into cell movement, formation of the three groups of leader, follower, and stationary cells was not observed in spheroid assays. These assays were used here to estimate basic migration rates of GBM cells, suggesting that *in vitro* migration assays result in a proof-of-principle than they resemble the complex reality

of three dimension *in vivo* conditions (Humpel, 2015).

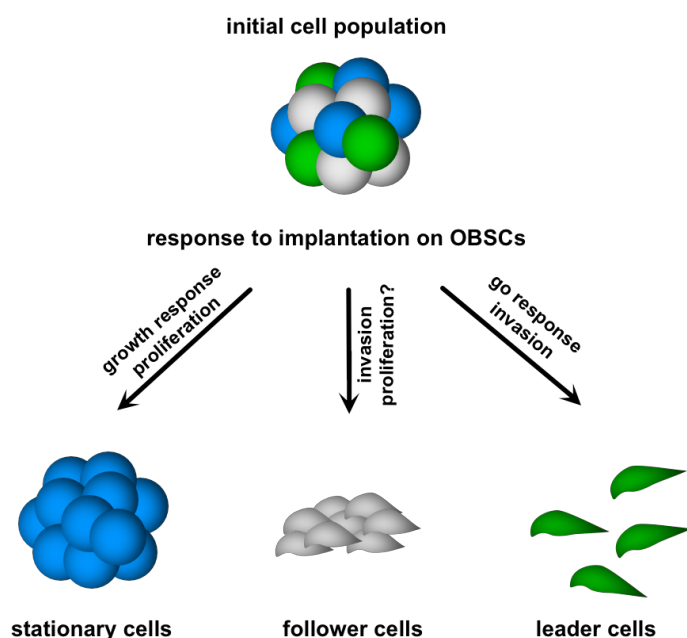


Figure 5-2: Go or growth response of GBM cells implanted on OBSCs

In line with the ‘go versus grow’ hypothesis described by Dhruv *et al.* (2013), from the present observations the hypothesis may be drawn that microenvironmental influences induced subgroup formation (Figure 5-2). While stationary cells may be driven to a ‘growing’ response – proliferative and non-invasive phenotype – a ‘go’ response is activated in leader cells – invasive and non-/less proliferative phenotype. Deeper

insight into the gene expression regulation was needed to classify follower cells, which appear in-between both states.

To challenge this hypothesis, the isolation method established in this work (see paragraph 4.2.2) was used to isolate cells of each fraction and enabled a straightforward analysis procedure for differential gene expression analysis.

5.2.2. Directed invasion of glioma cells in OBSCs

Several ‘active’ and ‘passive’ extracellular components are known to contribute to cancer invasion. Glioma cells are known to preferentially migrate along existing brain structures (reviewed in Cuddapah *et al.* 2014). This concept has been substantiated, as it was shown that vascular co-option and migration along white matter tracts are important features of glioma cell invasion (Friedl and Alexander, 2011; Nevo *et al.* 2014). In line with these factors, glioma cells implanted on OBSCs in this work were often found to invade the tissue in certain directions, whereas directed invasion was not seen in spheroid assays *in vitro*. In some cases, cells seemed to pass through narrow passages before spreading in a diffuse manner (Figure 4-3), supporting the hypothesis that glioma cells are attracted by certain structures (Cuddapah *et al.* 2014). For example, ECM structures including hyaluronic acid, proteoglycans, glycoproteins, and fibrous glycoproteins passively provide structural support and act as guiding scaffold or barrier for cancer cells (Hynes, 2009) and thus may attract and induce leader cells.

Additionally, cancer cells can be actively supported via proteolysis, for example, by MMPs released either from glioma or tumour infiltrating immune cells, or both (Joseph *et al.* 2014). Proteolysis loosens the ECM providing space to invade and can also cause release of cytokines and growth factors such as FGF, TGF β , and VEGF bound to ECM components (Hynes, 2009), which can further promote invasion. Thus, composition and interaction facilitates proliferation, migration, and invasion (Hynes, 2009) of cancer cells and can generate specific stem cell niches – such as perivascular, hypoxic, or acidic – that contribute to the fate of BTICs (Calabrese *et al.* 2007; Hjelmeland *et al.* 2011). Such mechanisms may still be observed in OBSCs as it was shown that capillaries, although no longer functional due to absent circulation, survive in organotypic slices and still seem to secrete a cocktail of cytokines that may indeed influence other cells in the slices (reviewed in Humpel, 2015).

Local growth factor release and presence of attractive ECM structures may be the cause for observed directed infiltration of the GBM cells. To further investigate this hypothesis, immunohistochemical staining of OBSCs (Norberg *et al.* 1999) after leader cell formation can likely resolve locally enhanced growth factor receptor presence or leader cell presence adjacent to certain structures such as blood vessels. The isolation technique developed in this work may provide a framework to compare differential gene expression of non-neoplastic cells, such as immune cells known to invade gliomas, surrounding leader cells with those in invasion-free areas of OBSCs. This may reveal possible invasion-supporting functions of non-neoplastic cells.

The challenging hypothesis may be drawn that disseminated brain tumour progenitor cells are led by the combined influences of microenvironment and specialised leader cells to colonise niches adjacent to the tumour. Located within the tumour, stationary cells may escape initial therapeutic treatments and may be attracted back to the initial tumour site after resection. For instance, cytokine release (such as $\text{TNF}\alpha$, $\text{TGF}\beta$, VEGF as described above) upon wound healing may induce new leader cells which drive invasion and re-colonisation of the parenchymal wound, thus inducing local tumour recurrence. Leader cells are likely the driving population for invasion, leading to local and distant recurrence after resection (see the expanded model in Figure 5-3). Due to their specific phenotype, leader cells or microenvironment factors that induce leader cells may be targeted specifically in therapeutic strategies and their reduction may reduce or abolish recurrences. A reduced pace or lower extension of recurrences could result in more localised, later recurrences and may reduce the risk of distant relapses.

During migration, brain infiltrating glioma cells are confronted with a complex interconnected ECM as well as several cell types present in the brain such as microglia, astrocytes, and neurons. Most studies investigating glioma cell invasion by expression profiling did not address the complex composition of heterogeneous GBMs. Important insights into the GBM landscape were gained from analysis of a large set of GBM samples provided by The Cancer Genome Atlas (TCGA). For example, the Verhaak classification describing each subtype with specific genetic alterations and gene expression signatures (Verhaak *et al.* 2010) based on gene expression and whole genome sequencing data was provided by the Cancer Genome Atlas Research Network in 2008. Other studies investigating glioma cell invasion focused on the tumour core and the infiltrative zone. Delic *et al.*, (2012) made a reasonable attempt by comparing gene expression profiles of laser capture microdissected human primary tumour

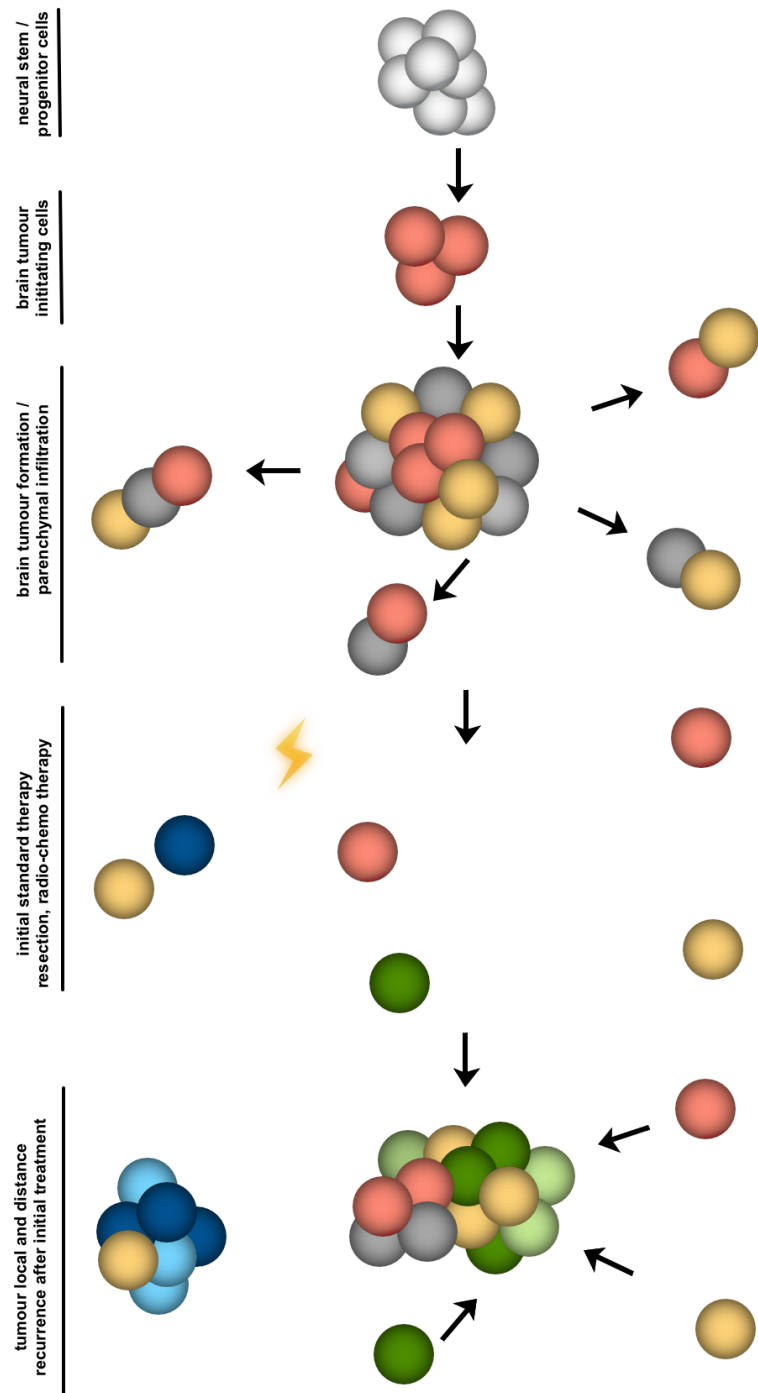


Figure 5-3: Expanded model of GBM formation, infiltration, and recurrence driven by BTICs

tissue specimens. Even more insight into the complex tumour cell and micro-environment interplays which are relevant for induction of invasion was provided by Nevo *et al.* (2014) with microarray profiling based on a human glioma stem cell xenograft model. The group revealed gene expression changes *in situ* between invading glioma cells compared to tumour core, and, in addition, changes in host cells residing within the infiltrated microenvironment relative to the unaffected cortex (Nevo *et al.* 2014). They identified molecules selectively expressed by invasive glioma cells, which may provide a starting point to identify microenvironmental cues that could induce leader cells. However, studies on the single cell level that distinguish between leader and follower cells in the infiltrative zone have not been reported.

The phenomenon of leader, follower, and stationary cell formation in OBSCs was assumed to depend on micro-environmental influences, and likely inter-cell contacts and/or communication to maintain a collective infiltration led by leader cells. To address this

hypothesis, cells of all three fractions were compared on the level of gene expression. Deeper investigation of underlying mechanisms was required to characterise the cells after separation into leader, follower, and stationary subpopulations. To isolate these cells, a micromanipulator adapter was developed. Unlike other physical separation methods such as flow sorting or laser capture approaches, this new technique did not bear the risk of affecting RNA preservation as occurs during fixation. A further important objective is the possibility to re-cultivate isolated vital single cells. Investigation of each fraction preserves progenitor features that cause the generation of a phenotypically identical population of leader cells during each re-implantation.

The present method may extend the results of two recent studies using combined epigenetic and genetic approaches to provide major insights in the complex evolutionary processes underlying the mechanisms driving malignant progression of low grade gliomas (Mazor *et al.* 2015), and the mechanisms of treatment resistance in GBM (Kim *et al.* 2015). As detailed above, Kim *et al.* (2015) performed whole exome sequencing of pairs of GBMs before and after therapy with temozolomide and described two predominant patterns at recurrence: linear evolution for locally and branched evolution of distally recurrent tumours. Mazor *et al.* (2015) analysed pairs of tumour samples, at diagnosis and after progression, and found that both genetic events and epigenetic events differed in recurrent tumours compared to respective non-treated primary tumours. They also described that hypermethylated G-CIMP-positive tumours frequently lost CpG methylation, especially in a gene subset after progression. This might indicate the loss of methylation as a driving force that activates transcription of genes that then turn into oncogenes (Mazor *et al.* 2015). In this context, the present method may serve for future studies of genetic and epigenetic evolution. The method provides the framework to model branched evolution, to analyse it during various stages, and to focus on leader cells that alone make distant tumour formation possible. Profound investigation of branched evolution may determine the key evolutionary changes necessary for leader cell formation in the right environment.

5.2.3. Gene expression profiling of leader, follower and stationary GBM cells

By nature of the different observed phenotypes of leader, follower, and stationary cells it seemed reasonable to assume that the invading cells differ in their gene regulatory networks from stationary cells rather than on genomic alterations due to clonal evolution (Tabassum and Polyak, 2015; Sottoriva *et al.* 2015) which occurred within this short time of incubation. To further exclude possible variance of intratumoural heterogeneity present in GBMs that might be preserved in primary progenitor cell culture (Sottoriva *et al.* 2013), the established cell line U87 was used for method establishment.

In general, established methods require at least 50,000 cells for gene expression profile analyses (Hartmann and Klein, 2006). These quantities could not be reached with the presented single cell isolation method. Thus, single cell analysis or even better analysis of small pools of single cells to reduce variances was a reasonable choice for the small amount of leader cells to be expected. Single cell transcripts were amplified using the method developed by Klein *et al.* (2002) to analyse the transcriptome of single micrometastatic cells. Quality PCRs revealed that even from a single cell cDNA, libraries could be generated, which is in general agreement with earlier studies (Hartmann and Klein, 2006). In addition, a pool of 20 cells per sample should decrease variability between the samples of each subpopulation in analysis of the microarray data.

A straightforward analysis procedure was presented which demonstrated a clear separation of leader cells from non-leader cells after hierarchical cluster analysis based on the gene expression profiles (Figure 4-17). Follower and stationary cells did not cluster separately, which was contrary to expectations and revealed high genetic similarity of both subgroups despite different phenotypes. To verify this similarity, a three pair-wise comparison of the information to which group the samples belong (Figure 4-18), was applied in cooperation with by Xin Lu, in the Department of Experimental Medicine and Therapy Research, Faculty of Medicine, University of Regensburg. In this analysis, follower and stationary populations could be distinguished based on DEGs with only a minor subset of genes being regulated similarly in both compared to leader cells. Nonetheless, follower and stationary cells are difficult to distinguish as revealed by the nearest neighbour analysis, which again clustered leader and non-leader cells separately, but did not distinguish follower and stationary cells in-between the non-leader group. Worth noting is the separate clustering of follower sample 7.

Hierarchical clustering and nearest neighbour analysis indicate that this sample ranged intermediately between leader and non-leader samples. This is most likely due to an accidental mingling of leader and follower cells during isolation and indicates the need of further confirmation of the results obtained here.

The observation of high similarity between follower and stationary cells is likely reasonable, in the context that normal stem cells depend on microenvironmental signals to reach an optimal balance between self-renewal, activation, and differentiation. This enables switching between stem and progenitor state (Borovski *et al.* 2011). As has been recently reviewed, a similar concept may apply to cancer stem and progenitor cells (Medema, 2013). In line with the hypothesis that subgroup formation is influenced by the microenvironment, Medema postulates that cancer stem cells may not be as autonomous as originally thought. Several studies propose a role for the microenvironment that constructs a cancer stem cell niche. In gliomas, this niche is postulated to be near endothelial cells, which might influence stemness by secreted factors (Calabrese *et al.* 2007). Based on our preliminary microarray data, it may be hypothesised that stationary cells generate their own niche at the implantation site due to microenvironmental influences (Calabrese *et al.* 2007). The presence of endothelial cells in blood vessels at the lateral ventricle or the close proximity to the SVZ may be responsible for induction (Vescovi *et al.* 2006). Simultaneously, differentiation of a cell fraction into leader cells could be induced by stimuli such as the presence of white matter tracts or a different response to blood vessel presence (Cuddapah *et al.* 2014; Nguyen-Ngoc *et al.* 2012). Cells seem to invade collectively (Friedl *et al.* 2012), hence it appears reasonable to conclude that leader cells somehow influence others to follow. Thus, further analysis of DEGs may reveal different expression of cell-cell contacts and/or cytokines between leader and non-leader cells.

As follower and stationary cells seem to possess high similarity, follower cells might be more flexible than leader cells and convert back to stationary cells in suitable niches. This would enable the formation of a new stem cell niche (Medema, 2013), or, as in *in vivo* situations, of a new tumour bulk (Kong *et al.* 2011; Claes *et al.* 2007). Initial re-culturing and re-implantation of stationary cells in OBSCs confirmed flexibility of the cells as formation of all three subpopulations was observed (data not shown). This promising finding should be further validated. Nevertheless, based on these observations, formation of leader cells was proposed to be necessary for infiltration, rendering leader cells as the major target to localise GBM repopulating cells in their respective niches.

5.2.4. The signature of leader cells

Several signalling pathways play a dual role in controlling cell growth and survival, as well as cell migration and invasion (Alexander & Friedl, 2012). Those ambiguous pathways include p53, Ras GTPase, small Rho GTPases, integrins, growth factor receptors and cadherins (Alexander & Friedl, 2012), as well as c-myc and NF- κ B signalling likely depending on micro-anatomical niche stimuli (Dhruv *et al.* 2013). Moreover, as described earlier, the main responsibility for acquisition of strong invasive potential of brain tumour cells may be attributed to EMT (Carro *et al.* 2010). EMT may account for the transformation of a subset into leaders with an infiltrative phenotype, but as a central question in collective invasion it remains to be unravelled how a subpopulation of cancer cells acquires infiltrative abilities.

It was shown that foremost mesenchymal BTICs and GBM cell lines were highly proliferative and invasive. The initial steps of local invasion require activation of signalling pathways which control cytoskeletal dynamics in the cells that induce cell- matrix and cell-cell junctions turnover in order to activate cell migration into the surrounding tissue (Friedl & Alexander, 2011). Recently, small molecule inhibition of mammalian Diaphanous family formins, which are Rho GTPase-directed effectors that regulate the F-actin cytoskeleton, were shown to inhibit migration glioma cell lines *in vitro* and invasion of U87 *in situ* in brain slice cultures (Arden *et al.* 2015). This finding stresses that invasion of glioma cells can be targeted. Single factor inhibition has often led to encouraging results, as GBM cell aggressiveness was reduced *in vitro* and often in *in vivo* animal models, but failed to be translated successfully into clinical approaches. Indicating that one target alone will not restrict invasion of GBM completely, thus it is important to identify signalling nodes, such as transcription factors, that regulate genes that lead to invasive leader cell formation.

The present study used reverse-engineered approaches based on mRNA expression rates identified in a microarray analysis to identify transcription factors which potentially trigger invasion and cause signalling changes during leader cell formation. In contrast, Dhruv *et al.* (2013) directly analysed transcription factor presence in the nuclear fraction of migrating and non-migrating cells. This method was not transferable to the present study as it was based on protein extraction of nuclear fractions, which requires a high number of cells that cannot be isolated with the single cell isolation method. Therefore, the presented transcription factor identification utilised established and published reverse-engineered methods based on mRNA expression rates. Moreover, the method of Dhruv *et al.* (2013) does take actual gene

expression into account, which cannot be equalled with transcription factor presence in the nucleus as expression of their target genes may be prevented by other levels of regulation such as methylation. However, the presented method does not consider post-transcriptional regulation.

Extracellular signals that are suggested to induce cell transition into the leader phenotype are usually processed by modulation of transcription factor activities. In response to extracellular signals, cellular receptors lead to transcription factors, which are activated or inhibited mediating required changes of gene expression. In general, transcription factor expression is stable and regulated via phosphorylation (e.g. STAT3) or inhibitors (e.g. NF- κ B – I κ B). Therefore, their activity can hardly be measured by their own gene expression, but rather by target gene expression. ISMARA (Balwierz *et al.* 2014) and ConsensuPathDB (Kamburov *et al.* 2013) analyses utilised the identified DEGs to reveal a set of transcription factors with increased activity in leader cells. Some of the detected transcription factors are well known to play essential roles during glioma cell invasion, including STAT3 (Carro *et al.* 2010) and NF- κ B (Dhruv *et al.* 2013).

In this work, a set of transcription factors is verified in samples of leader, follower, and stationary cells obtained from mesenchymal BTICs analysed in the OBSC model as well as in fresh patient tumour biopsies. The aim of which is to reveal a consistent signature that identifies leader cells with high sensitivity and specificity. In correlation to annotated DEGs, this signature may serve as basis to determine most of those genes relevant to induce and maintain migration and invasion. Although detailed analysis of these samples is currently ongoing, it can be proposed that the leader cell signature will assist in screening for pharmacological substances that inhibit its expression. Inhibition of this expression pattern will likely result in inhibition of leader cell formation as well as invasion.

The results obtained in this study raised several important questions central to the understanding of glioma infiltration. Formation of the specialised cell populations of leader, follower, and stationary cells was revealed, emphasising the importance of the OBSC model as an innovative and potent *in situ* method that is way closer to the *in vivo* situation. Additionally, this observation indicates that there is a heterogeneous cell population within a GBM tumour, which may result in the need of different drugs to effectively target them all. In contrast, quick relapse of GBM may be due to rapid changes in gene expression which cause the formation of leader, follower, and stationary cells. Switching between

the states when necessary seems reasonable, indicating possible pathways for relapse. Diffuse infiltration of the brain parenchyma by glioma cells is an early event, which renders them incurable by local therapy (Louis, 2006). Hence, deciphering mechanisms inducing infiltration may provide the knowledge to specifically identify and target leader cells. Therefore, the summarised data present a new method of deciphering different gene expression profiles between observed leader, follower, and stationary cells. This currently leads to a signature which specifically identifies leader cells with the aim to understand and then inhibit their formation.

Based on the presented findings, the initial model depicted in the introduction (Figure 3-7) has to be expanded by several other components to be considered to localise GBMs, as detailed in Figure 5-4. Tumour formation still requires the formation of BTICs, likely from aberrant NPCs (Modrek, 2014), while according to the proposed hypothesis specialised subpopulations are necessary to drive brain infiltration and tumour recurrence. Taken together, the findings suggest the need to target multiple pathways at the junction of invasive rim and microenvironment to prevent leader cell formation as a viable option for glioma therapy.

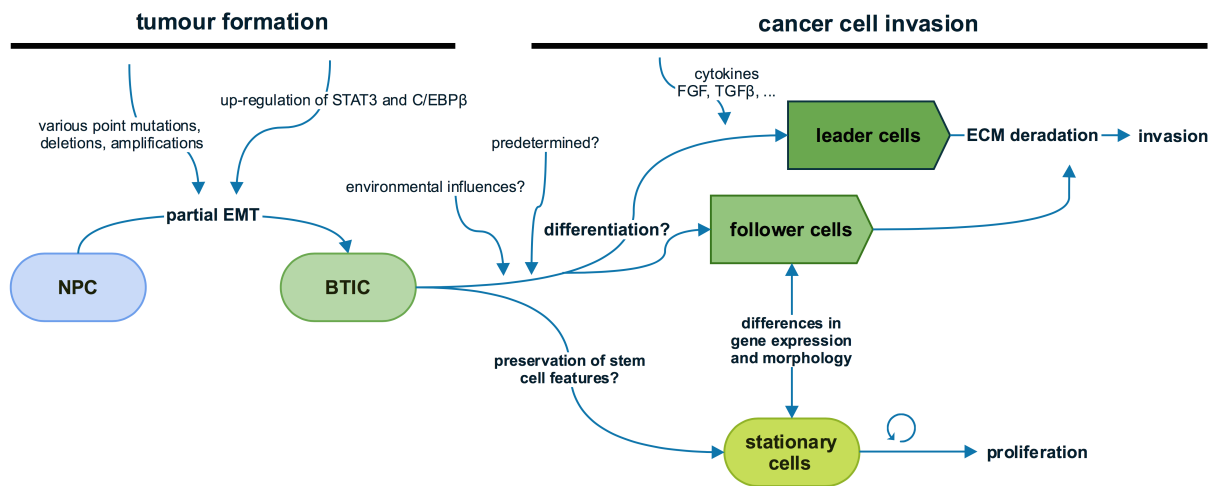


Figure 5-4: Schematic illustration of glioma formation and postulated role of BTICs

This illustration expands the initial model (introduction, Figure 3-7), suggesting that leader cells emerging from a BTIC population are the major factor responsible for GBM maintenance, invasion, and thus recurrence. BTICs may divide in subgroups of leader, follower, and stationary cells. Different mechanisms separate the cells into morphologically and functionally different subtypes, with leader cells initiating invasion into the surrounding tissue.

5.3. Clustering proneural and mesenchymal BTICs and TCs according to their proliferation and migration rates

The cancer stem cell hypothesis postulates that tumours arise from, and are maintained by a subpopulation of cells with stem cell properties. Cancer stem cells are defined by their ability to long-term self-renew, multilineage differentiation, and production of tumourigenic offspring which cause the cellular heterogeneity of a tumour (Singh *et al.* 2003). As detailed previously, BTICs display many of the properties characteristic for cancer stem cells (Singh *et al.* 2004), and BTIC lines have become a valuable tool to model GBM (Moeckel *et al.* 2014; Cusulin *et al.* 2015). The BTIC lines used in the present work were phenotypically diverse, with the majority of proneural lines growing in spheres and mesenchymal lines grew adherently, however, both were similar in their stem cell marker expression (Nestin, SOX2, and CD133) (Moeckel *et al.* 2014).

It was shown that sphere formation is not a premise for self-renewing growth and tumour formation, since glioma cells growing as monolayers were also tumourigenic (Cusulin *et al.* 2015). Despite their phenotypic divergence, the present set of heterogeneous primary BTICs had not been analysed before for unifying patterns according to which they might cluster. Therefore, in parallel to analysis of BTICs in the OBSC model, they were classified *in vitro*, first, by their expression of transcription factors that regulate critical signalling pathways, second, their proliferation, and third, their migration capacities. Correlation of proliferation and migration rates enabled subgroup specific clustering of the cells.

5.3.1. Deciphering transcription factor protein expression of BTIC and GBM cell lines

Overall, initially addressed protein expression of the analysed transcription factors STAT3, C/EBP β , c-myc, AMPK, mTOR, and SMAD2/3 revealed an heterogeneous expression pattern with high inter-line diversities (see section 4.3.1.1). This selection of transcription factors was chosen according to their relevance in signalling pathways associated with proliferation and/or migration. Special focus was set on STAT3 and C/EBP β due to their function in GBM invasion described by previous studies (Carro *et al.* 2010; Xia *et al.* 2015; Poli & Camporeale, 2015).

The data generated in this work could indicate that different compositions of dysregulated gene and protein expression are necessary to constitute tumour cell growth. Since, one constitutively active growth-enhancing signal is not enough to induce the formation of a tumour, but rather needs to be accompanied by the loss or gain of critical other key functions (Van Meir *et al.* 2010). However, total STAT3 was found to be distinctly increased in mesenchymal compared to proneural BTICs which corresponds to previously determined results (Carro *et al.* 2010) (Figure 4-23A and Figure 4-24A). Interestingly, increased activity as measured by phosphorylation status of Y705 and S727 was not observed in mesenchymal compared to proneural BTIC. This may be indicative for a constitutive activation of STAT3, which causes the mesenchymal lineage. Indeed, an engineered mutant form of STAT3 which is constitutively active and does not require phosphorylation, termed STAT3C (Bromberg *et al.* 1999), has been shown to trigger a metabolic switch by enhancing aerobic glycolysis, and reduce oxidative phosphorylation as well as mitochondrial activation (Poli & Camporeale, 2015). However, no naturally mutation has so far been detected that induces constitutive activation of STAT3 (Calò *et al.* 2003). In contrast, proneural BTICs may use oxidative phosphorylation preferentially. This corresponds to and is the subject of current investigations (unpublished work of Seliger *et al.*). Interestingly, GBM cell lines displayed elevated phosphorylation levels of STAT3 at S727 instead of increased total STAT3. Recently, there is increasing awareness of pSTAT S727 importance in mitochondria function. It can localise to mitochondria and preserve oxidative phosphorylation, control the opening of the mitochondrial permeability transition pore, as well as promote survival and resistance to apoptosis (Poli & Camporeale, 2015). Thus, the data generated here indicate that GBM cell lines may depend more on phosphorylation of STAT at S727 than on constitutively active STAT3 similar to mesenchymal BTICs.

In line, with elevated STAT3, the protein expression of the LAP1 and 2 isoforms of C/EBP β were elevated in mesenchymal compared to proneural BTICs (Figure 4-23B and Figure 4-24B), which is in general agreement with previously published findings (Carro *et al.* 2010). In contrast, GBM cell lines revealed slightly increased LIP expression and distinctly elevated LAP1 and 2 expression compared to BTICs, corresponding to the often observed mesenchymal drift in long-term GBM cell cultures (Tso *et al.* 2006). Thus, at least in the view of low C/EBP β isoform expression, proneural BTICs were not targets of the mesenchymal drift.

As c-myc has pivotal function in growth control, differentiation as well as apoptosis, and its abnormal expression is associated with malignancy of GBMs (Herms *et al.* 1999), its moderate expression in all groups was expected (Figure 4-23C and Figure 4-24C). Although, c-myc is a known down-stream target of STAT3 (Bromberg *et al.* 1999), its expression was lowest in mesenchymal BTICs, which had higher total STAT3 levels than the other groups. The active phosphorylated form – able to induce transcription – was not elevated in any group distinctly, it likely did not have an effect on c-myc protein expression. Thus, c-myc seemed to be more autonomously induced than STAT3 dependent, at least on protein expression level. However, STAT3 is only one among several c-myc activation triggers. The observation of elevated c-myc in proneural cells, which are barely invasive, at least *in situ*, is in line with the finding that c-myc depletion causes a phenotypic switch of glioma cells from a proliferative phenotype to a migratory phenotype accompanied by a decrease in cell proliferation (Dhruv *et al.* 2013). Although, a high degree of interline diversity calls for caution. This indicates a more STAT3 independent c-myc signalling, since STAT3 is known to enhance invasion (Carro *et al.* 2010).

Akhanvan *et al.* (2010) reviewed function of mTOR as an important factor in gliomagenesis, because of its key role in the PI3K signalling pathway, where it controls cell growth, metabolism, and autophagy. Moreover, mTOR can act either indirectly via SOCS3 or directly on STAT3 downstream of IL-6 (Howie *et al.* 2014). Thus, it was unexpected that mTOR was not subject to any great variations between cell lines (Figure 4-25A and Figure 4-26A). As seen in Figure 4-24A, pSTAT3 S727 was up-regulated in GBM cell lines, especially in A172, which might explain the observed increase of (p)mTOR. Indeed, Yokogami *et al.* (2000) demonstrated that mTOR is able to phosphorylate the STAT3 S727 site. In agreement to these findings, the present data provide an encouraging hint towards an mTOR pSTAT3 S727 interaction, which is a novel finding in GBM and thus should to be explored further.

The role of the metabolic master switch AMP kinase is discussed controversially, with functions either as a tumour suppressor or contextual promoter (Liang & Mills, 2013). On the one hand, AMPK is known to inhibit mTOR and thus thought to act as a tumour suppressor. On the other hand, AMPK may promote cell survival and oncogenic transformation in response to certain extrinsic and intrinsic stress factors, due to its wide spectrum of signalling based on the important function of AMPKs in monitoring and maintaining cellular energy homeostasis (Liang & Mills, 2013). Contradicting to the known

inhibitory function of active AMPK on mTOR, high levels of phosphorylated and total AMPK as well as mTOR were observed in proneural and GBM cells (Figure 4-25B and Figure 4-26B), especially in A172. In mesenchymal BTICs, total AMPK and mTOR expression was moderate, however, low levels of phosphorylated AMPK correlated with increased phosphorylated mTOR. This observation may indicate an impaired AMPK / mTOR signalling in proneural BTICs and GBM cell lines, a theory worthy of further investigation. However, reviewing (p)mTOR and (p)AMPK protein expression in BTICs, it remains difficult to draw conclusions based on their expression levels. In relation to proposed deeper investigation of metabolism in the cell lines investigated in this work, mTOR and AMPK should be explored further. The role of AMPK may depend on the degree of its activation, presence of AMPK isoforms, interaction with other signalling cascades such as p53, and other extrinsic and intrinsic processes activated in a cell (Liang & Mills, 2013). Therefore, it is important to further investigate AMPK regulation not independently, but in a cellular context.

Phosphorylated pSMAD2/3 is generally shown to investigate changes in the classical TGF β signalling pathway (Figure 4-25C and Figure 4-26C). Increased levels of active SMAD2/3 were assumed, hence the TGF β /SMAD2/3 signal pathway is known to be activated in human brain glioma cells (Zhao *et al.* 2015), and has been confirmed in proneural BTICs and GBM cell lines. It was interesting that GBM and BTIC lines did not cluster together here, although both groups exhibited increased proliferation rates compared to proneural BTICs. Previously, TGF β /SMAD2/3 signalling has been shown to promote GBM proliferation (Bruna *et al.* 2007). However, this would have to be the subject of a deeper investigation of the influence of TGF β on gliomas and the role of SMAD2/3 in this signalling pathway (current investigation of Meyer and Seliger *et al.*).

It is difficult to draw any particular conclusion from the p44/42 MAPK (ERK1/2) expression pattern (Figure 4-25D and Figure 4-26D), although distinct interline disparities were observed in phosphorylated p44/42 MAPK. The present data were in line with Glassman *et al.*, (2011) who described constitutive activity of the MAPK/ERK1/2 signalling pathway. Although, Zohrabian *et al.* (2009) described an important role of MAPK signalling pathways in glioma motility and growth, significantly increased expression of (p)p44/42 MAPK in cells with enhanced motility was neither observed nor could the present data be correlated with differences in cell proliferation, migration, or GBM subtype. EGF receptor activity functions via Ras small GTPase activation on the Raf-MEK-ERK pathway, which includes

p44/42 MAPK (Roberts & Der, 2007). EGF receptor amplification or other alterations are common in GBMs (Roth & Weller, 2014), thus further investigations may need to view p44/42 MAPK in this context.

The presented transcription factor expression profiles of proneural and mesenchymal BTICs as well as GBM cell lines revealed inter-line variances, and rarely, transcription factor levels were characteristic for one group. Thus, the possibility that all lines are genetically distinct even within the subgroups and that this contributes to disparities within the results might not be excluded. As transcription factors often require phosphorylation to influence target gene transcription, it is important to analyse the phosphorylation status, as performed here. For deeper insights, transcriptional activities of the factors should be investigated by analysis of mRNA expression of their target genes in order to address the complexity of the initial question if group specific patterns can be determined.

The individual analysis of several transcription factors conducted in this work provided a general overview, however, failed to reveal unique patterns within the analysed groups. Therefore, an integrative analysis is required to enable study of the interplay of all transcription factors. This may be accomplished by the previously described integrative approach for identification of a leader cell signature, which identifies transcription factor activities based on their motif presence in differentially expressed genes. Nonetheless, the data generated here provides first evidence that cell metabolism with special regard to pSTAT3 S727 is an important topic for further research. These encouraging hints should be validated in a larger set of samples to eliminate disparities within the results and reveal new mechanisms of and interactions between the transcription factors in GBM.

5.3.2. Correlation of proliferation and migration rates distinguished proneural and mesenchymal BTICs and TCs

The next step towards identification of a pattern which could distinguish proneural and mesenchymal groups was the analysis of proliferation rates (see section 4.3.1.2). Glassmann *et al.* (2011) describe doubling times of common human glioma cell lines, among those A172 (17.6 h) and U87 (25.3 h) were measured by DAPI staining and cell counting. In contrast, proliferation data generated in this work were reported after CyQuant assay measurement, which ensured no cell loss due to washing steps. Likely due to passaging effects, A172 revealed an increased doubling time of 33.9 h, while U87 corresponded well to the

Glassmann study with 30.9 h (Table 4-2). Therefore, doubling times of primary BTICs classified according to Verhaak *et al.* (2010) were not yet reported and the data generated here broadly corresponded to the literature. The CyQuant assay, therefore, was assumed to be suitable for characterising BTIC and TC proliferation.

Dramatically different profiles were identified in proneural compared to mesenchymal and GBM lines (Table 4-2, Figure 4-34A), as their doubling times were roughly twice that of mesenchymal and GBM lines. The striking difference in proliferation of proneural and mesenchymal primary cell lines was a novel finding, indicating that both groups can be separated according to it, at least *in vitro*. The study of Philips *et al.* (2006) described dramatically increased survival of patients with proneural GBMs, which they correlated with low proliferation rates. This was not yet been confirmed with primary progenitor cells defined according to the Verhaak classification (Verhaak *et al.* 2010). Moreover, proliferation analysis provided compelling evidence that progenitor and differentiated state of primary lines may not be differentiated, as every pair showed doubling times roughly within the same range. Despite multilineage differentiation (data not shown), which resulted in loss of stem cell marker expression (CD133⁺, Nestin⁺), and acquisition of differentiated neural cell markers (GFAP⁺, β -III tubulin⁺) (Singh *et al.* 2003), proliferative capacities of progenitor and differentiated pairs have not been previously investigated, and surprisingly, were not observed to be altered distinctly. Thus, the differentiated tumour stem cell immunophenotype still represents potent proliferative cells. In addition, expectations were matched as cells of the mesenchymal subtype could not be separated from GBM cell lines, as long-term culturing usually causes a mesenchymal drift (Tso *et al.* 2006).

Determining basic migration rates was another step towards distinction of all cell subgroups from each other. Again Glassmann *et al.* (2011) provided a reference for glioma cell line migration calculated on basis of single cell time-lapse microscopy. They report average migration rates of $363 \pm 134 \mu\text{m day}^{-1}$ for A172, and $179 \pm 91 \mu\text{m day}^{-1}$ for U87 (\pm SD), while here rates of $560 \pm 73 \mu\text{m day}^{-1}$ (A172), and $620 \pm 29 \mu\text{m day}^{-1}$ (U87) were observed (Table 4-3). It seems reasonable that single cell tracking (Glassmann *et al.* 2011) is more accurate than calculating average migration rates from spheroid assays, where a falsification by cell proliferation can increase the reported migration rates. However, since single cell time-lapse microscopy would have been more complex for analysis of all cell lines used, spheroid assays were considered as better choice in regards to availability, time- and cost-efficiency. For deeper investigation, it might be useful to validate the data by single cell

migration tracing. Here, estimated migration rates were within an acceptable range, as single cell velocities of $1 \mu\text{m min}^{-1}$ or even faster were described in experimental settings for cancer cells (Friedl *et al.* 2012).

To date, proneural and mesenchymal progenitor and differentiated pairs have not been investigated regarding their migration potentials. In contrast to proliferation, analysis of *in vitro* migration rates provided a clear separation of BTICs and TCs (Table 4-3, Figure 4-34 B). While proneural and mesenchymal BTICs as well as GBM cell lines were indistinguishable in view of migration rates, proneural TCs could be separated by significantly reduced and mesenchymal TCs by significantly increased migration rates. These encouraging results may provide hints to distinguish BTICs and TCs in culture before immunohistochemical staining for stemness or differentiation markers. As described and discussed above, proneural BTIC migration was analysed on laminin coated surfaces, since only adherent cells could be analysed for migration capacity.

Given that proneural TCs revealed decreased locomotion upon differentiation, while it was increased in mesenchymal cells, proneural BTICs may differentiate into less invasive descendants, whereas mesenchymal BTICs could undergo further EMT during differentiation, resulting in higher locomotion. However, this hypothesis requires further investigations, since in the OBSC model no significant differences could be revealed between proneural BTICs and TCs, whereas mesenchymal BTICs showed enhanced locomotion compared to their differentiated counter parts. As it will be discussed in the next chapter, this divergence likely results from migration modes that differ between the 2D *in vitro* setting, where cells adhere to a substrate on one side in a barrier-free surrounding and the 3D *in situ* model, where cells adhere at several sides to the ECM and likely need proteolytic activity to form a track (Friedl & Alexander, 2011). Still, the set of *in vitro* migration data provided insight in the general behaviour of proneural and mesenchymal cells.

Based on the encouraging results received from proliferation and migration assays it appeared obvious to plot them in a 2-dimensional coordinate system. Migration rates ($\mu\text{m day}^{-1}$) were depicted on the x-axis correlated to the respective proliferation rates (% increase day^{-1}). This revealed a separation according to the given groups (Figure 4-34C). Overall, proneural BTICs and TCs clustered closely in their groups, while mesenchymal cells had a larger distribution, which may account for higher inter-line diversities. Overall, correlation of proliferation and migration rates revealed distinct patterns for BTICs and their respective TCs that, at least

in vitro, may serve as classification reference for other not yet categorised primary glioma cell specimen, and hint to their differentiation status, as well as precursor state.

Previous studies analysed BTICs in attempt to assign them to subgroups, but comparisons of BTICs and TCs have not been made to reveal differences in proliferation and migration among them (Günther *et al.* 2008; Cusulin *et al.* 2015; Mao *et al.* 2013). Günther *et al.* (2008) analysed BTIC lines based on their phenotypic growth and differentiation behaviour and revealed that they differ in gene expression. Here, characteristic growth patterns were observed between proneural, often growing in spheres, and mesenchymal BTICs, usually growing adherently. However, patterns were not subtype exclusive and upon differentiation, all cells grew adherently which prevented phenotypical indication of a specific subtype.

Mao *et al.* (2013) described two distinct glioma stem cell subtypes that were divided in proneural and mesenchymal groups by transcriptomic profiling. In line with the data generated in this work, they showed that mesenchymal subtypes were more aggressive *in vitro* as well as *in vivo* than the proneural group. Cusulin *et al.* (2015) extended this observation by dividing a set of BTICs in stem- and progenitor-like precursor states. They associated the stem-like lines to the proneural subtype and concluded that they maintain more stem cell features and contain a higher proportion of tumour initiating cells than progenitor-like lines, associated to the mesenchymal subtype. Hence, they stress the hypothesis that the mesenchymal subtype may be hierarchically downstream of the proneural one (Cusulin *et al.* 2015). This hierarchy in tumour evolution bases on the mesenchymal shift of GBMs upon recurrence (Phillips *et al.* 2006) and the analysis of temporal sequence of driver events during tumourigenesis, indicating that the majority of non-GCIMP mesenchymal GBMs evolve from a proneural-like precursor (Ozawa *et al.* 2014). Bearing this in mind, the revealed distinct differences between proneural and mesenchymal BTICs and TCs by correlation of their proliferation and migration abilities calls for future investigation of their hierarchical positions during tumour evolution to add another clue to different precursor states of both subgroups.

In summary, correlation of proliferation and migration abilities could characterise each subgroup, see Figure 5-5. This correlation may improve BTIC characterisation and hint towards subtype indication, differentiation status, tumour evolution, and precursor state, although it can only serve as an initial characterisation and must be extended beyond by clonogenicity, tumour take, and genetic profiling.

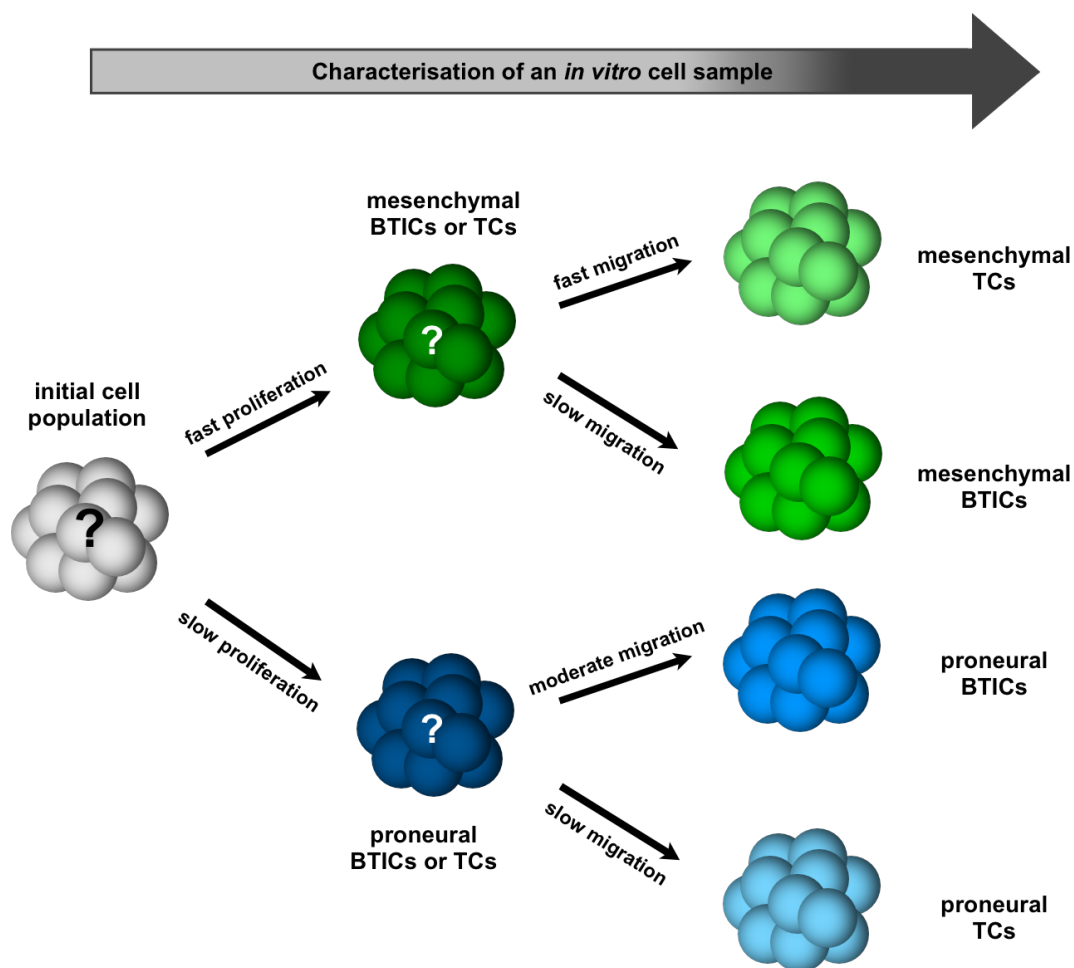


Figure 5-5: Characterisation of an initial *in vitro* glioma cell population by correlation of proliferation and migration rates

5.4. Diclofenac and ibuprofen restrict GBM cells via modulation of STAT3 signalling

GBM are not only characterised by infiltration of the brain. Enhanced mitotic activity and angiogenesis are additional hallmarks. Moreover, inflammation is an important contributor to the development and progression of human cancers. Non-steroidal anti-inflammatory drugs (NSAIDs) have been associated with anti-tumourigenic effects in different tumour entities (Sørensen *et al.* 2003; Ulrich *et al.* 2006) such as breast (Harris *et al.* 2006) or prostate cancer (Andrews *et al.* 2002). As outlined in the introduction (see paragraph 3.3.4), traditional NSAIDs are non-selective COX-1 and -2 inhibitors. These include ibuprofen (Warner *et al.* 1999) and diclofenac (Giuliano & Warner, 1999). Non-selective inhibition of COX-2 leads to decreased prostaglandin synthesis (Ulrich *et al.* 2006), which is important because

prostaglandin E2 was associated with tumour cell promotion (Marx, 2001). Thus, the NSAIDs ibuprofen and diclofenac may be candidates for a supportive therapy of gliomas. For glioma, research has generally focused on diclofenac, and data on other NSAIDs, such as ibuprofen, is limited.

Previous studies (Chirasani *et al.* 2013; Gottfried *et al.* 2013) revealed that diclofenac treatment of human and murine GBM cell lines caused c-myc inhibition followed by decreased gene expression of glucose transporter 1, as well as decreased LDH-A, and lactate secretion (Gottfried *et al.* 2013). Moreover, diclofenac inhibited STAT3 phosphorylation and lactate formation, induced cell cycle arrest at G2/M, and delayed tumour growth in an *in vivo* animal model (Chirasani *et al.* 2013). Based on this knowledge, the current study was designed to evaluate the effects of the NSAIDs diclofenac and ibuprofen on the proliferation and migration level in several human glioma cells (see section 4.3.3.1). Significantly decreased migration and proliferation of all GBM cell lines were observed from both diclofenac and ibuprofen treatment. In agreement with the preceding studies (Chirasani *et al.* 2013; Gottfried *et al.* 2013), increasing concentrations increasingly enhanced attenuating effects on cell proliferation. Current findings of the same effects on migration *in vitro* expand the prior findings. In the experimental setting, diclofenac was used at concentrations routinely reached in patients who take these medications (FDA information for diclofenac: www.drugs.com/pro/diclofenac.html). In contrast, ibuprofen concentrations exceeding appropriate physiological concentrations (FDA information for ibuprofen: www.drugs.com/pro/ibuprofen.html), but within the IC₅₀ range (Table 5-1; Leidgens *et al.* 2015), led to most significant effects in *in vitro* assays. However, further investigations (Leidgens *et al.* 2015) revealed that long-term treatment in routinely recommended concentrations has promising inhibitory effects on cell cycle and cell proliferation. In addition, higher ibuprofen concentrations may be reached in regions of blood-brain-barrier disruption, which can accompany gliomas (Cuddapah *et al.* 2014). For instance, localised increases in ibuprofen concentration in regions of interest may be possible by use of ibuprofen nanocarriers (Clond *et al.* 2013).

A dose-dependent highly significant restriction of cell migration by ibuprofen and diclofenac was observed. Bearing in mind that NF- κ B inhibition reduced GBM cell migration (Dhruv *et al.* 2013), a possible explanation for the observed effect is the known inhibition of nuclear translocation of NF- κ B by both NSAIDs. Diclofenac prevents TNF α induced NF- κ B

translocation (Fredriksson *et al.* 2011), while ibuprofen prevents degradation of I κ B α , the NF- κ B inhibitory protein in prostate cancer (Palayoor *et al.* 1999).

The simultaneous restriction of migration and proliferation indicates that ibuprofen and diclofenac restrict both growing and going signals. Despite similar effects on proliferation of both NSAIDs (Figure 4-35), ibuprofen more efficiently reduced migration of GBM cell lines than diclofenac (Figure 4-36). The greatest effect was observed on U87 cells, which revealed extreme differences in average migration rates at control conditions (Table 4-6). In contrast to proliferation assays, migration assays with both treatments were not performed in parallel, indicating that high variances are due to different passages used. During diclofenac assays, cells revealed a basic migration rate of about 153 $\mu\text{m day}^{-1}$, which were consistent between DMSO and non-treated (data not shown) control conditions. During spheroid assays performed with ibuprofen treatment, migration rates were increased 10-fold, while for estimating basic migration, the rate was moderate ($\sim 620 \mu\text{m day}^{-1}$, Table 4-4). However, such high variances were not observed in any other cell line. Further studies should address variances in migration and proliferation of U87 cells by parallel assay performance and more replicates.

The results obtained here were in general agreement with previous publications that revealed reduced extracellular lactate levels upon diclofenac treatment and a significant reduction of glioma cell migration (Seliger *et al.* 2013), in addition, reduced lactate levels are accompanied by a dose-dependent inhibition of cell growth (Chirasani *et al.* 2013; Gottfried *et al.* 2013). Based on the reports of diclofenac influence on lactate, the influence of ibuprofen was investigated. Indeed, ibuprofen reduced lactate levels, but to a lower extent than diclofenac (Leidgens *et al.* 2015). To explain these functional data, a potential COX-independent mechanism for both NSAIDs was assumed. Many highly proliferating solid tumours are characterised by intrinsic or induced expression of transcription factors which affect the cell cycle. High expression and activation of STAT3 (Carro *et al.* 2010; Buettner *et al.* 2002) and c-myc (Herms *et al.* 1999) are well known to be pathophysiological mechanisms in malignant gliomas. pSTAT3 Y705 levels were substantially reduced in presence of diclofenac. Diclofenac is known to have an impact on LDH-A (Chirasani *et al.* 2013), which is a direct target of c-myc (Shim *et al.* 1997), and can itself be induced by STAT3 (Buettner *et al.* 2002). Therefore, STAT3 and c-myc were investigated as possible modulators of the observed functional effects.

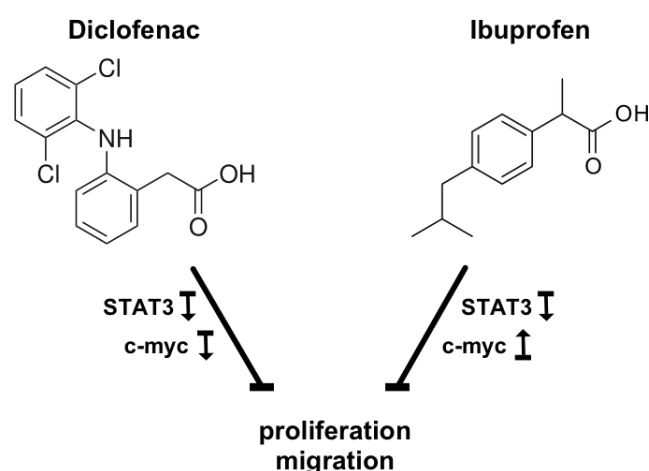


Figure 5-6: Influence of diclofenac or ibuprofen on GBM cells

Diclofenac and ibuprofen reduce GBM cell proliferation and migration. Both NSAIDs reduce STAT3 levels, but have reciprocal impact on c-myc.

Indeed, both agents decreased STAT3 phosphorylation at its physiologically active Y705 (Figure 4-37). Against expectation, c-myc expression was enhanced significantly after treatment with ibuprofen, whereas diclofenac reduced c-myc, indicating different cellular responses (Figure 5-6).

Depletion of c-myc led to enhanced migration and its expression was increased in migration restricted GBM cells, which was also associated with decreased transcriptional activity of NF- κ B (Dhruv *et al.* 2013). It, therefore,

seems reasonable that ibuprofen may restrict migration via c-myc induction and prevention of NF- κ B nuclear translocation by stabilisation of I κ B α (Palayoor *et al.* 1999). As proliferation is also restricted, which could be likely upon c-myc induction, STAT3 signalling could impact this mechanism. In contrast, diclofenac could restrict GBM cell proliferation and migration via repression of all three signalling pathways. For instance, the described transcription factor profiling provides a suitable framework for future studies to resolve these assumptions. Transcription factor profiling may reveal differential activation of the indicated transcription factors between GBM cells between non-restricted – control – and proliferation as well as migration restricted – NSAID treatment – conditions.

A full elaboration of the signalling pathways affected by ibuprofen and diclofenac is a remaining challenge which was beyond the scope of this study. The focus was set on STAT3 due to its known contribution to GBM and to limit the complexity of multi-target effects which contribute to GBM cell restriction upon diclofenac and ibuprofen treatment. To further investigate the impact of STAT3 inhibition, the specific inhibitor Stattic, which prevents STAT3 phosphorylation and thus activation, was applied to GBM cells (see paragraph 4.3.3.2; Leidgens *et al.* 2015). Overall, the highest applied Stattic concentrations were necessary to reduce proliferation and migration of GBM cell lines by half (IC₅₀) (see Table 5-1). Physiological concentrations of diclofenac decreased proliferation by half, whereas higher concentrations seem to be necessary for migration. Ibuprofen proved to be

effective only at concentrations exceeding the physiological concentrations, but was efficient on long-term low dosage treatment (Leidgens *et al.* 2015). These results support that STAT3 seems to be an important factor contributing to proliferation and migration of GBM cells.

Category	IC ₅₀ Stattic		IC ₅₀ Diclofenac		IC ₅₀ Ibuprofen	
GBM lines	Proliferation	Migration	Proliferation	Migration	Proliferation	Migration
A172	15 – 20 μ M	\geq 15 μ M	0.1 – 0.2 mM	> 0.2 mM	1 – 2 mM	> 2 mM
HTZ349	\geq 20 μ M	\geq 15 μ M	0.1 – 0.2 mM	> 0.2 mM	1 – 2 mM	\geq 1 mM
U87	\geq 15 μ M	10 – 15 μ M	0.1 – 0.2 mM	> 0.2 mM	1 – 2 mM	1 – 2 mM
GBM lines	15 – 20 μ M	10 – 15 μ M	0.1 – 0.2 mM	> 0.2 mM	1 – 2 mM	\geq 2 mM

Table 5-1: Proliferation and migration inhibitory effect of Stattic, diclofenac, and ibuprofen on GBM lines

As expected, Stattic efficiently decreased phosphorylation at the Y705 residue and further led to c-myc decrease (Figure 4-38). In addition, significantly reduced LDH-A mRNA expression levels were observed in two of three GBM cell lines (Figure 4-39) as well as a decrease of LDH activity, corresponding to effects observed after diclofenac treatment (Leidgens *et al.* 2015). This may indicate a comparable inhibiting influence of diclofenac on STAT3 which leads to down-regulation of c-myc and further decreases LDH-A mRNA expression, LDH activity, and lactate levels (Leidgens *et al.* 2015). In contrast, ibuprofen namely repressed STAT3 phosphorylation at Y705, but induced c-myc. Thus, decreases in, to a lesser extent, LDH-A mRNA expression, LDH activity, and lactate levels may hardly be surprising. In addition, Stattic exhibited comparable effects on cell proliferation (Figure 4-40) and migration (Figure 4-44), supporting the substantial role of STAT3 in this regulation cascade.

Although not directly proven, restriction of STAT3 phosphorylation at Y705 could constitute a COX-independent mechanism of the anti-tumourigenic efficacy of ibuprofen and diclofenac. However, the variety of effects of NSAIDs on GBM remains unravelled and molecular mechanisms related to resistance need to be studied in detail.

Nevertheless, the *in vitro* results of this study combined with further studies (Leidgens *et al.* 2015) may indicate a potential of diclofenac and ibuprofen to augment GBM treatment in patients, due to their migration and proliferation inhibiting effects. The results presented here suggest the need to evaluate the response and their efficacy as an adjuvant therapy in patients with high-grade gliomas, especially glioblastomas, as more effective chemo-preventive regimens are needed for treatment. Further comparative studies with different NSAIDs and

in vivo studies are necessary to affirm the conclusions drawn from these analyses on the spectra of positive effects of diclofenac and ibuprofen in GBM.

5.5. Specific STAT3 inhibition via Stattic restricts glioma cells *in vitro* and *in situ*

At normal conditions and during development, the activation of STAT3 and its induction of gene transcription are strictly regulated (Buettner *et al.* 2002). However, emerging evidence supports the idea that STAT3 is required to maintain a transformed phenotype (Bromberg, 2001) and plays an important role in oncogenesis, in line with the observations generated in this work. Extensive approaches have been performed to identify and understand aberrant regulation of STAT3 and its impact on proliferation, migration, and invasion. Among those, Bromberg *et al.* (2001) reported that dominant-negative STAT3 abrogated oncogenic transformation, whereas constitutively activated STAT3C mutants induced it. Furthermore, the study of Carro *et al.* (2010) revealed STAT3 in human glioma cells to be essential to maintain the tumour initiating capacity and the ability to invade the normal brain, as well as the combined expression of C/EBP β and STAT3 to be linked to the mesenchymal state of primary GBM (Carro *et al.* 2010).

These findings indicated STAT3 as a promising target for anticancer therapy. Supportive of that idea was evidence of STAT3 inhibition upon ibuprofen or diclofenac treatment, which caused restriction of GBM cell proliferation and migration in this work. The inhibiting effects of specific STAT3 inhibition by Stattic were also explored in BTICs and their differentiated counterparts (see paragraph 4.3.3.2). Indeed, proliferation and migration could be inhibited significantly in all subgroups *in vitro*, using different Stattic concentrations (Table 4-7). This achievement correlated well with enhanced transcriptional activity of STAT3 observed during transcription factor profiling in leader cells, which led to proof-of-principle testing in OBSCs. Expectations were confirmed as clear restriction of brain slice tissue infiltration by glioma cells was revealed upon Stattic treatment (see paragraph 4.3.4).

Although, *in vitro* studies reported cell cytotoxicity even with low Stattic concentrations, and *in vivo* animal studies revealed no signs of side effects using Stattic rates distinctly exceeding those concentrations used *in vitro*. Missing side effects are likely due to the fact that STAT3 may not be essential for viability of normal cells in adult mammals (Bromberg, 2002), although ablation of STAT3 led to early embryonic lethality (Levy & Lee,

2002). Lin *et al.* (2010) demonstrated high cell cytotoxicity rates in GBM cell lines *in vitro* even with low Stattic concentrations (0.73 μ M U87 and 0.84 μ M U251), whereas others administered about 17.75 μ M Stattic (Scuto *et al.* 2011) or about 47.35 μ M (Spitzner, Ebner *et al.* 2014) without side effects in their animal models. Therefore, Stattic was used in concentrations ranging from 0.625 to 20 μ M to reveal minimal dosages required for proliferation and migration restriction *in vitro*. Within the concentration spectra, migration and proliferation of all lines was reduced significantly (see paragraph 4.3.3.2). The range spread from lower concentrations required for BTICs to increasing concentrations for TCs and GBM cell lines (Table 4-7). According to the cancer stem cell model, tumour recurrence after initial treatment results from remaining, therapy-resistant cancer stem cells (Medema, 2013). In contrast to this theory, substantially lower Stattic concentrations were required to restrict proliferation of BTICs than of differentiated cells (GBM cell lines and TCs), indicating a more important role of STAT3 in BTIC proliferation than in differentiated cells. Although, therapy-resistance of cancer stem cells is widely assumed, it lacks conclusive experimental evidence (Medema, 2013). Consequently, it may not be excluded that inhibition of a central transcription factor as STAT3 has profound consequences for those tumour cells (cancer stem cells, BTICs) that contain self-renewal and multilineage differentiation capacity in contrast to more differentiated tumour cells, especially since loss of STAT3 was shown to be lethal in embryonic stem cells (Levy & Lee, 2002).

BTICs were far more sensitive to Stattic regarding reduction of proliferation than to migration (see Table 4-7). In contrast, similar IC₅₀ concentrations were sufficient to reduce proliferation and migration in differentiated TCs and GBM lines. This further supports a more important role of STAT3 in BTIC proliferation than in differentiated cells. According to the literature, this may indicate a dual role for STAT3 in progenitor (BTIC) and differentiated tumour cells. Such a dual role is also known from literature describing STAT3 to be critically involved in cell survival and cell cycle progression, particularly via induction of c-myc and several cyclins (Hirano *et al.* 2000), as well as to contribute essentially to maintain the ability to invade the normal brain (Carro *et al.* 2010). Consistent with these findings, STAT3 was part of the leader cell signature established with U87 cells. It is likely that BTICs depend more on STAT3 for their cell cycle progression, while STAT3 contributes equally to migration and proliferation in differentiated tumour cells.

These encouraging results were translated to the established *in situ* model (see section 4.3.4). Although, *in vivo* animal studies injected higher Stattic concentrations into established tumours (Scuto, Ebner *et al.* 2011; Spitzner, *et al.* 2014), 15 μ M of Stattic was applied in the OBSC model. This concentration was chosen mainly according to its efficient effect in the *in vitro* studies, but also partly because Stattic was added to the media two days after implantation of the spheroids onto the brain tissue. Worth noting was that STAT3 inhibition by Stattic resulted in a dramatic anti-infiltrative effects *in situ* (see Table 4-8 and Table 4-9). Again, proneural BTICs and TCs were barely infiltrative, but one proneural line (BTIC as well as TC) showed enhanced expansion (measured by maximum distance, see Figure 5-28) 7 days after implantation, which explains the high discrepancy between control and treatment. In this context, after 14 days (see Figure 4-48 and Table 4-8), fluorescence of these cells was not longer detectable, assuming STAT3 inhibition led to cell death over the long-term. While the data might imply that proneural BTICs and TCs, especially RAV17, are more resistant to STAT3 inhibition, it is difficult to draw conclusions due to their minimal infiltration of brain tissue.

In contrast, Stattic treatment had undeniable anti-infiltrative effects on mesenchymal BTICs, TCs, and U87 (Table 4-8 and Table 4-9). Interestingly, mesenchymal TCs were more sensitive to STAT3 inhibition than BTIC. Regarding the maximum distance day⁻¹ travelled by the cells, TCs (~2.34 μ m) were outperformed by BTICs (~15.56 μ m). In opposition to *in situ* results, *in vitro* assays did show dependency of BTICs on STAT3 for proliferation, but less for migration. These effects were observed at distinctly lower Stattic concentrations, suggesting that the OBSC microenvironment reduced dependency of BTICs on STAT3 and has high impact of infiltration capacity of tumour cells. However, BTIC infiltration was still highly significantly restricted by Stattic treatment.

In agreement with Scuto *et al.*, (2011), who reported a strong STAT3-dependency of activated B cell-like diffuse large B cell lymphoma *in vivo*, but less *in vitro*, the present *in vitro* results were not as dramatic as the *in situ* results. This implies that mesenchymal TCs depend strongly on STAT3 for brain parenchyma infiltration, while mesenchymal BTICs are more resistant to STAT3 inhibition *in situ* than *in vitro*. Thus, the tumour microenvironment seems to play a critical role on STAT3 dependency of mesenchymal tumour cells. STAT3 signalling is known to be important for the crosstalk between tumour and stroma cells (Yu *et al.* 2007), and through control of expression of multiple target genes of STAT3 may be involved in induction and/or propagation of infiltration.

In summary, STAT3 inhibition was demonstrated here to exert remarkable restriction of proliferation and migration *in vitro* and *in situ*, indicating that STAT3 is an important target for further therapy approaches of high-grade gliomas. However, the microenvironment seems to play an important role as it might modulate STAT3 dependency of the cells, indicating the need to evaluate tumour cell response to inhibitors *in vivo* or in an *in vivo*-like assay system. Until now, only a few specific STAT3 inhibitors, but not Stattic, have been translated to clinical trials. For instance, OPB-31121, which specifically inhibits STAT3 phosphorylation without affecting JAK kinase similarly to Stattic, recently demonstrated STAT3 inhibition in patients with advanced solid tumours in a phase I trial (Oh *et al.* 2015). Although, the component was applied orally for 28 days only and caused adverse gastrointestinal events to varying extents, it was tolerated and had potential to stabilise (n = 8) or reduce (n = 2) tumours (n = 18) (Oh *et al.* 2015), however, no brain tumour patient was included in the study. It, therefore, remains to be seen whether OPB-31121 is able to cross the blood-brain barrier and to have an effect on gliomas.

Targeted delivery of such small molecules to tumour cells is challenging. A local application may be a more favourable option than STAT3 inhibition in the entire organism, and could cause systemic side effects. With regard to the animal studies demonstrating strong tumour reduction by local injection of Stattic (Scuto *et al.* 2011; Spitzner, *et al.* 2014), local application at the tumour site may delay or even prevent local recurrence. However, it remains to be investigated if STAT3 inhibitors can be delivered to all brain regions without systemic side effects in order to target infiltrative cells which colonise niches far off the initial tumour site.

6. Concluding remarks and future perspectives

High-grade gliomas, especially GBM, are highly complex, heterogeneous tumours. Infiltration into the parenchyma constitutes an early, but still largely unexplored event in the progression of gliomas which contributes mainly to treatment difficulties. The propagation of malignant GBM cells and their invasion into the healthy brain is a primary cause of tumour recurrence and its associated morbidity. Identification of factors related to the invasion of BTICs into surrounding brain tissue from the initial tumour site – the transition from stationary into invading cells – still remains a central challenge for future research.

The present study provides insights into previously unknown characteristics of primary and differentiated BTICs in regards to their motility, proliferation, and sensitivity to STAT3 inhibition. This work has increased understanding of the dynamic nature and complexities of glioma cells, offering new perspectives for improved therapies and future developments.

Here, the high infiltrative potential of mesenchymal GBM cells *in vitro* and *in situ* was determined. In contrast, proneural cells were negligibly invasive *in situ*, indicating the importance of further investigations of intratumoural heterogeneity, possible dependencies on GBM subtypes, or interplays between them. A critical question that remains is how the seemingly diverse infiltration capacities of proneural and mesenchymal GBM cells are regulated and what physiologic stimuli are involved in these processes.

Unravelling the dynamics and complexity of glioma cell invasion and its induction by microenvironmental cues may provide new targets for developing effective future glioma treatments. An integrated understanding of how different GBM subtypes contribute to infiltration remains a central question to be answered.

Since deciphering the roles of subtypes in heterogeneous GBM is a long-term goal, an important short-term objective should be the improvement of existing standard therapy. Combined adjuvant therapies may prolong the current median survival rate or improve quality of life for affected patients. The findings of the present study suggest the need to evaluate the response to NSAIDs and their efficacy as an adjuvant therapy in patients with high-grade gliomas, especially GBM. Ibuprofen and diclofenac exhibited anti-tumourigenic effects on GBM cell lines *in vitro* (Leidgens *et al.* 2015). Although it was not conclusively proven, restriction of STAT3 phosphorylation and c-myc modulation could constitute mechanisms of their GBM restricting capacities. Therefore, future comparative investigations should elucidate their molecular mechanisms of action.

A remaining critical question is how the seemingly diverse effects on c-myc expression are differentially regulated by ibuprofen and diclofenac. Subsequently, specific inhibition of STAT3 has shown to exert remarkable restriction of proliferation and migration *in vitro* and *in situ*. This suggests that STAT3 is an important target for further therapy approaches of high-grade gliomas, and is supported by the identification of STAT3 being part of the leader cell signature in this work. The results presented here indicate that there may be value in the investigation of Stattic or other STAT3 specific inhibitors in clinical trials. However, whether STAT3 inhibitors can be delivered to all brain regions without systemic side effects remains to be investigated. Targeted delivery of such small molecules to tumour cells is challenging, but may be applicable in combination with targets identified by infiltrative cell profiling such as the leader cell signature presented in this work.

In addition to STAT3 and c-myc, various other tumour cellular functions were affected by ibuprofen and diclofenac (Leidgens *et al.* 2015). Therefore, a combination of specific STAT3 signalling inhibition and NSAID treatment could prove to be an even more effective therapy, using synergistic effects on tumour growth and diffuse infiltration.

Complementary to the previously described broad approach non-specifically targeting GBM cells, it remains important to decipher the factors causing glioma cells to infiltrate the parenchyma. To date, the dependency and interaction with the ECM of progeny cells in general, the different GBM subtypes, and their adaptive development away from the tumour cell fraction has not been adequately investigated. Curing infiltrative gliomas is highly improbable by techniques that cannot selectively destroy the tumour cells residing in niches far away from the parental tumour. Therefore, bottom-up approaches investigating the onset and cause of infiltration will probably shed light on the infiltrative growth pattern of gliomas.

The findings of the present study may provide the basis for such a bottom-up approach. In contrast to *in vitro* migration assays, the *in situ* OBSC model led to the discovery of three phenotypically distinct cell populations. Those leader, follower, and stationary cells emerged from initial populations with leader cells likely inducing and leading infiltration similar to observations in breast cancer (Cheung *et al.* 2013). This indicates that the cell population of a GBM tumour responds heterogeneously to its microenvironment. It seems reasonable that after resection, residual tumour cells switch between leader, follower, and stationary states if necessary, causing rapid GBM relapse.

Deciphering mechanisms responsible for inducing infiltration is therefore important in order to specifically identify and target leader cells. Here, a newly developed micromanipulator adapter to isolate different cell subpopulations from OBSCs, single cell RNA expression analysis, and bioinformatic analyses were employed to establish a novel integrated approach for the investigation of GBM progenitor cell invasion. This straightforward analysis procedure enabled a detailed comparison between all three cell types and revealed a specific leader cell expression profile. Indeed, invasive leader cells exhibited a markedly distinct expression pattern in comparison to follower and stationary cells. The leader cell-specific expression signature may allow further understanding of how the leader cell fraction drives invasion in response to the environment. Expression of a selection of transcription factors, chosen according to their relevance in glioma, is validated in leader, follower, and stationary cells received from mesenchymal BTIC lines after incubation in the OBSC model. Additionally, tumour cells obtained from invasive rim and tumour centre of fresh patient material after 5-ALA guided tumour resections are analysed. Transcription factors that are consistently detected in leader, but not in follower or stationary cells will serve to reliably identify leader cells. This could eventually lead to the identification of novel biomarkers for leader, follower, and stationary cells to target them specifically in future treatment strategies.

An important hypothesis, drawn from the present results, is that the leader cell population is the progenitor-cell derived subpopulation of GBM, which drives invasion and infiltration of the brain parenchyma. If this is true, the leader subpopulation constitutes a relevant and therapeutic target. Therefore, investigations of the function, adaption, interaction with the microenvironment, and mechanisms of invasion of the leader cell subpopulation, are necessary.

An approach to target leader formation cells and their function can be a high-throughput screening assay. Such an approach may be the combination of a reproducible matrix for consistent induction, coupled with a reporter system to verify leader cell formation.

The OBSC model enables the investigation and dissociation of events within infiltrative and non-infiltrative cells, as well as in the microenvironment, for several molecular, as well as at the cellular, levels. Thus, it is highly relevant for the investigation of invasion in GBM. Such a model also enables investigators to observe therapeutic approaches in an *in situ* setting, closely resembling the native cell environment. However, the model is frail and

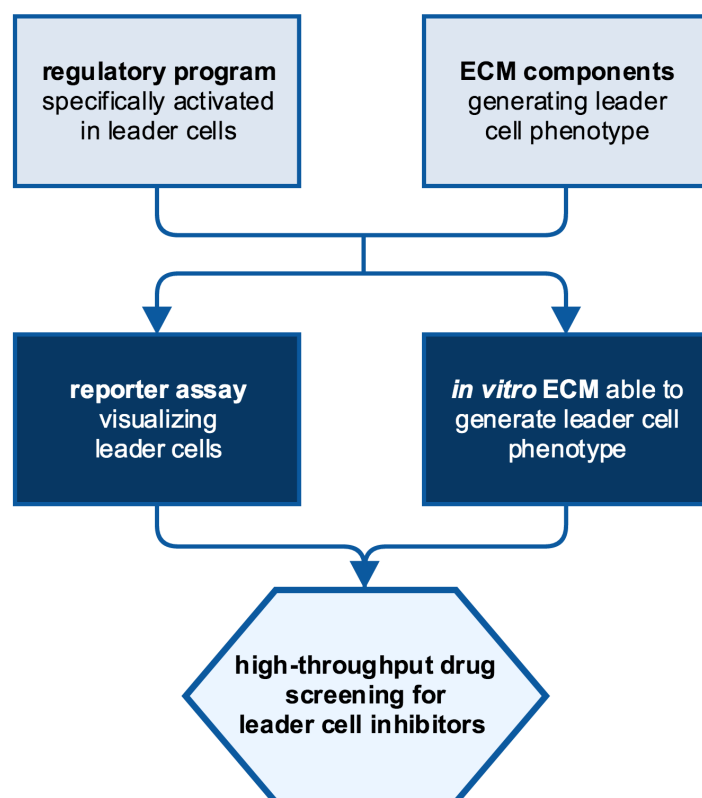


Figure 6-1: Possible work-flow to enable drug screening for leader cell inhibition

reproducible conditions cannot be guaranteed in this setup. Therefore, the development of an artificial assay providing a defined matrix especially adapted to the tumour microenvironment in the grey matter of the brain would be a challenging, but valuable future goal. Such a matrix may become a reliable model to follow invasion of human glioma progenitor cells online in a time- and space sensitive manner. If this is attained, a reproducible high-throughput screening of a potentially therapeutic agents would be feasible.

A further requirement for the development of a high-throughput therapeutic agent screening assay requires a reporter for specifically labelling leader cells. The results of the microarray analysis conducted here indicate that a combination of certain promoter sequences with reporter genes could be possible to achieve this goal. In combination with an *in vitro* assay of a defined matrix, the reporter assay would improve fast systematic screening for inhibitory substances, which prevent leader cell formation and consequently tumour cell invasion. In the future, such a reproducible high-throughput assay may be established in a workflow as depicted in Figure 6-1. Agents identified to be effective by means of such an approach might be promising for translation into clinical testing and provide a missing tool to meet an unmet therapeutic need in high-grade gliomas.

7. Materials and Methods

7.1. Materials

7.1.1. Chemicals and Reagents

Article	Order number	Company
β -Mercaptoethanol	M6250	Sigma-Aldrich, USA
6-Aminohexanoic acid	3113.1	Carl Roth, Karlsruhe, Germany
37% HCl	100317	Merck, Darmstadt, Germany
AEBSF	A8456	Sigma-Aldrich, USA
Agar Agar	A5431	Sigma-Aldrich, USA
Acrylamid/Bisacrylamid	1-610-185	Bio Rad, Munich, Germany
Agarose LE	840004	Biozym, Hessisch Oldendorf, Germany
Ammonium persulfate	A3678	Sigma-Aldrich, USA
Ampicillin Sodium Salt	A9518	Sigma-Aldrich, USA
Boric acid	100165	Merck, Darmstadt, Germany
Bromphenol blue	114391	Fluka, Switzerland
BSA	82-100-6	Sigma-Aldrich, USA
BSA Standard	UP36859D	VWR, USA
Deoxycholate	30970	Sigma-Aldrich, USA
Diclofenac sodium salt	D6899	Sigma-Aldrich, USA
Dithiothreitol (DTT)	D9779	Sigma-Aldrich, USA

Article	Order number	Company
DMSO	4720.4	Carl Roth, Karlsruhe, Germany
Ethanol	9065. 4	Carl Roth, Karlsruhe, Germany
Ethidium bromide	46067	Fluka, Switzerland
Glacial acetic acid	100063	Merck, Darmstadt, Germany
Glucose (D+) Monohydrate	108342	Merck, Darmstadt, Germany
Glycerol	0219399691	ICN Biomedicals, USA
Glycine	33226	Sigma-Aldrich, USA
Halt buffer	78420	Thermo Scientific, USA
Ibuprofen Sodium salt	I4883	Sigma-Aldrich, USA
Isobuthanol	100985	Merck, Darmstadt, Germany
Isopropanol	CP41.1	Carl Roth, Karlsruhe, Germany
L-Ascorbic acid (Vitamin C)	A4403	Sigma-Aldrich, USA
Low melt agarose	840 100	Biozym, Hessisch Oldendorf, Germany
Methanol	106018	Merck, Darmstadt, Germany
NaCl	9265.1	Carl Roth, Karlsruhe, Germany
Na ₂ EDTA-2H ₂ O	E5134	Sigma-Aldrich, USA
NaOH	38210	Fluka, Switzerland
Peptone	P0556	Fluka, Switzerland
Ponceau S	P3504	Sigma-Aldrich, USA
Re-blot mild	2502	Chemicon, USA
Roti coll 1	0258.1	Carl Roth, Karlsruhe, Germany
SDS	817034	Merck, Darmstadt, Germany
Stattic	ab120952	Abcam, UK
TEMED	T7024	Sigma-Aldrich, USA
Tris Base	T1503	Sigma-Aldrich, USA
Tris-HCl	T3253	Sigma-Aldrich, USA
Triton-X 100	T8787	Sigma-Aldrich, USA
Trypan blue	T8154	Sigma-Aldrich, USA
Tryptone (Bacto)	211705	BD, USA
Tween-20	9127.1	Carl Roth, Karlsruhe, Germany
Xylene Cyanol	110590	Merck, Darmstadt, Germany
Yeast Extract	92144	Fluka, Switzerland

7.1.2. Disposable Materials

Article	Order number	Company
0.2 µm syringe filter	723-2520	Thermo Scientific, USA
23 G 1 ¼ 0.6 × 30, BD Microlance 3	300700	BD, USA
10 µl tips	70.1131	Sarstedt, Nümbrecht, Germany
200 µl tips	70.760.012	Sarstedt, Nümbrecht, Germany
1000 µl tips	70.762.010	Sarstedt, Nümbrecht, Germany
1.5 ml tubes	72706	Sarstedt, Nümbrecht, Germany
2 ml tubes	72695500	Sarstedt, Nümbrecht, Germany
10 ml syringe, BD Luer-Lok Tip	300912	BD, USA
20 ml syringe, BD Plastipak Luer-Lok	300629	BD, USA
15 ml tubes	62554502	Sarstedt, Nümbrecht, Germany
50 ml tubes	62547254	Sarstedt, Nümbrecht, Germany
6-well plates, TPP	TPP92006	Faust, Switzerland
6-well plates, Falcon	353502	OMNILAB, Munich, Germany
10 cm Petri dishes, TPP	TPP93100	Faust, Switzerland
96-well plates, U-bottom, TPP	TPP92097	Faust, Switzerland
96-well plates, F-bottom, TPP	TPP92096	Faust, Switzerland
Cell culture flasks – T25, TPP	TPP90026	Faust, Switzerland
Cell culture flasks – T75, TPP	TPP90076	Faust, Switzerland
Cell culture inserts, 0.4 µm, Falcon	353090	OMNILAB, Munich, Germany
Cryo tubes	4796837	VWR, USA
Cell scraper	83 18 30	Sarstedt, Nümbrecht, Germany
Feather disposable scalpel No. 22	02.001.30.022	pfm medical, Cologne, Germany
Inserts	80209	Ibidi, Martinsried, Germany
Lab-Tek II, 4-chamber slide	154526	Nunc, USA
Object slides, Superfrost	ET07.1	Carl Roth, Karlsruhe, Germany
Pasteur pipettes	6121719	VWR, USA
Pre-Separation filters (30 µm)	130041407	Miltenyi, Bergisch Gladbach, Germany
PVDF membrane	39-4010	Peqlab, Erlangen, Germany
Roti NC membrane	HP 41.1	Carl Roth, Karlsruhe, Germany
Tissue culture plate, F-bottom	353046	OMNILAB, Munich, Germany
Steritop sterile filter	SCGPT01RE	Merck-Millipore, USA
Vibratome injector blades	1304	Schick, USA
Whatman paper	588-3192	VWR, USA

7.1.3. Equipment

Function	Device specification	Company
-80 °C freezer	Forma 900	Thermo Scientific, USA
60 / 200 °C heating cabinet	ED-115	WTB binder, Tuttlingen, Germany
Agarose gel chambers	PerfectBlue Gelsystem Mini S (40-0708) and Mini L (40-1214)	Peqlab, Erlangen, Germany
Agarose gel documentation	Serial N	Peqlab, Erlangen, Germany
Autoclave	Systec VE-150	Systec, Wetzlar, Germany
Binocular	MDG13	Wild Heerbrugg, Switzerland
Cell culture centrifuge	Megafuge 10.R	Thermo Scientific, USA
Cell incubator	HeraCell incubator	ThermoScientific, USA
Cell culture water bath	Water bath 1083	GFL, Burgwedel, Germany
Centrifuge, refrigerated	Centrifuge 5417R	Eppendorf, Hamburg, Germany
Centrifuge	Heraeus Variofuge 3.0R, #8074 rotor	Thermo Scientific, USA
Fine scale	handy H51	Sartorius, Göttingen, Germany
Fluorescence microscope	Zeiss Axio Observer.Z1	Visitron Systems GmbH, Puchheim, Germany
Fluorescence microscope	Olympus IX81	Olympus, Japan
Freezing container	5100-0001	Nalgene, USA
Heating block	Thermomixer 5436	Eppendorf, Hamburg, Germany
Heating stirrer	MR3001	Heidolph, Schwabach, Germany
Hemocytometer	Neubauer hemacytometer	Carl Roth, Karlsruhe, Germany
Light microscope	Fluovert Type 090-123.012	Leitz, Wetzlar, Germany
Light microscope camera	ProgRes C3	Jenoptik, Jena, Germany
Live cell imaging microscope	Leica DMI6000 B microscope	Leica, Wetzlar, Germany
Laminar flow	HeraSafe laminar flow	ThermoScientific, USA
Microwave	HF 12021	Siemens, Munich, Germany
Nanophotometer	IMPLEN P300	Kisker Biotech, Steinfurth, Germany
PCR machine	Mastercycler epgradient S	Eppendorf, Hamburg, Germany
pH meter	CG842	Schott, SI Analytics GmbH, Mainz, Germany
Plate reader	VarioSkan Flash Multimode Reader	Thermo Scientific, USA
Power supply	EC400P Series 90	E-C Apparatus Corporation, USA
qRT-PCR machine	Mx3005P	Agilent, USA
Scale	Universal U4800P	Sartorius, Göttingen, Germany

Function	Device specification	Company
Scale	BP21005	Sartorius, Göttingen, Germany
SDS-Page system	PerfectBlue Dual Gel Twin S (45-1010-C)	Peqlab, Erlangen, Germany
Semi-Dry-Blotter	‘PEGASUS’	Phase, Lübeck, Germany
Shaker	Forma Orbital Shaker, type 420	Thermo Scientific, USA
Shaker	Forma Orbital Shaker, type 481	Thermo Scientific, USA
Shaker	GFL 3017	GFL, Burgwedel, Germany
Vibratome	VT 1000S	Leica, Wetzlar, Germany
Vortex	Vortex Genie 2	Scientific industries, USA
Water bath	WNB 7	Memmert, Schwabach, Germany
Water filter system	Q-POD, Milli-Q	Millipore, USA
Western blot imager	ImageQuant LAS 500	GE Healthcare, Life Sciences, USA

7.1.4. Bioinformatic Analysis Software

Software	Function	Reference
GraphPad Prism, version 6.0f	Statistical analysis	GraphPad Software, USA
ImageJ, version 1.48 *	Image processing and analysis	National Institutes of Health, USA
Mendeley, version 1.15	Citation management	Mendeley Ltd., UK
Microsoft Office 2011	Further analyses and documentation	Microsoft, USA
MxPro QPCR Software	q-RT-PCR evaluation	Agilent Technologies, USA
Primer3, web based	Primer design	(Untergasser <i>et al.</i> 2012)
Pixelmator, version 3.3.2	Image editor	Pixelmator Team, Lithuania
VisiView	Microscope software	Visitron Systems GmbH, Puchheim, Germany

*Three extending macros were written for ImageJ for image processing. The macro ‘convertMetaTifs’ converts Meta files (.tif) of the fluorescence microscope software VisiView into Joint Photographic Experts Group (JPEG) files, the colour information pictures were pseudotyped for green or red fluorescence. ‘transformImages’ converts Tagged Image File Format (TIFF) files of the fluorescence microscope software VisiView or the Western Blot Imager into JPEG files regardless of colour information. The last macro ‘transformImagesWithContrast’ works as the TIFF macro above, however, during conversion, contrast enhancement occurs. The macro source code is listed in the appendix section 9.4.3.

7.1.5. Biological Materials

7.1.5.1. Primary Cell Culture and Cell Lines

Primary human brain tumour initiating cells (BTIC) are derived from human brain tumour tissue (resected at the department for Neurosurgery, Regensburg University Hospital) and established according to (Moeckel *et al.* 2014) at the laboratory of NeuroOncolgy, University Hospital Regensburg:

Primary human brain tumour initiating cells:

Name	Histology	Classification	Growth behaviour
RAV17	Primary GBM	proneural	spheres
RAV19	Primary GBM	proneural	spheres
RAV39	Primary GBM	proneural	spheres
RAV57	Primary GBM	proneural	semiadherent
RAV01	Primary GBM	mesenchymal	adherent
RAV21	Primary GBM	mesenchymal	adherent
RAV24	Primary Gliosarcoma (WHO grade IV)	mesenchymal	semiadherent
RAV26	Primary GBM	mesenchymal	adherent
RAV27	Secondary GBM	mesenchymal	adherent
RAV28	Primary GBM	mesenchymal	adherent

Human GBM cell lines:

Name	Histology	Growth behaviour	Reference
A172	GBM (WHO grade IV)	adherent	(Giard <i>et al.</i> 1973)
HTZ349	GBM (WHO grade IV)	adherent	(Bogdahn <i>et al.</i> 1989)
U-87 MG	Anaplastic astrocytoma (WHO grade III)	adherent	(Clark <i>et al.</i> 2010)
HEK 293T	Variant of human embryonic kidney (HEK) cells	adherent	(Graham <i>et al.</i> 1977); kindly provided by Prof. Geley, Division of Molecular Pathophysiology, Innsbruck Medical University, Austria

7.1.5.2. Bacterial Strain

For plasmid expression for lentivirus production, the bacterial strain *Escherichia coli* DH5 α was kindly provided by Prof. Wetzel, Department of Molecular Neuroscience, University Hospital Regensburg and has the following characteristics:

endA1, hsdR17, supE44, thi-1, recA1, gyrA (Na^r), relA1, Δ (lacIZYA-argF)-U169, deoR, Φ 80dlac Δ (lacZ)M15

7.1.5.3. Rat Strains

For brain slice culture preparation Long-Ewans, Sprague Dawley or Wistar rats (Charles River, Germany) were obtained from an in-house facility. Animal care was conducted in house, according to institutional guidelines with a 12 h light / 12 h dark cycle and *ad libitum* access to food and water. Animal age ranged between P8 and P12. The rat pups were killed by cervical dislocation.

7.1.5.4. Cell Culture Media, Reagents and Supplements

Article	Order number	Company
Accutase®	A 6964	Sigma-Aldrich, USA
basic Fibroblast Growth Factor – human (FGF)	130-093-842	Miltenyi, Bergisch Gladbach, Germany
Blasticidine S HCL	A11139-03	Life technologies, Gibco, USA
DMSO	A994.2	Carl Roth, Karlsruhe, Germany
Dulbecco's Phosphate Buffered Saline 1x (PBS)	D8537	Sigma-Aldrich, USA
Dulbecco's Modified Eagle's Medium low glucose (DMEM)	D6046	Sigma-Aldrich, USA
Dulbecco's Modified Eagle's Medium/Ham's Nutrient Mixture F12 (DMEM/F12)	D6421	Sigma-Aldrich, USA
Epidermal Growth Factor – human (EGF)	130-097-751	Miltenyi, Bergisch Gladbach, Germany
Fetal Bovine Serum (FBS)	S0115 (Lot: 0317A)	Biochrom, Berlin, Germany
Hank's Balanced Salt Solution (HBSS)	H6648	Life technologies, Gibco, USA
Horse Serum	26050-088 (Lot: 634813D)	Life technologies, Gibco, USA

Article	Order number	Company
Insulin Transferrin Sodium Selenite Supplement (ITS)	I1884-1VL	Sigma-Aldrich, USA
Laminin	354 232	Corning, USA
Leibovitz media	F1315	Biochrom, Berlin, Germany
Lipofectamine® 2000 Transfection Reagent	12566014	Life technologies, Gibco, USA
L-Glutamine	G7513	Sigma-Aldrich, USA
MEM non essential amino acids	M7145	Sigma-Aldrich, USA
MEM powder	11700-077	Life technologies, Gibco, USA
MEM Vitamin Solution (100x)	M6895	Sigma-Aldrich, USA
Metafectene	T020-20	Biontex, Munich, Germany
Neurobrew (B-27 supplement)	130-097-263	Miltenyi, Bergisch Gladbach, Germany
Opti-MEM	51 985 026	Invitrogen, Gibco, USA
Penicillin/Streptomycin	P4333	Sigma-Aldrich, USA
Puromycin dihydrochloride	P8833	Sigma-Aldrich, USA
RHB-A Stem Cell Media	SCS-SF-NB-01	StemCells, USA
Sodium Bicarbonate Solution (7.5%)	S8761	Sigma-Aldrich, USA
Trypan Blue Solution	15250-061	Life technologies, Gibco, USA
Trypsin-EDTA	T3924	Sigma-Aldrich, USA

7.1.5.5. General Cell Culture Media and Supplements

Dulbecco's modified Eagle's medium (DMEM) (500 ml)

10% (v/v) FBS, 50 U (v/v) Penicillin, 0.05% (v/v) Streptomycin, 2 mM (w/v) L-Glutamine, 1% (v/v) MEM Vitamin Solution, 1% (v/v) MEM non essential amino acids

500 ml DMEM was supplemented with 50 ml FBS and 5 ml of each Penicillin/Streptomycin, L-Glutamine and MEM Vitamin Solution. The media was stored at 4 °C for up to two weeks.

Dulbecco's modified Eagle's medium /Ham's F-12 (DMEM/F12) (500 ml)

50 U (v/v) Penicillin, 0.05% (v/v) Streptomycin, 2 mM (v/v) L-Glutamine, 1% (v/v) MEM non essential amino acids, 1% (v/v) MEM Vitamin Solution

500 ml DMEM/F12 were supplemented with 5 ml of each Penicillin/Streptomycin, L-Glutamine, MEM non essential amino acids and MEM Vitamin Solution. The media was stored at 4 °C for up to two weeks. Before use, aliquots of 50 ml were supplemented with 1x B27 supplement and each 50 µl of EGF and FGF stock solutions.

Epidermal Growth Factor (EGF) stock solution (20 ng μl^{-1})

1 mg lyophilised sterile EGF powder was dissolved in 50 ml of 0.1% (w/v) BSA dissolved in ddH₂O. Aliquots were frozen at -20 °C.

basic Fibroblast Growth Factor (FGF) stock solution (20 ng μl^{-1})

1 mg lyophilised sterile FGF powder was dissolved in 50 ml of 0.1% (w/v) BSA dissolved in ddH₂O. Aliquots were frozen at -20 °C.

Leibovitz/Live Cell Imaging Media (50 ml)

50 U (v/v) Penicillin, 0.05% (v/v) Streptomycin, 2 mM (w/v) L-Glutamine, 25 mM (w/v) D-glucose, 1% (v/v) MEM Vitamin Solution, 1% (v/v) MEM non essential amino acids, depending on cell line: 10% (v/v) FBS

50 ml Leibovitz was supplemented with 0.5 ml of each Penicillin/Streptomycin, L-Glutamine, D-glucose and MEM Vitamin Solution. Depending on the normal growth media < 5 ml FBS were added as well. The media was stored at 4 °C for up to two weeks.

Puromycin stock solution (10 $\mu\text{g } \mu\text{l}^{-1}$)

10 mg lyophilised sterile Puromycin powder was dissolved in 1 ml of ddH₂O. Aliquots were frozen at -20 °C.

RHB-A+ media (50 ml)

1% EGF (v/v), 1% FGF (v/v)

50 ml of RHB-A media (supplemented with 50 U (v/v) Penicillin and 50 $\mu\text{g } \mu\text{l}^{-1}$ Streptomycin in 500 ml) were supplemented with 50 μl of each EGF and FGF stock solutions. The media was stored at 4 °C for up to one week.

7.1.5.6. Brain Slice Culture Media**Preparation media (1 L)**

5% (v/v) horse serum, 1.6% MEM powder, 50 U (v/v) Penicillin, 0.05% (v/v) Streptomycin, 25 mM (w/v) D-glucose, 2 mM (w/v) L-Glutamine, 1 mM (w/v) Tris base

16 g MEM powder were dissolved in 1 L ddH₂O and supplemented with 10 ml D-glucose, 10 ml L-Glutamine, 10 ml Penicillin/Streptomycin, 10 ml 1 M Tris base and 50 ml horse serum.

The pH was adjusted to 7.4 with 37% HCl and the media was stored at 4 °C for up to two weeks.

Culture media (100 ml)

25% (v/v) horse serum, 25% (v/v) HBSS, 0.8% MEM powder, 0.58% (w/v) Sodium Bicarbonate, 50 U (v/v) Penicillin, 0.05% (v/v) Streptomycin, 0.05% (w/v) ITS, 25 mM (w/v) D-glucose, 4 mM (w/v) L-Glutamine, 4 mM (w/v) Vitamin C, 0.5 mM (w/v) Tris base

0.8 g MEM powder were dissolved in 44.57 ml ddH₂O and 25 ml HBSS and supplemented with 1.2 ml D-glucose, 2 ml L-Glutamine, 1 ml Penicillin/Streptomycin, 100 µl Vitamin C, 50 µl ITS, 580 µl 7.5% Sodium bicarbonate, 500 ml 1 M Tris base and 25 ml horse serum.

The pH was adjusted to 7.4 with 37% HCl and the media was stored at 4 °C for up to two weeks.

7.1.6. Antibodies

Primary antibodies:

Antigen	Source	Dilution	Dilution Buffer	Order Number	Company
(p)AMPK	Rabbit	1:1000	2.5% BSA	2535S	Cell Signaling, USA
AMPK	Rabbit	1:1000	2.5% BSA	2603S	Cell Signaling, USA
c-myc	Rabbit	1:1000	2.5% BSA	5605S	Cell Signaling, USA
C/EBPβ	Rabbit	1:1000	2.5% BSA	ab 32358	Abcam, UK
GAPDH	Goat	1:5000	1% milk	SC48167	Santa Cruz, USA
(p)mTOR	Rabbit	1:1000	2.5% BSA	5536S	Cell Signaling, USA
mTOR	Rabbit	1:1000	2.5% BSA	2983S	Cell Signaling, USA
(p)p42/44 MAPK	Rabbit	1:500	2.5% BSA	4370S	Cell Signaling, USA
p42/44 MAPK	Rabbit	1:500	2.5% BSA	4695S	Cell Signaling, USA
(p)SMAD2/3	Rabbit	1:500	2.5% BSA	3101S	Cell Signaling, USA
SMAD2/3	Rabbit	1:500	2.5% BSA	3102S	Cell Signaling, USA
(p)STAT3 S727	Rabbit	1:1000	2.5% BSA	9134S	Cell Signaling, USA
(p)STAT3 Y705	Rabbit	1:1000	2.5% BSA	9145S	Cell Signaling, USA
STAT3	Rabbit	1:2000	1% milk	4904S	Cell Signaling, USA

Secondary antibodies:

Antigen	Source	Dilution	Dilution Buffer	Order Number	Company
HRP- α goat	Donkey	1:5000	1% milk	SC-2020	Santa Cruz, USA
HRP- α rabbit	Goat	1:1000 – 5000	Depending on 1 st antibody buffer	541088	Biozym, Hessisch Oldendorf, Germany

7.1.7. Oligonucleotides

7.1.7.1. Primer

Primer	Sequence	Distributor
LDH-A forward	5'- GGTTGGTGCTGTTGGCATGG -3'	Metabion, Martinsried, Germany
LDH-A reverse	5'- TGCCCCAGCCGTGATAATGA -3'	
RPLPO forward	5'- CTGTCTGCAGATTGGCTACCC -3'	
RPLPO reverse	5'- GATGGATCAGCCAAGAAGGC -3'	

7.1.7.2. siRNA and shRNA

Gene	Sequence	Fluorescence labelling	Distributor
<i>STAT3</i>	5'- GCAAAGAATCACATGCCACT -3'	GFP	Metabion, Martinsried, Germany
<i>C/EBPβ</i>	5'- CGACTTCCTCTCCGACCTCTT -3'	RFP	
scrambled control	5'- TTCTCCGAACGTGTCACGTTT -3'	GFP/RFP	

universal negative control shRNA sequences:

Sense	Loop	Antisense
pLenti-H1-(shRNA-Neg-control)-Rsv(RFP-Bsd):		
5'- GTCTCCACGCGCAGTACATTT	cgag	AAATGTACTGCGCGTGGAGAC -3'
pLenti-H1-(shRNA-Neg-Control)- Rsv(GFP-Puro):		
5'- GTCTCCACGCGCAGTACATTT	cgag	AAATGTACTGCGCGTGGAGAC -3'

7.1.8. Plasmid Vectors

Detailed vector maps of the vectors modified according to custom specifications U57 pHR SFFV GFP, pLenti-H1-(shRNA-Neg-control)-Rsv(GFP-Bsd) and pLenti-H1-(shRNA-Neg-control)-Rsv(RFP-Bsd) are given in the appendix section 9.4.2.

Plasmid	Source
psPAX2	kindly provided by Prof. Geley, Division of Molecular Pathophysiology, Innsbruck Medical University, Austria
pCMV-VSV-G	
U57 pHR SFFV GFP	
pLenti-H1-(shRNA-Neg-control)-Rsv(GFP-Bsd)	Amsbio, Frankfurt/Main, Germany
pLenti-H1-(shRNA-Neg-control)-Rsv(RFP-Bsd)	

7.1.9. Bacterial Cultivation

285 mM Ampicillin (10 ml)

1 g Ampicillin was dissolved in 10 ml ddH₂O to reach 100 mg ml⁻¹ prior to sterile filtration. Aliquots were stored at -20 °C.

Luria Broth (LB) media (1 L)

10% (v/v) FBS, 50 U (w/v) Penicillin, 0.05% (w/v) Streptomycin, 2 mM (w/v) L-Glutamine, 1% (v/v) MEM Vitamin Solution, 1% (v/v) MEM non essential amino acids

10 g Peptone and 5 g of each Yeast Extract and NaCl were dissolved in 1 L ddH₂O. The pH was adjusted to 7.5 with 5 M NaOH before autoclaving. Media was stored at 4 °C for up to two months.

Prior to use, the media was supplemented with 100 µg ml⁻¹ Ampicillin.

For the preparation of LB-Agar, 15 g of Agar Agar was added per litre solution prior to autoclaving.

0.1 M CaCl₂ (1 L)

11.09 g CaCl₂ was dissolved in 1 L ddH₂O, sterile filtered and stored at RT.

0.1 M MgCl₂ (1 L)

20.33 g MgCl₂ was dissolved in 1 L ddH₂O, sterile filtered and stored at RT.

7.1.10. Enzymes and Enzyme Buffers

Article	Sequence	Cut pattern	Order number	Company
<i>AgeI</i>	5' -ACCGGT-3' 3' -TGGCCA-5'	5' -A CCGGT-3' 3' -TGGCC A-5'	R0552L	New England Biolabs, USA
<i>BamHI</i>	5' -GGATCC-3' 3' -CCTAGG-5'	5' -G GATCC-3' 3' -CCTAG G-5'	R0136L	New England Biolabs, USA
<i>EcoRI</i>	5' -GAATTC-3' 3' -CTTAAG-5'	5' -G AATTC-3' 3' -CTTAA G-5'	R0101L	New England Biolabs, USA
<i>HindIII</i>	5' -AAGCTT-3' 3' -TTCGAA-5'	5' -A AGCTT-3' 3' -TTCGA A-5'	R0104L	New England Biolabs, USA
<i>XbaI</i>	5' -TCTAGA-3' 3' -AGATCT-5'	5' -T CTAGA-3' 3' -AGATC T-5'	R0145L	New England Biolabs, USA
CutSmart Buffer			B7204S	New England Biolabs, USA
NEBuffer 2.1			B7202S	New England Biolabs, USA
NEBuffer 3.1			B7203S	New England Biolabs, USA
RNase A			19101	Qiagen, Hilden, Germany

7.1.11. Kits

Article	Order number	Company
BCA assay	UP95425A	VWR, USA
CyQuant Direct Cell Proliferation Assay	C35012	Invitrogen, USA
ECL Western Blot Bright	541021	Biozym, Hessisch Oldendorf, Germany
Halt Inhibitor Cocktail	78440	Perbio, Sweden
NucleoBond® Xtra Maxi	740414	Macherey & Nagel, Düren, Germany
NucleoSpin®	740955250	Macherey & Nagel, Düren, Germany
PCR Mycoplasma Test Kit I/C	PK-CA91-1096	Promocell, Heidelberg, Germany
QIAprep Spin Miniprep Kit	27106	Qiagen, Hilden, Germany
QIAGEN Plasmid Maxi Kit	12165	Qiagen, Hilden, Germany
QIAGEN RNeasy Mini Kit	74106	Qiagen, Hilden, Germany
Reverse Transcription System	A3500	Promega, Mannheim, Germany
SYBR Green Jump Start Kit	S4438	Promega, Mannheim, Germany

7.1.12. Molecular Weight Marker

Article	Order number	Company
O'GeneRuler DNA Ladder	SM1133	Fermentas, USA
Prestained protein ladder	SM1811	Fermentas, USA
Quantitas DNA Marker	250200	Biozym, Hessisch Oldendorf, Germany

7.1.13. Solution and Buffers

7.1.13.1. General Buffers

5% (w/v) Agarose (100 ml)

5 g of low melting Agarose was added to 100 ml 1x PBS. The solution was boiled in a microwave until the Agarose was dissolved. The solution was stored at 60 °C over night before use.

10% (w/v) D-Glucose (50 ml)

5 g D-Glucose was dissolved in 50 ml ddH₂O and sterile filtered. Aliquots were stored at -20 °C.

50% (v/v) Glycerol (10 ml)

5 ml glycerol was dissolved in 5 ml ddH₂O. Aliquots were stored at RT.

10 µg/ml ITS (10 ml)

100x ITS powder was dissolved in 10 ml ddH₂O and sterile filtered. Aliquots were stored at -20 °C.

0.5 M Na₂EDTA pH 8.0 (1 L)

106.12 g Na₂EDTA-2 was dissolved in 800 ml ddH₂O. pH was adjusted with NaOH pellets (~ 20 g) and the volume adjusted to 1 L. The solution was stored at RT.

10 mM Stattic stock solution (10 ml)

10 mg lyophilised sterile Stattic powder was pre-dissolved in 1.106 ml DMSO and diluted with RHB-A to 10 mM. Aliquots were frozen at -20 °C and kept in the dark.

4.5 mM Vitamin C (10 ml)

8 g Vitamin C was dissolved in 10 ml ddH₂O. Aliquots were stored at -20 °C.

7.1.13.2. DNA Buffers

10x DNA loading buffer (10 ml)

60% (v/v) glycerol, 3.3 (w/v) Tris base pH 7.4, 46.4 mM Xylene Cyanol, 37 mM bromphenol blue

Each 25 mg bromphenol blue and Xylene Cyanol were dissolved in 3.3 ml 1 M Tris base. 6 ml glycerol and 0.7 ml ddH₂O were added. Aliquots were stored at -20 °C.

10x TBE buffer (1 L)

890 mM boric acid, 890 mM Tris base, 4% (w/v) Na₂EDTA pH 8.0

108 g Tris base, 55 g boric acid were dissolved in 800 ml ddH₂O. Then 40 ml 0.5 M Na₂EDTA was added and the volume adjusted to 1 L. The solution was stored at RT.

50x TAE buffer (1 L)

2 M Tris base, 0.95 M glacial acetic acid, 10% (w/v) Na₂EDTA pH 8.0

242 g Tris base was dissolved in 500 ml ddH₂O. Then 100 ml 0.5 M Na₂EDTA and 57.1 ml glacial acetic acid were added and the volume adjusted to 1 L. The solution was stored at RT.

1.5% (w/v) Agarose (100 ml)

1.5 g Agarose was added to 100 ml 1x TBE buffer. The solution was boiled in a microwave until the Agarose was dissolved. The solution was stored at 60 °C for up to one week. Previous to gel casting, 5 µl Ethidium bromide was added to 40 ml Agarose solution.

7.1.13.3. Protein Buffers

5% (w/v) BSA blocking solution (100 ml)

5 g of BSA was dissolved in 100 ml of TBS-T and stored for up to one week at 4 °C.

5% (w/v) milk blocking solution (100 ml)

5 g of non-fat dry milk powder was dissolved in 1 ml of TBS-T and stored at 4 °C.

5x Laemmli Protein loading buffer (100 ml)

60 mM Tris-HCl pH 6.8, 10% (v/v) glycerol, 3% (w/v) SDS, 5% (v/v) β-mercaptoethanol, 37 mM bromphenol blue

6 ml 1 M Tris-HCL pH 6.8, 10 ml of glycerol, 15 ml 20% SDS, 5 ml β-mercaptoethanol and 25 mg bromphenol blue were added to 64 ml of ddH₂O. Aliquots were stored at -20 °C.

10% (w/v) Ammonium persulfate (APS) (20 ml)

1 g APS was dissolved in 10 ml ddH₂O. Aliquots were frozen at -20 °C.

10x SDS (1 L)

1.9 M Glycine, 250 mM Tris base, 35 mM SDS

144.1 g Glycine, 30.3 g Tris base, and 10 g SDS were dissolved in 800 ml of ddH₂O, then the volume was adjusted to 1 L. The solution was stored at RT.

10x TBS (1 L)/TBS-T (1 L)

1.5 M NaCl, 500 mM Tris base, (0.1% Tween-20)

60.5 g Tris base and 87.6 g NaCl were dissolved in 800 ml ddH₂O, then the pH was adjusted to 7.5 and the volume to 1 L. For 1x TBS-T 100 ml of 10x stock solution was diluted in 900 ml ddH₂O and 1 ml Tween-20 was added. The solutions were stored at RT.

Anode I buffer (1 L)

30 mM Tris base, 20% (v/v) Methanol

3.63 g Tris base was dissolved in 1 L ddH₂O, then 200 ml Methanol was added. The solution was stored at 4 °C.

Anode II buffer (1 L)

300 mM Tris base, 20% (v/v) Methanol

36.34 g Tris base was dissolved in 1 L ddH₂O, then 200 ml Methanol was added. The solution was stored at 4 °C.

Cathode buffer (1 L)

25 mM Tris base, 40 mM 6-Aminohexanoic acid, 20% (v/v) Methanol

3.03 g Tris base and 5.24 g 6-Aminohexanoic acid were dissolved in 1 L ddH₂O. Then 200 ml Methanol was added. The solution was stored at 4 °C.

RIPA Protein isolation buffer (100 ml)

50 mM Tris-HCl, 150 mM NaCl, 0.5% (v/v) Triton-X 100, 0.5% Deoxycholate, 100x (v/v) Halt buffer, 0.001% (w/v) AEBSF, 0.001% (w/v) DTT

877 mg NaCl was dissolved in 100 ml of 500 mM Tris-HCl pH 8.0 stock solution, then 500 ml Triton-X 100 and 500 mg Deoxycholate were added. Aliquots were stored at -20 °C. Prior to use 10 µl Halt buffer and each 1 µl of AEBSF and DTT were added.

Ponceau S (500 ml)

0.1 % (w/v) Ponceau S, 5 % (v/v) acetic acid

1 g Ponceau S was dissolved in 950 ml ddH₂O, then 50 ml of acetic acid was added. The solution was stored at RT.

Ponceau S Destaining solution (500 ml)

20 mM Tris base

1.2 g Tris base was dissolved in 500 ml ddH₂O. The solution was stored at RT.

7.2. Methods

7.2.1. Cell Culture methods

7.2.1.1. General Cell Culture

7.2.1.1.1. Culture, seeding, passaging

Once primary BTIC cultures were established, they were grown in RHB-A+ medium. They either grew adherently or in spheres. GBM cell lines were grown as adherent monolayers in DMEM medium. Cells were cultured at normoxic conditions at 37 °C with 21% O₂, 5% CO₂ and 95% humidity.

Cells were split as required when the cells reached approximately 80% confluence, as the maximal confluence should not exceed 70 – 90%. Generally, for continuous culture, the cells were split once or twice a week at sterile conditions in a laminar flow hood. Cells were checked regularly for *Mycoplasma* contamination to ensure *Mycoplasma*-free cell cultures.

Adherent cells: Media was discarded and the cell layer washed with 1xPBS prior to detachment by Trypsin-EDTA (GBM cell lines) or Accutase (BTICs). Cells were washed either with media (with 10% FBS) to inactivate Trypsin (GBM cells) or 1x PBS (adherent BTICs). The whole suspension was reabsorbed several times to obtain single cells in suspension. The cells were pelleted by 5 min of centrifugation at 1,200 xg at RT. After discarding the supernatant, the cells were resuspended in fresh medium and seeded according to requirements or at the desired splitting ratio (1:1 up to 1:8).

Spheres: The media containing all cells was centrifuged at 1,200 xg at RT for 5 min to pellet all cells. After discarding the supernatant, the cells were resuspended in 2.5 ml Accutase and left for dissociation at 37 °C in a water bath. If necessary, cells were passed through a 30 µm cell strainer before subsequent centrifugation. Cells were inoculated according to requirements or split at a ratio from 1:1 up to 1:5.

Differentiation of BTICs: BTIC cultures could be differentiated by replacement of RHB-A+ medium with DMEM containing 10% FBS. Cells were left at least 14 days under serum conditions to achieve a complete differentiation. Each primary line existed as pair of BTICs as well as a differentiated population.

7.2.1.1.2. Cell number determination

The cell number of single cell solutions was determined by counting on a hemacytometer. In general, 40 µl of cell suspension were mixed with 10 µl Trypan blue solution to differentiate between viable and dead cells. Cell numbers were calculated according to the following formula:

$$\text{cells/ml} = \frac{\text{amount of counted cells} \times df \times cf}{\text{amount of counted squares} \times sv}$$

cf = conversion factor µl in L: 1 L = 1×10^6 µl

df = dilution factor (here: 1.25)

sv = volume of one square = 0.1 µl

7.2.1.1.3. Thawing, freezing, and harvesting cells

Thawing: A frozen stock of approximately 1×10^6 cells ml⁻¹ from liquid nitrogen or -80 °C storage was thawed quickly in a 37 °C water bath to avoid formation of intracellular ice crystals. The cell suspension was transferred into a 15 ml tube filled with 10 ml culture media and centrifuged for 5 min at 1,200 g at RT to remove DMSO contained in the frozen stock. The supernatant was removed and the pellet resuspended in an appropriate amount of culture media, then transferred to a 25 or 75 cm² culture flask depending on cell viability.

Freezing: Cells were harvested as described below at cell densities of approximately 1×10^6 cells ml⁻¹ in culture media containing 10% (v/v) DMSO. 1.5 ml of cell suspension was transferred into cryo vials, stored in a freezing container and transferred quickly to -80 °C.

The use of DMSO assured a slow freezing (48 h) of the cells, minimizing disruption of the cell membrane.

Harvesting: Pellets were generated for either protein or mRNA extraction. Cells were harvested by scrapping them from the media surface, or, in the case of spheres, by centrifugation after washing once with 1x PBS. The pellets were washed again with 1.5 ml 1x PBS and transferred into a 2 ml Eppi before centrifugation for 10 min at 2,500 xg at RT. The supernatant was immediately discarded and the pellets were frozen in liquid nitrogen followed by storage at -80 °C until subsequent protein or RNA extraction.

7.2.1.1.4. Laminin coating

In order to seed cells normally grown in spheres as adherent monolayers, the culture vessel surfaces had to be coated with laminin. According to the concentration of the laminin stock solution, laminin was diluted in an adequate amount of PBS (generally 1:198). The vessels were filled until completely covered with solution (approximately 500 µl/well using 6-well plates) and incubated at 37 °C for at least 3 h. To avoid drying of the vessels after coating, the solution had to be replaced quickly by media or 1x PBS. The slides were ready for immediate use, which is recommended, but could be stored for up to 2 days at 4 °C if covered in 1x PBS.

7.2.1.2. Transfection Methods

7.2.1.2.1. siRNA Transfection

Transfection of cells with siRNAs was performed according to the manufacturer's manual with LipofectamineTM 2000. Cell confluence at the time of transfection was desired to be between 70 – 80%. Transfection was performed either in 6-well format or as batch trans-formation before seeding the cells into Ibidi Inserts. With each transfection, control batches with Lipofectamine alone and control siRNA were used. Transfection rates were estimated by fluorescence levels as all siRNAs used were fluorescently labelled, see paragraph 7.1.7.2.

Component	Ibidi insert	6-well
siRNA	1 pmol	30 pmol
diluted in Opti-MEM	25 µl	250 µl
Lipofectamine	1.5 µl	5 µl
diluted in Opti-MEM	25 µl	250 µl

Lipofectamine was diluted in Opti-MEM and incubated for 5 min at RT. Meanwhile, siRNAs (100 pmol stock) were diluted in Opti-MEM, the diluted Lipofectamine was added after the incubation period. The solution was mixed by inversion of the tube 4 – 6 times and incubated for 20 min at RT. Lipofectamine was added to media lacking siRNA for the Lipofectamine only control.

6-well plates: Cells were seeded 24 h prior to transfection in 2 ml of cell specific culture media lacking Pen/Strep. If cells did not normally grow adherently, they were seeded into laminin coated wells. On the following day, media was removed before 500 µl siRNA-Lipofectamine mixture was added to each well while gently shaking the plate. Cells were incubated for 4 h before 500 µl/well cell specific media without Pen/Strep was added. 24 h later, cell specific media was used to replace the transfection mixture.

Batch transfection: Cells were detached and adjusted to $1 - 5 \times 10^5$ cells (according to cell proliferation rate) during the 20-min incubation step of Lipofectamine with the siRNA. 50 µl of siRNA-Lipofectamine mixture was added to 50 µl of cell suspension, gently mixed and equally distributed into the two Ibidi insert chambers place in 24-well plates or 60 mm dishes. After 4 h of incubation, 50 µl/insert cell-specific media without Pen/Strep was added. Cells were incubated for 24 to 48 h before insert removal.

7.2.1.2.2. Lentiviral Infection

In order to monitor cell movement when implanted onto OBSC, lentiviral infections were performed to establish cells stably expressing fluorescence markers. Unlike transient siRNA transfection, stable integration by viral infection provides constant expression of fluorescence markers. The proneural BTICs RAV17, RAV19, and RAV57 were transduced with the shRNA control vector pLenti-H1-(shRNA-Neg-control)-Rsv(RFP-Bsd) carrying a RFP encoding gene under H1 promoter control as well as a blasticidin (Bsd) resistance gene with a RSV promoter. Cell line U87 as well as mesenchymal BTICs RAV21, RAV26 and RAV27 were transduced with U57 pHR SFFV GFP plasmid encoding a GFP gene under SFFV/U3 promoter control, see paragraph 7.1.7.2. Cells were transduced using a second-generation packaging system consisting of the plasmid psPAX2 encoding packaging related genes and the vector pVSV-G carrying genes relevant for envelope generation. All procedures connected to lentiviral particle production, harvesting and infection of target cells were handled in accordance with GenTSV (genetic technology safety regulations) at stage 2.

Lentiviral particle production: Infectious lentiviral particles were produced in 293T cells, containing a SV40 Large T-antigen, necessary for replication of transfected plasmids, which contain a SV40 origin of replication. One day prior to transfection, 293T cells were seeded at 2.5×10^6 cells in 10 cm dishes in DMEM + 10% FBS.

Component	Concentration
Expression plasmid	10 µg
psPAX2	5 µg
pVSV-G	5 µg
diluted in Opti-MEM	250 µl
Metafectene	60 µl
diluted in Opti-MEM	250 µl

Expression, packaging, and envelope plasmids were diluted in Opti-MEM at appropriate amounts. Corresponding volume (1:1) of Metafectene pre-diluted in Opti-MEM was added to the plasmid mixture, carefully mixed by 4–6 x inversions and left for incubation for 5 min at RT. Meanwhile, media of the 293T cells was refreshed with antibiotics-free DMEM + 10% FBS. The transfection solution was added drop wise to the virus producing cells, which were then incubated for 24 h. After 24 h, first cells begin to lyse due to the viral particle production inside. At this point, media was changed to target-cell cultivation media. Since initial trials revealed effective infection preventing capacities of RHB-A, DMEM/F12 media was used for BTIC infection. For U87, normal DMEM + 10% FBS was used.

Infection of target cells: Target cells were seeded one day prior to infection in 6-well plates (2–3 wells/condition) in a concentration appropriate to their proliferation rate to reach 70–80% confluence at the time of infection. Proneural cells were seeded on laminin-coated vessels to achieve growth in monolayers, since trials revealed low infection rates of spheres. Cultivation media was removed and the target cells rinsed with 1x PBS once. In order to produce media containing lentiviral particles, media was aspirated from the 293T cell vessel and filtered (0.2 µm). Subsequently, 2 ml of the obtained media was added onto the target cells. 293T cells were cultivated with fresh target cell media for another day. Infection was performed by spinoculation as initial experiments revealed that BTICS were not able to survive infection with the infection enhancing reagent polybrene, which required 48 h of exposure to lentiviral particles and polybrene. During spinoculation, target cells were exposed

to lentiviral particles for only 1 h and, to enhance infection rates, plates were centrifuged at 900 xg for 1 h. Afterwards, the cells were incubated in their general cultivation media for 24 h before a second infection. Infections were performed twice, at 48 and 72 h after 293T transfection. 24 h after the last infection, antibiotic selection with $13 \mu\text{g ml}^{-1}$ Bsd (stock: 10 mg ml^{-1}) was started to select those cells that genomically incorporated and expressed the RFP vector. Cells transduced with the GFP vector, which lacked an antibiotic selection gene, were enriched and sent for FACS sorting at the Department of Hematology & Oncology, University Hospital Regensburg. Cells were considered as S1 material after two media exchanges.

7.2.1.3. Inhibitor Treatment

The STAT3 specific inhibitor V, Stattic (Schust *et al.* 2006) was used to inhibit STAT3 functionality, by preventing phosphorylation of the transcription factor. Stattic (short for STAT three inhibitory compound) is a non-peptidic small molecule was identified by Schust and colleagues in 2006 by screening chemical libraries. Stattic is a 6-nitro-benzo[b]thiophene-1,1-dioxide 1, which selectively inhibits the function of the STAT3 SH2 domain. Thus, STAT3 activation through cell surface receptors like the interleukin 6 (IL-6) receptor, which activates STAT3 via its SH2 domain by phosphorylation of the tyrosine residue 705, is prevented. After phosphorylation, this SH2 domain is required for STAT3 dimerization, which is essential to enter the nucleus to alter gene expression (Zhong *et al.* 1994).

It has been shown that the inhibitory effect of Stattic increases by time and temperature, with optimal inhibitory efficacy at the physiologically relevant temperature of 37 °C (Schust *et al.* 2006) indicating an alkylation of STAT3 (McMurray, 2006). It is likely that Stattic modifies the cysteine residue 687, which is located at the opposite side of the phosphopeptide binding face (McMurray, 2006) and leads to alkylation of STAT3. In this case, Stattic alters the SH2 domain conformation so that STAT3 can no longer be recruited by tyrosine kinases, thus preventing STAT3 from being transformed into an active state. Additionally, this explains the selectivity of Stattic for STAT3, since the corresponding amino acid to Cys687 is a tyrosine in STAT1 and STAT5 (McMurray, 2006), which are closely related to STAT3, however, not affected by this compound.

Western blot: Stattic was applied at concentrations ranging from 0.625 μM to 20 μM . For Western blot analysis, cells were seeded 24 h prior to treatment, which was carried out with concentrations between 5 to 20 μM over 24 h.

Spheroid and proliferation assays: For spheroid and proliferation assays, equal Stattic concentrations were applied ranging from 0.625 to 20 μM . For proliferation analysis, cells were seeded 48 h prior to treatment, and then culture media was replaced by Stattic containing media. Spheroids were transferred with 100 μl media to dilute the double concentrations of Stattic applied to the target wells in advance. An example scheme for Stattic treatments according to which both assays were performed is shown in Figure 7-1.

OBSC: Stattic was applied at a concentration 15 μM in the OBSC culture media, two days after spheroid implantation. Stattic was applied every second day with the regular media exchange.

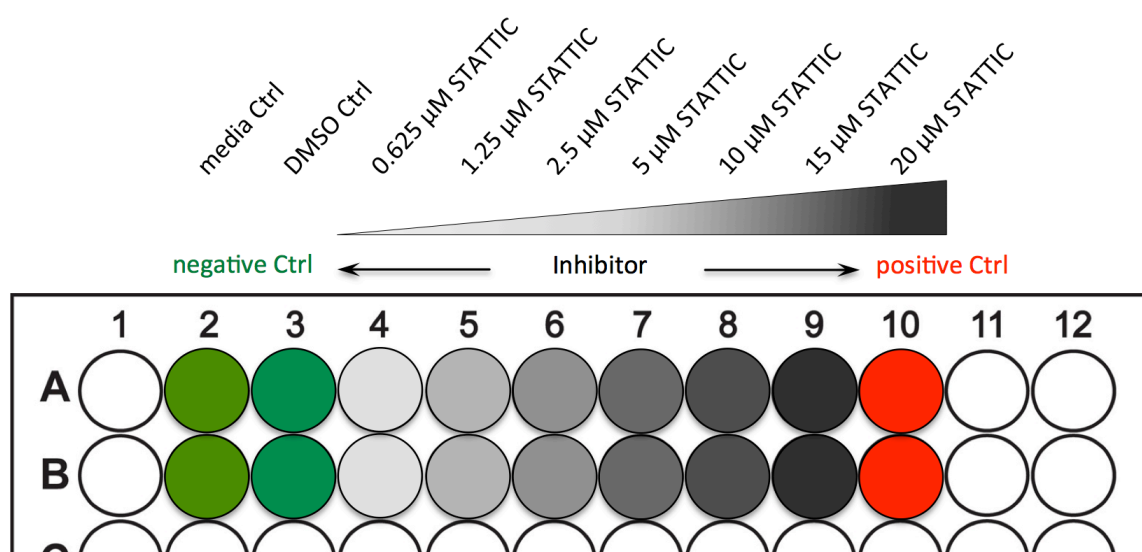


Figure 7-1: Stattic treatment assay layout

All proliferation and spheroid assays for Stattic treatment were conducted according to this scheme. Media and DMSO Control in column 2 and 3, followed by increasing Stattic concentrations ranging from 0.625 to 20 μM . The highest Stattic concentration also served as positive control.

7.2.1.4. Proliferation Assays

7.2.1.4.1. CyQuant proliferation assay

The CyQuant Direct Proliferation Assay was utilised to measure cell proliferation at treatment conditions in 96-well plate format according to manufacturer's protocols. Assays were performed in duplicates, two consecutive passages per cell line with three wells/treatment each turn. CyQuant measurements were collected during supervision of Lisa Rauer's Master thesis (Rauer, 2015) by Judith Proske and Lisa Rauer.

Assay protocol: Cells were detached, dissociated into single cell suspension and cell numbers were determined as described above. Depending on prior observations of proliferation rates, cells were seeded at densities of 2.5, 3.75 or 5×10^4 cells ml^{-1} with 100 μl /well and incubated at normoxic conditions. After 72 h, cultivation media was removed completely and replaced by Static treatment and appropriate controls, according to treatment concentrations and layout as described in section 7.2.1.3. Proliferation was either measured directly, or at 48 and 96 h respectively. 100 μl /well CyQuant Direct Solution (11.7 ml culture medium, 48 μl green fluorescent nucleic acid stain and 240 μl background suppressor) were applied 1 h prior to measurement with standard FITC filter settings (excitation at 480 nm, emission at 535 nm). Every step involving CyQuant dye handling required exclusion of light. Blank values measured at every time point (100 μl media) and serial cell number dilutions served as references.

Analysis: Background fluorescence was removed by subtraction of blank values, then values were normalised by division to the 0 h value, followed by 2-way ANOVA analysis to determine significant differences between treatments at different time points. GraphPad Prism software was used for calculation and graphical analysis. Significances were depicted for control compared to treatment. Detailed statistics comparing treatments among one another are listed in the statistics on the enclosed CD.

Calculation of the growth constant λ , doubling time and proliferation day^{-1} : For each condition respectively, the average of 6 measurements was calculated and used for calculations. In order to calculate absolute proliferation rates per day in %, the initial fluorescence at 0 h was subtracted from the values at 48 h and 96 h. The growth constant λ [min^{-1}] was first calculated for the two timeframes 0–48 and 0–96 h by use of the following formula:

$$\lambda = \ln \left(\frac{N_t/N_0}{t} \right)$$

N_0 = fluorescence/cell density at 0 h

N_t = fluorescence/cell density at time point t

t = time point

Depending on the growth curve, the mean λ of both was calculated, or λ_{48h} was further applied. Only in the event cell proliferation reached a plateau between 48 and 96 h, λ_{48h} was applied, otherwise the mean. Depending on λ , the doubling time t_d was calculated in h by use of the following formula:

$$t_d = \frac{\ln 2}{\lambda}$$

λ = growth constant

Mean proliferation per day (p) was calculated according to the formula for percentage growth:

$$p = \left(\frac{N_t}{N_0} \right)^{1/t} - 1$$

N_0 = fluorescence/cell density at 0 h

N_t = fluorescence/cell density at time point t

t = time point

7.2.1.4.2. Crystal violet proliferation assay

Crystal violet stains the DNA of cells, allowing fluorometric measurement of the increase of DNA as an indicator of cell proliferation. The assays were performed according to (Leidgens *et al.* 2015) to measure effects of diclofenac or ibuprofen on GBM cell lines.

7.2.1.5. Migration assays

7.2.1.5.1. Spheroid assay

Spheroid assays allow monitoring of cell migration over time across various treatments while simultaneously allowing quantification of migration rates. Assays were performed in triplicates, three consecutive passages per cell line with three spheroids/treatment each turn.

Spheroid formation: 200 µl of cell suspension at a density of 2.5×10^4 cells ml⁻¹ was inoculated into 96-well plates (F-bottom) coated with 100 µl of 1% agarose in 1x PBS 20 – 30 min prior to addition of cell suspension. Agarose coating forces the cells to form spheroids independent of their normal growth pattern. After 48 h, spheroids were isolated with 100 µl media using 200 µl pipette tips (at a 180° angle to the well) and transferred into U-bottom 96-well plates. Wells either contained 100 µl of normal growth media as a control or respective concentrations of Stattic as described in section 7.2.1.3. Laminin coating of U-bottom plates (see paragraph 7.2.1.1.4) was necessary for proneural BTICs to allow for adherence and migration.

Monitoring and quantification of migration: Pictures of spheroids were taken at 0, 16, 24, 40, and 48 h at 2.5 fold magnification on a Fluovolt light microscope. Spheroid size was measured with ImageJ software using the freehand selection tool. Figure 7-2 presents a representative measurement of spheroids at 40 h under different treatment conditions. ImageJ scale was set to 460 pixel/1000 µm according to scale and picture resolution (2080 × 1542), thus output data was given in µm. All values were normalised to the initial spheroid size at 0 h by division. Normalisation, comparison by 2-way ANOVA, and graphic realisation were done with GraphPad Prism software. Deviations are depicted as SD and significances for control compared to treatment. Detailed statistics comparing treatments among one another are listed in the statistics on the enclosed CD.

Calculation of mean migration day⁻¹: In order to calculate absolute migration rates per day in µm, the 0 h initial spheroid sizes were subtracted from the area measured at 24 h. The remaining area was assumed to be an ideal circle area. The radius was calculated by:

$$r = \sqrt{A/\pi}$$

r = radius = migration/day

A = area (area₂₄ – area₀)

π = mathematical constant

and assumed as average migration speed per day. For each condition, the average of 9 spheroids in total was calculated and assumed as average migration speed day⁻¹. Correspondingly, standard deviations define the range around the average migration.

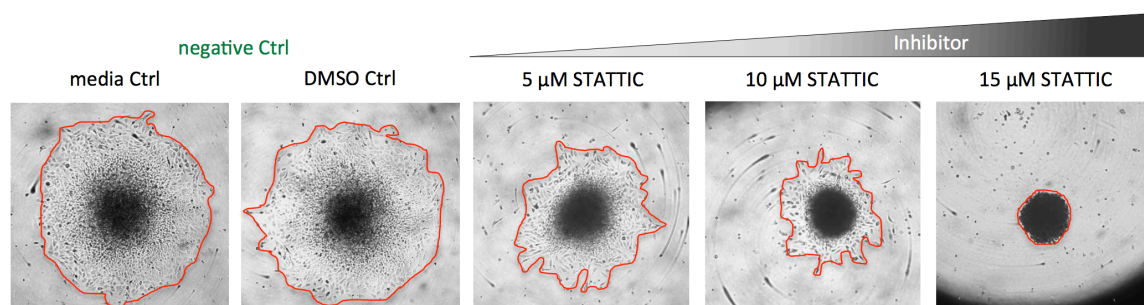


Figure 7-2: Measurement of spheroid area

At every time point (here: 40 h), the circumference of each spheroid was measured as pictured above by use of ImageJ free hand tool.

7.2.1.5.2. Wound healing assay

The wound healing assay is a modified version of a scratch assay. Instead of scratching a gap into an existent cell layer, Ibidi inserts (silicon culture-inserts) are used to generate a 500 μm cell-free gap between two cell layers. Live Cell Imaging was used for wound healing assays. In preparation, Ibidi inserts were stuck onto a Petri dish or a 4-chamber LabTek. Then, 80 μl of cell suspension was added to achieve a density of $1 - 2.5 \times 10^5$ cells ml^{-1} within each chamber. Cells were incubated for 24 – 48 h before inserts were removed and CO_2 -free media was applied. For Stattic treatment, media containing 5, 10, or 15 μM Stattic was added to different compartments of the LabTek. As Stattic is dissolved in DMSO, appropriate controls were carried out. Live cell imaging was performed at 10-fold magnification. Successively, the cell free gaps were positioned in focus and marked for recording. When fluorescence labelled cells were used, the appropriate fluorescence channels were recorded in addition. Three to four positions were marked for recording within each gap and pictures were taken every hour, for duration of 48 h, until the gap was closed (at least at control conditions). Cells stayed viable during the long imaging period due to an incubation chamber surrounding the microscope.

Subsequently, cell free spaces were measured in ImageJ (U.S. National Institutes of Health) at different time points (e.g. 0, 16, 24, 40, and 48 h, depending on cell motility). Using the data obtained in this analysis, migration rates were calculated in GraphPad Prism software. Values were first normalised to the 0 h value: $100 \times \text{Value Baseline}^{-1}$, then, 2-way ANOVA analysis allowed for determination of significant differences between treatments at different time points.

7.2.2. Organotypic Brain Slice Culture

7.2.2.1. Preparation

Organotypic brain slice cultures (OBSC) preparations were established on the basis of different publications (Gogolla *et al.* 2006; Gähwiler *et al.* 1997; Eyüpoglu *et al.* 2005) and adapted to our requirements.

Preliminaries for OBSC preparation: OBSC preparation was performed at most sterile conditions in a laminar flow hood. According to pup number, 6-well plates were filled with 1.2 ml/well of brain slice culture media and placed in a CO₂ incubator. One pup yielded approximately 3 – 5 slices with 2 – 3 hemispheres cultured/well. 5% low melting agarose in 1x PBS was prepared one day in advance and stored at 60 °C to eliminate air bubbles. Prior to use, the solution was placed in a water bath to cool down to 37 °C.

All materials such as filter paper, small fine tweezers, small scissors, scalpel, Vibratome blades, fine round-end spatula, flat-end spatula and big round-end spatula were sterilised and placed next to the Vibratome in the laminar flow together with one 3.5 cm and one 10 cm dish per pup. The Vibratome chamber was filled with ice-cold preparation media and cooled by ice. One 10 cm dish filled with 15 ml preparation media was placed on ice next to the Vibratome.

OBSC preparation: According to common and national guidelines and permissions for animal experiments, rat pups were killed by cervical dislocation with a large pair of sterilised scissors. After decapitation, the head was flushed with 70% isopropanol and transferred to a Petri dish placed in the laminar flow. The skin was removed by cutting along the middle vein starting at the neck until between the eyes, and then the skin was pulled aside. Using small scissors, the exposed skull was opened along the middle vein by inserting the scissors into the foramen magnum and cutting open along the middle line ending between the eyes. The two halves were pushed aside gently with fine tweezers to reveal the brain. Using a fine spatula (round-end), the whole brain was aseptically removed and placed in ice-cold preparation media directly to wash away remaining blood. Afterwards, the brain was dried carefully on a filter paper and placed, with the ventral side up, in the middle of a 3.5 µm dish, covered with 5% agarose and set on ice for polymerization. The agarose provided a scaffold to increase brain stability during the cutting process. After polymerization, the embedded brain was cut in a cuboid form and fixed with tissue glue on the Vibratome

plate (orientation: ventral site up, front in direction of the blade). 350 μm thick axial slices were cut with Vibratome settings at 3 – 5 speed and a frequency of 8. When floating in preparation media, the slices were transferred carefully with a big spatula into the 10 cm dish prepared beforehand. Slices were kept in preparation media and on ice whenever possible.

Slices were reviewed under a binocular to select those with completely preserved hippocampal structure showing clearly CA1, CA2, CA3 regions, dentate gyrus and entorhinal

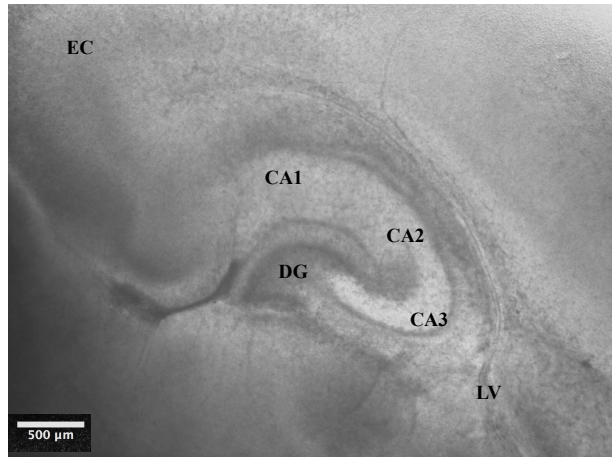


Figure 7-3: Organotypic brain slice

Image of an exemplary OBSC at 2.5 fold magnification taken before implantation. The lateral ventricle was considered as implantation site due to initial experiments. EC = entorhinal cortex, CA = *cornu ammonis*, DG = dentate gyrus, LV = lateral ventricle

cortex as shown in Figure 7-3. Those slices were either transferred to the insert membranes completely or separated in the two hemispheres with a spatula. If necessary, slices were unfolded and arranged by use of a small sterilised brush. However, slices were touched as little as possible. Three hemispheres were transferred onto insert membranes each, remaining media was soaked off the membrane and the inserts transferred into the equilibrated 6-well plate in the incubator. Slices were cultured 24 h before implantation.

7.2.2.2. Culture

Slices were kept in culture for up to 21 days in a humidified incubator at 37 °C with 5% CO₂. Media was exchanged every other day. Slices were exposed to media with the side facing the membrane, whereas their upper side was exposed to the controlled atmosphere. Any media soaking through the membrane was removed when the media was exchanged to keep the slices exposed to air. For imaging, the plate with slices was taken out of the incubator for ½ h at maximum to avoid any damage of the tissue.

7.2.2.3. Implantation of Glioma Cells

Two days before implantation, cells stably expressing a fluorescent marker, were seeded onto agarose coated 96-well plates (1×10^4 cells/well), as described for spheroid assays in paragraph 7.2.1.5.1. Slices were incubated for 24 h prior to implantation to adjust to the incubation atmosphere. Spheroids were picked from the agarose in as little media as possible and dropped onto the lateral ventricle, facing the hippocampal formation. One spheroid was implanted per hemisphere.

7.2.2.4. Monitoring Migration and Invasion

On the day of implantation, the entire hippocampus formation and the implantation site were imaged at 2.5 fold magnification under a light microscope. Using a fluorescent microscope, pictures at 5-fold magnification were taken to visualise the implanted spheroids. Progression of migration and invasion into the surrounding tissue was monitored once a week. Using Pixelmator software, several single images of one infiltrated area were merged into a complete picture of the whole area when necessary. Picture resolution (original: picture resolution 1.600×1.200 pixels) and scale were ensured during the merging process. Migration rates were estimated with similar principles as used for spheroid assays (see paragraph 7.2.1.5.1). The maximum distances travelled and the spatial area expansion by cells were measured 7 and 14 days after implantation on OBSCs with ImageJ. The measurement scale was set to 332 pixels/1000 μm according to the image scale factor, thus output data was specified in μm or μm^2 depending on the type of measurement. Additionally, spheroid size and radius were measured at implantation day. To calculate maximum invasion rates, values were normalised by subtraction of the initial spheroid radius. Then values were normalised to one day and averaged. The difference of the distances travelled between Static treated cells were compared to the control and a percentage proportion was calculated. The proportion of distance travelled by cells after treatment was calculated on the basis of the distance covered by respective control cells. Additionally, spatial expansion of the area covered by cells was measured since the infiltration on OBSCs was not radial as assumed for spheroid assays. Again, the percentage proportion of area covered by cells upon treatment was calculated on basis of the spatial expansion of respective control cells. All measurements were performed in triplicates, normalisation, comparison by 2-way ANOVA and graphic realisation were performed with GraphPad Prism software.

Significances are depicted for control compared to treatment. Deviations were depicted as SEM for area and SD for maximum distance related values.

7.2.2.5. Isolation of Single Cells

In order to isolate single cells from the invading rim or the non-invasive centre, an adapter for the Eppendorf Micromanipulator (InjectMan NI 2 and CellTram Air, Eppendorf, Hamburg, Germany) was developed to achieve a precise cutting of the respective regions. In cooperation with the Physics Mechanic Workshop, Faculty of Physics, University of Regensburg, an adapter was designed and manufactured from a 0.6×30 23 G $1 \frac{1}{4}$ cannula. Due to the attachment to the Micromanipulator, the adapter permitted absorption and transfer of separated tissue fragments.

For cell isolation, the membrane holding the OBSCs was cut from the insert. Remaining media was soaked off and the membrane (parts where no OBSCs were located) was glued to an object slide with tissue glue. Once the glue had dried, OBSC culture media was applied onto OBSCs and the slide placed under the microscope (Figure 7-4).

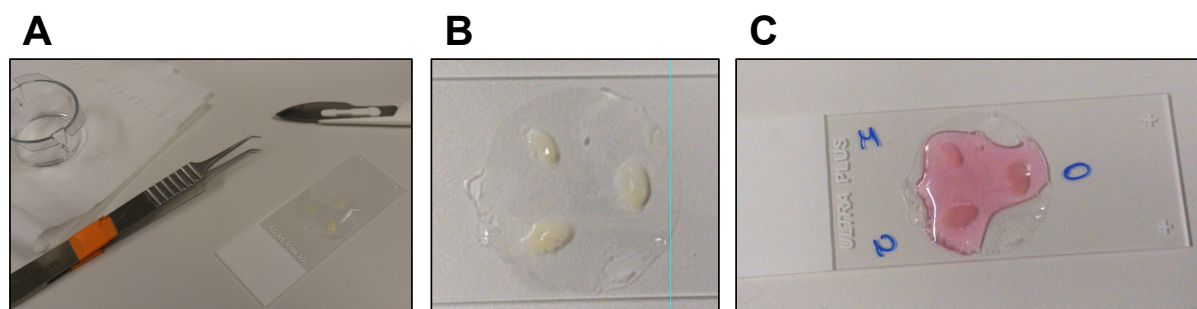


Figure 7-4: OBSC preparation for single cell isolation

(A) Membrane holding the OBSC were cut off the insert and (B) glued onto an object slide. Once the adhesive had set (C), the OBSC were covered with culture media and transferred to the microscope.

By use of this cannula-like adapter, small regions containing the cells of interest (leader, follower, or stationary) were cut from an OBSC, gathered in the cannula and transferred into a fresh well containing 1x PBS. The transfer and additional resorbing of the tissue fragment caused separation of single cells from the tissue without further need of enzymatic dissociation. Those single cells were picked by use of a capillary attached to the micromanipulator. The collected cells were transferred into cell lysis buffer immediately and frozen at -80°C to proceed with mRNA isolation followed by cDNA library preparation from single cells or pools of 20 cells.

7.2.2.6. cDNA libraries, quality PCRs, and microarrays

Further processing of collected cells into cDNA libraries, validation of cDNA libraries via quality PCRs, and microarray hybridization was performed according to (Hartmann and Klein, 2006) in the Department of Experimental Medicine and Therapy Research, Faculty of Medicine, University of Regensburg. cDNA library generation was performed based on isolation of the cellular mRNA by oligo-dT beads, followed by cDNA synthesis using random octamer and oligo-dT₍₁₅₎ primers, poly-G tailing, and PCR amplification (Hartmann & Klein, 2006). In total, 8 pools of each leader, follower, and stationary cells (20 cells/pool) were compared. The samples were hybridised to Agilent-014850 Whole Human Genome Microarray 4x44K chips, which possess 19,596 registered *Target Entrez Gene RNAs*. Four samples were hybridised to every chip and scanned (Axon Gene Pix 4400A, Molecular Devices, USA) prior to calculation of fluorescence intensity with the corresponding software (GenePixPro 7.0, Molecular Devices, USA).

Detailed bioinformatic processing to compare the three groups and identify a leader cell specific transcription factor signature was performed by Xin Lu, in the Department of Experimental Medicine and Therapy Research, Faculty of Medicine, University of Regensburg. The following briefly describes the established analysis parameters, algorithms, and methods utilised.

DEG analysis: Differentially expressed genes (DEG) were identified with the Limma-package that analyses gene expression data from microarray and RNA-Sequencing technologies (Ritchie *et al.* 2015). Both single-channel and two-colour microarrays can be analysed. Here, one-colour microarrays were used. The input data was imported in raw data format (*.gpr files). After background correction, the differentially expressed genes were identified. The algorithm employed – Linear Models – uses pairwise comparison to separate the input data into hierarchical groups. To reduce the probability of increased rates of Type I errors during multiple comparisons, a false discovery rate (FDR) approach was used with a q-value of 0.05.

Three pair wise comparison: The differentially expressed genes among the three types of cells were detected by performing three pair-wise comparisons into one Fisher's exact-test. This made it possible to assess whether the expected values of a quantitative variable within several pre-defined groups differ from each other. This method is also integrated in the Limma-package, and reveals if the three cells types are genetically truly different from each other. In comparison to the DEG analysis, this method used the information of pre-defined subgroups to compare them pairwise and to determine if the groups possess pronounced differences as expected. A q-value of < 0.05 was applied to the data as well as FDR.

Nearest neighbour analysis: Unsupervised clustering was performed to indicate a natural difference between leader and non-leader cells by identification of the nearest neighbours. Unsupervised clustering is a set of methods that extrapolates information about non-labelled data. It can be used to distinguish cell subtypes, without prior categorization, based on the natural expression features of the subtypes. The input data for this analysis was the normalised (by quantile normalisation) expression data. The unsupervised learning algorithm *k*-means was used, as it is widely used for clustering. *k*-means seeks to segregate the data (n observations) into k clusters such that the variances within the regions are minimised. Each observation belongs to the cluster with the nearest mean, serving as a prototype of the cluster. The number (k) of expected clusters serves as an input parameter for the algorithm. According to the dataset, k was set to 2 and 3 to cluster the expression data for the 4.000 probes with maximum variance. SigClust was used as a statistical method for testing the significance of the clustering results (Liu *et al.* 2008). The significance of the association with the distinct sample types was calculated by Fisher's test ($p < 3.3 \times 10^{-5}$).

ISMARA: The Integrated Motif Activity Response Analysis models raw genome-wide expression or chromatin modification data. It can be used to computationally predict regulatory sites for transcription factors (Balwierz *et al.* 2014). It runs automated in a web-based tool called ISMARA (Integrated System for Motif Activity Response Analysis) (Balwierz *et al.* 2014), which identifies key, or groups of, transcription factors as well as micro RNAs driving expression and makes detailed predictions regarding their regulatory roles. The ISMARA analysis identified the most significant transcription factor binding motifs where leader cells were significantly distinct from follower and stationary cells. The whole dataset was utilised for ISMARA analysis.

Interaction network analysis: Interaction network analysis was performed to identify differentially regulated transcription factors between leader and non-leader cells. ConsensusPathDB-human was utilised, which integrates interaction networks in *Homo sapiens*, including binary and complex protein-protein, genetic, metabolic, signalling, gene regulatory and drug-target interactions, as well as biochemical pathways. Data originate from currently 32 public resources for interactions (<http://consensuspathdb.org>) and interactions that were curated from literature. The interaction data are integrated in a complementary manner to avoid redundancies. This results in a seamless interaction network containing different types of interactions (Kamburov *et al.* 2013). For ConsensusPathDB analysis, the top 78 differentially expressed genes were included with a threshold q-value of < 0.01 .

7.2.3. Molecular Biological Analyses

7.2.3.1. Polymerase Chain Reaction (PCR)

Cell culture samples were checked for Mycoplasma contamination on a regular basis. The Promokine Kit detects a wide spectrum of Mycoplasma strains known as cell culture contaminants by use of primers amplifying a 479 bp sequence within the 16S rRNA operon coding region of the Mycoplasma genome.

1 ml supernatant of highly confluent cell cultures were frozen every other week and used for Mycoplasma detection according to manufacturer's protocols. Negative controls contained sterile water instead of DNA template.

The PCRs were performed according to the following manufacturer's protocol in given reaction tubes already containing a MasterMix with internal control DNA, nucleotides, primer, and Hot-Start Taq DNA Polymerase.

PCR batch (1-fold):

Component	Sample	Rehydration buffer	DNA-free ddH ₂ O
Test samples	2 µl	23 µl	
Positive control		23 µl	2 µl
Negative control		23 µl	2 µl

PCR program:

Degrees	Duration	Repetitions	Step
95 °C	2 min		Activation of Taq DNA Polymerase
94 °C	30 sec	40 ×	Denaturation
55 °C	30 sec		Annealing
72 °C	40 sec		Extension
4 °C	∞		Cool down

After PCR, the samples were stored at -20 °C or directly used for agarose gel electrophoresis.

7.2.3.2. Agarose Gel Electrophoresis

4.5 µl Ethidium bromide (0.5 µg ml⁻¹) was added to 90 ml of 1.5% agarose solution and poured into a gel chamber equipped with an appropriate comb. After polymerization, the gel was covered with TAE buffer and the comb removed carefully. A DNA ladder served as reference for base pair size. In general, 15 µl of the samples were mixed with 1.5 µl 10x DNA loading buffer and applied into the gel slots. Cell culture supernatants tested for Mycoplasma contamination already contained loading buffer from the test reaction and were loaded directly (15 µl).

Electrophoresis was carried out at 100 V and 300 mA for 45 min. Afterwards, bands were checked and a picture of the gel was taken with exposure to UV light at 254 nm specific for Ethidium bromide intercalated into DNA.

7.2.3.3. Quantitative real-time PCR

RNA isolation, cDNA synthesis and qRT-PCR runs were performed as described in (Leidgens *et al.* 2015).

qRT-PCR batch (1-fold):

Component	Volume
SYBR Green Mastermix	11 µl
primer forward	0.5 µl
primer reverse	0.5 µl
nuclease-free H ₂ O	6 µl
cDNA (1:25)	4 µl
total volume	22 µl

qRT-PCR program:

Degrees	Duration	Repetitions	Step
95 °C	15 min		Initial denaturation
95 °C	15 sec	35 ×	Denaturation
58 °C	30 sec		Annealing
72 °C	30 sec		Extension
65 – 95 °C	10 min		Melting curve

7.2.3.4. Plasmid Isolation

7.2.3.4.1. Generation of CaCl₂ competent *E. coli* DH5α

100 µl *E. coli* containing glycerol stock was added to 5 ml of LB media and grown over night at 37 °C while shaking at 200 xg. 1 ml of overnight culture was added to 500 ml preheated LB media and grown at 37 °C while shaking at 200 xg until OD₆₀₀ 0.3 – 0.4. Bacteria were spun down at 3,500 xg at 4 °C for 11 min. The pellet was resuspended in 125 ml of 0.1 M MgCl₂ (ice cold) on ice and incubated for 10 min on ice before spinning down at 2,500 xg at 4 °C for 11 min. The pellets were resuspended in 50 ml of ice cold 0.1 M CaCl₂ and left on ice for 20 min. Bacteria were pelleted for 11 min at 2,500 xg at 4 °C and

resuspended in 12.5 ml ice-cold 0.1 M CaCl_2 with 15% glycerol. Aliquots of 200 μl were dispensed and frozen immediately in liquid nitrogen.

7.2.3.4.2. Heat shock transformation of CaCl_2 competent *E. coli* DH5 α

Plasmids, see paragraph 7.1.8, were transformed into CaCl_2 competent *E. coli* DH5 α cells for amplification. One aliquot of competent DH5 α cells per transformation was thawed on ice before addition of plasmid DNA (100 ng) and incubated on ice for $\frac{1}{2}$ h. Heat shock was performed for 60 sec at 42 °C in a water bath and cells were transferred onto ice immediately afterwards and incubated for 10 min. 500 μl LB media were added and cells grown for 1 h at 37 °C while agitating at 200 xg. 200 μl of the suspension were plated on LB agar plates supplemented with 100 $\mu\text{l ml}^{-1}$ ampicillin as all plasmids used possessed an ampicillin resistance and incubated over night at 37 °C.

After successful transformation, clones were picked for plasmid isolation and inoculated in 5 ml LB media (with 100 $\mu\text{l ml}^{-1}$ ampicillin) for ~ 8 h incubation at 37 °C shaking at 200 xg. The pre-culture was used for plasmid isolation at mini scale or 200 μl were added to 100 ml ampicillin supplemented LB media and grown overnight at 37 °C while agitating at 200 xg for plasmid isolation at midi scale. Glycerol stocks were prepared the next day by addition of 500 μl culture to 500 μl 50% glycerol, stocks were stored at -80 °C.

7.2.3.4.3. Plasmid isolation at mini scale

For plasmid isolation at mini scale, the Miniprep Kit was used according to the manufacturer's protocol. 1.5 ml over-night culture was centrifuged for 1 min at 13,000 xg. The supernatant was discarded, the pellet resuspended in 250 μl of buffer 1, followed by addition of 250 μl of buffer 2 and 4 – 6x inversions to mix thoroughly and incubation for 3 min. Then, 250 μl buffer 3 were added and the samples inverted again before 5 min of centrifugation at 13,000 xg. 500 μl supernatant were added to 1 ml 100% ethanol, inverted 2x, incubated for 2 min and centrifuged at 13,000 xg for 10 min. The precipitated DNA was washed with 500 μl 70% ethanol and centrifuged for 10 min at 13,000 xg at RT. The supernatant was decanted carefully, remaining liquid was removed through incubation at 37 °C for $\frac{1}{2}$ h. Precipitated DNA was solubilised in 80 μl ddH $_2$ O with 10 $\mu\text{g ml}^{-1}$ RNase A.

7.2.3.4.4. Plasmid isolation at midi scale

Midi preps were performed to generate large amounts of plasmid DNA using the QIAGEN Plasmid Maxi Kit according to the manufacturer's protocol and modified where necessary. 200 ml culture were centrifuged for 10 min at 4,700 xg and 4 °C. Subsequently, the supernatant was discarded, the pellet resuspended in 10 ml buffer P1 before addition of 10 ml buffer P2. The tube was inverted 4 – 6x to mix thoroughly prior to 5 min of incubation. 10 ml buffer P3 (chilled previously on ice) were added, followed by 4 – 6x inversion and 20 min of incubation on ice. Lysed bacteria were centrifuged for 60 min at 4,700 xg at 4 °C. Meanwhile, columns were equilibrated with 10 ml QBT buffer. The supernatant was passed through a filter before addition onto the columns to remove any remaining cell debris. Once the supernatant had passed through, the tip was washed twice with 30 ml of QC buffer. Plasmid DNA was eluted with 15 ml of QF buffer and precipitated with 10.5 ml isopropanol prior to 30 min of centrifugation at 4,700 xg at 4 °C. The DNA pellet was washed with 5 ml 70% ethanol and centrifuged for another 10 min. The received DNA precipitate was air dried for 15 min before solubilisation in 300 µl ddH₂O over night at 4 °C. On the following day the amount and purity of the DNA was measured at the NanoPhotometer.

7.2.3.4.5. Control restriction of plasmid DNA

Control restrictions of plasmid DNA resulting from mini preparation were performed to ensure correct plasmid content. The different vectors, see section 7.1.8, were digested as presented below:

Plasmid	Enzyme (cutting positions)	Fragment sizes
psPAX2	<i>EcoRI</i> (1 720 / 6 094 bp)	4 374 / 6 329 bp
	<i>BamHI</i> (7 367 / 8 374 / 8 711 bp)	337 / 1 007 / 9 359 bp
pCMV-VSV-G	<i>AgeI</i> (2 401 bp) and <i>XbaI</i> (6 358 bp)	2 406 / 3 957 bp
U57 pHR SFFV GFP	<i>BamHI</i> (526 / 1 248 bp)	722 / 10 326 bp
pLenti-H1-(shRNA-Neg-control)-Rsv(GFP-Bsd)	<i>HindIII</i> (2 919 / 6 509 / 7 065 / 7 649 bp)	556 / 584 / 3 397 / 3 590 bp
pLenti-H1-(shRNA-Neg-control)-Rsv(RFP-Bsd)	<i>HindIII</i> (2 708 / 6 298 / 6 854 / 7 438 bp)	556 / 584 / 3 143 / 3 590 bp

Single or double restrictions were performed according to the following scheme:

Component	Concentration
plasmid DNA	10 μ l
CutSmart Buffer / NEBuffer 2.1/3.1	3 μ l
restriction enzyme I	0.5 μ l
<i>restriction enzyme II</i>	<i>0.5 μl</i>
ddH ₂ O	ad 30 μ l

The restriction reactions were mixed on ice and restriction itself performed for 1 h at 37 °C. Resulting fragments were checked by agarose gel electrophoresis analysis, see paragraph 7.2.3.2. When plasmid vectors revealed correct cutting patterns, plasmids were propagated further for midi preparation.

7.2.4. Protein Biochemical Analyses

7.2.4.1. Preparation of Whole Protein Lysates

Protein isolation: Whole protein lysates were prepared either from cell pellets frozen at -80 °C or cells lysed directly. Depending on the frozen pellet size, 50 – 200 μ l RIPA buffer was added, the pellets were thawed on ice and vortexed frequently until they were completely resuspended. For direct lysis, cells seeded in 10 cm dishes were transferred on ice, washed once with 1x PBS before addition of 200 μ l RIPA buffer, and finally scraped off the dish. Lysed cells were incubated for 10 min on ice before centrifugation for 10 min at 14,000 xg at 4 °C. Afterwards, the supernatant was transferred into fresh tubes.

Measurement of protein content: Protein content was measured by use of BCA assay (bicinchoninic acid assay), a biochemical assay determining the total concentration of protein in a solution. Analysis was performed according to the manufacturer's protocol in 96-well plates. Samples were diluted 1:10 in 1x PBS in a total volume of 25 μ l/well and measured in triplicates. Blanks were taken with RIPA buffer instead of a sample. As a reference, a standard dilution row at concentrations of 2000, 1000, 750, 500, 250, 125, 62.5, 0 μ g ml⁻¹ BSA diluted 1:10 in RIPA stock buffer was measured each time in duplicates. 200 μ l of BCA solution at a 1:50 ratio (reagent A to B) was added to each well before. After 30 min of incubation at 37 °C, the optical density (OD) was measured at 540 nm. OD values correspond

to protein concentration in $\mu\text{g } \mu\text{l}^{-1}$. Triplicates were averaged and the blank value subtracted to determine absolute concentrations. To ensure equal loading in PAGE, every sample was diluted to an equal protein amount of $2 \mu\text{g } \mu\text{l}^{-1}$ aliquot in 1x PBS.

Sample preparation for SDS-PAGE: Samples were either subjected to SDS-PAGE directly after preparation or stored at -80°C . Before use, 5x Laemmli buffer was added to the samples, then heat- inactivation was carried out for 10 min at 75°C .

7.2.4.2. SDS Polyacrylamide Gel Electrophoresis

SDS-PAGE was carried out using glass cassettes and electrophoresis modules assembled according to the manufacturer's instructions. The cassettes were filled with 10 – 12% resolving gel solution, which was covered immediately with 100% isobutanol. Approximately 1.5 cm space was left for the stacking gel. After polymerisation (20 – 30 min), the remaining isobutanol was soaked off and the stacking gel solution was added upon the resolving gel. An appropriate comb was inserted to create wells for sample loading and the gel was left for polymerisation.

Resolving gel (10 ml)	10%	12%	Stacking gel (5 ml)
ddH ₂ O	7.9 ml	6.6 ml	3.4 ml
30% Bis-Acrylamide	6.7 ml	8.0 ml	830 μl
1.5 M Tris (pH 8.8)	5.0 ml	5.0 ml	—
1.0 M Tris (pH 6.8)	—	—	630 μl
10% SDS	200 μl	200 μl	50 μl
10% APS	200 μl	200 μl	50 μl
TEMED	8 μl	8 μl	5 μl

For running SDS-PAGE, the electrophoresis chamber was filled with 1x SDS electrophoresis buffer. The protein samples were mixed with SDS loading buffer and heated for 10 min at 75°C . After a short centrifugation, 25 μl of the denatured protein samples were loaded into the wells, likewise 5 μl of the protein ladder. Electrophoresis was performed at 80 V and maximal amperage until the samples percolated through the resolving gel (first 20 min). Afterwards, the voltage was increased to 120 V and maximum amperage for approximately 1.5 h. Thus, proteins were separated according to size. After SDS-PAGE, Western blot analysis was performed.

7.2.4.3. Western blot

After SDS-PAGE, Western blot analyses were performed for transferring proteins from the SDS gel onto a nitrocellulose or PVDF membrane. SDS gels were incubated in a cathode buffer for 10 min with shaking. Meanwhile, each three Whatman blotting papers were submerged in cathode, anode I and anode II buffer, while the membrane was submerged in anode I buffer (previous equilibration for PVDF membrane occurred in 100% Methanol for 1 min). To assemble a blot, three papers soaked with cathode buffer were laid onto the cathode plate followed by the gel. Afterwards, a membrane and on top the three papers soaked in anode I buffer were stacked onto the gel followed by those soaked with anode II buffer. Air bubbles were removed before the anode plate was laid on top.

Blotting was performed at 45 mA for one gel or 90 mA for two gels, for 1.5 h at 4 °C. Subsequently, membranes were stained with Ponceau S solution for 5 min to verify successful separation. Then, membranes were destained for 2 min while shaking, followed by incubation in blocking solution for 1 h at RT while shaking. Washing the membrane with TBS-T buffer for each 10 min three times after the blocking step. The incubation with primary antibodies was performed overnight (used antibodies and dilutions are given in paragraph 7.1.6).

On the following day, blots were washed again, three times with TBS-T and the secondary antibody was applied. Incubation with secondary HRP-coupled antibodies was carried out for 1 – 2 h at RT. Afterwards, membranes were washed three times for 10 min with TBS-T and protein detection was carried out by ECL chemiluminescence reaction. Membranes were incubated for 20 sec up to 2 min in a 1:1 mixture of the ECL solutions. Signals were visualised with a Western Blot Imager and saved in TIFF format. Using GraphPad Prism software, images were analysed for band intensity. Band intensities were compared to the loading control and in case of treatment, to the corresponding control afterwards.

8. Bibliography

- Adamson, C. *et al.*, 2009. Glioblastoma multiforme: a review of where we have been and where we are going. *Expert opinion on investigational drugs*, 18(8), pp.1061–83.
- Agudelo-Garcia, P. & Jesus, J. De, 2011. Glioma cell migration on three-dimensional nanofiber scaffolds is regulated by substrate topography and abolished by inhibition of STAT3 signaling. *Neoplasia*, 13(9), pp.831–840.
- Aguilar-Morante, D. *et al.*, 2011. Decreased CCAAT/enhancer binding protein β expression inhibits the growth of glioblastoma cells. *Neuroscience*, 176, pp.110–9.
- Akhavan, D., Cloughesy, T.F. & Mischel, P.S., 2010. mTOR signaling in glioblastoma: Lessons learned from bench to bedside. *Neuro-Oncology*, 12(8), pp.882–889.
- Alexander, S. & Friedl, P., 2012. Cancer invasion and resistance: interconnected processes of disease progression and therapy failure. *Trends in molecular medicine*, 18(1), pp.13–26.
- Alonso, M.M. *et al.*, 2011. Genetic and epigenetic modifications of Sox2 contribute to the invasive phenotype of malignant gliomas. *PloS one*, 6(11), p.e26740.
- Andrews, J. *et al.*, 2002. Superior effectiveness of ibuprofen compared with other NSAIDs for reducing the survival of human prostate cancer cells. *Cancer Chemotherapy and Pharmacology*, 50(4), pp.277–284.

- Arden, J.D. *et al.*, 2015. Small molecule agonists of mammalian Diaphanous-related (mDia) formins reveal an effective glioblastoma anti-invasion strategy. *Molecular biology of the cell*.
- Balwierz, P.J. *et al.*, 2014. ISMARA: automated modeling of genomic signals as a democracy of regulatory motifs. *Genome Research*, 24(5), pp.869–884.
- Beadle, C. *et al.*, 2008. The role of myosin II in glioma invasion of the brain. *Molecular biology of the cell*, 19(8), pp.3357–68.
- Beier, D., Wischhusen, J., *et al.*, 2008. CD133 expression and cancer stem cells predict prognosis in high-grade oligodendroglial tumors. *Brain pathology (Zurich, Switzerland)*, 18(3), pp.370–7.
- Beier, D. *et al.*, 2007. CD133+ and CD133- glioblastoma-derived cancer stem cells show differential growth characteristics and molecular profiles. *Cancer Research*, 67(9), pp.4010–4015.
- Beier, D., Röhrl, S., *et al.*, 2008. Temozolomide preferentially depletes cancer stem cells in glioblastoma. *Cancer research*, 68(14), pp.5706–15.
- Bellail, A.C. *et al.*, 2004. Microregional extracellular matrix heterogeneity in brain modulates glioma cell invasion. *The international journal of biochemistry & cell biology*, 36(6), pp.1046–69.
- Bendfeldt, K. *et al.*, 2007. Basic fibroblast growth factor modulates density of blood vessels and preserves tight junctions in organotypic cortical cultures of mice: a new in vitro model of the blood-brain barrier. *The Journal of neuroscience : the official journal of the Society for Neuroscience*, 27(12), pp.3260–7.
- Bleeker, F.E., Molenaar, R.J. & Leenstra, S., 2012. Recent advances in the molecular understanding of glioblastoma. *Journal of Neuro-Oncology*, 108(1), pp.11–27.
- Bogdahn, U. *et al.*, 1989. Autocrine tumor cell growth-inhibiting activities from human malignant melanoma. *Cancer research*, 49(19), pp.5358–63.
- Borovski, T. *et al.*, 2011. Cancer stem cell niche: the place to be. *Cancer research*, 71(3), pp.634–9.

- Brantley, E.C. *et al.*, 2008. Loss of protein inhibitors of activated STAT-3 expression in glioblastoma multiforme tumors: Implications for STAT-3 activation and gene expression. *Clinical Cancer Research*, 14(15), pp.4694–4704.
- Bromberg, J., 2002. Stat proteins and oncogenesis. *The Journal of clinical investigation*, 109(9), pp.1139–42.
- Bromberg, J.F., 2001. Activation of STAT proteins and growth control. *BioEssays : news and reviews in molecular, cellular and developmental biology*, 23(2), pp.161–9.
- Bromberg, J.F. *et al.*, 1999. Stat3 as an oncogene. *Cell*, 98(3), pp.295–303.
- Bruna, A. *et al.*, 2007. High TGF β -Smad Activity Confers Poor Prognosis in Glioma Patients and Promotes Cell Proliferation Depending on the Methylation of the PDGF-B Gene. *Cancer Cell*, 11(February), pp.147–160.
- Buettner, R., Mora, L.B. & Jove, R., 2002. Activated STAT signaling in human tumors provides novel molecular targets for therapeutic intervention. *Clinical Cancer Research*, 8(4), pp.945–954.
- Calabrese, C. *et al.*, 2007. A Perivascular Niche for Brain Tumor Stem Cells. *Cancer Cell*, 11(January), pp.69–82.
- Calò, V. *et al.*, 2003. STAT proteins: from normal control of cellular events to tumorigenesis. *Journal of cellular physiology*, 197(2), pp.157–68.
- Cancer Genome Atlas Research Network, 2008. Comprehensive genomic characterization defines human glioblastoma genes and core pathways. *Nature*, 455(7216), pp.1061–8.
- Cancer Genome Atlas Research Network *et al.*, 2015. Comprehensive, Integrative Genomic Analysis of Diffuse Lower-Grade Gliomas. *The New England journal of medicine*, 372(26), pp.2481–98.
- Carro, M.S. *et al.*, 2010. The transcriptional network for mesenchymal transformation of brain tumours. *Nature*, 463(7279), pp.318–325.
- Charles, N.A. *et al.*, 2011. The brain tumor microenvironment. *Glia*, 59(8), pp.1169–80.
- Cheung, K.J. *et al.*, 2013. Collective invasion in breast cancer requires a conserved Basal epithelial program. *Cell*, 155(7), pp.1639–51.

- Chirasani, S.R. *et al.*, 2013. Diclofenac inhibits lactate formation and efficiently counteracts local immune suppression in a murine glioma model. *International journal of cancer. Journal international du cancer*, 132(4), pp.843–53.
- Choi, S.Y.C. *et al.*, 2014. Lessons from patient-derived xenografts for better in vitro modeling of human cancer. *Advanced drug delivery reviews*, 79-80, pp.222–37.
- Claes, A., Idema, A.J. & Wesseling, P., 2007. Diffuse glioma growth: a guerilla war. *Acta neuropathologica*, 114(5), pp.443–58.
- Le Clainche, C. & Carlier, M.-F., 2008. Regulation of actin assembly associated with protrusion and adhesion in cell migration. *Physiological reviews*, 88(2), pp.489–513.
- Clark, M.J. *et al.*, 2010. U87MG decoded: The genomic sequence of a cytogenetically aberrant human cancer cell line. *PLoS Genetics*, 6(1).
- Clond, M.A. *et al.*, 2013. Reactive Oxygen Species-Activated Nanoprodrug of Ibuprofen for Targeting Traumatic Brain Injury in Mice. *PLoS ONE*, 8(4), pp.2–11.
- Cloughesy, T.F., Cavenee, W.K. & Mischel, P.S., 2014. Glioblastoma: From Molecular Pathology to Targeted Treatment. *Annual Review of Pathology: Mechanisms of Disease*, 9(1), pp.1–25.
- Cuddapah, V.A. *et al.*, 2014. A neurocentric perspective on glioma invasion. *Nature reviews. Neuroscience*, 15(7), pp.455–65.
- Cusulin, C. *et al.*, 2015. Precursor States of Brain Tumor Initiating Cell Lines Are Predictive of Survival in Xenografts and Associated with Glioblastoma Subtypes. *Stem Cell Reports*, 5, pp.1–9.
- Darnell, J.E., Kerr, I.M. & Stark, G.R., 1994. Jak-STAT pathways and transcriptional activation in response to IFNs and other extracellular signaling proteins. *Science (New York, N.Y.)*, 264(5164), pp.1415–21.
- Das, S., Srikanth, M. & Kessler, J., 2008. Cancer stem cells and glioma. *Nature clinical practice. Neurology*, 4(8), pp.427–35.
- Delic, S., *et al.*, 2012. “Identification and Functional Validation of CDH11, PCSK6 and SH3GL3 as Novel Glioma Invasion-Associated Candidate Genes.” *Neuropathology and Applied Neurobiology* 38 (2), pp. 201–12.

- Demuth, T. *et al.*, 2008. Glioma cells on the run - the migratory transcriptome of 10 human glioma cell lines. *BMC genomics*, 9, p.54.
- Demuth, T. *et al.*, 2001. Migratory activity of human glioma cell lines in vitro assessed by continuous single cell observation. *Clinical & experimental metastasis*, 18(7), pp.589–597.
- Demuth, T. & Berens, M.E., 2004. Molecular mechanisms of glioma cell migration and invasion. *Journal of neuro-oncology*, 70(2), pp.217–28.
- Dhruv, H.D. *et al.*, 2013. Reciprocal activation of transcription factors underlies the dichotomy between proliferation and invasion of glioma cells. *PloS one*, 8(8), p.e72134.
- Eisele, G. *et al.*, 2014. Cilengitide treatment of newly diagnosed glioblastoma patients does not alter patterns of progression. *Journal of neuro-oncology*, 117(1), pp.141–5.
- Eyüpoglu, I.Y. *et al.*, 2005. Malignant glioma-induced neuronal cell death in an organotypic glioma invasion model. Technical note. *Journal of neurosurgery*, 102(4), pp.738–44.
- Farrell, C.L., Megyesi, J. & Del Maestro, R.F., 1988. Effect of ibuprofen on tumor growth in the C6 spheroid implantation glioma model. *Journal of neurosurgery*, 68(6), pp.925–930.
- Fredriksson, L. *et al.*, 2011. Diclofenac inhibits tumor necrosis factor- α -induced nuclear factor- κ B activation causing synergistic hepatocyte apoptosis. *Hepatology*, 53(6), pp.2027–2041.
- Friedl, P. *et al.*, 2012. Classifying collective cancer cell invasion. *Nature cell biology*, 14(8), pp.777–83.
- Friedl, P. & Alexander, S., 2011. Cancer invasion and the microenvironment: plasticity and reciprocity. *Cell*, 147(5), pp.992–1009.
- Friedl, P. & Gilmour, D., 2009. Collective cell migration in morphogenesis, regeneration and cancer. *Nature reviews. Molecular cell biology*, 10(7), pp.445–57.
- Friedl, P. & Wolf, K., 2010. Plasticity of cell migration: a multiscale tuning model. *The Journal of cell biology*, 188(1), pp.11–9.
- Friedl, P. & Wolf, K., 2003. Tumour-cell invasion and migration: diversity and escape mechanisms. *Nature reviews. Cancer*, 3(5), pp.362–74.

- Gähwiler, B.H. *et al.*, 1997. Organotypic slice cultures: a technique has come of age. *Trends in neurosciences*, 20(10), pp.471–7.
- Galli, R. *et al.*, 2004. Isolation and characterization of tumorigenic, stem-like neural precursors from human glioblastoma. *Cancer research*, 64(19), pp.7011–21.
- Giard, D.J. *et al.*, 1973. In vitro cultivation of human tumors: establishment of cell lines derived from a series of solid tumors. *Journal of the National Cancer Institute*, 51(5), pp.1417–1423.
- Giuliano, F. & Warner, T.D., 1999. Ex vivo assay to determine the cyclooxygenase selectivity of non-steroidal anti-inflammatory drugs. *British journal of pharmacology*, 126(8), pp.1824–1830.
- Glassmann, A. *et al.*, 2011. Pharmacological targeting of the constitutively activated MEK/MAPK-dependent signaling pathway in glioma cells inhibits cell proliferation and migration. *International Journal of Oncology*, 39(6), pp.1567–1575.
- Gogolla, N. *et al.*, 2006. Preparation of organotypic hippocampal slice cultures for long-term live imaging. *Nature protocols*, 1(3), pp.1165–71.
- Gottfried, E. *et al.*, 2013. New Aspects of an Old Drug - Diclofenac Targets MYC and Glucose Metabolism in Tumor Cells. *PLoS ONE*, 8(7).
- Graham, F.L. *et al.*, 1977. Characteristics of a human cell line transformed by DNA from human adenovirus type 5. *The Journal of general virology*, 36(2977), pp.59–74.
- Gritsenko, P.G., Ilina, O. & Friedl, P., 2012. Interstitial guidance of cancer invasion. *The Journal of pathology*, 226(2), pp.185–99.
- Grzmil, M. *et al.*, 2011. MAP kinase-interacting kinase 1 regulates SMAD2-dependent TGF- β signaling pathway in human glioblastoma. *Cancer research*, 71(6), pp.2392–402.
- Günther, H.S. *et al.*, 2008. Glioblastoma-derived stem cell-enriched cultures form distinct subgroups according to molecular and phenotypic criteria. *Oncogene*, 27(20), pp.2897–2909.
- Haeger, A. *et al.*, 2014. Cell jamming: collective invasion of mesenchymal tumor cells imposed by tissue confinement. *Biochimica et biophysica acta*, 1840(8), pp.2386–95.
- Hall, A., 2009. The cytoskeleton and cancer. *Cancer and Metastasis Reviews*, 28(1-2), pp.5–14.

- Hanahan, D. & Weinberg, R.A., 2011. Hallmarks of cancer: The next generation. *Cell*, 144(5), pp.646–674.
- Harris, R.E., Beebe-Donk, J. & Alshafie, G.A., 2006. Reduction in the risk of human breast cancer by selective cyclooxygenase-2 (COX-2) inhibitors. *BMC cancer*, 6, p.27.
- Hartmann, C.H. & Klein, C.A., 2006. Gene expression profiling of single cells on large-scale oligonucleotide arrays. *Nucleic acids research*, 34(21), p.e143.
- Hermes, J.W. *et al.*, 1999. C-MYC oncogene family expression in glioblastoma and survival. *Surgical Neurology*, 51, pp.536–542.
- Hirano, T., Ishihara, K. & Hibi, M., 2000. Roles of STAT3 in mediating the cell growth, differentiation and survival signals relayed through the IL-6 family of cytokine receptors. *Oncogene*, 19(21), pp.2548–56.
- Hjelmeland, B. *et al.*, 2011. Acidic stress promotes a glioma stem cell phenotype. *Cell death and differentiation*, 18, pp.829–840.
- Hoelzinger, D.B. *et al.*, 2005. Gene expression profile of glioblastoma multiforme invasive phenotype points to new therapeutic targets. *Neoplasia (New York, N.Y.)*, 7(1), pp.7–16.
- Homma, J. *et al.*, 2006. Increased expression of CCAAT/enhancer binding protein beta correlates with prognosis in glioma patients. *Oncology reports*, 15(3), pp.595–601.
- Hou, L.C. *et al.*, 2006. Recurrent glioblastoma multiforme: a review of natural history and management options. *Neurosurgical focus*, 20(4), p.E5.
- Howie, D., Waldmann, H. & Cobbold, S., 2014. Nutrient Sensing via mTOR in T Cells Maintains a Tolerogenic Microenvironment. *Frontiers in Immunology*, 5(August), pp.1–14.
- Humpel, C., 2015. Organotypic brain slice cultures: A review. *Neuroscience*, 305(August), pp.86–98.
- Hynes, R.O., 2009. The extracellular matrix: not just pretty fibrils. *Science (New York, N.Y.)*, 326(5957), pp.1216–9.
- Ignatova, T.N. *et al.*, 2002. Human cortical glial tumors contain neural stem-like cells expressing astroglial and neuronal markers in vitro. *Glia*, 39(3), pp.193–206.

- Johnsen, J.I. *et al.*, 2004. Cyclooxygenase-2 is expressed in neuroblastoma, and nonsteroidal anti-inflammatory drugs induce apoptosis and inhibit tumor growth in vivo. *Cancer Research*, 64(20), pp.7210–7215.
- Jones, L.J. *et al.*, 2001. Sensitive determination of cell number using the CyQUANT® cell proliferation assay. *Journal of Immunological Methods*, 254(1-2), pp.85–98.
- Joseph, J.V. *et al.*, 2014. TGF- β is an inducer of ZEB1-dependent mesenchymal transdifferentiation in glioblastoma that is associated with tumor invasion. *Cell death & disease*, 5(10), p.e1443.
- Kalluri, R., 2009. EMT: When epithelial cells decide to become mesenchymal-like cells. *Journal of Clinical Investigation*, 119(6), pp.1417–1419.
- Kamburov, A. *et al.*, 2013. The ConsensusPathDB interaction database: 2013 Update. *Nucleic Acids Research*, 41(D1), pp.793–800.
- Kienast, Y. *et al.*, 2010. Real-time imaging reveals the single steps of brain metastasis formation. *Nature medicine*, 16(1), pp.116–122.
- Kim, J. *et al.*, 2015. Spatiotemporal Evolution of the Primary Glioblastoma Genome. *Cancer cell*, 28(3), pp.318–28.
- Klein, C.A. *et al.*, 2002. Combined transcriptome and genome analysis of single micrometastatic cells. *Nature biotechnology*, 20(4), pp.387–92.
- Kong, D. *et al.*, 2011. Cancer Stem Cells and Epithelial-to-Mesenchymal Transition (EMT)-Phenotypic Cells: Are They Cousins or Twins? *Cancers*, 3(1), pp.716–29.
- Kovács, R., Papageorgiou, I. & Heinemann, U., 2011. Slice cultures as a model to study neurovascular coupling and blood brain barrier in vitro. *Cardiovascular psychiatry and neurology*, 2011, p.646958.
- Lane, S.W., Williams, D. a & Watt, F.M., 2014. Modulating the stem cell niche for tissue regeneration. *Nature biotechnology*, 32(8), pp.795–803.
- Leidgens, V. *et al.*, 2015. Ibuprofen and Diclofenac Restrict Migration and Proliferation of Human Glioma Cells by Distinct Molecular Mechanisms. *PloS one*, 10(10), p.e0140613.
- Levy, D. & Lee, C., 2002. What does Stat3 do? *The Journal of Clinical Investigation*, 109(9), pp.1143–1148.

- Li, Z. *et al.*, 2009. Turning cancer stem cells inside out: An exploration of glioma stem cells signalling pathways. *Journal of Biological Chemistry*, 284(25), pp.16705–16709.
- Liang, J. & Mills, G.B., 2013. AMPK: A contextual oncogene or tumor suppressor? *Cancer Research*, 73(10), pp.2929–2935.
- Lin, N. *et al.*, 2014. Prevalence and clinicopathologic characteristics of the molecular subtypes in malignant glioma: A multi-institutional analysis of 941 cases. *PLoS ONE*, 9(4), pp.1–5.
- Liu, Y. *et al.*, 2008. Statistical Significance of Clustering for High-Dimension, Low-Sample Size Data. *Journal of the American Statistical Association*, 103(483), pp.1281–1293.
- Louis, D.N. *et al.*, 2014. International Society of Neuropathology-Haarlem Consensus Guidelines for Nervous System Tumor Classification and Grading. *Brain pathology (Zurich, Switzerland)*, (July), pp.1–7.
- Louis, D.N., 2006. Molecular pathology of malignant gliomas. *Annual review of pathology*, 1, pp.97–117.
- Louis, D.N. *et al.*, 2007. The 2007 WHO classification of tumours of the central nervous system. *Acta neuropathologica*, 114(2), pp.97–109.
- Mani, S. a *et al.*, 2008. The epithelial-mesenchymal transition generates cells with properties of stem cells. *Cell*, 133(4), pp.704–15.
- Mao, P. *et al.*, 2013. Mesenchymal glioma stem cells are maintained by activated glycolytic metabolism involving aldehyde dehydrogenase 1A3. *Proceedings of the National Academy of Sciences of the United States of America*, 110(21), pp.8644–9.
- Marusyk, A. & Polyak, K., 2013. Cancer. Cancer cell phenotypes, in fifty shades of grey. *Science (New York, N.Y.)*, 339(6119), pp.528–9.
- Marx, J., 2001. Cancer research. Anti-inflammatories inhibit cancer growth--but how? *Science (New York, N.Y.)*, 291(5504), pp.581–2.
- Mazor, T. *et al.*, 2015. DNA Methylation and Somatic Mutations Converge on the Cell Cycle and Define Similar Evolutionary Histories in Brain Tumors. *Cancer Cell*, 28(3), pp.307–317.
- McMurray, J.S., 2006. A new small-molecule Stat3 inhibitor. *Chemistry & biology*, 13(11), pp.1123–4.

- Medema, J.P., 2013. Cancer stem cells: the challenges ahead. *Nature cell biology*, 15(4), pp.338–44.
- Van Meir, E.G. *et al.*, 2010. Exciting new advances in neuro-oncology: the avenue to a cure for malignant glioma. *CA: a cancer journal for clinicians*, 60(3), pp.166–93.
- Meyer, M. *et al.*, 2014. Single cell derived clonal analysis of human glioblastoma links functional and genomic heterogeneity. *Proceedings of the National Academy of Sciences of the United States of America*, In Press, pp.1–6.
- Modrek, A.S., 2014. Brain stem cells as the cell of origin in glioma. *World Journal of Stem Cells*, 6(1), p.43.
- Moeckel, S. *et al.*, 2014. Response-predictive gene expression profiling of glioma progenitor cells in vitro. *PloS one*, 9(9), p.e108632.
- Nevo, I. *et al.*, 2014. Identification of molecular pathways facilitating glioma cell invasion in situ. *PloS one*, 9(11), p.e111783.
- Nguyen-Ngoc, K.-V. *et al.*, 2012. ECM microenvironment regulates collective migration and local dissemination in normal and malignant mammary epithelium. *Proceedings of the National Academy of Sciences of the United States of America*, 109(39), pp.E2595–604.
- Noraberg, J., Kristensen, B.W. & Zimmer, J., 1999. Markers for neuronal degeneration in organotypic slice cultures. *Brain research. Brain research protocols*, 3(3), pp.278–90.
- Noushmehr, H. *et al.*, 2010. Identification of a CpG island methylator phenotype that defines a distinct subgroup of glioma. *Cancer cell*, 17(5), pp.510–22.
- Oh, D. *et al.*, 2015. Phase I Study of OPB-31121, an Oral STAT3 Inhibitor, in Patients with Advanced Solid Tumors. , pp.1–9.
- Ohgaki, H. & Kleihues, P., 2013. The definition of primary and secondary glioblastoma. *Clinical cancer research : an official journal of the American Association for Cancer Research*, 19(4), pp.764–72.
- Onken, J. *et al.*, 2014. Versican isoform V1 regulates proliferation and migration in high-grade gliomas. *Journal of neuro-oncology*.

- Ortensi, B. *et al.*, 2013. Cancer stem cell contribution to glioblastoma invasiveness. *Stem cell research & therapy*, 4, p.18.
- Ostrom, Q.T. *et al.*, 2014. CBTRUS Statistical Report: Primary Brain and Central Nervous System Tumors Diagnosed in the United States in 2007-2011. *Neuro-Oncology*, 16(suppl 4), pp.iv1–iv63.
- Ozawa, T. *et al.*, 2014. Most Human Non-GCIMP Glioblastoma Subtypes Evolve from a Common Proneural-like Precursor Glioma. *Cancer Cell*, 26(2), pp.288–300.
- Palayoor, S.T. *et al.*, 1999. Constitutive activation of IkappaB kinase alpha and NF-kappaB in prostate cancer cells is inhibited by ibuprofen. *Oncogene*, 18(51), pp.7389–7394.
- Parra-Bonilla, G. *et al.*, 2013. Lactate dehydrogenase a expression is necessary to sustain rapid angiogenesis of pulmonary microvascular endothelium. *PloS one*, 8(9), p.e75984.
- Patel, A.P. *et al.*, 2014. Single-cell RNA-seq highlights intratumoral heterogeneity in primary glioblastoma. *Science (New York, N.Y.)*, 344(6190), pp.1396–401.
- Phillips, H.S. *et al.*, 2006. Molecular subclasses of high-grade glioma predict prognosis, delineate a pattern of disease progression, and resemble stages in neurogenesis. *Cancer cell*, 9(3), pp.157–73.
- Poli, V. & Camporeale, A., 2015. STAT3-Mediated Metabolic Reprograming in Cellular Transformation and Implications for Drug Resistance. *Frontiers in oncology*, 5(June), p.121.
- Polyak, K. & Weinberg, R. a, 2009. Transitions between epithelial and mesenchymal states: acquisition of malignant and stem cell traits. *Nature reviews. Cancer*, 9(4), pp.265–73.
- Rao, S.S. *et al.*, 2013. Mimicking white matter tract topography using core-shell electrospun nanofibers to examine migration of malignant brain tumors. *Biomaterials*, 34(21), pp.5181–90.
- Rauer, L., 2015. Metformin and Stattic as additive inhibitors of STAT3 in malignant glioma cells. *Master's Thesis*. University of Regensburg.
- Reya, T. *et al.*, 2001. Stem cells, cancer, and cancer stem cells. *Nature*, 414(6859), pp.105–11.

- Ridley, A.J. *et al.*, 2003. Cell migration: integrating signals from front to back. *Science (New York, N.Y.)*, 302(December), pp.1704–1709.
- Riemenschneider, M.J. *et al.*, 2010. Molecular diagnostics of gliomas: state of the art. *Acta neuropathologica*, 120(5), pp.567–84.
- Ritchie, M.E. *et al.*, 2015. limma powers differential expression analyses for RNA-sequencing and microarray studies. *Nucleic acids research*, 43(7), p.e47.
- Roberts, P.J. & Der, C.J., 2007. Targeting the Raf-MEK-ERK mitogen-activated protein kinase cascade for the treatment of cancer. *Oncogene*, 26, pp.3291–3310.
- Roth, P. & Weller, M., 2014. Challenges to targeting epidermal growth factor receptor in glioblastoma: escape mechanisms and combinatorial treatment strategies. *Neuro-oncology*, 16(suppl 8), pp.viii14–viii19.
- Rushing, E.J. & Wesseling, P., 2015. Towards an integrated morphological and molecular WHO diagnosis of central nervous system tumors. *Current Opinion in Neurology*, p.1.
- Sanai, N., Alvarez-Buylla, A. & Berger, M.S., 2005. Neural stem cells and the origin of gliomas. *The New England journal of medicine*, 353(8), pp.811–22.
- Santra, M. *et al.*, 2006. Ectopic expression of doublecortin protects adult rat progenitor cells and human glioma cells from severe oxygen and glucose deprivation. *Neuroscience*, 142(3), pp.739–52.
- Scheel, C. & Weinberg, R. a., 2012. Cancer stem cells and epithelial-mesenchymal transition: Concepts and molecular links. *Seminars in Cancer Biology*, 22(5-6), pp.396–403.
- Schust, J. *et al.*, 2006. Stattic: a small-molecule inhibitor of STAT3 activation and dimerization. *Chemistry & biology*, 13(11), pp.1235–42.
- Scuto, A. *et al.*, 2011. STAT3 inhibition is a therapeutic strategy for ABC-like diffuse large B-cell lymphoma. *Cancer research*, 71(9), pp.3182–8.
- Seliger, C. *et al.*, 2013. Lactate-modulated induction of THBS-1 activates transforming growth factor (TGF)-beta2 and migration of glioma cells in vitro. *PloS one*, 8(11), p.e78935.
- Shelton, L.M. *et al.*, 2010. A novel pre-clinical in vivo mouse model for malignant brain tumor growth and invasion. *Journal of neuro-oncology*, 99(2), pp.165–76.

- Sherry, M.M. *et al.*, 2009. STAT3 is required for proliferation and maintenance of multipotency in glioblastoma stem cells. *Stem cells (Dayton, Ohio)*, 27(10), pp.2383–92.
- Shim, H. *et al.*, 1997. c-Myc transactivation of LDH-A: implications for tumor metabolism and growth. *Proceedings of the National Academy of Sciences of the United States of America*, 94(13), pp.6658–6663.
- Singh, A. & Settleman, J., 2010. EMT, cancer stem cells and drug resistance: an emerging axis of evil in the war on cancer. *Oncogene*, 29(34), pp.4741–4751.
- Singh, S.K. *et al.*, 2003. Identification of a cancer stem cell in human brain tumors. *Cancer Research*, 63, pp.5821–5828.
- Singh, S.K. *et al.*, 2004. Identification of human brain tumour initiating cells. *Nature*, 432(7015), pp.396–401.
- Sørensen, H.T. *et al.*, 2003. Risk of cancer in a large cohort of nonaspirin NSAID users: a population-based study. *British journal of cancer*, 88(11), pp.1687–1692.
- Sottoriva, A. *et al.*, 2015. A Big Bang model of human colorectal tumor growth. *Nature Genetics*, 47(3), pp.209–216.
- Sottoriva, A. *et al.*, 2013. Intratumor heterogeneity in human glioblastoma reflects cancer evolutionary dynamics. *Proceedings of the National Academy of Sciences of the United States of America*, 110(10), pp.4009–14.
- Spitzner, M., Roesler, B., *et al.*, 2014. STAT3 inhibition sensitizes colorectal cancer to chemoradiotherapy in vitro and in vivo. *International journal of cancer*, 134(4), pp.997–1007.
- Spitzner, M., Ebner, R., *et al.*, 2014. STAT3: A Novel Molecular Mediator of Resistance to Chemoradiotherapy. *Cancers*, 6(4), pp.1986–2011.
- Stupp, R. *et al.*, 2005. Radiotherapy plus Concomitant and Adjuvant Temozolomide for Glioblastoma. *New England Journal of Medicine*, 352(10), pp.987–996.
- Sturm, D. *et al.*, 2012. Hotspot Mutations in H3F3A and IDH1 Define Distinct Epigenetic and Biological Subgroups of Glioblastoma. *Cancer Cell*, 22(4), pp.425–437.
- Sullivan, J.P. *et al.*, 2014. Brain Tumor Cells in Circulation are Enriched for Mesenchymal Gene Expression. *Cancer Discovery*, (November), pp.1299–1310.

- Sundar, S.J. *et al.*, 2014. The role of cancer stem cells in glioblastoma. *Neurosurgical focus*, 37(6), p.E6.
- Tabassum, D.P. & Polyak, K., 2015. Tumorigenesis: it takes a village. *Nature reviews. Cancer*, 15(8), pp.473–83.
- Tso, C.-L. *et al.*, 2006. Primary glioblastomas express mesenchymal stem-like properties. *Molecular cancer research : MCR*, 4(9), pp.607–619.
- Ulrich, C.M., Bigler, J. & Potter, J.D., 2006. Non-steroidal anti-inflammatory drugs for cancer prevention: promise, perils and pharmacogenetics. *Nature reviews. Cancer*, 6(2), pp.130–140.
- Untergasser, A. *et al.*, 2012. Primer3-new capabilities and interfaces. *Nucleic Acids Research*, 40(15), pp.1–12.
- Valster, A. *et al.*, 2005. Cell migration and invasion assays. *Methods (San Diego, Calif.)*, 37(2), pp.208–15.
- Venere, M. *et al.*, 2011. Cancer stem cells in gliomas: identifying and understanding the apex cell in cancer's hierarchy. *Glia*, 59(8), pp.1148–54.
- Verhaak, R.G.W. *et al.*, 2010. Integrated genomic analysis identifies clinically relevant subtypes of glioblastoma characterized by abnormalities in PDGFRA, IDH1, EGFR, and NF1. *Cancer cell*, 17(1), pp.98–110.
- Vescovi, A.L., Galli, R. & Reynolds, B., 2006. Brain tumour stem cells. *Nature reviews. Cancer*, 6(6), pp.425–36.
- Villalva, C. *et al.*, 2011. STAT3 is essential for the maintenance of neurosphere-initiating tumor cells in patients with glioblastomas: a potential for targeted therapy? *International journal of cancer. Journal international du cancer*, 128(4), pp.826–38.
- Vinet, J. *et al.*, 2012. Neuroprotective function for ramified microglia in hippocampal excitotoxicity. *Journal of neuroinflammation*, 9(1), p.27.
- Vlashi, E. & Pajonk, F., 2014. Cancer stem cells, cancer cell plasticity and radiation therapy. *Seminars in cancer biology*, pp.1–8.

- Warner, T.D. *et al.*, 1999. Nonsteroid drug selectivities for cyclo-oxygenase-1 rather than cyclo-oxygenase-2 are associated with human gastrointestinal toxicity: a full in vitro analysis. *Proceedings of the National Academy of Sciences of the United States of America*, 96(13), pp.7563–7568.
- Wen, P.Y. & Kesari, S., 2008. Malignant gliomas in adults. *The New England journal of medicine*, 359(5), pp.492–507.
- Xia, P., Zhang, R. & Ge, G., 2015. C/EBP β Mediates TNF- α -Induced Cancer Cell Migration by Inducing MMP Expression Dependent on p38 MAPK. *Journal of cellular biochemistry*, (April), doi: 10.1002/jcb.25219.
- Xiong, A. *et al.*, 2014. Transcription Factor STAT3 as a Novel Molecular Target for Cancer Prevention. *Cancers*, 6(2), pp.926–57.
- Yokogami, K. *et al.*, 2000. Serine phosphorylation and maximal activation of STAT3 during CNTF signaling is mediated by the rapamycin target mTOR. *Current biology: CB*, 10(1), pp.47–50.
- Yu, H. *et al.*, 2014. Revisiting STAT3 signalling in cancer: new and unexpected biological functions. *Nature Reviews Cancer*, 14(11), pp.736–746.
- Yu, H., Kortylewski, M. & Pardoll, D., 2007. Crosstalk between cancer and immune cells: role of STAT3 in the tumour microenvironment. *Nature Reviews Immunology*, 7(1), pp.41–51.
- Yu, H., Pardoll, D. & Jove, R., 2009. STATs in cancer inflammation and immunity: a leading role for STAT3. *Nature reviews. Cancer*, 9(11), pp.798–809.
- Zarkoob, H. *et al.*, 2013. Investigating the link between molecular subtypes of glioblastoma, epithelial-mesenchymal transition, and CD133 cell surface protein. *PloS one*, 8(5), p.e64169.
- Zhao, H. *et al.*, 2015. TGF- β /Smad2/3 signal pathway involves in U251 cell proliferation and apoptosis. *Gene*, 562(1), pp.76–82.
- Zhong, Z., Wen, Z. & Darnell, J.E., 1994. Stat3: a STAT family member activated by tyrosine phosphorylation in response to epidermal growth factor and interleukin-6. *Science (New York, N.Y.)*, 264(5155), pp.95–98.
- Zohrabian, V.M. *et al.*, 2009. Rho/ROCK and MAPK signaling pathways are involved in glioblastoma cell migration and proliferation. *Anticancer research*, 29(1), pp.119–23.

9. Appendix

9.1. List of Abbreviations

~	Approximately
°C	Degree Celsius
2D	Two Dimensional
3D	Three Dimensional
5-ALA	5-Aminolevulinic Acid
α	Alpha
β	Beta
π	Pi
μg	Microgram
μm	Micrometre
μl	Microliter
AMPK	Adenosine Monophosphate-Activated Protein Kinase
ANOVA	Analysis of Variance
APS	Ammonium Persulfate
bp	Base Pair
BCPC	Brain Cancer Propagating Cell
BSA	Bovine Serum Albumin
Bsd	Blasticidin
BTIC	Brain Tumour Initiating Cell
BTSC	Brain Tumour Stem Cell
cm	Centimetre
c-myc	Cellular Homologue to Myelocytomatosis Viral Oncogene
cDNA	Complementary DNA
CA	<i>Cornu Ammonis</i>
CaCl_2	Calcium Chloride
CD	Cluster of Differentiation
C/EBP	CCAAT/Enhancer Binding Protein
CI	Confidence Interval
COX	Cyclooxygenase
Ctrl	Control
CSC	Cancer Stem Cell

ddH ₂ O	Double-Distilled Water
div	Days <i>in vitro</i>
DAPI	4',6-diamidino-2-phenylindole
DEG	Differentially Expressed Genes
DMEM	Dulbecco's Modified Eagle's Medium
DMSO	Dimethylsulfoxide
DNA	Deoxyribonucleic Acid
DTT	Dithiothreitol
e.g.	<i>exempli gratia</i>
<i>E. coli</i>	<i>Escherichia coli</i>
EC	Entorhinal Cortex
ECM	Extracellular Matrix
EDTA	Ethylenediaminetetraacetic Acid
EF1 α	Elongation Factor 1 α
EGF	Epidermal Growth Factor
EGFR	Epidermal Growth Factor Receptor
EMT	Epithelial to Mesenchymal Transition
ERK	Extracellular Signal-Regulated Protein Kinase
F-actin	Filamentous Actin
F12	Ham's Nutrient Mixture F12
FACS	Fluorescence-Activated Cell Sorting
FAK	Focal Adhesion Kinase
FBS	Fetal Bovine Serum
FCS	Fetal Calf Serum
FDA	Food and Drug Administration
FDR	False Discovery Rate
FGF	Fibroblast Growth Factor
g	Gram
G1	Gap Phase 1 (cell cycle)
G2/M	Gap Phase 2 / Mitosis (cell cycle)
G-CIMP	– Cytosine – phosphate – Guanine Island Methylator Phenotype
GAPDH	Glyceraldehyde 3-Phosphate Dehydrogenase
GBM	Glioblastoma
GFP	Green Fluorescent Protein
GTP	Guanosine Triphosphate

h	Hour
HCL	Hydrochloride
HE	Hematoxylin and Eosin Stain
HRP	Horseradish Peroxidase
I κ B	Inhibitor of NF- κ B
IC50	Half Maximal Inhibitory Concentration
IDH	Isocitrate Dehydrogenase
IL	Interleukin
ISMARA	Integrated System for Motif Activity Response Analysis
JAK	Janus Kinase
kDa	Kilo Dalton
L	Litre
LAP	Liver-enriched Activator Protein
LDH-A	Lactate Dehydrogenase A
LIP	Liver-enriched Inhibitory Protein
LV	Lateral Ventricle
M	Molar
mA	Milliampere
mg	Milligram
min	Minute(s)
mm	Millimetre
ml	Millilitre
mRNA	Messenger RNA
mTOR	Mammalian Target Of Rapamycin
MAPK	Mitogen-Activated Protein Kinase
MEK	Mitogen-Activated Protein Kinase Kinase
MET	Mesenchymal to Epithelial Transition
MgCl ₂	Magnesium Chloride
MMP	Matrix Metalloproteinase
ng	Nanogram
nm	Nanometre
non-leader	Follower and Stationary Cells
n.s.	Not Significant

NaCl	Sodium Chloride
NaOH	Sodium Hydroxide
NF- κ B	Nuclear Factor κ -light-chain-enhancer of Activated B Cells
NSAID	Non-Steroidal Anti-Inflammatory Drug
NSC	Neural Stem Cell
NPC	Neural Progenitor Cell
oligo	Oligonucleotide
oligo-dT	Short Single-stranded Sequence of Deoxythymine (dT)
OBSC	Organotypic Brain Slice Culture
OD	Optical density
p	Phosphorylated
poly-G tailing	Polyadenylation, Addition of poly-G tail to mRNA
PAGE	Polyacrylamide Gel Electrophoresis
PBS	Phosphate Buffered Saline
PDGF	Platelet-Derived Growth Factor
PI3K	Phosphatidylinositol-3-Kinase
PIAS	Protein Inhibitor of Activated STAT
PTEN	Phosphatase and Tensin Homolog
PVDF	Polyvinylidene Difluoride
qRT-PCR	Quantitative Real-Time PCR
RFP	Red Fluorescent Protein
RNA	Ribonucleic Acid
RPLPO	Ribosomal Subunit Protein
RT	Room Temperature
sec	Second(s)
shRNA	Small Hairpin RNA
siRNA	Small Interfering RNA
S	Serine
S phase	Synthesis phase (cell cycle)
SD	Standard Deviation
SDS	Sodium Dodecyl Sulphate
SEM	Standard Error of the Mean
SH	Src Homology Domain

SOCS	Suppressor of Cytokine Signalling
SOX	Sex Determining Region Y (SRY)–box
STAT	Signal Transducers and Activator of Transcription
STAT3C	Engineered mutant Constitutively active STAT3
Stattic	STAT3 Inhibitory Compound
SVZ	Subventricular Zone
TAZ	Transcriptional Co-activator with PDZ-binding Motif
TBS(-T)	Tris Buffered Saline (with Tween-20)
TC	Tumour Cell
TCGA	The Cancer Genome Atlas
TF	Transcription Factor
TGF	Transforming Growth Factor
TIC	Tumour Initiating Cell
TNF	Tumour Necrosis Factor
TP53	Tumour Protein p53
uPA	urokinase-type Plasminogen Activator
U	Unit
U87	U-87 MG
US	United States
V	Volt
VEGF	Vascular Endothelial Growth Factor
WHO	World Health Organisation
xg	Relative Centrifugal Force
Y	Tyrosine
ZEB	Zinc-finger Enhancer Binding

9.2. List of Figures

Introduction

3-1: Proposed genetic pathways operative in the evolution of primary and secondary GBM	9
3-2: Sequential genetic changes define the molecular landscape of GBM subtypes	11
3-3: Reconstruction of evolution of intratumoural heterogeneity in GBM	13
3-4: Hypothetical concepts of intrinsic GBM cellular heterogeneity	14
3-5: Clonal dynamic during tumour growth and clonal cooperation within heterogeneous tumours	15
3-6: Infiltration of the brain by malignant glioma cells	19
3-7: Possible origins of BTIC and their role in GBM formation	22
3-8: Two distinct forms of invasion	23
3-9: Simplified illustration of STAT3 signalling, adapted from Xiong <i>et al.</i> (2014)	27
3-10: Work packages of the present PhD project	32

Results

4-1: Implantation of U87-GFP cells on an organotypic brain slice	35
4-2: Periodic monitoring of U87-GFP invasiveness in OBSCs	36
4-3: Composite image of U87-GFP invasiveness after 3 weeks in OBSC	37
4-4: Evaluation of serial implantation of U87-GFP cells in OBSC	38
4-5: Periodic monitoring of mesenchymal BTICs RAV21, 26 and 27 in OBSCs	40
4-6: Invasion pattern of RAV21 in OBSCs after 3 weeks in culture	41
4-7: Area expansion and maximum distance covered by mesenchymal BTICs and TCs in OBSCs	41
4-8: Periodic monitoring of proneural BTICs RAV17, RAV19, and RAV57 in OBSCs	42
4-9: Area expansion and maximum distance covered by proneural BTICs and TCs in slice cultures	43

4-10: Average area expansion and maximum distance covered by proneural and mesenchymal glioma cells in slice cultures _____	44
4-11: Simultaneous implantation of proneural (RAV57) and mesenchymal (RAV26) in OBSC _____	46
4-12: Simultaneous implantation of proneural (RAV57) and mesenchymal (RAV27) in OBSC _____	47
4-13: Formation of distinct U87 cell populations in the OBSC model _____	49
4-14: Equipment setup of the micromanipulator with the newly developed adapter _____	50
4-15: Isolation of single cells from the OBSC model _____	51
4-16: Representative quality PCRs on cDNA libraries _____	51
4-17: Hierarchic cluster analysis of differentially expressed genes of leader versus non-leader U87 cells _____	53
4-18: Three pair wise comparison of differentially expressed genes of leader, follower, and stationary U87 cells _____	54
4-19: Heat-map of leader, follower and stationary subpopulation clustering after <i>k-means</i> clustering _____	55
4-20: Schematic view of transcription factor identification based on DEGs _____	56
4-21: Exemplary ISMARA transcription factor binding motifs _____	57
4-22: Representative Western blots depicting basal expression levels of transcription factors in BTIC and GBM cell lines _____	59
4-23: Basal protein expression of (p)STAT3, C/EBP β , and c-myc in proneural, mesenchymal BTIC, and GBM lines _____	61
4-24: Basal protein expression of (p)STAT3, C/EBP β , and c-myc in single BTIC and GBM lines _____	62
4-25: Basal protein expression of (p)mTOR, (p)AMPK, (p)SMAD, and (p)p42/44 MAPK in proneural, mesenchymal BTIC and GBM lines _____	64
4-26: Basal protein expression of (p)mTOR, (p)AMPK, (p)SMAD, and (p)p42/44 MAPK in single BTIC and GBM lines _____	65
4-27: Basic proliferation rates for GBM cell lines A172, HTZ349, and U87 _____	68

4-28: Basic proliferation rates of BTICs compared to their differentiated pair of TCs _____	69
4-29: Basic proliferation rates of proneural compared to mesenchymal lines _____	70
4-30: Basic migration rates for GBM cell lines A172, HTZ349, and U87 _____	73
4-31: Basic migration capacities of BTICs compared to respective TCs _____	74
4-32: Basic migration capacities of proneural compared to mesenchymal lines _____	75
4-33: Representative BTICs compared to their differentiated TCs _____	78
4-34: Scatter plots comparing proliferation and migration of BTICs, TCs, and GBM cell lines _____	80
4-35: GBM cell line proliferation after diclofenac or ibuprofen treatment _____	83
4-36: GBM cell line migration after diclofenac or ibuprofen treatment _____	85
4-37: Protein expression in GBM cell lines after diclofenac or ibuprofen treatment _____	87
4-38: Exemplary Western blots of protein expression in GBM lines after Stattic treatment _	88
4-39: Quantitative real-time PCR of GBM cell lines after Stattic treatment _____	89
4-40: Proliferation of GBM cell lines after Stattic treatment _____	91
4-41: Proliferation of proneural BTICs and corresponding TCs after Stattic treatment ____	92
4-42: Proliferation of mesenchymal BTICs and corresponding TCs after Stattic treatment _	94
4-43: Spheroid assay with Stattic treatment of GBM lines A172, HTZ349, and U87 _____	96
4-44: Migration of GBM cell lines after Stattic treatment _____	97
4-45: Migration of proneural BTICs and corresponding TCs after Stattic treatment _____	98
4-46: Migration of mesenchymal BTICs and corresponding TCs after Stattic treatment __	100
4-47: Decreased OBSC infiltration by U87 glioma cells with Stattic treatment _____	103
4-48: Decreased OBSC infiltration by proneural BTIC and TC lines with Stattic treatment	104
4-49: Decreased OBSC infiltration by mesenchymal BTIC and TC lines with Stattic treatment _____	107

Discussion

5-1: GBM formation and diffuse infiltration driven by BTICs _____	116
5-2: Go or growth response of GBM cells implanted on OBSCs _____	123

5-3: Expanded model of GBM formation, infiltration, and recurrence driven by BTICs	126
5-4: Schematic illustration of glioma formation and postulated role of BTICs	132
5-5: Characterisation of an initial in vitro glioma cell population by correlation of proliferation and migration rates	141
5-6: Influence of diclofenac or ibuprofen on GBM cells	144

Concluding and future perspectives

6-1: Possible work-flow to enable drug screening for leader cell inhibition	154
---	-----

Materials and Methods

7-1: Static treatment assay layout	179
7-2: Measurement of spheroid area	183
7-3: Organotypic brain slice	185
7-4: OBSC preparation for single cell isolation	187

Appendix

9-1: Stacked basal expression levels of (p)STAT3, C/EBP β , (p)mTOR and (p)AMPK	227
9-2: Stacked basal expression levels of (p)SMAD and (p)p42/44 MAPK	227
9-3: Western blot quantification corresponding to Figure 4-37	229
9-4: Western blot quantification corresponding to Figure 4-38	230
9-5: Wound healing assay of GBM lines A172 and HTZ349 with Static treatment	231

9.3. List of Tables

Results

4-1: Overview of average invasion day-1 of U87, primary BTICs, and TCs in the OBSC model _____	45
4-2: Overview of growth constant, doubling time, and proliferation day-1 for GBM and primary cell lines _____	72
4-3: Overview of average migration day-1 of GBM and primary cell lines _____	77
4-4: Summarised characteristics of GBM cell lines _____	79
4-5: Summarised characteristics of BTIC lines _____	81
4-6: Summary of doubling times and migration rates of GBM cell lines after NSAID treatment _____	86
4-7: Proliferation and migration inhibitory effects of Stattic on BTIC and TC _____	102
4-8: Percentage spatial expansion of glioma cells on OBSCs was decreased by 15 μ M Stattic _____	110
4-9: Maximum distance covered by glioma cells on OBSCs was decreased upon 15 μ M of Stattic treatment _____	111

Discussion

5-1: Proliferation and migration inhibitory effect of Stattic, diclofenac, and ibuprofen on GBM lines _____	145
---	-----

Appendix

9-1: Detailed proliferation rates of GBM cells after NSAID treatment, see Figure 4-35 and Table 4-6 _____	228
9-2: Detailed migration rates of GBM cells after NSAID treatment, see Figure 4-36 and Table 4-6 _____	228
9-3: Average proliferation rate per day after Stattic treatment _____	232
9-4: Average migration rates of BTIC, TC and GBM cell lines after Stattic treatment _____	233
9-5: Spatial cell expansion on OBSCs after Stattic treatment _____	234

9-6: Average invasion per day on OBSCs after Stattic treatment	235
--	-----

9.4. Supporting Material

9.4.1. Detailed and Further Diagrams

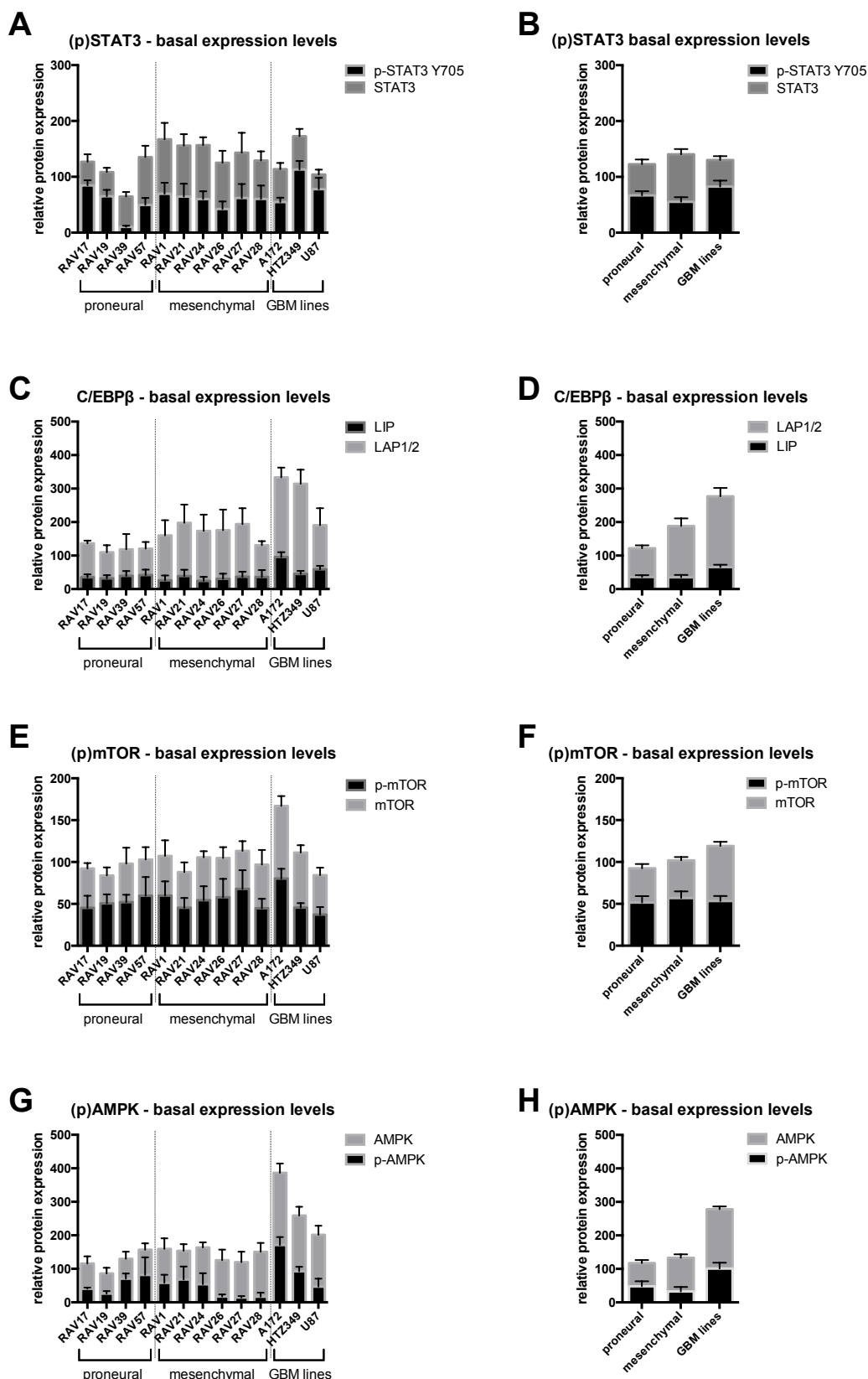
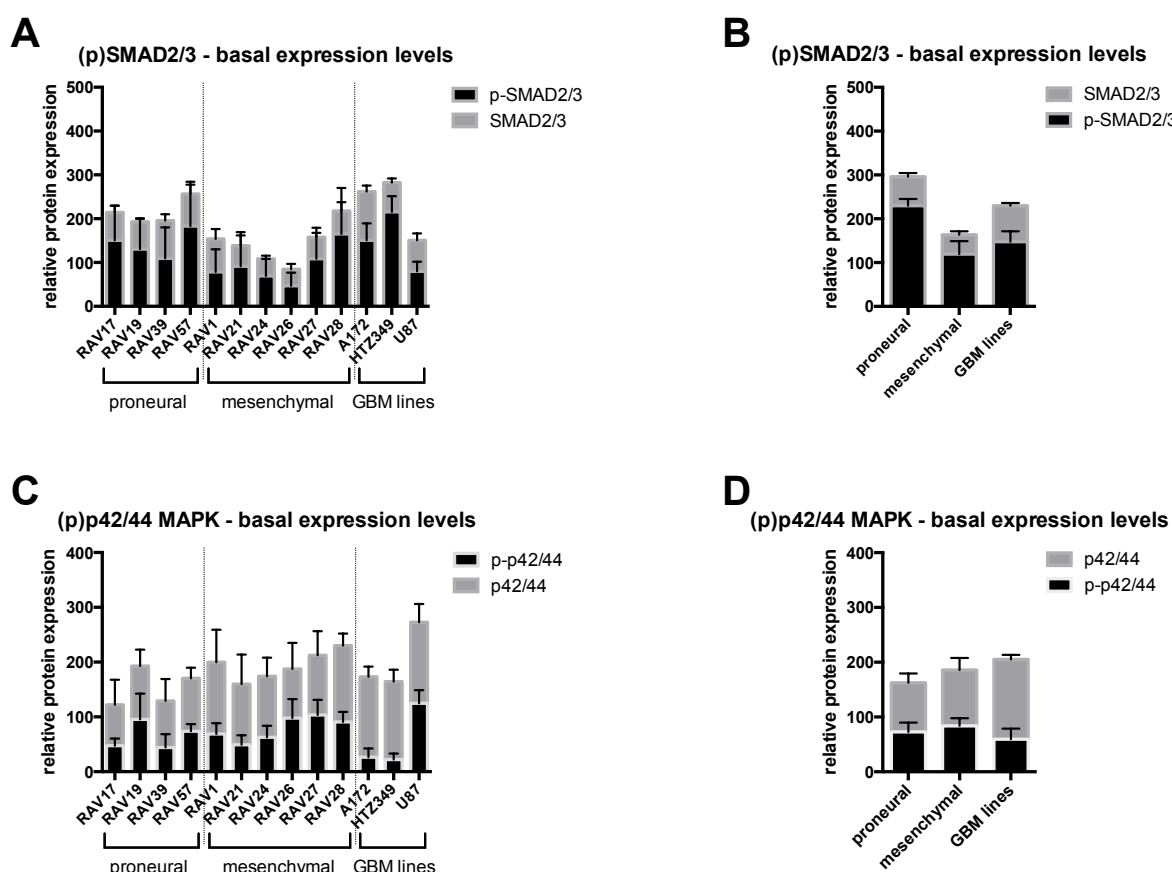


Figure 9-1: Stacked basal expression levels of (p)STAT3, C/EBP β , (p)mTOR and (p)AMPK

Supplement to Figure 4-23 to Figure 4-26. (A) Combined expression levels of pSTAT3 Y705 and STAT3 showed lower overall expression in proneural than mesenchymal BTICs. RAV39 displayed the lowest expression, whereas in RAV57 overall STAT3 expression appears similar to mesenchymal BTICs. STAT3 expression in GBM lines resembled the expression titre in mesenchymal BTIC. (B) Overall STAT3 expression was observed to be similar in proneural and mesenchymal BTICs, whereas GBM lines showed a slightly increased expression. (C) Overall C/EBP β expression increased from proneural to mesenchymal BTICs (up to ~2-fold increase) and was highest in GBM lines (~3.3-fold from RAV19 to A172). RAV28 resembled C/EBP β expression levels as observed in proneural BTICs. (D) Grouped data confirmed the previous findings. (E) Overall mTOR expression varied in between the cell lines, remarkably higher expression was observed in A172, ~1.7-fold compared to RAV26. (F) mTOR expression was increased in GBM lines compared to proneural and mesenchymal BTICs. (G) RAV19 showed less overall AMPK expression, only ~0.5-fold compared to RAV57. GBM lines, especially A172 revealed higher AMPK expression (up to ~4-fold) than BTICs. (H) Added together, both BTIC groups exhibited equal AMPK expression levels that were higher (~2.3-fold) than in GBM lines. Experiments were performed in triplicates, each group (proneural, mesenchymal, GBM lines) consisted of three representative cell lines (n = 9); values represent mean \pm SEM.

**Figure 9-2: Stacked basal expression levels of (p)SMAD and (p)p42/44 MAPK**

Supplement to Figure 4-25 and Figure 4-26. (A) Proneural BTICs displayed increased SMAD expression titres than mesenchymal BTICs. RAV57 exhibited the highest (~2.8-fold) and RAV26 the lowest (~0.9-fold) SMAD expression levels. GBM lines A172 and HTZ349 displayed high total SMAD expression, and U87 exhibited only half as much. (B) Added together, proneural BTICs displayed the highest SMAD expression levels, while mesenchymal BTICs exhibited approximately half the expression. SMAD titre of GBM cell line was located in between expression levels of proneural and mesenchymal BTICs. (C) p42/44 MAPK expression varied in between all lines. (D) Added together, a small increase of p42/44 MAPK expression was revealed in proneural compared to mesenchymal (1.12-fold) BTICs. Expression was observed to be further increased in GBM lines (1.18-fold). Experiments were performed in triplicates, each group (proneural, mesenchymal, GBM lines) consisted of three representative cell lines (n = 9); values represent mean \pm SEM.

Category	λ	t(d)	ρ	λ	t(d)	ρ	λ	t(d)	ρ	λ	t(d)	ρ
Diclofenac in mM	none			0.05			0.1			0.2		
A172	0.595	27.958	81.306	0.527	31.580	69.347	0.432	38.468	54.103	0.204	81.611	24.595
HTZ349	0.552	30.161	73.595	0.519	32.040	68.071	0.374	44.501	45.328	0.093	178.310	0.389
U87	0.588	28.304	79.993	0.505	32.957	65.659	0.395	42.117	48.436	0.141	117.863	15.159
average GBM lines	0.578	28.808	78.298	0.517	32.192	67.692	0.400	41.695	49.289	0.146	125.928	13.381
Ibuprofen in mM	none			0.5			1.0			2.0		
A172	0.595	27.958	81.306	0.500	33.284	64.841	0.405	41.061	49.951	0.092	180.269	9.667
HTZ349	0.552	30.161	73.595	0.499	33.353	64.671	0.398	41.776	48.915	-	-	-
U87	0.588	28.304	79.993	0.505	32.957	65.659	0.395	42.117	48.436	-	-	-
average GBM lines	0.578	28.808	78.298	0.501	33.198	65.057	0.399	41.651	49.101	0.031	60.090	3.222

Table 9-1: Detailed proliferation rates of GBM cells after NSAID treatment, see Figure 4-35 and Table 4-6

Treatment of GBM cell lines with either diclofenac or ibuprofen caused a concentration-dependent decrease of the growth invariants (λ), resulting in increased doubling times (t(d)) and slower percentage growth (ρ).

Category	$\mu\text{m day}^{-1}$	Range (\pm SD)	$\mu\text{m day}^{-1}$	Range (\pm SD)	$\mu\text{m day}^{-1}$	Range (\pm SD)	$\mu\text{m day}^{-1}$	Range (\pm SD)
Diclofenac in mM	none		0.05		0.1		0.2	
A172	527.938	407.946 – 647.930	431.438	335.706 – 527.169	456.688	340.609 – 572.766	368.250	267.695 – 468.805
HTZ349	785.375	719.341 – 851.409	687.438	618.336 – 756.539	645.750	578.020 – 713.480	477.375	434.402 – 520.348
U87	152.688	66.503 – 238.872	118.063	2.918 – 233.207	74.687	-18.764 – 168.139	94.063	14.255 – 173.870
average GBM lines	488.667	210.674 – 766.659	412.313	159.236 – 665.389	392.375	135.136 – 649.614	313.229	133.218 – 493.241
Ibuprofen in mM	none		0.5		1.0		2.0	
A172	613.547	441.927 – 785.166	605.757	444.317 – 767.197	619.485	447.298 – 791.671	439.382	186.183 – 625.565
HTZ349	1003.462	773.515 – 1233.409	721.900	569.716 – 874.085	555.918	452.519 – 659.317	309.984	241.641 – 378.327
U87	1591.345	1506.178 – 1676.512	1238.461	1071.724 – 1405.198	1162.158	1022.105 – 1302.211	739.453	597.614 – 881.291
average GBM lines	1069.451	907.207 – 1231.696	855.373	695.252 – 1015.493	779.187	640.641 – 917.733	496.273	364.151 – 628.394

Table 9-2: Detailed migration rates of GBM cells after NSAID treatment, see Figure 4-36 and Table 4-6

Migration rates of GBM cell lines were decreased concentration-dependent, after treatment with either diclofenac or ibuprofen.

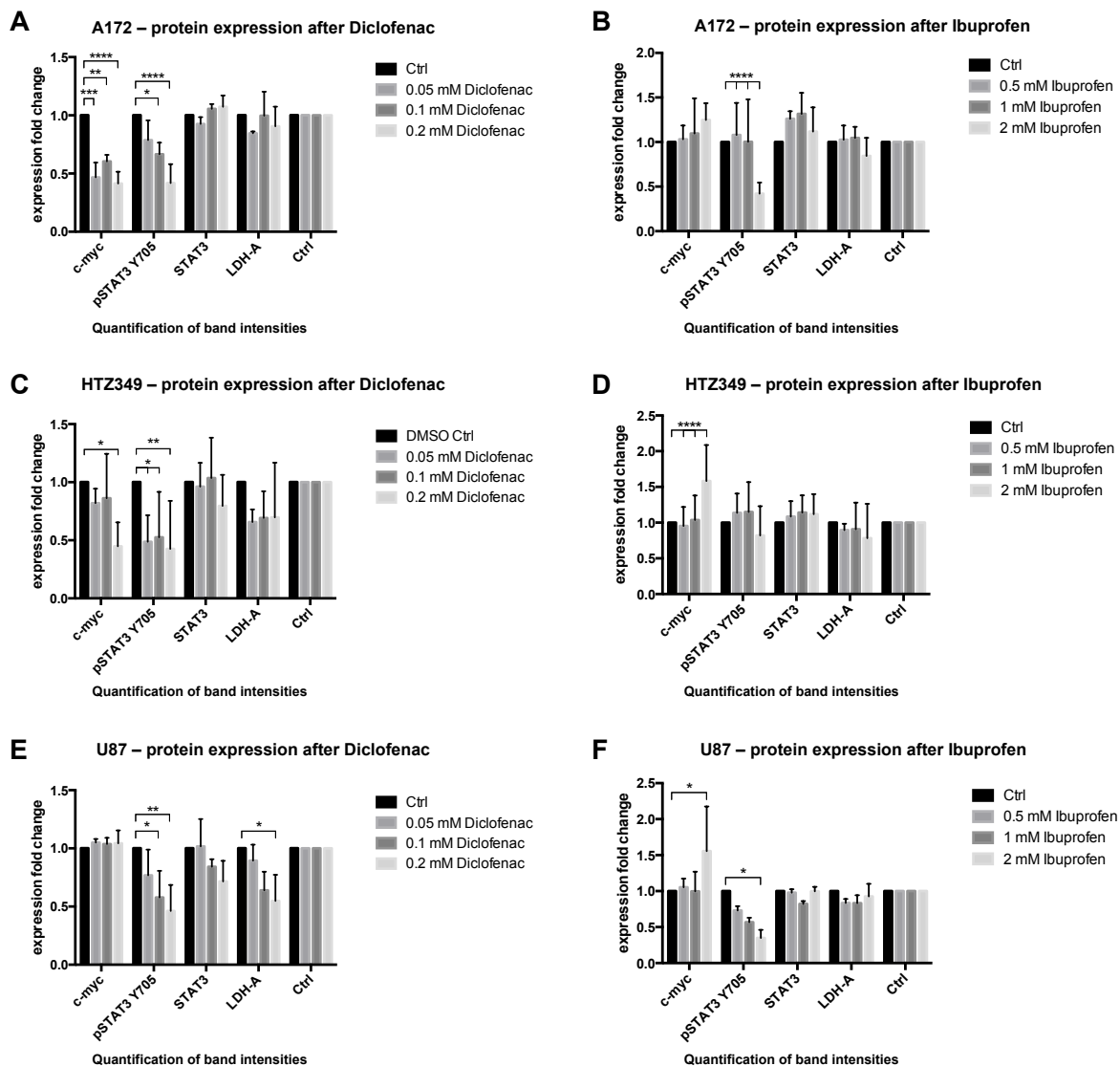


Figure 9-3: Western blot quantification corresponding to Figure 4-37

Protein expression quantification in GBM cell lines after diclofenac or ibuprofen treatment (A, B) Concentration depend, diclofenac or ibuprofen reduced STAT3 phosphorylation significantly without affecting total STAT3 levels in A172. c-myc expression was significantly down regulated by diclofenac, whereas ibuprofen increased c-myc expression. LDH-A titres were reduced upon diclofenac or ibuprofen treatment, but not to significant extent. (C) In HTZ349, diclofenac reduced pSTAT3 and c-myc concentration dependently. LDH-A titres were reduced, but not to significant extent. (D) Expression of c-myc was significantly increased in a concentration-dependent manner after ibuprofen treatment. pSTAT3 levels were reduced, but not to significant extent. (E, F) In U87, diclofenac or ibuprofen reduced STAT3 phosphorylation significantly in a concentration depend way, without affecting total STAT3 levels. Expression of c-myc was not altered by diclofenac, whereas ibuprofen led to a significant increase of c-myc expression. Upon diclofenac treatment, a significant decrease in LDH-A expression was observed, in a concentration-dependent manner. Ibuprofen exhibited no effect on LDH-A expression titres. All Western blots were performed in triplicates; values represent mean \pm SD; Statistics: 95% CI (A172, U87) or 90% CI (HTZ349), ns: $p > 0.05$, *: $p \leq 0.05$, **: $p \leq 0.01$, ***: $p \leq 0.001$, ****: $p \leq 0.0001$.

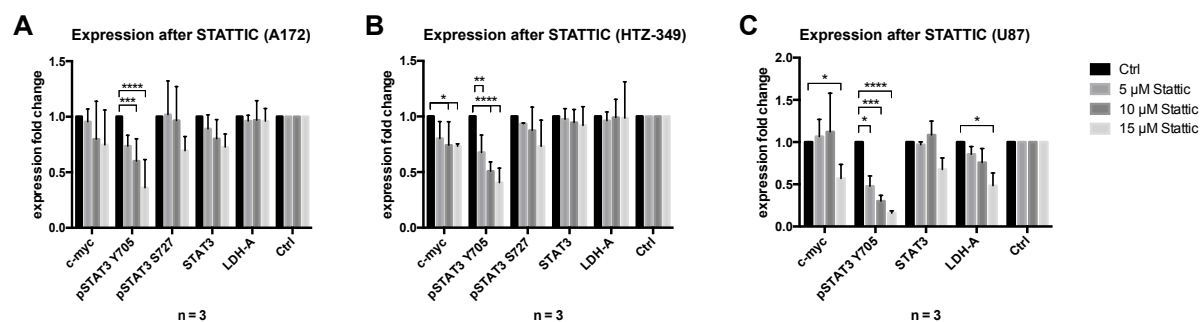


Figure 9-4: Western blot quantification corresponding to Figure 4-38

(A) Phosphorylated STAT3 Y705 levels were decreased in a concentration-dependent way in A172 upon Stattic treatment, compared to DMSO control. In a similar way c-myc expression was decreased. pSTAT3 S727 and STAT3 expression were decreased upon treatment with 15 μM Stattic, but not significantly. LDH-A titre was not altered by Stattic treatment. (B) In HTZ349, pSTAT3 Y705 and c-myc expression levels were significantly decreased in concentration dependent manner after Stattic treatment. pSTAT3 S727, STAT3, and LDH-A expression were not altered by Stattic. (C) In U87 exposed to Stattic, pSTAT3 Y705 and LDH-A were decreased significantly in a concentration-dependent manner. STAT3 was decreased upon treatment with 15 μM Stattic, but not statistically significant. Expression of c-myc was decreased with 15 μM Stattic significantly, despite an initial increase. All experiments were performed in triplicates; values represent mean \pm SD; expression was normalised to GAPDH control; 2way ANOVA analysis with Tukey's multiple comparisons test, 95% CI, ns: $p > 0.05$, *: $p \leq 0.05$, **: $p \leq 0.01$, ***: $p \leq 0.001$, ****: $p \leq 0.0001$.

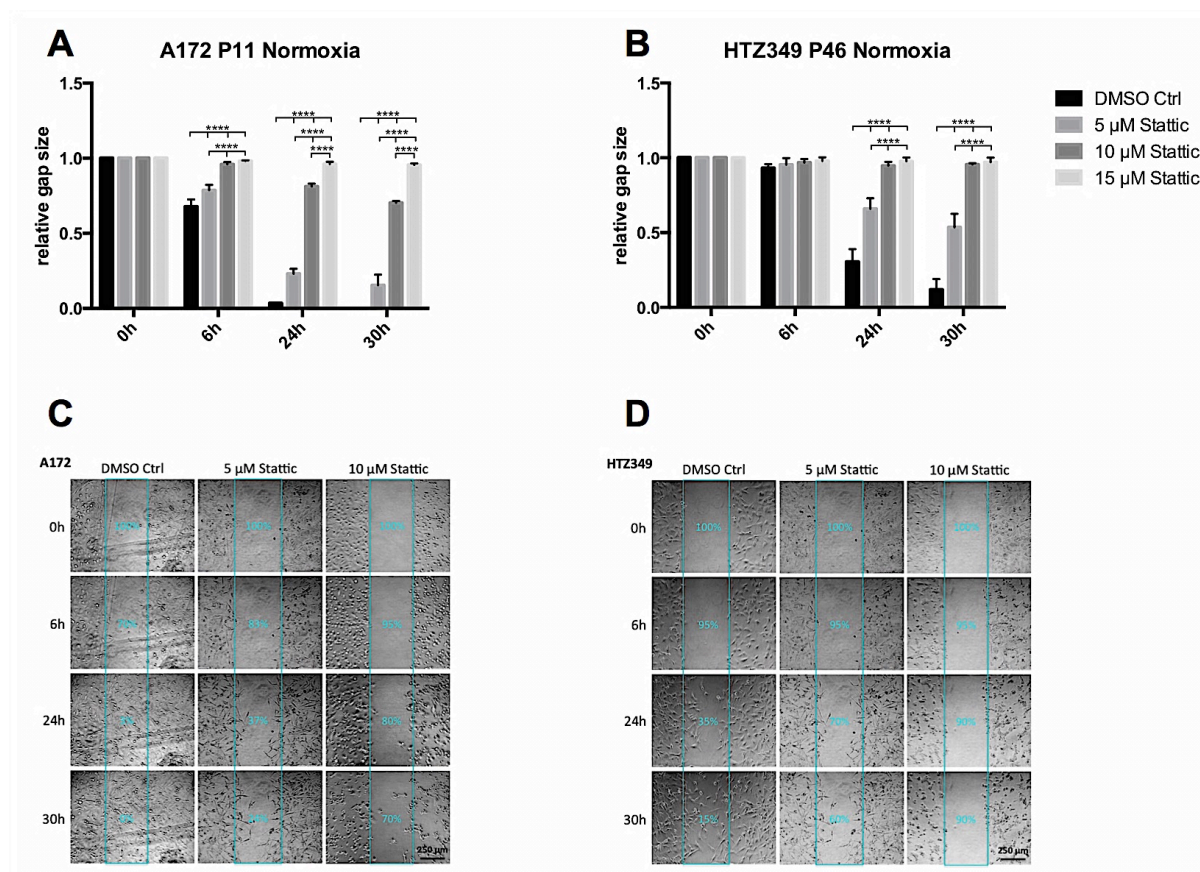


Figure 9-5: Wound healing assay of GBM lines A172 and HTZ349 with Stattic treatment

(A) A172 cells showed reduced migration, resulting in delayed gap closing, when treated with Stattic. The gap closure delay was concentration-dependent. Upon 15 μ M of Stattic treatment, the gap size remained similar to the initial gap size. With all concentrations migration of A172 cells was significantly decreased. (B) HTZ349 cells displayed reduced migration upon Stattic treatment. Migration was significantly reduced from 24 h on with all Stattic concentrations used. (C) Representative phase contrast pictures (taken at the same position at each time point) of A172 cells treated with control (DMSO) or 5, 10 μ M Stattic taken at 0, 6, 24 and 30 h. The turquoise rectangles mark the initial gap size that was measured for evaluation. Within the rectangles the percentage of cell free space is depicted. (D) Representative phase contrast pictures of HTZ349 cells. All experiments were performed in triplicates; values represent mean \pm SD; relative area expression was normalised to spheroid size at 0 h; 2way ANOVA analysis with Tukey's multiple comparisons test, ns: $p > 0.05$, *: $p \leq 0.05$, **: $p \leq 0.01$, ***: $p \leq 0.001$, ****: $p \leq 0.0001$.

Category	Mean of Proliferation day ⁻¹ (%)								
GBM lines	DMSO	0.625 μ M Stattic	1.25 μ M Stattic	2.5 μ M Stattic	5 μ M Stattic	10 μ M Stattic	15 μ M Stattic	20 μ M Stattic	
A172	54.606	57.755	54.903	67.281	52.980	42.637	34.360	10.530	
HTZ349	45.335	46.630	45.737	48.047	46.677	36.957	36.630	25.433	
U87	80.260	92.325	97.036	84.754	77.681	39.734	33.338	11.428	
GBM lines	65.654	65.679	62.937	63.173	56.179	49.562	39.802	14.128	
BTIC									
RAV17	36.526	41.184	26.257	21.643	17.677	-	-	-	
RAV19	22.132	19.541	6.653	-	-	-	-	-	
RAV57	35.117	31.664	25.270	23.579	-	-	-	-	
proneural BTIC	35.280	21.347	19.627	11.071	-	-	-	-	
RAV21	70.543	74.643	75.759	33.204	8.452	-	-	-	
RAV26	43.660	43.234	35.984	-	-	-	-	-	
RAV27	90.295	89.411	80.845	50.778	-	-	-	-	
mesenchymal BTIC	66.472	69.499	68.756	33.118	-	-	-	-	
TC	DMSO	0.625 μ M Stattic	1.25 μ M Stattic	2.5 μ M Stattic	5 μ M Stattic	10 μ M Stattic	15 μ M Stattic	20 μ M Stattic	
RAV17	24.893	17.756	17.047	19.519	1.475	-	-	-	
RAV19	30.750	26.646	22.746	18.331	17.983	8.680	-	-	
RAV57	41.203	31.208	40.152	37.193	33.480	29.073	0.685	-	
proneural TC	29.088	16.800	20.430	24.651	17.009	10.543	-	-	
RAV21	73.330	30.635	54.880	65.119	57.927	36.112	-	-	
RAV26	78.886	80.336	70.923	66.613	60.972	45.545	-	-	
RAV27	50.992	39.498	59.671	52.773	51.347	30.763	4.492	-	
mesenchymal TC	66.746	49.325	57.200	51.255	48.486	36.354	5.184	-	

Table 9-3: Average proliferation rate per day after Stattic treatment

Mean proliferation (percentage growth) within one day was estimated on basis of the fluorescence increase as measured in CyQUANT assays. In each case Stattic reduced the proliferation ability with increasing concentrations. In general BTICs displayed more rapidly response than TCs, and TCs at lower dosages than GBM cell lines. In case of proliferation rates fell below initial values, those were marked by –.

Category	Mean of migration/day; in μm									
	DMSO Ctrl	0.625 μM Stattic	1.25 μM Stattic	2.5 μM Stattic	5 μM Stattic	10 μM Stattic	15 μM Stattic	20 μM Stattic		
GBM lines										
A172	557.18 (\pm 79.93)	499.01 (\pm 50.88)	503.39 (\pm 47.3)	468.36 (\pm 43.34)	426.98 (\pm 49.32)	332.01 (\pm 44.76)	257.39 (\pm 91.12)	132.97 (\pm 32.03)		
HTZ349	519.18 (\pm 56.12)	484.87 (\pm 75.78)	484.11 (\pm 73.3)	455.96 (\pm 92.05)	423.84 (\pm 97.42)	306.17 (\pm 93.55)	224.39 (\pm 119.20)	95.95 (\pm 20.01)		
U87	626.93 (\pm 31.44)	573.75 (\pm 48.52)	545.38 (\pm 63.08)	521.67 (\pm 95.51)	440.5 (\pm 125.78)	352.9 (\pm 83.94)	255.32 (\pm 74.8)	263.84 (\pm 98.81)		
GBM lines	567.89 (\pm 72.76)	519.21 (\pm 69.76)	510.96 (\pm 65.16)	482.0 (\pm 82.68)	430.44 (\pm 92.69)	330.36 (\pm 76.53)	245.7 (\pm 94.26)	164.25 (\pm 93.97)		
BTIC										
RAV17	558.37 (\pm 58.22)	520.4 (\pm 25.56)	499.37 (\pm 33.68)	496.56 (\pm 30.35)	429.67 (\pm 27.88)	318.58 (\pm 39.14)	118.36 (\pm 77.65)	85.29 (\pm 5.52)		
RAV19	697.04 (\pm 28.86)	672.58 (\pm 34.95)	671.61 (\pm 20.31)	618.69 (\pm 15.2)	577.48 (\pm 50.91)	403.74 (\pm 138.48)	125.5 (\pm 60.43)	134.15 (\pm 62.34)		
RAV57	590.42 (\pm 26.05)	516.62 (\pm 59.27)	478.88 (\pm 43.53)	450.4 (\pm 44.16)	348.49 (\pm 103.33)	203.99 (\pm 90.76)	110.53 (\pm 27.02)	100.28 (\pm 11.95)		
proneural BTIC	615.28 (\pm 71.81)	569.87 (\pm 84.49)	549.95 (\pm 93.9)	521.88 (\pm 78.67)	451.88 (\pm 116.85)	308.77 (\pm 125.95)	118.02 (\pm 56.94)	106.57 (\pm 41.02)		
RAV21	539.64 (\pm 19.46)	509.12 (\pm 14.25)	505.84 (\pm 9.13)	501.54 (\pm 15.76)	478.29 (\pm 17.24)	218.88 (\pm 131.14)	178.27 (\pm 80.53)	114.73 (\pm 10.86)		
RAV26	654.55 (\pm 32.84)	555.75 (\pm 17.51)	512.97 (\pm 31.25)	440.84 (\pm 38.31)	343.22 (\pm 31.43)	260.5 (\pm 23.96)	180.22 (\pm 68.36)	131.86 (\pm 31.85)		
RAV27	732.97 (\pm 105.53)	691.82 (\pm 107.51)	679.23 (\pm 95.47)	648.54 (\pm 125.33)	596.76 (\pm 138.34)	411.41 (\pm 123.43)	154.35 (\pm 61.7)	103.97 (\pm 21.23)		
mesenchymal BTIC	585.57 (\pm 99.76)	566.01 (\pm 98.97)	530.31 (\pm 115.14)	472.76 (\pm 132.01)	296.93 (\pm 131.38)	170.95 (\pm 68.91)	116.85 (\pm 24.98)	103.97 (\pm 21.23)		
TC										
RAV17	276.82 (\pm 16.03)	261.96 (\pm 13.2)	240.90 (\pm 43.42)	248.52 (\pm 20.39)	207.0 (\pm 13.1)	114.59 (\pm 38.12)	58.78 (\pm 19.85)	48.54 (\pm 10.97)		
RAV19	343.06 (\pm 36.47)	312.67 (\pm 25.97)	290.95 (\pm 10.82)	279.78 (\pm 19.83)	274.96 (\pm 28.82)	187.08 (\pm 42.99)	136.99 (\pm 75.27)	110.84 (\pm 45.28)		
RAV57	852.76 (\pm 72.04)	816.86 (\pm 68.28)	801.63 (\pm 47.63)	788.3 (\pm 71.68)	694.04 (\pm 125.05)	348.86 (\pm 123.07)	104.94 (\pm 59.99)	66.42 (\pm 4.558)		
proneural TC	490.88 (\pm 266.16)	463.83 (\pm 258.56)	444.49 (\pm 260.72)	438.87 (\pm 255.73)	392.0 (\pm 230.84)	216.85 (\pm 125.04)	100.23 (\pm 63.58)	77.41 (\pm 37.79)		
RAV21	826.11 (\pm 32.0)	793.39 (\pm 21.37)	781.39 (\pm 18.7)	751.17 (\pm 35.32)	704.96 (\pm 116.85)	539.87 (\pm 137.01)	363.09 (\pm 233.54)	267.82 (\pm 175.23)		
RAV26	1047.26 (\pm 42.0)	1014.16 (\pm 29.95)	949.62 (\pm 35.95)	945.77 (\pm 31.92)	801.7 (\pm 112.96)	377.31 (\pm 197.1)	251.95 (\pm 144.31)	169.14 (\pm 70.24)		
RAV27	1017.7 (\pm 77.0)	984.64 (\pm 31.12)	975.57 (\pm 66.47)	936.58 (\pm 65.44)	823.13 (\pm 111.89)	555.86 (\pm 207.05)	269.17 (\pm 93.13)	179.83 (\pm 42.58)		
mesenchymal TC	963.69 (\pm 112.53)	930.73 (\pm 103.24)	902.19 (\pm 97.77)	877.84 (\pm 101.79)	776.6 (\pm 109.16)	491.01 (\pm 194.12)	294.74 (\pm 168.33)	205.59 (\pm 116.42)		

Table 9-4: Average migration rates of BTIC, TC and GBM cell lines after Stattic treatment

Mean migration velocities within one day were estimated on basis of the area covered by cells as measured for the evaluation of the spheroid assays. Since radial and non-directed migration was presumed, the covered area after 24 h was assumed as an ideal circle surface area, and its radius calculated. In each case Stattic reduced the migration rate with increasing concentrations. In general, BTICs responded to lower dosages than TCs, than GBM cell lines.

Category	Area normalized to initial size (μm^2) – Ctrl		Area normalized to initial size (μm^2) – 15 μM Stattic	
	Area (\pm SEM)	Percentage increase (%)	Area (\pm SEM)	Percentage increase (%)
GBM lines				
U87	6711977.00 (\pm 419894.10)	1807.371	1387484.00 (\pm 606720.40)	646.354
BTIC				
RAV17	102522.50 (\pm 21230.77)	122.677	256077.20 (\pm 18654.45)	150.969
RAV19	143848.30 (\pm 44784.91)	136.349	–	0.000
RAV57	303277.70 (\pm 12046.75)	143.577	–	80.151
average proneural BTIC	183216.10 (\pm 33960.27)	135.604	0.00	95.020
RAV21	4054593.00 (\pm 664703.80)	2286.962	118619.80 (\pm 24174.92)	149.327
RAV26	10473650.00 (\pm 4235590.00)	6477.487	28805.27 (\pm 186868.10)	112.404
RAV27	16328060.00 (\pm 2911078.00)	8842.317	132718.40 (\pm 25175.78)	183.365
average mesenchymal BTIC	10285430.00 (\pm 2319168.00)	5852.507	93381.15 (\pm 57238.64)	144.333
TC				
RAV17	48528.07 (\pm 36545.76)	111.717	–	81.156
RAV19	46939.59 (\pm 13790.98)	115.373	–	0.000
RAV57	55983.64 (\pm 21724.59)	109.824	–	84.725
average proneural TC	50483.77 (\pm 12977.73)	111.746	–	55.284
RAV21	2371200.00 (\pm 742511.10)	1592.585	–	50.057
RAV26	5471551.00 (\pm 2190640.00)	2171.891	41917.63 (\pm 15125.73)	118.646
RAV27	4793739.00 (\pm 710859.10)	3558.679	67089.87 (\pm 13000.77)	149.847
average mesenchymal TC	4054740.00 (\pm 733066.60)	2383.450	33336.63 (\pm 18910.89)	89.393

Table 9-5: Spatial cell expansion on OBSCs after Stattic treatment

Area expansion on OBSCs of proneural, mesenchymal BTICs, and glioma cell line U87 in μm^2 , normalised to initial spheroid size. Rates of control and after Stattic treatment (15 μM) were calculated (for each line: n = 6; for aggregated data: n = 18).

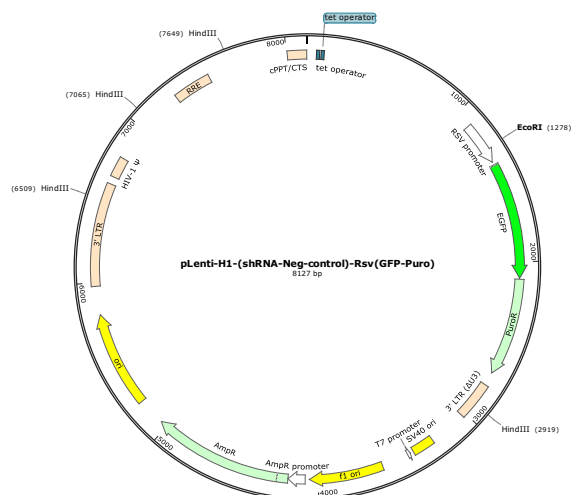
Category	Ctrl		15 μ M Static	
GBM lines	Invasion day ⁻¹ (μ m)	Range (Standard deviation)	Invasion day ⁻¹ (μ m)	Range (Standard deviation)
U87	147.99	117.21 – 178.77	47.858	26.53 – 69.19
BTIC				
RAV17	14.95	3.92 – 25.98	6.454	2.36 – 10.55
RAV19	2.47	1.00 – 3.93	3.815	0.00 – 10.30
RAV57	12.45	8.16 – 16.74	4.746	0.00 – 10.89
average proneural BTIC	9.96	1.43 – 18.48	5.075	0.00 – 10.44
RAV21	125.56	100.76 – 150.37	19.464	2.60 – 36.33
RAV26	179.0	149.57 – 208.42	11.610	0.00 – 27.19
RAV27	220.30	153.27 – 287.32	15.612	6.55 – 24.68
average mesenchymal BTIC	174.95	117.08 – 232.82	15.562	1.78 – 29.35
TC				
RAV17	4.34	2.09 – 6.60	4.124	0.00 – 8.45
RAV19	2.61	1.60 – 3.62	6.011	0.00 – 14.36
RAV57	12.51	0.0 – 28.75	0.904	0.00 – 2.41
average proneural TC	6.49	0.0 – 16.44	3.686	0.00 – 9.29
RAV21	53.16	30.58 – 75.74	0.553	0.00 – 1.91
RAV26	213.75	151.78 – 276.32	2.876	0.00 – 7.04
RAV27	149.48	120.60 – 178.35	3.575	1.79 – 5.36
average mesenchymal TC	121.82	42.76 – 200.87	2.335	0.00 – 5.22

Table 9-6: Average invasion per day on OBSCs after Static treatment

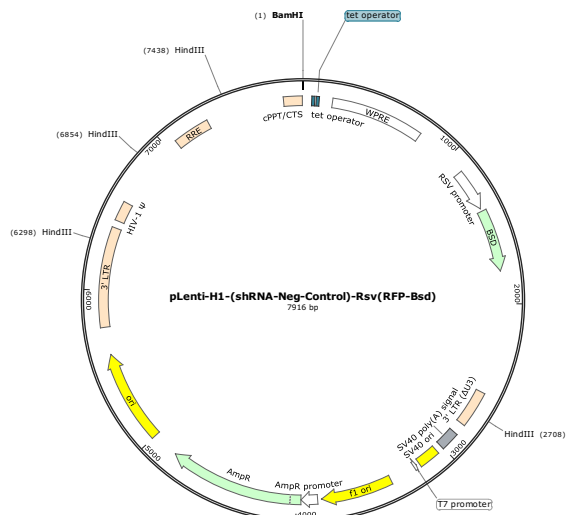
Average OBSCs invasion by proneural, mesenchymal BTICs and glioma cell line U87 in μ m day⁻¹. Rates of control and after Static treatment (15 μ M) were calculated (for each line: n = 6; for aggregated data: n = 18).

9.4.2. Vector Charts

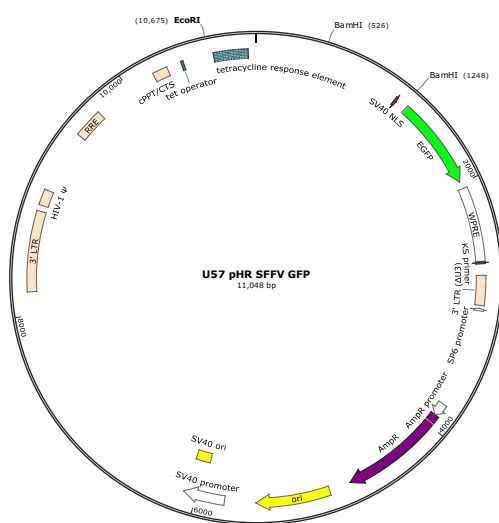
pLenti-H1-(shRNA-Neg-control)-
Rsv(GFP-Bsd):



pLenti-H1-(shRNA-Neg-control)-
Rsv(RFP-Bsd):



U57 pHR SFFV GFP:



9.4.3. ImageJ Macros

9.4.3.1. convertMetaTifs.ijm

```
function contains(string, shouldContainPart) {
    return (indexOf(string, shouldContainPart) != -1);
}

folder = getDirectory("Choose Source Folder");
destFolder = getDirectory("Select destination Folder");
setBatchMode(true);
images = getFileList(folder);
for (imageIndex = 0; imageIndex < images.length; imageIndex++) {
    showProgress(imageIndex, images.length);
    imageName = images[imageIndex];
    if (endsWith(imageName, ".nd")) {
        continue;
    }
    if (File.isDirectory(folder + imageName)) {
        continue;
    }
    if (!endsWith(imageName, ".tif")) {
        continue;
    }
    if (contains(imageName, "RED")) {
        open(folder + imageName);
        run("Channels Tool... ");
        run("Red");
        saveAs("Jpeg", destFolder + imageName);
        run("Close");
        continue;
    }
    if (contains(imageName, "GFP.tif")) {
        open(folder + imageName);
        run("Channels Tool... ");
        run("Green");
        saveAs("Jpeg", destFolder + imageName);
        run("Close");
        continue;
    }
    open(folder + imageName);
    saveAs("Jpeg", destFolder + imageName);
    continue;
}
```

9.4.3.2. **transformImages.ijm**

```
folder = getDirectory("Choose Source Folder");
destFolder = getDirectory("Select destination Folder");
//print ("Converting all Images in " + folder + " to " + destFolder);

setBatchMode(true);
images = getFileList(folder);
for (imageIndex = 0; imageIndex < images.length; imageIndex++) {
    showProgress(imageIndex, images.length);
    image = images[imageIndex];
    open(folder + image);
    saveAs("Jpeg", destFolder + image);
//    print ("Image " + image);
}
```

9.4.3.3. **transformImagesWithContrast.ijm**

```
folder = getDirectory("Choose Source Folder");
destFolder = getDirectory("Select destination Folder");
//print ("Converting all Images in " + folder + " to " + destFolder);

setBatchMode(true);
images = getFileList(folder);
for (imageIndex = 0; imageIndex < images.length; imageIndex++) {
    showProgress(imageIndex, images.length);
    image = images[imageIndex];
    open(folder + image);
    run("Enhance Contrast", "saturated=0.4 normalize");
    saveAs("Jpeg", destFolder + image);
//    print ("Image " + image);
}
```

9.5. Curriculum Vitae

9.5.1. Publications

V. Leidgens, C. Seliger, B. Jachnik, T. Welz, P. Leukel, A. Vollmann-Zwerenz, U. Bogdahn, M. Kreutz, O. M. Grauer, P. Hau; Ibuprofen and diclofenac restrict migration and proliferation of human glioma cells by distinct molecular mechanisms; PLoS One (2015)

J. Onken, S. Moeckel, P. Leukel, V. Leidgens, F. Baumann, U. Bogdahn, A. Vollmann-Zwerenz, P. Hau; Versican isoform V1 regulates proliferation and migration in high-grade gliomas; J Neurooncol. (2014)

V. Gawrisch, N. Patwary, M. Rüttgers, E. Kerkhoff, M.J. Riemenschneider, U. Bogdahn, A. Vollmann-Zwerenz, C.A. Klein, P. Hau; P03.02: *In situ* organotypic brain slice culture migration model to dissect infiltrative from stationary human brain tumor initiating cells; Neuro Oncol (2014)

9.5.2. Contributions to Conferences

Poster presentation

NeuroOnkologische Arbeitsgemeinschaft (NOA) – 17. Jahrestagung

Heidelberg, Germany, July 2015

V. Leidgens, C. Seliger, P. Leukel, A. Vollmann-Zwerenz, L. Rauer, U. Bogdahn, M. Kreutz, P. Sander, O.M. Grauer, P. Hau; Ibuprofen and diclofenac inhibit migration and proliferation of human glioma cell lines *in vitro*

Oral presentation

NeuroOnkologische Arbeitsgemeinschaft (NOA) – 16. Jahrestagung

Bonn, Germany, June 2014

Isolation of infiltrative and stationary human brain tumor initiating cells in an *in situ* organotypic slice culture migration model

Poster presentation

International Meeting of the German Society for Cell Biology (DGZ)

Regensburg, Germany, March 2014

V. Gawrisch, N. Patwary, M. Rüttgers, C.A. Klein, E. Kerkhoff, M.J. Riemenschneider, U. Bogdahn, A. Vollmann-Zwerenz, P. Hau; Dissection of migrating from non-migrating human brain tumor initiating cells in an *in situ* organotypic slice culture migration model

Poster presentation

4th Quadrennial Meeting of the World Federation of Neuro-Oncology

San Francisco, USA, November 2013

V. Gawrisch, M. Rüttgers, P. Weigell, E. Kerkhoff, M.J. Riemenschneider, U. Bogdahn, A. Vollmann-Zwerenz, P. Hau; An *in situ* organotypic slice culture migration model to dissect migrating from non-migrating human brain tumor initiating cells

Poster presentation

10th Annual Meeting of the European Association of Neuro-Oncology

Marseille, France, September 2012

V. Gawrisch, M. Rüttgers, A. Vollmann-Zwerenz, P. Hau; Migratory capacity of brain tumor initiating cells: A Molecular and Cellular Dissection of Tumor Initiating Cells in High-Grade Gliomas

9.5.3. Awards

3rd pRED Discovery Oncology Award

3rd place

3rd pRED Discovery Oncology Award Symposium

Pathophysiology of the extracellular matrix – basic concepts and therapeutic approaches for cancer therapy – Roche, pRED

Penzberg, Germany, October 2015

V. Leidgens; Identification of ECM components inducing human brain tumour initiating cell invasion

Best Talk Award

NeuroOnkologische Arbeitsgemeinschaft (NOA) – 16. Jahrestagung

Bonn, Germany, June 2014

V. Leidgens; Isolation of infiltrative and stationary human brain tumor initiating cells in an *in situ* organotypic slice culture migration model

9.6. Acknowledgements

Completing my PhD and realising this thesis was an amazing journey, one which would not have been possible without support and encouragement of many exceptional people:

First of all, I would like to express my sincere gratitude my supervisor Prof. Dr. Peter Hau, for introducing me to glioblastoma research, providing insight and expertise. I am grateful for the opportunity to work on this fantastic PhD project, his willingness to take over the supervision, continuous support, valuable advice, crucial remarks, and thoughtful comments during my progress.

I would also like to thank the mentors of my dissertation, Prof. Dr. Eugen Kerkhoff and Prof. Dr. Markus Riemenschneider, for their interest, guidance, and invaluable advice during this time. I would like to thank Prof. Dr. Dr. Ghazaleh Tabatabai for her willingness to evaluate my thesis. I express my gratitude to Prof. Dr. Tobias Pukrop and Prof. Dr. Christoph Klein for their insightful questions, time and willingness to be part of the dissertation committee.

I am grateful to Prof. Dr. Ulrich Bogdahn for the possibility to work in his institute. In addition, to Prof. Dr. Eugen Kerkhoff and his group for advice and assistance for live cell imaging and actin experiments improving our published manuscript.

Especially I would like to thank Prof. Dr. Christoph Klein for his enthusiasm as well as continuous support in characterising the leader cells, which led to the strong collaboration that evolved and pushed this project forward.

I am very thankful for all participants involved in this joint research, Nina, Sandra, Kathrin, and Barbara, as well as Xin for taking care of the microarray data. And of course Tom, whose enthusiasm during the adapter development never ended. I very much appreciated this during the hours we spent sitting in the dark picking hundreds of cells.

My special thanks also to Prof. Dr. Martin Proescholdt for his kind collaboration, support, and thought-provoking advice to promote and improve my work.

I express my gratitude to Dr. Maria Stella Carro and Prof. Dr. Stephan Geley for great internships in their labs, familiarising me with lentiviral transduction and providing valuable insight and thoughtful advice.

The NeuroOncology lab gains my deepest thanks for their invaluable help regarding technical as well as scientific questions and providing thought-provoking questions during research work. Thank you Arabel, Birgit, Corinna, Ina, Judith, and Sylvia for creating such a wonderful working environment, and also all the fun we had together outside of shared scientific interests. Sincere thanks are due to Birgit who is always ready to help, probably the most important person in the lab keeping everything organised and everybody cheerful with your contagious laughter.

I have to expand this special thanks to all other members of the D4 floor. Annette, Tobias, Dagmar, Eva-Maria, and Lohmi deserve special gratitude for sharing expertise, lab space, as well as fun and a lot of cake. I am grateful that the group has been a source of friendships as well as good advice and collaboration. This is also true for former colleagues Petra, Maike, and Paul as well as current and former students in the lab Valeria, Anne-Louise, Anne, Patrizia, Suomi, Lisa, and Eva. It was great working next to you all, you contributed to make my PhD time unforgettable.

I gratefully acknowledge the funding sources without which I would not have been able to develop my scientific discoveries. I was funded by the BMBF within the framework of the Nationalen Genomforschungsnetz (NGFN) and by the Wilhelm Sander Stiftung.

Thank you Annette, Daniel, Jenni, and Sandra for being the best friends I can imagine. I am grateful for your constant faith in me and encouraging words, whenever needed not only during my thesis. Let's see what's up for us next.

I am deeply indebted to my family, my brother and especially my parents for their unconditional loving and great constant encouragement throughout the years. Who are always behind me with all their thrust and love and without their constant trust, love and support, this thesis would not have been possible. I owe my family much more than I would ever be able to express, thus I keep it simple: Thank you so much for your unconditional love and care.

Janusz gains my deepest thanks for being there for me, listening to all the new ideas that fascinated me, but also giving me the much-needed support when nothing seemed to go forward anymore. You carried me when the work appeared to overwhelm me, and supported me to work through the night to get this thesis done. Thanks for these past years of exciting PhD life that you lived with me and anyway starting in the adventure of our marriage. Thank you for the love and affection that you give me every day, being an enrichment for my life.

*Die Wissenschaft fängt eigentlich erst da an interessant zu werden,
wo sie aufhört.*

- Justus von Liebig

Don't give up.

Not ever.

Not for one single day.

Be safe, if you can be.

But always be amazing.

- Clara Oswald

1. Detailed Statistics

1.1. Proliferation assays

Statistics to proliferation assays depicted in chapter 4.3.3.2.2 (see from page 90), Figures 4-40 to 4-42. Statistics were calculated by two-way ANOVA (multiple comparisons: within each column row means are compared to each other (simple effects within columns); $\alpha = 0.05$; 95% CI; Tukey's multiple comparisons test).

A172	Significance	Adjusted p-value	Significance	Adjusted p-value
Category	48 h		96 h	
DMSO vs. 0.625 μ M Stattic	n.s.	> 0.9999	n.s.	0.7744
DMSO vs. 1.25 μ M Stattic	n.s.	> 0.9999	n.s.	0.9221
DMSO vs. 2.5 μ M Stattic	n.s.	0.7115	n.s.	0.9992
DMSO vs. 5 μ M Stattic	n.s.	> 0.9999	n.s.	0.9999
DMSO vs. 10 μ M Stattic	n.s.	0.8309	n.s.	0.9502
DMSO vs. 15 μ M Stattic	n.s.	0.2681	n.s.	0.9969
DMSO vs. 20 μ M Stattic	***	0.0003	n.s.	0.5266
0.625 μ M Stattic vs. 1.25 μ M Stattic	n.s.	> 0.9999	n.s.	0.1458
0.625 μ M Stattic vs. 2.5 μ M Stattic	n.s.	0.9096	n.s.	0.4002
0.625 μ M Stattic vs. 5 μ M Stattic	n.s.	0.9987	n.s.	0.5258
0.625 μ M Stattic vs. 10 μ M Stattic	n.s.	0.5900	n.s.	0.9995
0.625 μ M Stattic vs. 15 μ M Stattic	n.s.	0.1180	n.s.	0.3682
0.625 μ M Stattic vs. 20 μ M Stattic	****	< 0.0001	n.s.	> 0.9999
1.25 μ M Stattic vs. 2.5 μ M Stattic	n.s.	0.7343	n.s.	0.9958
1.25 μ M Stattic vs. 5 μ M Stattic	n.s.	> 0.9999	n.s.	0.9925
1.25 μ M Stattic vs. 10 μ M Stattic	n.s.	0.8119	n.s.	0.2881
1.25 μ M Stattic vs. 15 μ M Stattic	n.s.	0.2502	n.s.	0.9994
1.25 μ M Stattic vs. 20 μ M Stattic	***	0.0003	n.s.	0.0581
2.5 μ M Stattic vs. 5 μ M Stattic	n.s.	0.5795	n.s.	> 0.9999
2.5 μ M Stattic vs. 10 μ M Stattic	n.s.	0.0534	n.s.	0.6607
2.5 μ M Stattic vs. 15 μ M Stattic	**	0.0035	n.s.	> 0.9999
2.5 μ M Stattic vs. 20 μ M Stattic	****	< 0.0001	n.s.	0.1945
5 μ M Stattic vs. 10 μ M Stattic	n.s.	0.9149	n.s.	0.7822
5 μ M Stattic vs. 15 μ M Stattic	n.s.	0.3784	n.s.	> 0.9999
5 μ M Stattic vs. 20 μ M Stattic	***	0.0006	n.s.	0.2916
10 μ M Stattic vs. 15 μ M Stattic	n.s.	0.9815	n.s.	0.6149
10 μ M Stattic vs. 20 μ M Stattic	*	0.0314	n.s.	0.9842
15 μ M Stattic vs. 20 μ M Stattic	n.s.	0.2710	n.s.	0.1808

HTZ349	Significance	Adjusted p-vale	Significance	Adjusted p-vale
Category	48 h		96 h	
DMSO vs. 0.625 μ M Stattic	n.s.	> 0.9999	n.s.	0.9997
DMSO vs. 1.25 μ M Stattic	n.s.	> 0.9999	n.s.	0.4643
DMSO vs. 2.5 μ M Stattic	n.s.	0.9998	n.s.	0.6478
DMSO vs. 5 μ M Stattic	n.s.	> 0.9999	n.s.	0.8064
DMSO vs. 10 μ M Stattic	n.s.	0.9237	n.s.	0.9972
DMSO vs. 15 μ M Stattic	n.s.	0.9086	n.s.	> 0.9999
DMSO vs. 20 μ M Stattic	n.s.	0.0720	***	0.0004
0.625 μ M Stattic vs. 1.25 μ M Stattic	n.s.	> 0.9999	n.s.	0.2034
0.625 μ M Stattic vs. 2.5 μ M Stattic	n.s.	> 0.9999	n.s.	0.3380
0.625 μ M Stattic vs. 5 μ M Stattic	n.s.	> 0.9999	n.s.	0.5004
0.625 μ M Stattic vs. 10 μ M Stattic	n.s.	0.8875	n.s.	0.9376
0.625 μ M Stattic vs. 15 μ M Stattic	n.s.	0.8698	n.s.	> 0.9999
0.625 μ M Stattic vs. 20 μ M Stattic	n.s.	0.0771	**	0.0022
1.25 μ M Stattic vs. 2.5 μ M Stattic	n.s.	> 0.9999	n.s.	> 0.9999
1.25 μ M Stattic vs. 5 μ M Stattic	n.s.	> 0.9999	n.s.	0.9993
1.25 μ M Stattic vs. 10 μ M Stattic	n.s.	0.9037	n.s.	0.8712
1.25 μ M Stattic vs. 15 μ M Stattic	n.s.	0.8863	n.s.	0.2407
1.25 μ M Stattic vs. 20 μ M Stattic	n.s.	0.0613	****	< 0.0001
2.5 μ M Stattic vs. 5 μ M Stattic	n.s.	> 0.9999	n.s.	> 0.9999
2.5 μ M Stattic vs. 10 μ M Stattic	n.s.	0.7326	n.s.	0.9584
2.5 μ M Stattic vs. 15 μ M Stattic	n.s.	0.7043	n.s.	0.3884
2.5 μ M Stattic vs. 20 μ M Stattic	*	0.0224	****	< 0.0001
5 μ M Stattic vs. 10 μ M Stattic	n.s.	0.8849	n.s.	0.9916
5 μ M Stattic vs. 15 μ M Stattic	n.s.	0.8670	n.s.	0.5579
5 μ M Stattic vs. 20 μ M Stattic	n.s.	0.0758	****	< 0.0001
10 μ M Stattic vs. 15 μ M Stattic	n.s.	> 0.9999	n.s.	0.9582
10 μ M Stattic vs. 20 μ M Stattic	n.s.	0.7737	****	< 0.0001
15 μ M Stattic vs. 20 μ M Stattic	n.s.	0.7991	**	0.0016

U87	Significance	Adjusted p-value	Significance	Adjusted p-value
Category	48 h		96 h	
DMSO vs. 0.625 μ M Stattic	n.s.	0.9340	***	0.0002
DMSO vs. 1.25 μ M Stattic	n.s.	0.7597	*	0.0201
DMSO vs. 2.5 μ M Stattic	n.s.	> 0.9999	n.s.	0.9743
DMSO vs. 5 μ M Stattic	n.s.	> 0.9999	****	< 0.0001
DMSO vs. 10 μ M Stattic	*	0.0367	****	< 0.0001
DMSO vs. 15 μ M Stattic	*	0.0103	****	< 0.0001
DMSO vs. 20 μ M Stattic	***	0.0001	****	< 0.0001
0.625 μ M Stattic vs. 1.25 μ M Stattic	n.s.	0.9997	n.s.	0.6822
0.625 μ M Stattic vs. 2.5 μ M Stattic	n.s.	0.9949	**	0.0038
0.625 μ M Stattic vs. 5 μ M Stattic	n.s.	0.8918	n.s.	> 0.9999
0.625 μ M Stattic vs. 10 μ M Stattic	***	0.0005	n.s.	0.2838
0.625 μ M Stattic vs. 15 μ M Stattic	****	< 0.0001	****	< 0.0001
0.625 μ M Stattic vs. 20 μ M Stattic	****	< 0.0001	****	< 0.0001
1.25 μ M Stattic vs. 2.5 μ M Stattic	n.s.	0.9374	n.s.	0.2290
1.25 μ M Stattic vs. 5 μ M Stattic	n.s.	0.7015	n.s.	0.5064
1.25 μ M Stattic vs. 10 μ M Stattic	***	0.0002	**	0.0010
1.25 μ M Stattic vs. 15 μ M Stattic	****	< 0.0001	****	< 0.0001
1.25 μ M Stattic vs. 20 μ M Stattic	****	< 0.0001	****	< 0.0001
2.5 μ M Stattic vs. 5 μ M Stattic	n.s.	0.9989	***	0.0008
2.5 μ M Stattic vs. 10 μ M Stattic	*	0.0112	****	< 0.0001
2.5 μ M Stattic vs. 15 μ M Stattic	**	0.0028	****	< 0.0001
2.5 μ M Stattic vs. 20 μ M Stattic	****	< 0.0001	****	< 0.0001
5 μ M Stattic vs. 10 μ M Stattic	n.s.	0.1153	n.s.	0.2548
5 μ M Stattic vs. 15 μ M Stattic	*	0.0420	****	< 0.0001
5 μ M Stattic vs. 20 μ M Stattic	***	0.0009	****	< 0.0001
10 μ M Stattic vs. 15 μ M Stattic	n.s.	0.9998	n.s.	0.0809
10 μ M Stattic vs. 20 μ M Stattic	n.s.	0.6380	**	0.0064
15 μ M Stattic vs. 20 μ M Stattic	n.s.	0.8803	n.s.	0.9525

GBM lines	Significance	Adjusted p-value	Significance	Adjusted p-value
Category	48 h		96 h	
DMSO vs. 0.625 μ M Stattic	n.s.	> 0.9999	n.s.	0.9998
DMSO vs. 1.25 μ M Stattic	n.s.	0.9998	n.s.	0.9789
DMSO vs. 2.5 μ M Stattic	n.s.	0.9999	n.s.	0.9592
DMSO vs. 5 μ M Stattic	n.s.	0.7479	n.s.	0.9876
DMSO vs. 10 μ M Stattic	n.s.	0.1720	n.s.	0.2932
DMSO vs. 15 μ M Stattic	**	0.0021	****	< 0.0001
DMSO vs. 20 μ M Stattic	****	< 0.0001	****	< 0.0001
0.625 μ M Stattic vs. 1.25 μ M Stattic	n.s.	0.9998	n.s.	0.8717
0.625 μ M Stattic vs. 2.5 μ M Stattic	n.s.	0.9999	n.s.	0.8167
0.625 μ M Stattic vs. 5 μ M Stattic	n.s.	0.7678	n.s.	0.9033
0.625 μ M Stattic vs. 10 μ M Stattic	n.s.	0.1928	n.s.	0.6475
0.625 μ M Stattic vs. 15 μ M Stattic	**	0.0029	***	0.0003
0.625 μ M Stattic vs. 20 μ M Stattic	****	< 0.0001	****	< 0.0001
1.25 μ M Stattic vs. 2.5 μ M Stattic	n.s.	> 0.9999	n.s.	> 0.9999
1.25 μ M Stattic vs. 5 μ M Stattic	n.s.	0.9427	n.s.	> 0.9999
1.25 μ M Stattic vs. 10 μ M Stattic	n.s.	0.3799	*	0.0246
1.25 μ M Stattic vs. 15 μ M Stattic	**	0.0085	****	< 0.0001
1.25 μ M Stattic vs. 20 μ M Stattic	****	< 0.0001	****	< 0.0001
2.5 μ M Stattic vs. 5 μ M Stattic	n.s.	0.9314	n.s.	> 0.9999
2.5 μ M Stattic vs. 10 μ M Stattic	n.s.	0.3555	*	0.0169
2.5 μ M Stattic vs. 15 μ M Stattic	**	0.0074	****	< 0.0001
2.5 μ M Stattic vs. 20 μ M Stattic	****	< 0.0001	****	< 0.0001
5 μ M Stattic vs. 10 μ M Stattic	n.s.	0.9635	*	0.0316
5 μ M Stattic vs. 15 μ M Stattic	n.s.	0.1803	****	< 0.0001
5 μ M Stattic vs. 20 μ M Stattic	****	< 0.0001	****	< 0.0001
10 μ M Stattic vs. 15 μ M Stattic	n.s.	0.8420	n.s.	0.1276
10 μ M Stattic vs. 20 μ M Stattic	***	0.0001	***	0.0009
15 μ M Stattic vs. 20 μ M Stattic	*	0.0240	n.s.	0.6385

RAV17 BTIC	Significance	Adjusted p-vale	Significance	Adjusted p-vale
Category	48 h		96 h	
DMSO vs. 0.625 μ M Stattic	n.s.	0.3028	n.s.	0.9971
DMSO vs. 1.25 μ M Stattic	n.s.	0.0965	n.s.	0.8595
DMSO vs. 2.5 μ M Stattic	**	0.0035	n.s.	0.6437
DMSO vs. 5 μ M Stattic	**	0.0022	n.s.	0.4015
DMSO vs. 10 μ M Stattic	n.s.	0.2776	*	0.0410
DMSO vs. 15 μ M Stattic	**	0.0054	***	0.0002
DMSO vs. 20 μ M Stattic	*	0.0108	***	0.0004
0.625 μ M Stattic vs. 1.25 μ M Stattic	n.s.	> 0.9999	n.s.	0.5099
0.625 μ M Stattic vs. 2.5 μ M Stattic	n.s.	0.6609	n.s.	0.3135
0.625 μ M Stattic vs. 5 μ M Stattic	n.s.	0.5610	n.s.	0.1609
0.625 μ M Stattic vs. 10 μ M Stattic	n.s.	> 0.9999	*	0.0131
0.625 μ M Stattic vs. 15 μ M Stattic	n.s.	0.7443	****	< 0.0001
0.625 μ M Stattic vs. 20 μ M Stattic	n.s.	0.8634	***	0.0001
1.25 μ M Stattic vs. 2.5 μ M Stattic	n.s.	0.8242	n.s.	0.9997
1.25 μ M Stattic vs. 5 μ M Stattic	n.s.	0.7342	n.s.	0.9886
1.25 μ M Stattic vs. 10 μ M Stattic	n.s.	> 0.9999	n.s.	0.4347
1.25 μ M Stattic vs. 15 μ M Stattic	n.s.	0.8885	*	0.0200
1.25 μ M Stattic vs. 20 μ M Stattic	n.s.	0.9599	*	0.0253
2.5 μ M Stattic vs. 5 μ M Stattic	n.s.	> 0.9999	n.s.	> 0.9999
2.5 μ M Stattic vs. 10 μ M Stattic	n.s.	0.9084	n.s.	0.7622
2.5 μ M Stattic vs. 15 μ M Stattic	n.s.	> 0.9999	n.s.	0.1311
2.5 μ M Stattic vs. 20 μ M Stattic	n.s.	> 0.9999	n.s.	0.1354
5 μ M Stattic vs. 10 μ M Stattic	n.s.	0.8539	n.s.	0.9085
5 μ M Stattic vs. 15 μ M Stattic	n.s.	> 0.9999	n.s.	0.2769
5 μ M Stattic vs. 20 μ M Stattic	n.s.	0.9995	n.s.	0.2723
10 μ M Stattic vs. 15 μ M Stattic	n.s.	0.9442	n.s.	0.9947
10 μ M Stattic vs. 20 μ M Stattic	n.s.	0.9808	n.s.	0.9882
15 μ M Stattic vs. 20 μ M Stattic	n.s.	> 0.9999	n.s.	> 0.9999

RAV19 BTIC	Significance	Adjusted p-vale	Significance	Adjusted p-vale
Category	48 h		96 h	
DMSO vs. 0.625 μ M Stattic	*	0.0372	****	< 0.0001
DMSO vs. 1.25 μ M Stattic	**	0.0046	****	< 0.0001
DMSO vs. 2.5 μ M Stattic	****	< 0.0001	****	< 0.0001
DMSO vs. 5 μ M Stattic	****	< 0.0001	****	< 0.0001
DMSO vs. 10 μ M Stattic	****	< 0.0001	****	< 0.0001
DMSO vs. 15 μ M Stattic	****	< 0.0001	****	< 0.0001
DMSO vs. 20 μ M Stattic	****	< 0.0001	****	< 0.0001
0.625 μ M Stattic vs. 1.25 μ M Stattic	n.s.	> 0.9999	****	< 0.0001
0.625 μ M Stattic vs. 2.5 μ M Stattic	****	< 0.0001	****	< 0.0001
0.625 μ M Stattic vs. 5 μ M Stattic	****	< 0.0001	****	< 0.0001
0.625 μ M Stattic vs. 10 μ M Stattic	****	< 0.0001	****	< 0.0001
0.625 μ M Stattic vs. 15 μ M Stattic	****	< 0.0001	****	< 0.0001
0.625 μ M Stattic vs. 20 μ M Stattic	****	< 0.0001	**	0.0039
1.25 μ M Stattic vs. 2.5 μ M Stattic	****	< 0.0001	****	< 0.0001
1.25 μ M Stattic vs. 5 μ M Stattic	****	< 0.0001	****	< 0.0001
1.25 μ M Stattic vs. 10 μ M Stattic	****	< 0.0001	****	< 0.0001
1.25 μ M Stattic vs. 15 μ M Stattic	****	< 0.0001	****	< 0.0001
1.25 μ M Stattic vs. 20 μ M Stattic	****	< 0.0001	****	< 0.0001
2.5 μ M Stattic vs. 5 μ M Stattic	****	< 0.0001	****	< 0.0001
2.5 μ M Stattic vs. 10 μ M Stattic	****	< 0.0001	****	< 0.0001
2.5 μ M Stattic vs. 15 μ M Stattic	****	< 0.0001	****	< 0.0001
2.5 μ M Stattic vs. 20 μ M Stattic	****	< 0.0001	n.s.	> 0.9999
5 μ M Stattic vs. 10 μ M Stattic	n.s.	0.9408	n.s.	> 0.9999
5 μ M Stattic vs. 15 μ M Stattic	n.s.	0.9594	n.s.	> 0.9999
5 μ M Stattic vs. 20 μ M Stattic	n.s.	0.9968	n.s.	> 0.9999
10 μ M Stattic vs. 15 μ M Stattic	n.s.	> 0.9999	n.s.	> 0.9999
10 μ M Stattic vs. 20 μ M Stattic	n.s.	0.9996	n.s.	> 0.9999
15 μ M Stattic vs. 20 μ M Stattic	n.s.	0.9999	****	< 0.0001

RAV57 BTIC	Significance	Adjusted p-vale	Significance	Adjusted p-vale
Category	48 h		96 h	
DMSO vs. 0.625 μ M Stattic	n.s.	> 0.9999	n.s.	0.1194
DMSO vs. 1.25 μ M Stattic	n.s.	0.9954	*	0.0302
DMSO vs. 2.5 μ M Stattic	n.s.	0.9886	*	0.0371
DMSO vs. 5 μ M Stattic	n.s.	0.2382	****	< 0.0001
DMSO vs. 10 μ M Stattic	**	0.0016	****	< 0.0001
DMSO vs. 15 μ M Stattic	**	0.0013	****	< 0.0001
DMSO vs. 20 μ M Stattic	****	< 0.0001	****	< 0.0001
0.625 μ M Stattic vs. 1.25 μ M Stattic	n.s.	0.9994	n.s.	> 0.9999
0.625 μ M Stattic vs. 2.5 μ M Stattic	n.s.	0.9974	n.s.	> 0.9999
0.625 μ M Stattic vs. 5 μ M Stattic	n.s.	0.2223	n.s.	0.5398
0.625 μ M Stattic vs. 10 μ M Stattic	***	0.0006	**	0.0016
0.625 μ M Stattic vs. 15 μ M Stattic	***	0.0006	***	0.0002
0.625 μ M Stattic vs. 20 μ M Stattic	****	< 0.0001	****	< 0.0001
1.25 μ M Stattic vs. 2.5 μ M Stattic	n.s.	> 0.9999	n.s.	> 0.9999
1.25 μ M Stattic vs. 5 μ M Stattic	n.s.	0.5970	n.s.	0.6473
1.25 μ M Stattic vs. 10 μ M Stattic	**	0.0073	**	0.0014
1.25 μ M Stattic vs. 15 μ M Stattic	**	0.0058	***	0.0002
1.25 μ M Stattic vs. 20 μ M Stattic	***	0.0003	****	< 0.0001
2.5 μ M Stattic vs. 5 μ M Stattic	n.s.	0.6829	n.s.	0.5985
2.5 μ M Stattic vs. 10 μ M Stattic	*	0.0110	**	0.0011
2.5 μ M Stattic vs. 15 μ M Stattic	**	0.0086	***	0.0001
2.5 μ M Stattic vs. 20 μ M Stattic	***	0.0005	****	< 0.0001
5 μ M Stattic vs. 10 μ M Stattic	n.s.	0.5251	n.s.	0.2079
5 μ M Stattic vs. 15 μ M Stattic	n.s.	0.3933	*	0.0405
5 μ M Stattic vs. 20 μ M Stattic	n.s.	0.1116	**	0.0039
10 μ M Stattic vs. 15 μ M Stattic	n.s.	> 0.9999	n.s.	0.9873
10 μ M Stattic vs. 20 μ M Stattic	n.s.	0.9951	n.s.	0.9212
15 μ M Stattic vs. 20 μ M Stattic	n.s.	> 0.9999	n.s.	> 0.9999

Proneural BTIC	Significance	Adjusted p-value	Significance	Adjusted p-value
Category	48 h		96 h	
DMSO vs. 0.625 μ M Stattic	n.s.	0.6679	*	0.0389
DMSO vs. 1.25 μ M Stattic	n.s.	0.4428	*	0.0298
DMSO vs. 2.5 μ M Stattic	*	0.0138	**	0.0043
DMSO vs. 5 μ M Stattic	***	0.0002	****	< 0.0001
DMSO vs. 10 μ M Stattic	****	< 0.0001	****	< 0.0001
DMSO vs. 15 μ M Stattic	****	< 0.0001	****	< 0.0001
DMSO vs. 20 μ M Stattic	****	< 0.0001	****	< 0.0001
0.625 μ M Stattic vs. 1.25 μ M Stattic	n.s.	> 0.9999	n.s.	> 0.9999
0.625 μ M Stattic vs. 2.5 μ M Stattic	n.s.	0.6751	n.s.	0.9948
0.625 μ M Stattic vs. 5 μ M Stattic	n.s.	0.0847	****	< 0.0001
0.625 μ M Stattic vs. 10 μ M Stattic	****	< 0.0001	****	< 0.0001
0.625 μ M Stattic vs. 15 μ M Stattic	****	< 0.0001	****	< 0.0001
0.625 μ M Stattic vs. 20 μ M Stattic	****	< 0.0001	****	< 0.0001
1.25 μ M Stattic vs. 2.5 μ M Stattic	n.s.	0.8709	n.s.	0.9956
1.25 μ M Stattic vs. 5 μ M Stattic	n.s.	0.1903	****	< 0.0001
1.25 μ M Stattic vs. 10 μ M Stattic	****	< 0.0001	****	< 0.0001
1.25 μ M Stattic vs. 15 μ M Stattic	****	< 0.0001	****	< 0.0001
1.25 μ M Stattic vs. 20 μ M Stattic	****	< 0.0001	****	< 0.0001
2.5 μ M Stattic vs. 5 μ M Stattic	n.s.	0.9183	***	0.0008
2.5 μ M Stattic vs. 10 μ M Stattic	**	0.0038	****	< 0.0001
2.5 μ M Stattic vs. 15 μ M Stattic	****	< 0.0001	****	< 0.0001
2.5 μ M Stattic vs. 20 μ M Stattic	****	< 0.0001	****	< 0.0001
5 μ M Stattic vs. 10 μ M Stattic	n.s.	0.2309	n.s.	0.9981
5 μ M Stattic vs. 15 μ M Stattic	*	0.0200	n.s.	0.8285
5 μ M Stattic vs. 20 μ M Stattic	*	0.0182	n.s.	0.7631
10 μ M Stattic vs. 15 μ M Stattic	n.s.	0.9771	n.s.	0.9934
10 μ M Stattic vs. 20 μ M Stattic	n.s.	0.9729	n.s.	0.9836
15 μ M Stattic vs. 20 μ M Stattic	n.s.	> 0.9999	n.s.	> 0.9999

RAV17 TC	Significance	Adjusted p-vale	Significance	Adjusted p-vale
Category	48 h		96 h	
DMSO vs. 0.625 μ M Stattic	n.s.	0.9900	n.s.	0.5954
DMSO vs. 1.25 μ M Stattic	n.s.	> 0.9999	**	0.0040
DMSO vs. 2.5 μ M Stattic	n.s.	> 0.9999	n.s.	0.2447
DMSO vs. 5 μ M Stattic	n.s.	0.1536	***	0.0002
DMSO vs. 10 μ M Stattic	***	0.0004	****	< 0.0001
DMSO vs. 15 μ M Stattic	****	< 0.0001	****	< 0.0001
DMSO vs. 20 μ M Stattic	***	0.0002	****	< 0.0001
0.625 μ M Stattic vs. 1.25 μ M Stattic	n.s.	0.9789	n.s.	0.4036
0.625 μ M Stattic vs. 2.5 μ M Stattic	n.s.	0.9909	n.s.	0.9960
0.625 μ M Stattic vs. 5 μ M Stattic	n.s.	0.5148	n.s.	0.0764
0.625 μ M Stattic vs. 10 μ M Stattic	**	0.0027	***	0.0010
0.625 μ M Stattic vs. 15 μ M Stattic	****	< 0.0001	****	< 0.0001
0.625 μ M Stattic vs. 20 μ M Stattic	**	0.0011	****	< 0.0001
1.25 μ M Stattic vs. 2.5 μ M Stattic	n.s.	> 0.9999	n.s.	0.9127
1.25 μ M Stattic vs. 5 μ M Stattic	n.s.	0.1189	n.s.	0.9912
1.25 μ M Stattic vs. 10 μ M Stattic	***	0.0003	n.s.	0.3320
1.25 μ M Stattic vs. 15 μ M Stattic	****	< 0.0001	*	0.0145
1.25 μ M Stattic vs. 20 μ M Stattic	***	0.0001	**	0.0045
2.5 μ M Stattic vs. 5 μ M Stattic	n.s.	0.1145	n.s.	0.4795
2.5 μ M Stattic vs. 10 μ M Stattic	***	0.0001	*	0.0276
2.5 μ M Stattic vs. 15 μ M Stattic	****	< 0.0001	***	0.0007
2.5 μ M Stattic vs. 20 μ M Stattic	****	< 0.0001	***	0.0001
5 μ M Stattic vs. 10 μ M Stattic	n.s.	0.4728	n.s.	0.8385
5 μ M Stattic vs. 15 μ M Stattic	*	0.0124	n.s.	0.1111
5 μ M Stattic vs. 20 μ M Stattic	n.s.	0.1967	n.s.	0.0622
10 μ M Stattic vs. 15 μ M Stattic	n.s.	0.6307	n.s.	0.8180
10 μ M Stattic vs. 20 μ M Stattic	n.s.	0.9929	n.s.	0.8205
15 μ M Stattic vs. 20 μ M Stattic	n.s.	0.9921	n.s.	> 0.9999

RAV19 TC	Significance	Adjusted p-vale	Significance	Adjusted p-vale
Category	48 h		96 h	
DMSO vs. 0.625 μ M Stattic	n.s.	> 0.9999	n.s.	0.2529
DMSO vs. 1.25 μ M Stattic	n.s.	0.2322	n.s.	> 0.9999
DMSO vs. 2.5 μ M Stattic	n.s.	0.0971	n.s.	0.5941
DMSO vs. 5 μ M Stattic	n.s.	0.6877	**	0.0042
DMSO vs. 10 μ M Stattic	***	0.0007	**	0.0069
DMSO vs. 15 μ M Stattic	****	< 0.0001	*	0.0188
DMSO vs. 20 μ M Stattic	****	< 0.0001	**	0.0025
0.625 μ M Stattic vs. 1.25 μ M Stattic	n.s.	0.1919	n.s.	0.2842
0.625 μ M Stattic vs. 2.5 μ M Stattic	n.s.	0.0710	n.s.	0.9995
0.625 μ M Stattic vs. 5 μ M Stattic	n.s.	0.7159	n.s.	0.4715
0.625 μ M Stattic vs. 10 μ M Stattic	***	0.0002	n.s.	0.6762
0.625 μ M Stattic vs. 15 μ M Stattic	****	< 0.0001	n.s.	0.8143
0.625 μ M Stattic vs. 20 μ M Stattic	****	< 0.0001	n.s.	0.3636
1.25 μ M Stattic vs. 2.5 μ M Stattic	n.s.	0.9990	n.s.	0.6345
1.25 μ M Stattic vs. 5 μ M Stattic	n.s.	0.9992	**	0.0050
1.25 μ M Stattic vs. 10 μ M Stattic	n.s.	0.2380	**	0.0083
1.25 μ M Stattic vs. 15 μ M Stattic	****	< 0.0001	*	0.0222
1.25 μ M Stattic vs. 20 μ M Stattic	***	0.0002	**	0.0030
2.5 μ M Stattic vs. 5 μ M Stattic	n.s.	0.9654	n.s.	0.2573
2.5 μ M Stattic vs. 10 μ M Stattic	n.s.	0.6459	n.s.	0.4073
2.5 μ M Stattic vs. 15 μ M Stattic	****	< 0.0001	n.s.	0.5691
2.5 μ M Stattic vs. 20 μ M Stattic	**	0.0022	n.s.	0.1857
5 μ M Stattic vs. 10 μ M Stattic	n.s.	0.1473	n.s.	0.9999
5 μ M Stattic vs. 15 μ M Stattic	****	< 0.0001	n.s.	0.9997
5 μ M Stattic vs. 20 μ M Stattic	***	0.0002	n.s.	> 0.9999
10 μ M Stattic vs. 15 μ M Stattic	*	0.0206	n.s.	> 0.9999
10 μ M Stattic vs. 20 μ M Stattic	n.s.	0.2000	n.s.	0.9988
15 μ M Stattic vs. 20 μ M Stattic	n.s.	0.9977	n.s.	0.9981

RAV57 TC	Significance	Adjusted p-vale	Significance	Adjusted p-vale
Category	48 h		96 h	
DMSO vs. 0.625 μ M Stattic	**	0.0043	****	< 0.0001
DMSO vs. 1.25 μ M Stattic	n.s.	0.9975	n.s.	0.9895
DMSO vs. 2.5 μ M Stattic	n.s.	0.9800	n.s.	0.0847
DMSO vs. 5 μ M Stattic	*	0.0142	****	< 0.0001
DMSO vs. 10 μ M Stattic	****	< 0.0001	****	< 0.0001
DMSO vs. 15 μ M Stattic	****	< 0.0001	****	< 0.0001
DMSO vs. 20 μ M Stattic	****	< 0.0001	****	< 0.0001
0.625 μ M Stattic vs. 1.25 μ M Stattic	*	0.0351	****	< 0.0001
0.625 μ M Stattic vs. 2.5 μ M Stattic	n.s.	0.0745	*	0.0184
0.625 μ M Stattic vs. 5 μ M Stattic	n.s.	> 0.9999	n.s.	0.8786
0.625 μ M Stattic vs. 10 μ M Stattic	****	< 0.0001	n.s.	0.9288
0.625 μ M Stattic vs. 15 μ M Stattic	****	< 0.0001	****	< 0.0001
0.625 μ M Stattic vs. 20 μ M Stattic	****	< 0.0001	****	< 0.0001
1.25 μ M Stattic vs. 2.5 μ M Stattic	n.s.	> 0.9999	n.s.	0.3203
1.25 μ M Stattic vs. 5 μ M Stattic	n.s.	0.0934	****	< 0.0001
1.25 μ M Stattic vs. 10 μ M Stattic	****	< 0.0001	****	< 0.0001
1.25 μ M Stattic vs. 15 μ M Stattic	****	< 0.0001	****	< 0.0001
1.25 μ M Stattic vs. 20 μ M Stattic	****	< 0.0001	****	< 0.0001
2.5 μ M Stattic vs. 5 μ M Stattic	n.s.	0.1783	n.s.	0.1541
2.5 μ M Stattic vs. 10 μ M Stattic	****	< 0.0001	****	< 0.0001
2.5 μ M Stattic vs. 15 μ M Stattic	****	< 0.0001	****	< 0.0001
2.5 μ M Stattic vs. 20 μ M Stattic	****	< 0.0001	****	< 0.0001
5 μ M Stattic vs. 10 μ M Stattic	****	< 0.0001	n.s.	0.0529
5 μ M Stattic vs. 15 μ M Stattic	****	< 0.0001	****	< 0.0001
5 μ M Stattic vs. 20 μ M Stattic	****	< 0.0001	****	< 0.0001
10 μ M Stattic vs. 15 μ M Stattic	****	< 0.0001	****	< 0.0001
10 μ M Stattic vs. 20 μ M Stattic	****	< 0.0001	****	< 0.0001
15 μ M Stattic vs. 20 μ M Stattic	n.s.	0.9980	**	0.0053

proneural TC	Significance	Adjusted p-vale	Significance	Adjusted p-vale
Category	48 h		96 h	
DMSO vs. 0.625 μ M Stattic	n.s.	0.6521	*	0.0470
DMSO vs. 1.25 μ M Stattic	*	0.0227	n.s.	0.2932
DMSO vs. 2.5 μ M Stattic	n.s.	0.7182	n.s.	0.9415
DMSO vs. 5 μ M Stattic	n.s.	0.1967	n.s.	0.0641
DMSO vs. 10 μ M Stattic	***	0.0001	***	0.0006
DMSO vs. 15 μ M Stattic	****	< 0.0001	****	< 0.0001
DMSO vs. 20 μ M Stattic	****	< 0.0001	****	< 0.0001
0.625 μ M Stattic vs. 1.25 μ M Stattic	n.s.	0.8089	n.s.	0.9878
0.625 μ M Stattic vs. 2.5 μ M Stattic	n.s.	> 0.9999	n.s.	0.5791
0.625 μ M Stattic vs. 5 μ M Stattic	n.s.	0.9988	n.s.	> 0.9999
0.625 μ M Stattic vs. 10 μ M Stattic	n.s.	0.1060	n.s.	0.8965
0.625 μ M Stattic vs. 15 μ M Stattic	****	< 0.0001	**	0.0038
0.625 μ M Stattic vs. 20 μ M Stattic	****	< 0.0001	***	0.0001
1.25 μ M Stattic vs. 2.5 μ M Stattic	n.s.	0.7059	n.s.	0.9632
1.25 μ M Stattic vs. 5 μ M Stattic	n.s.	0.9751	n.s.	0.9925
1.25 μ M Stattic vs. 10 μ M Stattic	n.s.	0.9050	n.s.	0.3493
1.25 μ M Stattic vs. 15 μ M Stattic	****	< 0.0001	****	< 0.0001
1.25 μ M Stattic vs. 20 μ M Stattic	***	0.0002	****	< 0.0001
2.5 μ M Stattic vs. 5 μ M Stattic	n.s.	0.9945	n.s.	0.6367
2.5 μ M Stattic vs. 10 μ M Stattic	n.s.	0.0614	*	0.0446
2.5 μ M Stattic vs. 15 μ M Stattic	****	< 0.0001	****	< 0.0001
2.5 μ M Stattic vs. 20 μ M Stattic	****	< 0.0001	****	< 0.0001
5 μ M Stattic vs. 10 μ M Stattic	n.s.	0.2619	n.s.	0.8908
5 μ M Stattic vs. 15 μ M Stattic	****	< 0.0001	**	0.0045
5 μ M Stattic vs. 20 μ M Stattic	****	< 0.0001	***	0.0001
10 μ M Stattic vs. 15 μ M Stattic	**	0.0033	n.s.	0.1839
10 μ M Stattic vs. 20 μ M Stattic	*	0.0160	*	0.0197
15 μ M Stattic vs. 20 μ M Stattic	n.s.	> 0.9999	n.s.	0.9962

RAV21 BTIC	Significance	Adjusted p-vale	Significance	Adjusted p-vale
Category	48 h		96 h	
DMSO vs. 0.625 μ M Stattic	n.s.	0.9992	n.s.	> 0.9999
DMSO vs. 1.25 μ M Stattic	n.s.	0.9919	n.s.	0.9945
DMSO vs. 2.5 μ M Stattic	*	0.0472	n.s.	0.0577
DMSO vs. 5 μ M Stattic	**	0.0027	****	< 0.0001
DMSO vs. 10 μ M Stattic	**	0.0030	****	< 0.0001
DMSO vs. 15 μ M Stattic	**	0.0011	****	< 0.0001
DMSO vs. 20 μ M Stattic	****	< 0.0001	****	< 0.0001
0.625 μ M Stattic vs. 1.25 μ M Stattic	n.s.	> 0.9999	n.s.	0.9996
0.625 μ M Stattic vs. 2.5 μ M Stattic	**	0.0091	n.s.	0.1099
0.625 μ M Stattic vs. 5 μ M Stattic	***	0.0004	****	< 0.0001
0.625 μ M Stattic vs. 10 μ M Stattic	***	0.0005	****	< 0.0001
0.625 μ M Stattic vs. 15 μ M Stattic	***	0.0002	****	< 0.0001
0.625 μ M Stattic vs. 20 μ M Stattic	****	< 0.0001	****	< 0.0001
1.25 μ M Stattic vs. 2.5 μ M Stattic	**	0.0040	n.s.	0.3093
1.25 μ M Stattic vs. 5 μ M Stattic	***	0.0002	***	0.0006
1.25 μ M Stattic vs. 10 μ M Stattic	***	0.0002	****	< 0.0001
1.25 μ M Stattic vs. 15 μ M Stattic	****	< 0.0001	****	< 0.0001
1.25 μ M Stattic vs. 20 μ M Stattic	****	< 0.0001	****	< 0.0001
2.5 μ M Stattic vs. 5 μ M Stattic	n.s.	0.9387	n.s.	0.3619
2.5 μ M Stattic vs. 10 μ M Stattic	n.s.	0.9480	****	< 0.0001
2.5 μ M Stattic vs. 15 μ M Stattic	n.s.	0.8476	****	< 0.0001
2.5 μ M Stattic vs. 20 μ M Stattic	n.s.	0.3631	****	< 0.0001
5 μ M Stattic vs. 10 μ M Stattic	n.s.	> 0.9999	****	< 0.0001
5 μ M Stattic vs. 15 μ M Stattic	n.s.	> 0.9999	****	< 0.0001
5 μ M Stattic vs. 20 μ M Stattic	n.s.	0.9952	****	< 0.0001
10 μ M Stattic vs. 15 μ M Stattic	n.s.	> 0.9999	n.s.	> 0.9999
10 μ M Stattic vs. 20 μ M Stattic	n.s.	0.9934	n.s.	0.9989
15 μ M Stattic vs. 20 μ M Stattic	n.s.	0.9997	n.s.	> 0.9999

RAV26 BTIC	Significance	Adjusted p-vale	Significance	Adjusted p-vale
Category	48 h		96 h	
DMSO vs. 0.625 μ M Stattic	n.s.	> 0.9999	**	0.0032
DMSO vs. 1.25 μ M Stattic	n.s.	0.3792	****	< 0.0001
DMSO vs. 2.5 μ M Stattic	****	< 0.0001	*	0.0109
DMSO vs. 5 μ M Stattic	****	< 0.0001	****	< 0.0001
DMSO vs. 10 μ M Stattic	****	< 0.0001	****	< 0.0001
DMSO vs. 15 μ M Stattic	****	< 0.0001	****	< 0.0001
DMSO vs. 20 μ M Stattic	****	< 0.0001	****	< 0.0001
0.625 μ M Stattic vs. 1.25 μ M Stattic	n.s.	0.5265	n.s.	0.8887
0.625 μ M Stattic vs. 2.5 μ M Stattic	****	< 0.0001	n.s.	> 0.9999
0.625 μ M Stattic vs. 5 μ M Stattic	****	< 0.0001	****	< 0.0001
0.625 μ M Stattic vs. 10 μ M Stattic	****	< 0.0001	****	< 0.0001
0.625 μ M Stattic vs. 15 μ M Stattic	****	< 0.0001	****	< 0.0001
0.625 μ M Stattic vs. 20 μ M Stattic	****	< 0.0001	****	< 0.0001
1.25 μ M Stattic vs. 2.5 μ M Stattic	****	< 0.0001	n.s.	0.6909
1.25 μ M Stattic vs. 5 μ M Stattic	****	< 0.0001	****	< 0.0001
1.25 μ M Stattic vs. 10 μ M Stattic	****	< 0.0001	****	< 0.0001
1.25 μ M Stattic vs. 15 μ M Stattic	****	< 0.0001	****	< 0.0001
1.25 μ M Stattic vs. 20 μ M Stattic	****	< 0.0001	****	< 0.0001
2.5 μ M Stattic vs. 5 μ M Stattic	****	< 0.0001	****	< 0.0001
2.5 μ M Stattic vs. 10 μ M Stattic	****	< 0.0001	****	< 0.0001
2.5 μ M Stattic vs. 15 μ M Stattic	****	< 0.0001	****	< 0.0001
2.5 μ M Stattic vs. 20 μ M Stattic	****	< 0.0001	****	< 0.0001
5 μ M Stattic vs. 10 μ M Stattic	n.s.	0.9998	*	0.0382
5 μ M Stattic vs. 15 μ M Stattic	n.s.	0.9974	n.s.	0.1498
5 μ M Stattic vs. 20 μ M Stattic	n.s.	0.9757	*	0.0287
10 μ M Stattic vs. 15 μ M Stattic	n.s.	> 0.9999	n.s.	> 0.9999
10 μ M Stattic vs. 20 μ M Stattic	n.s.	0.9994	n.s.	> 0.9999
15 μ M Stattic vs. 20 μ M Stattic	n.s.	> 0.9999	n.s.	> 0.9999

RAV27 BTIC	Significance	Adjusted p-vale	Significance	Adjusted p-vale
Category	48 h		96 h	
DMSO vs. 0.625 μ M Stattic	n.s.	> 0.9999	n.s.	0.9998
DMSO vs. 1.25 μ M Stattic	n.s.	0.9969	n.s.	0.8021
DMSO vs. 2.5 μ M Stattic	n.s.	0.1213	n.s.	0.1302
DMSO vs. 5 μ M Stattic	****	< 0.0001	****	< 0.0001
DMSO vs. 10 μ M Stattic	****	< 0.0001	****	< 0.0001
DMSO vs. 15 μ M Stattic	****	< 0.0001	****	< 0.0001
DMSO vs. 20 μ M Stattic	****	< 0.0001	****	< 0.0001
0.625 μ M Stattic vs. 1.25 μ M Stattic	n.s.	0.9971	n.s.	0.9676
0.625 μ M Stattic vs. 2.5 μ M Stattic	n.s.	0.1239	n.s.	0.3080
0.625 μ M Stattic vs. 5 μ M Stattic	****	< 0.0001	****	< 0.0001
0.625 μ M Stattic vs. 10 μ M Stattic	****	< 0.0001	****	< 0.0001
0.625 μ M Stattic vs. 15 μ M Stattic	****	< 0.0001	****	< 0.0001
0.625 μ M Stattic vs. 20 μ M Stattic	****	< 0.0001	****	< 0.0001
1.25 μ M Stattic vs. 2.5 μ M Stattic	n.s.	0.4763	n.s.	0.8489
1.25 μ M Stattic vs. 5 μ M Stattic	**	0.0017	****	< 0.0001
1.25 μ M Stattic vs. 10 μ M Stattic	**	0.0011	****	< 0.0001
1.25 μ M Stattic vs. 15 μ M Stattic	**	0.0014	****	< 0.0001
1.25 μ M Stattic vs. 20 μ M Stattic	**	0.0015	****	< 0.0001
2.5 μ M Stattic vs. 5 μ M Stattic	n.s.	0.5858	****	< 0.0001
2.5 μ M Stattic vs. 10 μ M Stattic	n.s.	0.5153	****	< 0.0001
2.5 μ M Stattic vs. 15 μ M Stattic	n.s.	0.5550	****	< 0.0001
2.5 μ M Stattic vs. 20 μ M Stattic	n.s.	0.5668	****	< 0.0001
5 μ M Stattic vs. 10 μ M Stattic	n.s.	> 0.9999	n.s.	0.2739
5 μ M Stattic vs. 15 μ M Stattic	n.s.	> 0.9999	n.s.	0.3041
5 μ M Stattic vs. 20 μ M Stattic	n.s.	> 0.9999	n.s.	0.2671
10 μ M Stattic vs. 15 μ M Stattic	n.s.	> 0.9999	n.s.	> 0.9999
10 μ M Stattic vs. 20 μ M Stattic	n.s.	> 0.9999	n.s.	> 0.9999
15 μ M Stattic vs. 20 μ M Stattic	n.s.	> 0.9999	n.s.	> 0.9999

mesenchymal BTIC	Significance	Adjusted p-vale	Significance	Adjusted p-vale
Category	48 h		96 h	
DMSO vs. 0.625 μ M Stattic	n.s.	0.9944	n.s.	0.9915
DMSO vs. 1.25 μ M Stattic	n.s.	0.9978	n.s.	0.9771
DMSO vs. 2.5 μ M Stattic	**	0.0056	n.s.	0.1411
DMSO vs. 5 μ M Stattic	****	< 0.0001	****	< 0.0001
DMSO vs. 10 μ M Stattic	****	< 0.0001	****	< 0.0001
DMSO vs. 15 μ M Stattic	****	< 0.0001	****	< 0.0001
DMSO vs. 20 μ M Stattic	****	< 0.0001	****	< 0.0001
0.625 μ M Stattic vs. 1.25 μ M Stattic	n.s.	> 0.9999	n.s.	> 0.9999
0.625 μ M Stattic vs. 2.5 μ M Stattic	***	0.0004	n.s.	0.6254
0.625 μ M Stattic vs. 5 μ M Stattic	****	< 0.0001	****	< 0.0001
0.625 μ M Stattic vs. 10 μ M Stattic	****	< 0.0001	****	< 0.0001
0.625 μ M Stattic vs. 15 μ M Stattic	****	< 0.0001	****	< 0.0001
0.625 μ M Stattic vs. 20 μ M Stattic	****	< 0.0001	****	< 0.0001
1.25 μ M Stattic vs. 2.5 μ M Stattic	***	0.0008	n.s.	0.6899
1.25 μ M Stattic vs. 5 μ M Stattic	****	< 0.0001	****	< 0.0001
1.25 μ M Stattic vs. 10 μ M Stattic	****	< 0.0001	****	< 0.0001
1.25 μ M Stattic vs. 15 μ M Stattic	****	< 0.0001	****	< 0.0001
1.25 μ M Stattic vs. 20 μ M Stattic	****	< 0.0001	****	< 0.0001
2.5 μ M Stattic vs. 5 μ M Stattic	n.s.	0.4041	****	< 0.0001
2.5 μ M Stattic vs. 10 μ M Stattic	n.s.	0.2878	****	< 0.0001
2.5 μ M Stattic vs. 15 μ M Stattic	n.s.	0.3818	****	< 0.0001
2.5 μ M Stattic vs. 20 μ M Stattic	n.s.	0.1257	****	< 0.0001
5 μ M Stattic vs. 10 μ M Stattic	n.s.	> 0.9999	***	0.0002
5 μ M Stattic vs. 15 μ M Stattic	n.s.	> 0.9999	****	< 0.0001
5 μ M Stattic vs. 20 μ M Stattic	n.s.	> 0.9999	****	< 0.0001
10 μ M Stattic vs. 15 μ M Stattic	n.s.	> 0.9999	n.s.	> 0.9999
10 μ M Stattic vs. 20 μ M Stattic	n.s.	> 0.9999	n.s.	0.9999
15 μ M Stattic vs. 20 μ M Stattic	n.s.	> 0.9999	n.s.	0.9999

RAV21 TC	Significance	Adjusted p-vale	Significance	Adjusted p-vale
Category	48 h		96 h	
DMSO vs. 0.625 μ M Stattic	****	< 0.0001	n.s.	0.8246
DMSO vs. 1.25 μ M Stattic	n.s.	0.1304	n.s.	0.8315
DMSO vs. 2.5 μ M Stattic	n.s.	0.8412	n.s.	0.8773
DMSO vs. 5 μ M Stattic	n.s.	0.2185	n.s.	0.0536
DMSO vs. 10 μ M Stattic	****	< 0.0001	*	0.0405
DMSO vs. 15 μ M Stattic	****	< 0.0001	****	< 0.0001
DMSO vs. 20 μ M Stattic	****	< 0.0001	****	< 0.0001
0.625 μ M Stattic vs. 1.25 μ M Stattic	n.s.	0.0503	n.s.	0.0673
0.625 μ M Stattic vs. 2.5 μ M Stattic	****	< 0.0001	n.s.	0.0863
0.625 μ M Stattic vs. 5 μ M Stattic	**	0.0063	n.s.	0.7851
0.625 μ M Stattic vs. 10 μ M Stattic	n.s.	0.9964	n.s.	0.7232
0.625 μ M Stattic vs. 15 μ M Stattic	*	0.0206	****	< 0.0001
0.625 μ M Stattic vs. 20 μ M Stattic	***	0.0003	****	< 0.0001
1.25 μ M Stattic vs. 2.5 μ M Stattic	n.s.	0.7797	n.s.	> 0.9999
1.25 μ M Stattic vs. 5 μ M Stattic	n.s.	0.9999	***	0.0002
1.25 μ M Stattic vs. 10 μ M Stattic	n.s.	0.2283	****	< 0.0001
1.25 μ M Stattic vs. 15 μ M Stattic	****	< 0.0001	****	< 0.0001
1.25 μ M Stattic vs. 20 μ M Stattic	****	< 0.0001	****	< 0.0001
2.5 μ M Stattic vs. 5 μ M Stattic	n.s.	0.9311	***	0.0002
2.5 μ M Stattic vs. 10 μ M Stattic	***	0.0007	***	0.0001
2.5 μ M Stattic vs. 15 μ M Stattic	****	< 0.0001	****	< 0.0001
2.5 μ M Stattic vs. 20 μ M Stattic	****	< 0.0001	****	< 0.0001
5 μ M Stattic vs. 10 μ M Stattic	*	0.0499	n.s.	> 0.9999
5 μ M Stattic vs. 15 μ M Stattic	****	< 0.0001	****	< 0.0001
5 μ M Stattic vs. 20 μ M Stattic	****	< 0.0001	****	< 0.0001
10 μ M Stattic vs. 15 μ M Stattic	**	0.0022	****	< 0.0001
10 μ M Stattic vs. 20 μ M Stattic	****	< 0.0001	****	< 0.0001
15 μ M Stattic vs. 20 μ M Stattic	n.s.	0.8894	n.s.	0.7035

RAV26 TC	Significance	Adjusted p-vale	Significance	Adjusted p-vale
Category	48 h		96 h	
DMSO vs. 0.625 μ M Stattic	n.s.	0.9506	n.s.	0.9960
DMSO vs. 1.25 μ M Stattic	n.s.	0.1178	n.s.	0.9357
DMSO vs. 2.5 μ M Stattic	*	0.0320	*	0.0135
DMSO vs. 5 μ M Stattic	****	< 0.0001	n.s.	0.0733
DMSO vs. 10 μ M Stattic	****	< 0.0001	**	0.0040
DMSO vs. 15 μ M Stattic	****	< 0.0001	****	< 0.0001
DMSO vs. 20 μ M Stattic	****	< 0.0001	****	< 0.0001
0.625 μ M Stattic vs. 1.25 μ M Stattic	**	0.0052	n.s.	> 0.9999
0.625 μ M Stattic vs. 2.5 μ M Stattic	***	0.0009	n.s.	0.7035
0.625 μ M Stattic vs. 5 μ M Stattic	****	< 0.0001	n.s.	0.9075
0.625 μ M Stattic vs. 10 μ M Stattic	****	< 0.0001	n.s.	0.6268
0.625 μ M Stattic vs. 15 μ M Stattic	****	< 0.0001	****	< 0.0001
0.625 μ M Stattic vs. 20 μ M Stattic	****	< 0.0001	****	< 0.0001
1.25 μ M Stattic vs. 2.5 μ M Stattic	n.s.	0.9996	n.s.	0.2128
1.25 μ M Stattic vs. 5 μ M Stattic	n.s.	0.0777	n.s.	0.5650
1.25 μ M Stattic vs. 10 μ M Stattic	****	< 0.0001	n.s.	0.1114
1.25 μ M Stattic vs. 15 μ M Stattic	****	< 0.0001	****	< 0.0001
1.25 μ M Stattic vs. 20 μ M Stattic	****	< 0.0001	****	< 0.0001
2.5 μ M Stattic vs. 5 μ M Stattic	n.s.	0.2397	n.s.	0.9991
2.5 μ M Stattic vs. 10 μ M Stattic	****	< 0.0001	n.s.	> 0.9999
2.5 μ M Stattic vs. 15 μ M Stattic	****	< 0.0001	****	< 0.0001
2.5 μ M Stattic vs. 20 μ M Stattic	****	< 0.0001	****	< 0.0001
5 μ M Stattic vs. 10 μ M Stattic	***	0.0001	n.s.	0.9965
5 μ M Stattic vs. 15 μ M Stattic	****	< 0.0001	****	< 0.0001
5 μ M Stattic vs. 20 μ M Stattic	****	< 0.0001	****	< 0.0001
10 μ M Stattic vs. 15 μ M Stattic	****	< 0.0001	****	< 0.0001
10 μ M Stattic vs. 20 μ M Stattic	****	< 0.0001	****	< 0.0001
15 μ M Stattic vs. 20 μ M Stattic	n.s.	0.9399	****	< 0.0001

RAV27 TC	Significance	Adjusted p-value	Significance	Adjusted p-value
Category	48 h		96 h	
DMSO vs. 0.625 μ M Stattic	n.s.	0.9995	n.s.	> 0.9999
DMSO vs. 1.25 μ M Stattic	n.s.	0.9999	n.s.	> 0.9999
DMSO vs. 2.5 μ M Stattic	n.s.	> 0.9999	n.s.	0.9998
DMSO vs. 5 μ M Stattic	n.s.	> 0.9999	n.s.	> 0.9999
DMSO vs. 10 μ M Stattic	n.s.	0.9850	n.s.	0.9985
DMSO vs. 15 μ M Stattic	n.s.	0.5755	n.s.	0.8972
DMSO vs. 20 μ M Stattic	n.s.	0.1583	****	< 0.0001
0.625 μ M Stattic vs. 1.25 μ M Stattic	n.s.	0.9793	n.s.	0.9992
0.625 μ M Stattic vs. 2.5 μ M Stattic	n.s.	0.9986	n.s.	0.9945
0.625 μ M Stattic vs. 5 μ M Stattic	n.s.	0.9993	n.s.	0.9979
0.625 μ M Stattic vs. 10 μ M Stattic	n.s.	> 0.9999	n.s.	0.9832
0.625 μ M Stattic vs. 15 μ M Stattic	n.s.	0.8770	n.s.	0.7934
0.625 μ M Stattic vs. 20 μ M Stattic	n.s.	0.4088	****	< 0.0001
1.25 μ M Stattic vs. 2.5 μ M Stattic	n.s.	> 0.9999	n.s.	> 0.9999
1.25 μ M Stattic vs. 5 μ M Stattic	n.s.	> 0.9999	n.s.	> 0.9999
1.25 μ M Stattic vs. 10 μ M Stattic	n.s.	0.8862	n.s.	> 0.9999
1.25 μ M Stattic vs. 15 μ M Stattic	n.s.	0.3141	n.s.	0.9589
1.25 μ M Stattic vs. 20 μ M Stattic	n.s.	0.0595	***	0.0001
2.5 μ M Stattic vs. 5 μ M Stattic	n.s.	> 0.9999	n.s.	> 0.9999
2.5 μ M Stattic vs. 10 μ M Stattic	n.s.	0.9750	n.s.	> 0.9999
2.5 μ M Stattic vs. 15 μ M Stattic	n.s.	0.5194	n.s.	0.9892
2.5 μ M Stattic vs. 20 μ M Stattic	n.s.	0.1319	***	0.0002
5 μ M Stattic vs. 10 μ M Stattic	n.s.	0.9833	n.s.	> 0.9999
5 μ M Stattic vs. 15 μ M Stattic	n.s.	0.5644	n.s.	0.9768
5 μ M Stattic vs. 20 μ M Stattic	n.s.	0.1527	***	0.0002
10 μ M Stattic vs. 15 μ M Stattic	n.s.	0.9763	n.s.	0.9974
10 μ M Stattic vs. 20 μ M Stattic	n.s.	0.6494	***	0.0004
15 μ M Stattic vs. 20 μ M Stattic	n.s.	0.9932	**	0.0038

mesenchymal TC	Significance	Adjusted p-value	Significance	Adjusted p-value
Category	48 h		96 h	
DMSO vs. 0.625 μ M Stattic	**	0.0027	n.s.	0.1265
DMSO vs. 1.25 μ M Stattic	n.s.	0.0913	n.s.	0.9998
DMSO vs. 2.5 μ M Stattic	***	0.0005	n.s.	0.8572
DMSO vs. 5 μ M Stattic	***	0.0002	n.s.	0.0790
DMSO vs. 10 μ M Stattic	****	< 0.0001	*	0.0137
DMSO vs. 15 μ M Stattic	****	< 0.0001	****	< 0.0001
DMSO vs. 20 μ M Stattic	****	< 0.0001	****	< 0.0001
0.625 μ M Stattic vs. 1.25 μ M Stattic	n.s.	0.9603	n.s.	0.2946
0.625 μ M Stattic vs. 2.5 μ M Stattic	n.s.	> 0.9999	n.s.	0.7208
0.625 μ M Stattic vs. 5 μ M Stattic	n.s.	0.9994	n.s.	0.9991
0.625 μ M Stattic vs. 10 μ M Stattic	**	0.0087	n.s.	> 0.9999
0.625 μ M Stattic vs. 15 μ M Stattic	****	< 0.0001	n.s.	0.0507
0.625 μ M Stattic vs. 20 μ M Stattic	****	< 0.0001	****	< 0.0001
1.25 μ M Stattic vs. 2.5 μ M Stattic	n.s.	0.8539	n.s.	0.9862
1.25 μ M Stattic vs. 5 μ M Stattic	n.s.	0.7183	n.s.	0.2792
1.25 μ M Stattic vs. 10 μ M Stattic	****	< 0.0001	n.s.	0.0786
1.25 μ M Stattic vs. 15 μ M Stattic	****	< 0.0001	****	< 0.0001
1.25 μ M Stattic vs. 20 μ M Stattic	****	< 0.0001	****	< 0.0001
2.5 μ M Stattic vs. 5 μ M Stattic	n.s.	> 0.9999	n.s.	0.8273
2.5 μ M Stattic vs. 10 μ M Stattic	*	0.0181	n.s.	0.4711
2.5 μ M Stattic vs. 15 μ M Stattic	****	< 0.0001	****	< 0.0001
2.5 μ M Stattic vs. 20 μ M Stattic	****	< 0.0001	****	< 0.0001
5 μ M Stattic vs. 10 μ M Stattic	*	0.0399	n.s.	0.9994
5 μ M Stattic vs. 15 μ M Stattic	****	< 0.0001	****	< 0.0001
5 μ M Stattic vs. 20 μ M Stattic	****	< 0.0001	****	< 0.0001
10 μ M Stattic vs. 15 μ M Stattic	****	< 0.0001	***	0.0003
10 μ M Stattic vs. 20 μ M Stattic	****	< 0.0001	****	< 0.0001
15 μ M Stattic vs. 20 μ M Stattic	n.s.	0.5367	****	< 0.0001

1.2. Migration assays

Statistics to migration assays depicted in chapter 4.3.3.2.3 (see from page 95), Figures 4-44 to 4-46. Statistics were calculated by two-way ANOVA (multiple comparisons: within each column row means are compared to each other (simple effects within columns); $\alpha = 0.05$; 95% CI; Tukey's multiple comparisons test).

A172	Significance	Adjusted p-vale	Significance	Adjusted p-vale
Category	16 h		24 h	
DMSO vs. 0.625 μ M Stattic	n.s.	0.9986	n.s.	0.4975
DMSO vs. 1.25 μ M Stattic	n.s.	> 0.9999	n.s.	0.9425
DMSO vs. 2.5 μ M Stattic	n.s.	0.9789	n.s.	0.1294
DMSO vs. 5 μ M Stattic	n.s.	0.5011	**	0.0010
DMSO vs. 10 μ M Stattic	*	0.0165	****	< 0.0001
DMSO vs. 15 μ M Stattic	**	0.0035	****	< 0.0001
DMSO vs. 20 μ M Stattic	***	0.0001	****	< 0.0001
0.625 μ M Stattic vs. 1.25 μ M Stattic	n.s.	0.9993	n.s.	0.9966
0.625 μ M Stattic vs. 2.5 μ M Stattic	n.s.	> 0.9999	n.s.	0.9988
0.625 μ M Stattic vs. 5 μ M Stattic	n.s.	0.9144	n.s.	0.4380
0.625 μ M Stattic vs. 10 μ M Stattic	n.s.	0.1292	***	0.0008
0.625 μ M Stattic vs. 15 μ M Stattic	*	0.0396	****	< 0.0001
0.625 μ M Stattic vs. 20 μ M Stattic	**	0.0027	****	< 0.0001
1.25 μ M Stattic vs. 2.5 μ M Stattic	n.s.	0.9858	n.s.	0.8515
1.25 μ M Stattic vs. 5 μ M Stattic	n.s.	0.5462	n.s.	0.0777
1.25 μ M Stattic vs. 10 μ M Stattic	*	0.0204	****	< 0.0001
1.25 μ M Stattic vs. 15 μ M Stattic	**	0.0045	****	< 0.0001
1.25 μ M Stattic vs. 20 μ M Stattic	***	0.0002	****	< 0.0001
2.5 μ M Stattic vs. 5 μ M Stattic	n.s.	0.9859	n.s.	0.8748
2.5 μ M Stattic vs. 10 μ M Stattic	n.s.	0.2805	*	0.0119
2.5 μ M Stattic vs. 15 μ M Stattic	n.s.	0.1060	***	0.0007
2.5 μ M Stattic vs. 20 μ M Stattic	**	0.0099	****	< 0.0001
5 μ M Stattic vs. 10 μ M Stattic	n.s.	0.8922	n.s.	0.4648
5 μ M Stattic vs. 15 μ M Stattic	n.s.	0.6504	n.s.	0.1072
5 μ M Stattic vs. 20 μ M Stattic	n.s.	0.1788	**	0.0087
10 μ M Stattic vs. 15 μ M Stattic	n.s.	> 0.9999	n.s.	0.9984
10 μ M Stattic vs. 20 μ M Stattic	n.s.	0.9531	n.s.	0.8330
15 μ M Stattic vs. 20 μ M Stattic	n.s.	0.9973	n.s.	0.9963

A172	Significance	Adjusted p-vale	Significance	Adjusted p-vale
Category	40 h		48 h	
DMSO vs. 0.625 μ M Stattic	***	0.0007	**	0.0014
DMSO vs. 1.25 μ M Stattic	**	0.0035	**	0.0031
DMSO vs. 2.5 μ M Stattic	****	< 0.0001	****	< 0.0001
DMSO vs. 5 μ M Stattic	****	< 0.0001	****	< 0.0001
DMSO vs. 10 μ M Stattic	****	< 0.0001	****	< 0.0001
DMSO vs. 15 μ M Stattic	****	< 0.0001	****	< 0.0001
DMSO vs. 20 μ M Stattic	****	< 0.0001	****	< 0.0001
0.625 μ M Stattic vs. 1.25 μ M Stattic	n.s.	> 0.9999	n.s.	> 0.9999
0.625 μ M Stattic vs. 2.5 μ M Stattic	n.s.	0.9829	n.s.	0.6590
0.625 μ M Stattic vs. 5 μ M Stattic	n.s.	0.0532	**	0.0039
0.625 μ M Stattic vs. 10 μ M Stattic	****	< 0.0001	****	< 0.0001
0.625 μ M Stattic vs. 15 μ M Stattic	****	< 0.0001	****	< 0.0001
0.625 μ M Stattic vs. 20 μ M Stattic	****	< 0.0001	****	< 0.0001
1.25 μ M Stattic vs. 2.5 μ M Stattic	n.s.	0.8880	n.s.	0.5217
1.25 μ M Stattic vs. 5 μ M Stattic	*	0.0155	**	0.0018
1.25 μ M Stattic vs. 10 μ M Stattic	****	< 0.0001	****	< 0.0001
1.25 μ M Stattic vs. 15 μ M Stattic	****	< 0.0001	****	< 0.0001
1.25 μ M Stattic vs. 20 μ M Stattic	****	< 0.0001	****	< 0.0001
2.5 μ M Stattic vs. 5 μ M Stattic	n.s.	0.4954	n.s.	0.5141
2.5 μ M Stattic vs. 10 μ M Stattic	****	< 0.0001	****	< 0.0001
2.5 μ M Stattic vs. 15 μ M Stattic	****	< 0.0001	****	< 0.0001
2.5 μ M Stattic vs. 20 μ M Stattic	****	< 0.0001	****	< 0.0001
5 μ M Stattic vs. 10 μ M Stattic	*	0.0228	**	0.0040
5 μ M Stattic vs. 15 μ M Stattic	****	< 0.0001	****	< 0.0001
5 μ M Stattic vs. 20 μ M Stattic	****	< 0.0001	****	< 0.0001
10 μ M Stattic vs. 15 μ M Stattic	n.s.	0.7912	n.s.	0.3696
10 μ M Stattic vs. 20 μ M Stattic	**	0.0034	****	< 0.0001
15 μ M Stattic vs. 20 μ M Stattic	n.s.	0.3485	n.s.	0.0923

HTZ349	Significance	Adjusted p-vale	Significance	Adjusted p-vale
Category	16 h		24 h	
DMSO vs. 0.625 μ M Stattic	n.s.	> 0.9999	n.s.	0.9574
DMSO vs. 1.25 μ M Stattic	n.s.	> 0.9999	n.s.	0.9416
DMSO vs. 2.5 μ M Stattic	n.s.	> 0.9999	n.s.	0.7555
DMSO vs. 5 μ M Stattic	n.s.	0.9978	n.s.	0.4370
DMSO vs. 10 μ M Stattic	n.s.	0.7690	**	0.0072
DMSO vs. 15 μ M Stattic	n.s.	0.7263	**	0.0023
DMSO vs. 20 μ M Stattic	n.s.	0.5437	***	0.0002
0.625 μ M Stattic vs. 1.25 μ M Stattic	n.s.	> 0.9999	n.s.	> 0.9999
0.625 μ M Stattic vs. 2.5 μ M Stattic	n.s.	> 0.9999	n.s.	> 0.9999
0.625 μ M Stattic vs. 5 μ M Stattic	n.s.	> 0.9999	n.s.	0.9889
0.625 μ M Stattic vs. 10 μ M Stattic	n.s.	0.9596	n.s.	0.2258
0.625 μ M Stattic vs. 15 μ M Stattic	n.s.	0.9438	n.s.	0.1113
0.625 μ M Stattic vs. 20 μ M Stattic	n.s.	0.8448	*	0.0195
1.25 μ M Stattic vs. 2.5 μ M Stattic	n.s.	> 0.9999	n.s.	> 0.9999
1.25 μ M Stattic vs. 5 μ M Stattic	n.s.	> 0.9999	n.s.	0.9932
1.25 μ M Stattic vs. 10 μ M Stattic	n.s.	0.9045	n.s.	0.2591
1.25 μ M Stattic vs. 15 μ M Stattic	n.s.	0.8772	n.s.	0.1316
1.25 μ M Stattic vs. 20 μ M Stattic	n.s.	0.7343	*	0.0243
2.5 μ M Stattic vs. 5 μ M Stattic	n.s.	> 0.9999	n.s.	> 0.9999
2.5 μ M Stattic vs. 10 μ M Stattic	n.s.	0.9498	n.s.	0.5239
2.5 μ M Stattic vs. 15 μ M Stattic	n.s.	0.9315	n.s.	0.3235
2.5 μ M Stattic vs. 20 μ M Stattic	n.s.	0.8220	n.s.	0.0841
5 μ M Stattic vs. 10 μ M Stattic	n.s.	0.9927	n.s.	0.8265
5 μ M Stattic vs. 15 μ M Stattic	n.s.	0.9881	n.s.	0.6385
5 μ M Stattic vs. 20 μ M Stattic	n.s.	0.9466	n.s.	0.2536
10 μ M Stattic vs. 15 μ M Stattic	n.s.	> 0.9999	n.s.	> 0.9999
10 μ M Stattic vs. 20 μ M Stattic	n.s.	> 0.9999	n.s.	0.9926
15 μ M Stattic vs. 20 μ M Stattic	n.s.	> 0.9999	n.s.	0.9996

HTZ349	Significance	Adjusted p-vale	Significance	Adjusted p-vale
Category	40 h		48 h	
DMSO vs. 0.625 μ M Stattic	n.s.	0.9990	n.s.	0.6367
DMSO vs. 1.25 μ M Stattic	n.s.	0.9624	n.s.	0.3386
DMSO vs. 2.5 μ M Stattic	n.s.	0.5930	*	0.0246
DMSO vs. 5 μ M Stattic	*	0.0306	****	< 0.0001
DMSO vs. 10 μ M Stattic	****	< 0.0001	****	< 0.0001
DMSO vs. 15 μ M Stattic	****	< 0.0001	****	< 0.0001
DMSO vs. 20 μ M Stattic	****	< 0.0001	****	< 0.0001
0.625 μ M Stattic vs. 1.25 μ M Stattic	n.s.	> 0.9999	n.s.	> 0.9999
0.625 μ M Stattic vs. 2.5 μ M Stattic	n.s.	0.9453	n.s.	0.8619
0.625 μ M Stattic vs. 5 μ M Stattic	n.s.	0.1902	*	0.0332
0.625 μ M Stattic vs. 10 μ M Stattic	****	< 0.0001	****	< 0.0001
0.625 μ M Stattic vs. 15 μ M Stattic	****	< 0.0001	****	< 0.0001
0.625 μ M Stattic vs. 20 μ M Stattic	****	< 0.0001	****	< 0.0001
1.25 μ M Stattic vs. 2.5 μ M Stattic	n.s.	0.9978	n.s.	0.9814
1.25 μ M Stattic vs. 5 μ M Stattic	n.s.	0.4651	n.s.	0.1147
1.25 μ M Stattic vs. 10 μ M Stattic	****	< 0.0001	****	< 0.0001
1.25 μ M Stattic vs. 15 μ M Stattic	****	< 0.0001	****	< 0.0001
1.25 μ M Stattic vs. 20 μ M Stattic	****	< 0.0001	****	< 0.0001
2.5 μ M Stattic vs. 5 μ M Stattic	n.s.	0.9142	n.s.	0.7005
2.5 μ M Stattic vs. 10 μ M Stattic	****	< 0.0001	****	< 0.0001
2.5 μ M Stattic vs. 15 μ M Stattic	****	< 0.0001	****	< 0.0001
2.5 μ M Stattic vs. 20 μ M Stattic	****	< 0.0001	****	< 0.0001
5 μ M Stattic vs. 10 μ M Stattic	**	0.0060	***	0.0001
5 μ M Stattic vs. 15 μ M Stattic	****	< 0.0001	****	< 0.0001
5 μ M Stattic vs. 20 μ M Stattic	****	< 0.0001	****	< 0.0001
10 μ M Stattic vs. 15 μ M Stattic	n.s.	0.8947	n.s.	0.4400
10 μ M Stattic vs. 20 μ M Stattic	*	0.0323	****	< 0.0001
15 μ M Stattic vs. 20 μ M Stattic	n.s.	0.6422	n.s.	0.1808

U87	Significance	Adjusted p-vale	Significance	Adjusted p-vale
Category	16 h		24 h	
DMSO vs. 0.625 μ M Stattic	n.s.	> 0.9999	n.s.	> 0.9999
DMSO vs. 1.25 μ M Stattic	n.s.	> 0.9999	n.s.	> 0.9999
DMSO vs. 2.5 μ M Stattic	n.s.	0.9986	n.s.	0.9258
DMSO vs. 5 μ M Stattic	n.s.	0.6275	n.s.	0.0682
DMSO vs. 10 μ M Stattic	n.s.	0.2046	***	0.0004
DMSO vs. 15 μ M Stattic	n.s.	0.0654	****	< 0.0001
DMSO vs. 20 μ M Stattic	n.s.	0.0553	****	< 0.0001
0.625 μ M Stattic vs. 1.25 μ M Stattic	n.s.	> 0.9999	n.s.	> 0.9999
0.625 μ M Stattic vs. 2.5 μ M Stattic	n.s.	> 0.9999	n.s.	0.9937
0.625 μ M Stattic vs. 5 μ M Stattic	n.s.	0.7890	n.s.	0.1999
0.625 μ M Stattic vs. 10 μ M Stattic	n.s.	0.3367	**	0.0023
0.625 μ M Stattic vs. 15 μ M Stattic	n.s.	0.1269	****	< 0.0001
0.625 μ M Stattic vs. 20 μ M Stattic	n.s.	0.1096	****	< 0.0001
1.25 μ M Stattic vs. 2.5 μ M Stattic	n.s.	> 0.9999	n.s.	0.9958
1.25 μ M Stattic vs. 5 μ M Stattic	n.s.	0.8359	n.s.	0.2226
1.25 μ M Stattic vs. 10 μ M Stattic	n.s.	0.3913	**	0.0028
1.25 μ M Stattic vs. 15 μ M Stattic	n.s.	0.1566	***	0.0001
1.25 μ M Stattic vs. 20 μ M Stattic	n.s.	0.1362	***	0.0001
2.5 μ M Stattic vs. 5 μ M Stattic	n.s.	0.9625	n.s.	0.7499
2.5 μ M Stattic vs. 10 μ M Stattic	n.s.	0.6456	*	0.0479
2.5 μ M Stattic vs. 15 μ M Stattic	n.s.	0.3360	**	0.0039
2.5 μ M Stattic vs. 20 μ M Stattic	n.s.	0.3018	**	0.0035
5 μ M Stattic vs. 10 μ M Stattic	n.s.	0.9989	n.s.	0.8811
5 μ M Stattic vs. 15 μ M Stattic	n.s.	0.9666	n.s.	0.4152
5 μ M Stattic vs. 20 μ M Stattic	n.s.	0.9551	n.s.	0.3987
10 μ M Stattic vs. 15 μ M Stattic	n.s.	> 0.9999	n.s.	0.9980
10 μ M Stattic vs. 20 μ M Stattic	n.s.	0.9999	n.s.	0.9975
15 μ M Stattic vs. 20 μ M Stattic	n.s.	> 0.9999	n.s.	> 0.9999

U87	Significance	Adjusted p-value	Significance	Adjusted p-value
Category	40 h		48 h	
DMSO vs. 0.625 μ M Stattic	n.s.	0.1330	n.s.	0.1115
DMSO vs. 1.25 μ M Stattic	n.s.	0.1953	*	0.0498
DMSO vs. 2.5 μ M Stattic	**	0.0040	**	0.0063
DMSO vs. 5 μ M Stattic	****	< 0.0001	****	< 0.0001
DMSO vs. 10 μ M Stattic	****	< 0.0001	****	< 0.0001
DMSO vs. 15 μ M Stattic	****	< 0.0001	****	< 0.0001
DMSO vs. 20 μ M Stattic	****	< 0.0001	****	< 0.0001
0.625 μ M Stattic vs. 1.25 μ M Stattic	n.s.	> 0.9999	n.s.	> 0.9999
0.625 μ M Stattic vs. 2.5 μ M Stattic	n.s.	0.9708	n.s.	0.9915
0.625 μ M Stattic vs. 5 μ M Stattic	**	0.0071	**	0.0057
0.625 μ M Stattic vs. 10 μ M Stattic	****	< 0.0001	****	< 0.0001
0.625 μ M Stattic vs. 15 μ M Stattic	****	< 0.0001	****	< 0.0001
0.625 μ M Stattic vs. 20 μ M Stattic	****	< 0.0001	****	< 0.0001
1.25 μ M Stattic vs. 2.5 μ M Stattic	n.s.	0.9345	n.s.	0.9994
1.25 μ M Stattic vs. 5 μ M Stattic	**	0.0038	*	0.0160
1.25 μ M Stattic vs. 10 μ M Stattic	****	< 0.0001	****	< 0.0001
1.25 μ M Stattic vs. 15 μ M Stattic	****	< 0.0001	****	< 0.0001
1.25 μ M Stattic vs. 20 μ M Stattic	****	< 0.0001	****	< 0.0001
2.5 μ M Stattic vs. 5 μ M Stattic	n.s.	0.1915	n.s.	0.1031
2.5 μ M Stattic vs. 10 μ M Stattic	****	< 0.0001	****	< 0.0001
2.5 μ M Stattic vs. 15 μ M Stattic	****	< 0.0001	****	< 0.0001
2.5 μ M Stattic vs. 20 μ M Stattic	****	< 0.0001	****	< 0.0001
5 μ M Stattic vs. 10 μ M Stattic	n.s.	0.3585	n.s.	0.2481
5 μ M Stattic vs. 15 μ M Stattic	**	0.0044	****	< 0.0001
5 μ M Stattic vs. 20 μ M Stattic	**	0.0067	***	0.0008
10 μ M Stattic vs. 15 μ M Stattic	n.s.	0.8212	n.s.	0.3544
10 μ M Stattic vs. 20 μ M Stattic	n.s.	0.8747	n.s.	0.6781
15 μ M Stattic vs. 20 μ M Stattic	n.s.	> 0.9999	n.s.	> 0.9999

GBM lines	Significance	Adjusted p-value	Significance	Adjusted p-value
Category	16 h		24 h	
DMSO vs. 0.625 μ M Stattic	n.s.	0.9993	n.s.	0.8011
DMSO vs. 1.25 μ M Stattic	n.s.	> 0.9999	n.s.	0.8887
DMSO vs. 2.5 μ M Stattic	n.s.	0.9856	n.s.	0.1755
DMSO vs. 5 μ M Stattic	n.s.	0.4153	***	0.0005
DMSO vs. 10 μ M Stattic	*	0.0114	****	< 0.0001
DMSO vs. 15 μ M Stattic	**	0.0021	****	< 0.0001
DMSO vs. 20 μ M Stattic	***	0.0003	****	< 0.0001
0.625 μ M Stattic vs. 1.25 μ M Stattic	n.s.	> 0.9999	n.s.	> 0.9999
0.625 μ M Stattic vs. 2.5 μ M Stattic	n.s.	> 0.9999	n.s.	0.9838
0.625 μ M Stattic vs. 5 μ M Stattic	n.s.	0.8398	n.s.	0.1351
0.625 μ M Stattic vs. 10 μ M Stattic	n.s.	0.0874	****	< 0.0001
0.625 μ M Stattic vs. 15 μ M Stattic	*	0.0233	****	< 0.0001
0.625 μ M Stattic vs. 20 μ M Stattic	**	0.0050	****	< 0.0001
1.25 μ M Stattic vs. 2.5 μ M Stattic	n.s.	0.9995	n.s.	0.9554
1.25 μ M Stattic vs. 5 μ M Stattic	n.s.	0.6817	n.s.	0.0843
1.25 μ M Stattic vs. 10 μ M Stattic	*	0.0406	****	< 0.0001
1.25 μ M Stattic vs. 15 μ M Stattic	**	0.0093	****	< 0.0001
1.25 μ M Stattic vs. 20 μ M Stattic	**	0.0017	****	< 0.0001
2.5 μ M Stattic vs. 5 μ M Stattic	n.s.	0.9601	n.s.	0.7357
2.5 μ M Stattic vs. 10 μ M Stattic	n.s.	0.2051	**	0.0012
2.5 μ M Stattic vs. 15 μ M Stattic	n.s.	0.0675	****	< 0.0001
2.5 μ M Stattic vs. 20 μ M Stattic	*	0.0174	****	< 0.0001
5 μ M Stattic vs. 10 μ M Stattic	n.s.	0.9067	n.s.	0.2723
5 μ M Stattic vs. 15 μ M Stattic	n.s.	0.6687	*	0.0308
5 μ M Stattic vs. 20 μ M Stattic	n.s.	0.3690	**	0.0034
10 μ M Stattic vs. 15 μ M Stattic	n.s.	> 0.9999	n.s.	0.9955
10 μ M Stattic vs. 20 μ M Stattic	n.s.	0.9939	n.s.	0.8697
15 μ M Stattic vs. 20 μ M Stattic	n.s.	> 0.9999	n.s.	0.9995

GBM lines	Significance	Adjusted p-vale	Significance	Adjusted p-vale
Category	40 h		48 h	
DMSO vs. 0.625 μ M Stattic	*	0.0236	**	0.0018
DMSO vs. 1.25 μ M Stattic	*	0.0188	***	0.0004
DMSO vs. 2.5 μ M Stattic	****	< 0.0001	****	< 0.0001
DMSO vs. 5 μ M Stattic	****	< 0.0001	****	< 0.0001
DMSO vs. 10 μ M Stattic	****	< 0.0001	****	< 0.0001
DMSO vs. 15 μ M Stattic	****	< 0.0001	****	< 0.0001
DMSO vs. 20 μ M Stattic	****	< 0.0001	****	< 0.0001
0.625 μ M Stattic vs. 1.25 μ M Stattic	n.s.	> 0.9999	n.s.	> 0.9999
0.625 μ M Stattic vs. 2.5 μ M Stattic	n.s.	0.7384	n.s.	0.5492
0.625 μ M Stattic vs. 5 μ M Stattic	***	0.0001	****	< 0.0001
0.625 μ M Stattic vs. 10 μ M Stattic	****	< 0.0001	****	< 0.0001
0.625 μ M Stattic vs. 15 μ M Stattic	****	< 0.0001	****	< 0.0001
0.625 μ M Stattic vs. 20 μ M Stattic	****	< 0.0001	****	< 0.0001
1.25 μ M Stattic vs. 2.5 μ M Stattic	n.s.	0.7799	n.s.	0.7949
1.25 μ M Stattic vs. 5 μ M Stattic	***	0.0002	****	< 0.0001
1.25 μ M Stattic vs. 10 μ M Stattic	****	< 0.0001	****	< 0.0001
1.25 μ M Stattic vs. 15 μ M Stattic	****	< 0.0001	****	< 0.0001
1.25 μ M Stattic vs. 20 μ M Stattic	****	< 0.0001	****	< 0.0001
2.5 μ M Stattic vs. 5 μ M Stattic	n.s.	0.0767	*	0.0236
2.5 μ M Stattic vs. 10 μ M Stattic	****	< 0.0001	****	< 0.0001
2.5 μ M Stattic vs. 15 μ M Stattic	****	< 0.0001	****	< 0.0001
2.5 μ M Stattic vs. 20 μ M Stattic	****	< 0.0001	****	< 0.0001
5 μ M Stattic vs. 10 μ M Stattic	***	0.0002	****	< 0.0001
5 μ M Stattic vs. 15 μ M Stattic	****	< 0.0001	****	< 0.0001
5 μ M Stattic vs. 20 μ M Stattic	****	< 0.0001	****	< 0.0001
10 μ M Stattic vs. 15 μ M Stattic	n.s.	0.3715	*	0.0267
10 μ M Stattic vs. 20 μ M Stattic	**	0.0021	****	< 0.0001
15 μ M Stattic vs. 20 μ M Stattic	n.s.	0.7110	n.s.	0.4147

RAV17 BTIC	Significance	Adjusted p-value	Significance	Adjusted p-value
Category	16 h		24 h	
DMSO vs. 0.625 μ M Stattic	n.s.	0.9999	n.s.	> 0.9999
DMSO vs. 1.25 μ M Stattic	n.s.	0.8969	n.s.	0.6075
DMSO vs. 2.5 μ M Stattic	n.s.	0.5650	*	0.0398
DMSO vs. 5 μ M Stattic	*	0.0167	****	< 0.0001
DMSO vs. 10 μ M Stattic	****	< 0.0001	****	< 0.0001
DMSO vs. 15 μ M Stattic	****	< 0.0001	****	< 0.0001
DMSO vs. 20 μ M Stattic	****	< 0.0001	****	< 0.0001
0.625 μ M Stattic vs. 1.25 μ M Stattic	n.s.	0.9939	n.s.	0.6524
0.625 μ M Stattic vs. 2.5 μ M Stattic	n.s.	0.8782	*	0.0483
0.625 μ M Stattic vs. 5 μ M Stattic	n.s.	0.0808	****	< 0.0001
0.625 μ M Stattic vs. 10 μ M Stattic	****	< 0.0001	****	< 0.0001
0.625 μ M Stattic vs. 15 μ M Stattic	****	< 0.0001	****	< 0.0001
0.625 μ M Stattic vs. 20 μ M Stattic	****	< 0.0001	****	< 0.0001
1.25 μ M Stattic vs. 2.5 μ M Stattic	n.s.	0.9997	n.s.	0.9343
1.25 μ M Stattic vs. 5 μ M Stattic	n.s.	0.4951	**	0.0042
1.25 μ M Stattic vs. 10 μ M Stattic	****	< 0.0001	****	< 0.0001
1.25 μ M Stattic vs. 15 μ M Stattic	****	< 0.0001	****	< 0.0001
1.25 μ M Stattic vs. 20 μ M Stattic	****	< 0.0001	****	< 0.0001
2.5 μ M Stattic vs. 5 μ M Stattic	n.s.	0.8545	n.s.	0.2026
2.5 μ M Stattic vs. 10 μ M Stattic	***	0.0002	****	< 0.0001
2.5 μ M Stattic vs. 15 μ M Stattic	****	< 0.0001	****	< 0.0001
2.5 μ M Stattic vs. 20 μ M Stattic	****	< 0.0001	****	< 0.0001
5 μ M Stattic vs. 10 μ M Stattic	n.s.	0.0608	**	0.0065
5 μ M Stattic vs. 15 μ M Stattic	***	0.0009	****	< 0.0001
5 μ M Stattic vs. 20 μ M Stattic	***	0.0007	****	< 0.0001
10 μ M Stattic vs. 15 μ M Stattic	n.s.	0.9584	n.s.	0.4403
10 μ M Stattic vs. 20 μ M Stattic	n.s.	0.9423	n.s.	0.3805
15 μ M Stattic vs. 20 μ M Stattic	n.s.	> 0.9999	n.s.	> 0.9999

RAV17 BTIC	Significance	Adjusted p-vale	Significance	Adjusted p-vale
Category	40 h		48 h	
DMSO vs. 0.625 μ M Stattic	n.s.	0.2447	n.s.	0.1958
DMSO vs. 1.25 μ M Stattic	***	0.0005	*	0.0289
DMSO vs. 2.5 μ M Stattic	****	< 0.0001	****	< 0.0001
DMSO vs. 5 μ M Stattic	****	< 0.0001	****	< 0.0001
DMSO vs. 10 μ M Stattic	****	< 0.0001	****	< 0.0001
DMSO vs. 15 μ M Stattic	****	< 0.0001	****	< 0.0001
DMSO vs. 20 μ M Stattic	****	< 0.0001	****	< 0.0001
0.625 μ M Stattic vs. 1.25 μ M Stattic	n.s.	0.5937	n.s.	0.9986
0.625 μ M Stattic vs. 2.5 μ M Stattic	****	< 0.0001	**	0.0032
0.625 μ M Stattic vs. 5 μ M Stattic	****	< 0.0001	****	< 0.0001
0.625 μ M Stattic vs. 10 μ M Stattic	****	< 0.0001	****	< 0.0001
0.625 μ M Stattic vs. 15 μ M Stattic	****	< 0.0001	****	< 0.0001
0.625 μ M Stattic vs. 20 μ M Stattic	****	< 0.0001	****	< 0.0001
1.25 μ M Stattic vs. 2.5 μ M Stattic	n.s.	0.0759	*	0.0373
1.25 μ M Stattic vs. 5 μ M Stattic	****	< 0.0001	****	< 0.0001
1.25 μ M Stattic vs. 10 μ M Stattic	****	< 0.0001	****	< 0.0001
1.25 μ M Stattic vs. 15 μ M Stattic	****	< 0.0001	****	< 0.0001
1.25 μ M Stattic vs. 20 μ M Stattic	****	< 0.0001	****	< 0.0001
2.5 μ M Stattic vs. 5 μ M Stattic	n.s.	0.4347	**	0.0029
2.5 μ M Stattic vs. 10 μ M Stattic	****	< 0.0001	****	< 0.0001
2.5 μ M Stattic vs. 15 μ M Stattic	****	< 0.0001	****	< 0.0001
2.5 μ M Stattic vs. 20 μ M Stattic	****	< 0.0001	****	< 0.0001
5 μ M Stattic vs. 10 μ M Stattic	****	< 0.0001	****	< 0.0001
5 μ M Stattic vs. 15 μ M Stattic	****	< 0.0001	****	< 0.0001
5 μ M Stattic vs. 20 μ M Stattic	****	< 0.0001	****	< 0.0001
10 μ M Stattic vs. 15 μ M Stattic	****	< 0.0001	****	< 0.0001
10 μ M Stattic vs. 20 μ M Stattic	****	< 0.0001	****	< 0.0001
15 μ M Stattic vs. 20 μ M Stattic	n.s.	0.9987	n.s.	0.9878

RAV19 BTIC	Significance	Adjusted p-vale	Significance	Adjusted p-vale
Category	16 h		24 h	
DMSO vs. 0.625 μ M Stattic	n.s.	0.6252	n.s.	0.0697
DMSO vs. 1.25 μ M Stattic	n.s.	0.4752	*	0.0134
DMSO vs. 2.5 μ M Stattic	n.s.	0.0804	**	0.0011
DMSO vs. 5 μ M Stattic	**	0.0018	****	< 0.0001
DMSO vs. 10 μ M Stattic	****	< 0.0001	****	< 0.0001
DMSO vs. 15 μ M Stattic	****	< 0.0001	****	< 0.0001
DMSO vs. 20 μ M Stattic	****	< 0.0001	****	< 0.0001
0.625 μ M Stattic vs. 1.25 μ M Stattic	n.s.	> 0.9999	n.s.	0.9998
0.625 μ M Stattic vs. 2.5 μ M Stattic	n.s.	0.9785	n.s.	0.9563
0.625 μ M Stattic vs. 5 μ M Stattic	n.s.	0.4081	n.s.	0.0598
0.625 μ M Stattic vs. 10 μ M Stattic	****	< 0.0001	****	< 0.0001
0.625 μ M Stattic vs. 15 μ M Stattic	****	< 0.0001	****	< 0.0001
0.625 μ M Stattic vs. 20 μ M Stattic	****	< 0.0001	****	< 0.0001
1.25 μ M Stattic vs. 2.5 μ M Stattic	n.s.	0.9951	n.s.	0.9992
1.25 μ M Stattic vs. 5 μ M Stattic	n.s.	0.5555	n.s.	0.2238
1.25 μ M Stattic vs. 10 μ M Stattic	***	0.0002	****	< 0.0001
1.25 μ M Stattic vs. 15 μ M Stattic	****	< 0.0001	****	< 0.0001
1.25 μ M Stattic vs. 20 μ M Stattic	****	< 0.0001	****	< 0.0001
2.5 μ M Stattic vs. 5 μ M Stattic	n.s.	0.9689	n.s.	0.6423
2.5 μ M Stattic vs. 10 μ M Stattic	**	0.0059	****	< 0.0001
2.5 μ M Stattic vs. 15 μ M Stattic	****	< 0.0001	****	< 0.0001
2.5 μ M Stattic vs. 20 μ M Stattic	****	< 0.0001	****	< 0.0001
5 μ M Stattic vs. 10 μ M Stattic	n.s.	0.1759	**	0.0013
5 μ M Stattic vs. 15 μ M Stattic	***	0.0002	****	< 0.0001
5 μ M Stattic vs. 20 μ M Stattic	***	0.0005	****	< 0.0001
10 μ M Stattic vs. 15 μ M Stattic	n.s.	0.5811	n.s.	0.1532
10 μ M Stattic vs. 20 μ M Stattic	n.s.	0.7042	n.s.	0.2132
15 μ M Stattic vs. 20 μ M Stattic	n.s.	> 0.9999	n.s.	> 0.9999

RAV19 BTIC	Significance	Adjusted p-vale	Significance	Adjusted p-vale
Category	40 h		48 h	
DMSO vs. 0.625 μ M Stattic	**	0.0042	*	0.0140
DMSO vs. 1.25 μ M Stattic	****	< 0.0001	**	0.0032
DMSO vs. 2.5 μ M Stattic	****	< 0.0001	****	< 0.0001
DMSO vs. 5 μ M Stattic	****	< 0.0001	****	< 0.0001
DMSO vs. 10 μ M Stattic	****	< 0.0001	****	< 0.0001
DMSO vs. 15 μ M Stattic	****	< 0.0001	****	< 0.0001
DMSO vs. 20 μ M Stattic	****	< 0.0001	****	< 0.0001
0.625 μ M Stattic vs. 1.25 μ M Stattic	n.s.	0.7652	n.s.	> 0.9999
0.625 μ M Stattic vs. 2.5 μ M Stattic	*	0.0184	***	0.0008
0.625 μ M Stattic vs. 5 μ M Stattic	****	< 0.0001	****	< 0.0001
0.625 μ M Stattic vs. 10 μ M Stattic	****	< 0.0001	****	< 0.0001
0.625 μ M Stattic vs. 15 μ M Stattic	****	< 0.0001	****	< 0.0001
0.625 μ M Stattic vs. 20 μ M Stattic	****	< 0.0001	****	< 0.0001
1.25 μ M Stattic vs. 2.5 μ M Stattic	n.s.	0.6998	**	0.0039
1.25 μ M Stattic vs. 5 μ M Stattic	*	0.0123	****	< 0.0001
1.25 μ M Stattic vs. 10 μ M Stattic	****	< 0.0001	****	< 0.0001
1.25 μ M Stattic vs. 15 μ M Stattic	****	< 0.0001	****	< 0.0001
1.25 μ M Stattic vs. 20 μ M Stattic	****	< 0.0001	****	< 0.0001
2.5 μ M Stattic vs. 5 μ M Stattic	n.s.	0.6892	n.s.	0.1049
2.5 μ M Stattic vs. 10 μ M Stattic	****	< 0.0001	****	< 0.0001
2.5 μ M Stattic vs. 15 μ M Stattic	****	< 0.0001	****	< 0.0001
2.5 μ M Stattic vs. 20 μ M Stattic	****	< 0.0001	****	< 0.0001
5 μ M Stattic vs. 10 μ M Stattic	****	< 0.0001	****	< 0.0001
5 μ M Stattic vs. 15 μ M Stattic	****	< 0.0001	****	< 0.0001
5 μ M Stattic vs. 20 μ M Stattic	****	< 0.0001	****	< 0.0001
10 μ M Stattic vs. 15 μ M Stattic	****	< 0.0001	****	< 0.0001
10 μ M Stattic vs. 20 μ M Stattic	****	< 0.0001	****	< 0.0001
15 μ M Stattic vs. 20 μ M Stattic	n.s.	> 0.9999	n.s.	> 0.9999

RAV57 BTIC	Significance	Adjusted p-vale	Significance	Adjusted p-vale
Category	16 h		24 h	
DMSO vs. 0.625 μ M Stattic	n.s.	0.9503	n.s.	0.6538
DMSO vs. 1.25 μ M Stattic	n.s.	0.9137	n.s.	0.4580
DMSO vs. 2.5 μ M Stattic	n.s.	0.5795	*	0.0303
DMSO vs. 5 μ M Stattic	**	0.0035	****	< 0.0001
DMSO vs. 10 μ M Stattic	****	< 0.0001	****	< 0.0001
DMSO vs. 15 μ M Stattic	****	< 0.0001	****	< 0.0001
DMSO vs. 20 μ M Stattic	****	< 0.0001	****	< 0.0001
0.625 μ M Stattic vs. 1.25 μ M Stattic	n.s.	> 0.9999	n.s.	> 0.9999
0.625 μ M Stattic vs. 2.5 μ M Stattic	n.s.	0.9984	n.s.	0.8797
0.625 μ M Stattic vs. 5 μ M Stattic	n.s.	0.1568	**	0.0017
0.625 μ M Stattic vs. 10 μ M Stattic	**	0.0019	****	< 0.0001
0.625 μ M Stattic vs. 15 μ M Stattic	**	0.0024	****	< 0.0001
0.625 μ M Stattic vs. 20 μ M Stattic	**	0.0024	****	< 0.0001
1.25 μ M Stattic vs. 2.5 μ M Stattic	n.s.	0.9996	n.s.	0.9638
1.25 μ M Stattic vs. 5 μ M Stattic	n.s.	0.2089	**	0.0050
1.25 μ M Stattic vs. 10 μ M Stattic	**	0.0032	****	< 0.0001
1.25 μ M Stattic vs. 15 μ M Stattic	**	0.0039	****	< 0.0001
1.25 μ M Stattic vs. 20 μ M Stattic	**	0.0040	****	< 0.0001
2.5 μ M Stattic vs. 5 μ M Stattic	n.s.	0.5711	n.s.	0.1683
2.5 μ M Stattic vs. 10 μ M Stattic	*	0.0256	***	0.0002
2.5 μ M Stattic vs. 15 μ M Stattic	*	0.0305	****	< 0.0001
2.5 μ M Stattic vs. 20 μ M Stattic	*	0.0309	****	< 0.0001
5 μ M Stattic vs. 10 μ M Stattic	n.s.	0.9050	n.s.	0.5929
5 μ M Stattic vs. 15 μ M Stattic	n.s.	0.9241	n.s.	0.4142
5 μ M Stattic vs. 20 μ M Stattic	n.s.	0.9254	n.s.	0.3921
10 μ M Stattic vs. 15 μ M Stattic	n.s.	> 0.9999	n.s.	> 0.9999
10 μ M Stattic vs. 20 μ M Stattic	n.s.	> 0.9999	n.s.	> 0.9999
15 μ M Stattic vs. 20 μ M Stattic	n.s.	> 0.9999	n.s.	> 0.9999

RAV57 BTIC	Significance	Adjusted p-vale	Significance	Adjusted p-vale
Category	40 h		48 h	
DMSO vs. 0.625 μ M Stattic	****	< 0.0001	****	< 0.0001
DMSO vs. 1.25 μ M Stattic	****	< 0.0001	****	< 0.0001
DMSO vs. 2.5 μ M Stattic	****	< 0.0001	****	< 0.0001
DMSO vs. 5 μ M Stattic	****	< 0.0001	****	< 0.0001
DMSO vs. 10 μ M Stattic	****	< 0.0001	****	< 0.0001
DMSO vs. 15 μ M Stattic	****	< 0.0001	****	< 0.0001
DMSO vs. 20 μ M Stattic	****	< 0.0001	****	< 0.0001
0.625 μ M Stattic vs. 1.25 μ M Stattic	n.s.	0.9759	n.s.	0.9153
0.625 μ M Stattic vs. 2.5 μ M Stattic	n.s.	0.4038	n.s.	0.1880
0.625 μ M Stattic vs. 5 μ M Stattic	****	< 0.0001	****	< 0.0001
0.625 μ M Stattic vs. 10 μ M Stattic	****	< 0.0001	****	< 0.0001
0.625 μ M Stattic vs. 15 μ M Stattic	****	< 0.0001	****	< 0.0001
0.625 μ M Stattic vs. 20 μ M Stattic	****	< 0.0001	****	< 0.0001
1.25 μ M Stattic vs. 2.5 μ M Stattic	n.s.	0.9710	n.s.	0.9432
1.25 μ M Stattic vs. 5 μ M Stattic	****	< 0.0001	****	< 0.0001
1.25 μ M Stattic vs. 10 μ M Stattic	****	< 0.0001	****	< 0.0001
1.25 μ M Stattic vs. 15 μ M Stattic	****	< 0.0001	****	< 0.0001
1.25 μ M Stattic vs. 20 μ M Stattic	****	< 0.0001	****	< 0.0001
2.5 μ M Stattic vs. 5 μ M Stattic	***	0.0005	****	< 0.0001
2.5 μ M Stattic vs. 10 μ M Stattic	****	< 0.0001	****	< 0.0001
2.5 μ M Stattic vs. 15 μ M Stattic	****	< 0.0001	****	< 0.0001
2.5 μ M Stattic vs. 20 μ M Stattic	****	< 0.0001	****	< 0.0001
5 μ M Stattic vs. 10 μ M Stattic	***	0.0003	****	< 0.0001
5 μ M Stattic vs. 15 μ M Stattic	****	< 0.0001	****	< 0.0001
5 μ M Stattic vs. 20 μ M Stattic	****	< 0.0001	****	< 0.0001
10 μ M Stattic vs. 15 μ M Stattic	n.s.	0.9306	n.s.	0.6533
10 μ M Stattic vs. 20 μ M Stattic	n.s.	0.9129	n.s.	0.5892
15 μ M Stattic vs. 20 μ M Stattic	n.s.	> 0.9999	n.s.	> 0.9999

proneural BTIC	Significance	Adjusted p-value	Significance	Adjusted p-value
Category	16 h		24 h	
DMSO vs. 0.625 μ M Stattic	n.s.	0.8240	n.s.	0.3962
DMSO vs. 1.25 μ M Stattic	n.s.	0.5662	n.s.	0.0508
DMSO vs. 2.5 μ M Stattic	n.s.	0.1189	***	0.0005
DMSO vs. 5 μ M Stattic	****	< 0.0001	****	< 0.0001
DMSO vs. 10 μ M Stattic	****	< 0.0001	****	< 0.0001
DMSO vs. 15 μ M Stattic	****	< 0.0001	****	< 0.0001
DMSO vs. 20 μ M Stattic	****	< 0.0001	****	< 0.0001
0.625 μ M Stattic vs. 1.25 μ M Stattic	n.s.	> 0.9999	n.s.	0.9937
0.625 μ M Stattic vs. 2.5 μ M Stattic	n.s.	0.9506	n.s.	0.4397
0.625 μ M Stattic vs. 5 μ M Stattic	*	0.0411	****	< 0.0001
0.625 μ M Stattic vs. 10 μ M Stattic	****	< 0.0001	****	< 0.0001
0.625 μ M Stattic vs. 15 μ M Stattic	****	< 0.0001	****	< 0.0001
0.625 μ M Stattic vs. 20 μ M Stattic	****	< 0.0001	****	< 0.0001
1.25 μ M Stattic vs. 2.5 μ M Stattic	n.s.	0.9962	n.s.	0.9417
1.25 μ M Stattic vs. 5 μ M Stattic	n.s.	0.1257	**	0.0011
1.25 μ M Stattic vs. 10 μ M Stattic	****	< 0.0001	****	< 0.0001
1.25 μ M Stattic vs. 15 μ M Stattic	****	< 0.0001	****	< 0.0001
1.25 μ M Stattic vs. 20 μ M Stattic	****	< 0.0001	****	< 0.0001
2.5 μ M Stattic vs. 5 μ M Stattic	n.s.	0.5819	n.s.	0.0863
2.5 μ M Stattic vs. 10 μ M Stattic	***	0.0002	****	< 0.0001
2.5 μ M Stattic vs. 15 μ M Stattic	****	< 0.0001	****	< 0.0001
2.5 μ M Stattic vs. 20 μ M Stattic	****	< 0.0001	****	< 0.0001
5 μ M Stattic vs. 10 μ M Stattic	n.s.	0.1637	**	0.0055
5 μ M Stattic vs. 15 μ M Stattic	**	0.0061	****	< 0.0001
5 μ M Stattic vs. 20 μ M Stattic	**	0.0075	****	< 0.0001
10 μ M Stattic vs. 15 μ M Stattic	n.s.	0.9776	n.s.	0.6713
10 μ M Stattic vs. 20 μ M Stattic	n.s.	0.9839	n.s.	0.6809
15 μ M Stattic vs. 20 μ M Stattic	n.s.	> 0.9999	n.s.	> 0.9999

proneural BTIC	Significance	Adjusted p-value	Significance	Adjusted p-value
Category	40 h		48 h	
DMSO vs. 0.625 μ M Stattic	****	< 0.0001	****	< 0.0001
DMSO vs. 1.25 μ M Stattic	****	< 0.0001	****	< 0.0001
DMSO vs. 2.5 μ M Stattic	****	< 0.0001	****	< 0.0001
DMSO vs. 5 μ M Stattic	****	< 0.0001	****	< 0.0001
DMSO vs. 10 μ M Stattic	****	< 0.0001	****	< 0.0001
DMSO vs. 15 μ M Stattic	****	< 0.0001	****	< 0.0001
DMSO vs. 20 μ M Stattic	****	< 0.0001	****	< 0.0001
0.625 μ M Stattic vs. 1.25 μ M Stattic	n.s.	0.6824	n.s.	0.9739
0.625 μ M Stattic vs. 2.5 μ M Stattic	**	0.0026	***	0.0008
0.625 μ M Stattic vs. 5 μ M Stattic	****	< 0.0001	****	< 0.0001
0.625 μ M Stattic vs. 10 μ M Stattic	****	< 0.0001	****	< 0.0001
0.625 μ M Stattic vs. 15 μ M Stattic	****	< 0.0001	****	< 0.0001
0.625 μ M Stattic vs. 20 μ M Stattic	****	< 0.0001	****	< 0.0001
1.25 μ M Stattic vs. 2.5 μ M Stattic	n.s.	0.4370	*	0.0464
1.25 μ M Stattic vs. 5 μ M Stattic	****	< 0.0001	****	< 0.0001
1.25 μ M Stattic vs. 10 μ M Stattic	****	< 0.0001	****	< 0.0001
1.25 μ M Stattic vs. 15 μ M Stattic	****	< 0.0001	****	< 0.0001
1.25 μ M Stattic vs. 20 μ M Stattic	****	< 0.0001	****	< 0.0001
2.5 μ M Stattic vs. 5 μ M Stattic	**	0.0067	****	< 0.0001
2.5 μ M Stattic vs. 10 μ M Stattic	****	< 0.0001	****	< 0.0001
2.5 μ M Stattic vs. 15 μ M Stattic	****	< 0.0001	****	< 0.0001
2.5 μ M Stattic vs. 20 μ M Stattic	****	< 0.0001	****	< 0.0001
5 μ M Stattic vs. 10 μ M Stattic	****	< 0.0001	****	< 0.0001
5 μ M Stattic vs. 15 μ M Stattic	****	< 0.0001	****	< 0.0001
5 μ M Stattic vs. 20 μ M Stattic	****	< 0.0001	****	< 0.0001
10 μ M Stattic vs. 15 μ M Stattic	****	< 0.0001	****	< 0.0001
10 μ M Stattic vs. 20 μ M Stattic	****	< 0.0001	****	< 0.0001
15 μ M Stattic vs. 20 μ M Stattic	n.s.	> 0.9999	n.s.	> 0.9999

RAV17 TC	Significance	Adjusted p-vale	Significance	Adjusted p-vale
Category	16 h		24 h	
DMSO vs. 0.625 μ M Stattic	n.s.	0.9805	n.s.	0.8356
DMSO vs. 1.25 μ M Stattic	n.s.	0.7032	n.s.	0.4409
DMSO vs. 2.5 μ M Stattic	n.s.	0.6951	n.s.	0.4030
DMSO vs. 5 μ M Stattic	n.s.	0.0574	***	0.0001
DMSO vs. 10 μ M Stattic	**	0.0028	****	< 0.0001
DMSO vs. 15 μ M Stattic	**	0.0086	****	< 0.0001
DMSO vs. 20 μ M Stattic	**	0.0051	****	< 0.0001
0.625 μ M Stattic vs. 1.25 μ M Stattic	n.s.	0.9985	n.s.	0.9996
0.625 μ M Stattic vs. 2.5 μ M Stattic	n.s.	0.9983	n.s.	0.9991
0.625 μ M Stattic vs. 5 μ M Stattic	n.s.	0.5285	*	0.0402
0.625 μ M Stattic vs. 10 μ M Stattic	n.s.	0.0885	****	< 0.0001
0.625 μ M Stattic vs. 15 μ M Stattic	n.s.	0.1842	****	< 0.0001
0.625 μ M Stattic vs. 20 μ M Stattic	n.s.	0.1308	****	< 0.0001
1.25 μ M Stattic vs. 2.5 μ M Stattic	n.s.	> 0.9999	n.s.	> 0.9999
1.25 μ M Stattic vs. 5 μ M Stattic	n.s.	0.9295	n.s.	0.1965
1.25 μ M Stattic vs. 10 μ M Stattic	n.s.	0.4095	***	0.0003
1.25 μ M Stattic vs. 15 μ M Stattic	n.s.	0.6165	***	0.0004
1.25 μ M Stattic vs. 20 μ M Stattic	n.s.	0.5139	***	0.0001
2.5 μ M Stattic vs. 5 μ M Stattic	n.s.	0.9331	n.s.	0.2222
2.5 μ M Stattic vs. 10 μ M Stattic	n.s.	0.4176	***	0.0004
2.5 μ M Stattic vs. 15 μ M Stattic	n.s.	0.6251	***	0.0005
2.5 μ M Stattic vs. 20 μ M Stattic	n.s.	0.5225	***	0.0001
5 μ M Stattic vs. 10 μ M Stattic	n.s.	0.9933	n.s.	0.5963
5 μ M Stattic vs. 15 μ M Stattic	n.s.	0.9996	n.s.	0.6237
5 μ M Stattic vs. 20 μ M Stattic	n.s.	0.9982	n.s.	0.4354
10 μ M Stattic vs. 15 μ M Stattic	n.s.	> 0.9999	n.s.	> 0.9999
10 μ M Stattic vs. 20 μ M Stattic	n.s.	> 0.9999	n.s.	> 0.9999
15 μ M Stattic vs. 20 μ M Stattic	n.s.	> 0.9999	n.s.	> 0.9999

RAV17 TC	Significance	Adjusted p-vale	Significance	Adjusted p-vale
Category	40 h		48 h	
DMSO vs. 0.625 μ M Stattic	n.s.	0.0579	n.s.	0.1613
DMSO vs. 1.25 μ M Stattic	****	< 0.0001	****	< 0.0001
DMSO vs. 2.5 μ M Stattic	**	0.0038	*	0.0335
DMSO vs. 5 μ M Stattic	****	< 0.0001	****	< 0.0001
DMSO vs. 10 μ M Stattic	****	< 0.0001	****	< 0.0001
DMSO vs. 15 μ M Stattic	****	< 0.0001	****	< 0.0001
DMSO vs. 20 μ M Stattic	****	< 0.0001	****	< 0.0001
0.625 μ M Stattic vs. 1.25 μ M Stattic	n.s.	0.4337	n.s.	0.0912
0.625 μ M Stattic vs. 2.5 μ M Stattic	n.s.	0.9963	n.s.	0.9997
0.625 μ M Stattic vs. 5 μ M Stattic	****	< 0.0001	****	< 0.0001
0.625 μ M Stattic vs. 10 μ M Stattic	****	< 0.0001	****	< 0.0001
0.625 μ M Stattic vs. 15 μ M Stattic	****	< 0.0001	****	< 0.0001
0.625 μ M Stattic vs. 20 μ M Stattic	****	< 0.0001	****	< 0.0001
1.25 μ M Stattic vs. 2.5 μ M Stattic	n.s.	0.9181	n.s.	0.3314
1.25 μ M Stattic vs. 5 μ M Stattic	*	0.0113	***	0.0004
1.25 μ M Stattic vs. 10 μ M Stattic	****	< 0.0001	****	< 0.0001
1.25 μ M Stattic vs. 15 μ M Stattic	****	< 0.0001	****	< 0.0001
1.25 μ M Stattic vs. 20 μ M Stattic	****	< 0.0001	****	< 0.0001
2.5 μ M Stattic vs. 5 μ M Stattic	****	< 0.0001	****	< 0.0001
2.5 μ M Stattic vs. 10 μ M Stattic	****	< 0.0001	****	< 0.0001
2.5 μ M Stattic vs. 15 μ M Stattic	****	< 0.0001	****	< 0.0001
2.5 μ M Stattic vs. 20 μ M Stattic	****	< 0.0001	****	< 0.0001
5 μ M Stattic vs. 10 μ M Stattic	****	< 0.0001	****	< 0.0001
5 μ M Stattic vs. 15 μ M Stattic	****	< 0.0001	****	< 0.0001
5 μ M Stattic vs. 20 μ M Stattic	****	< 0.0001	****	< 0.0001
10 μ M Stattic vs. 15 μ M Stattic	n.s.	0.6642	n.s.	0.1380
10 μ M Stattic vs. 20 μ M Stattic	n.s.	0.4493	*	0.0447
15 μ M Stattic vs. 20 μ M Stattic	n.s.	> 0.9999	n.s.	> 0.9999

RAV19 TC	Significance	Adjusted p-vale	Significance	Adjusted p-vale
Category	16 h		24 h	
DMSO vs. 0.625 μ M Stattic	n.s.	0.9045	n.s.	0.7809
DMSO vs. 1.25 μ M Stattic	n.s.	0.6095	n.s.	0.2152
DMSO vs. 2.5 μ M Stattic	n.s.	0.0700	**	0.0072
DMSO vs. 5 μ M Stattic	n.s.	0.0620	**	0.0032
DMSO vs. 10 μ M Stattic	****	< 0.0001	****	< 0.0001
DMSO vs. 15 μ M Stattic	****	< 0.0001	****	< 0.0001
DMSO vs. 20 μ M Stattic	****	< 0.0001	****	< 0.0001
0.625 μ M Stattic vs. 1.25 μ M Stattic	n.s.	0.9999	n.s.	0.9928
0.625 μ M Stattic vs. 2.5 μ M Stattic	n.s.	0.7927	n.s.	0.4934
0.625 μ M Stattic vs. 5 μ M Stattic	n.s.	0.7676	n.s.	0.3478
0.625 μ M Stattic vs. 10 μ M Stattic	*	0.0213	**	0.0059
0.625 μ M Stattic vs. 15 μ M Stattic	*	0.0147	****	< 0.0001
0.625 μ M Stattic vs. 20 μ M Stattic	**	0.0051	****	< 0.0001
1.25 μ M Stattic vs. 2.5 μ M Stattic	n.s.	0.9747	n.s.	0.9618
1.25 μ M Stattic vs. 5 μ M Stattic	n.s.	0.9679	n.s.	0.8997
1.25 μ M Stattic vs. 10 μ M Stattic	n.s.	0.0990	n.s.	0.1003
1.25 μ M Stattic vs. 15 μ M Stattic	n.s.	0.0734	**	0.0018
1.25 μ M Stattic vs. 20 μ M Stattic	*	0.0307	***	0.0002
2.5 μ M Stattic vs. 5 μ M Stattic	n.s.	> 0.9999	n.s.	> 0.9999
2.5 μ M Stattic vs. 10 μ M Stattic	n.s.	0.6974	n.s.	0.7494
2.5 μ M Stattic vs. 15 μ M Stattic	n.s.	0.6216	n.s.	0.0911
2.5 μ M Stattic vs. 20 μ M Stattic	n.s.	0.4159	*	0.0190
5 μ M Stattic vs. 10 μ M Stattic	n.s.	0.7254	n.s.	0.8674
5 μ M Stattic vs. 15 μ M Stattic	n.s.	0.6514	n.s.	0.1579
5 μ M Stattic vs. 20 μ M Stattic	n.s.	0.4449	*	0.0382
10 μ M Stattic vs. 15 μ M Stattic	n.s.	> 0.9999	n.s.	0.9542
10 μ M Stattic vs. 20 μ M Stattic	n.s.	> 0.9999	n.s.	0.7220
15 μ M Stattic vs. 20 μ M Stattic	n.s.	> 0.9999	n.s.	0.9998

RAV19 TC	Significance	Adjusted p-vale	Significance	Adjusted p-vale
Category	40 h		48 h	
DMSO vs. 0.625 μ M Stattic	****	< 0.0001	****	< 0.0001
DMSO vs. 1.25 μ M Stattic	****	< 0.0001	****	< 0.0001
DMSO vs. 2.5 μ M Stattic	****	< 0.0001	****	< 0.0001
DMSO vs. 5 μ M Stattic	****	< 0.0001	****	< 0.0001
DMSO vs. 10 μ M Stattic	****	< 0.0001	****	< 0.0001
DMSO vs. 15 μ M Stattic	****	< 0.0001	****	< 0.0001
DMSO vs. 20 μ M Stattic	****	< 0.0001	****	< 0.0001
0.625 μ M Stattic vs. 1.25 μ M Stattic	n.s.	0.3232	n.s.	0.4535
0.625 μ M Stattic vs. 2.5 μ M Stattic	**	0.0015	****	< 0.0001
0.625 μ M Stattic vs. 5 μ M Stattic	****	< 0.0001	****	< 0.0001
0.625 μ M Stattic vs. 10 μ M Stattic	****	< 0.0001	****	< 0.0001
0.625 μ M Stattic vs. 15 μ M Stattic	****	< 0.0001	****	< 0.0001
0.625 μ M Stattic vs. 20 μ M Stattic	****	< 0.0001	****	< 0.0001
1.25 μ M Stattic vs. 2.5 μ M Stattic	n.s.	0.6899	**	0.0043
1.25 μ M Stattic vs. 5 μ M Stattic	n.s.	0.1502	**	0.0012
1.25 μ M Stattic vs. 10 μ M Stattic	****	< 0.0001	****	< 0.0001
1.25 μ M Stattic vs. 15 μ M Stattic	****	< 0.0001	****	< 0.0001
1.25 μ M Stattic vs. 20 μ M Stattic	****	< 0.0001	****	< 0.0001
2.5 μ M Stattic vs. 5 μ M Stattic	n.s.	0.9920	n.s.	> 0.9999
2.5 μ M Stattic vs. 10 μ M Stattic	****	< 0.0001	****	< 0.0001
2.5 μ M Stattic vs. 15 μ M Stattic	****	< 0.0001	****	< 0.0001
2.5 μ M Stattic vs. 20 μ M Stattic	****	< 0.0001	****	< 0.0001
5 μ M Stattic vs. 10 μ M Stattic	***	0.0003	****	< 0.0001
5 μ M Stattic vs. 15 μ M Stattic	****	< 0.0001	****	< 0.0001
5 μ M Stattic vs. 20 μ M Stattic	****	< 0.0001	****	< 0.0001
10 μ M Stattic vs. 15 μ M Stattic	n.s.	0.2071	**	0.0072
10 μ M Stattic vs. 20 μ M Stattic	**	0.0076	****	< 0.0001
15 μ M Stattic vs. 20 μ M Stattic	n.s.	0.9681	n.s.	0.9246

RAV57 TC	Significance	Adjusted p-vale	Significance	Adjusted p-vale
Category	16 h		24 h	
DMSO vs. 0.625 μ M Stattic	n.s.	0.4509	n.s.	0.9872
DMSO vs. 1.25 μ M Stattic	n.s.	0.4356	n.s.	0.0716
DMSO vs. 2.5 μ M Stattic	n.s.	0.2437	n.s.	0.2011
DMSO vs. 5 μ M Stattic	n.s.	0.1919	n.s.	0.1781
DMSO vs. 10 μ M Stattic	n.s.	0.1249	**	0.0031
DMSO vs. 15 μ M Stattic	n.s.	0.9792	n.s.	0.0511
DMSO vs. 20 μ M Stattic	n.s.	0.2244	***	0.0002
0.625 μ M Stattic vs. 1.25 μ M Stattic	n.s.	> 0.9999	n.s.	0.5373
0.625 μ M Stattic vs. 2.5 μ M Stattic	n.s.	> 0.9999	n.s.	0.8094
0.625 μ M Stattic vs. 5 μ M Stattic	n.s.	> 0.9999	n.s.	0.7786
0.625 μ M Stattic vs. 10 μ M Stattic	n.s.	0.9993	n.s.	0.0783
0.625 μ M Stattic vs. 15 μ M Stattic	n.s.	0.9776	n.s.	0.4549
0.625 μ M Stattic vs. 20 μ M Stattic	n.s.	> 0.9999	*	0.0120
1.25 μ M Stattic vs. 2.5 μ M Stattic	n.s.	> 0.9999	n.s.	> 0.9999
1.25 μ M Stattic vs. 5 μ M Stattic	n.s.	> 0.9999	n.s.	> 0.9999
1.25 μ M Stattic vs. 10 μ M Stattic	n.s.	0.9995	n.s.	0.9897
1.25 μ M Stattic vs. 15 μ M Stattic	n.s.	0.9745	n.s.	> 0.9999
1.25 μ M Stattic vs. 20 μ M Stattic	n.s.	> 0.9999	n.s.	0.8259
2.5 μ M Stattic vs. 5 μ M Stattic	n.s.	> 0.9999	n.s.	> 0.9999
2.5 μ M Stattic vs. 10 μ M Stattic	n.s.	> 0.9999	n.s.	0.9084
2.5 μ M Stattic vs. 15 μ M Stattic	n.s.	0.8889	n.s.	0.9998
2.5 μ M Stattic vs. 20 μ M Stattic	n.s.	> 0.9999	n.s.	0.5591
5 μ M Stattic vs. 10 μ M Stattic	n.s.	> 0.9999	n.s.	0.9265
5 μ M Stattic vs. 15 μ M Stattic	n.s.	0.8385	n.s.	> 0.9999
5 μ M Stattic vs. 20 μ M Stattic	n.s.	> 0.9999	n.s.	0.5976
10 μ M Stattic vs. 15 μ M Stattic	n.s.	0.7345	n.s.	0.9958
10 μ M Stattic vs. 20 μ M Stattic	n.s.	> 0.9999	n.s.	0.9996
15 μ M Stattic vs. 20 μ M Stattic	n.s.	0.8723	n.s.	0.8814

RAV57 TC	Significance	Adjusted p-vale	Significance	Adjusted p-vale
Category	40 h		48 h	
DMSO vs. 0.625 μ M Stattic	***	0.0003	****	< 0.0001
DMSO vs. 1.25 μ M Stattic	****	< 0.0001	****	< 0.0001
DMSO vs. 2.5 μ M Stattic	****	< 0.0001	****	< 0.0001
DMSO vs. 5 μ M Stattic	****	< 0.0001	****	< 0.0001
DMSO vs. 10 μ M Stattic	****	< 0.0001	****	< 0.0001
DMSO vs. 15 μ M Stattic	****	< 0.0001	****	< 0.0001
DMSO vs. 20 μ M Stattic	****	< 0.0001	****	< 0.0001
0.625 μ M Stattic vs. 1.25 μ M Stattic	n.s.	0.9998	n.s.	0.3576
0.625 μ M Stattic vs. 2.5 μ M Stattic	n.s.	0.9939	n.s.	0.8622
0.625 μ M Stattic vs. 5 μ M Stattic	n.s.	0.9995	n.s.	0.9986
0.625 μ M Stattic vs. 10 μ M Stattic	****	< 0.0001	****	< 0.0001
0.625 μ M Stattic vs. 15 μ M Stattic	****	< 0.0001	****	< 0.0001
0.625 μ M Stattic vs. 20 μ M Stattic	****	< 0.0001	****	< 0.0001
1.25 μ M Stattic vs. 2.5 μ M Stattic	n.s.	> 0.9999	n.s.	0.9970
1.25 μ M Stattic vs. 5 μ M Stattic	n.s.	> 0.9999	n.s.	0.8206
1.25 μ M Stattic vs. 10 μ M Stattic	***	0.0007	***	0.0003
1.25 μ M Stattic vs. 15 μ M Stattic	****	< 0.0001	****	< 0.0001
1.25 μ M Stattic vs. 20 μ M Stattic	****	< 0.0001	****	< 0.0001
2.5 μ M Stattic vs. 5 μ M Stattic	n.s.	> 0.9999	n.s.	0.9975
2.5 μ M Stattic vs. 10 μ M Stattic	**	0.0027	****	< 0.0001
2.5 μ M Stattic vs. 15 μ M Stattic	****	< 0.0001	****	< 0.0001
2.5 μ M Stattic vs. 20 μ M Stattic	****	< 0.0001	****	< 0.0001
5 μ M Stattic vs. 10 μ M Stattic	***	0.0009	****	< 0.0001
5 μ M Stattic vs. 15 μ M Stattic	****	< 0.0001	****	< 0.0001
5 μ M Stattic vs. 20 μ M Stattic	****	< 0.0001	****	< 0.0001
10 μ M Stattic vs. 15 μ M Stattic	n.s.	0.0797	***	0.0001
10 μ M Stattic vs. 20 μ M Stattic	**	0.0017	****	< 0.0001
15 μ M Stattic vs. 20 μ M Stattic	n.s.	0.9677	n.s.	> 0.9999

proneural TC	Significance	Adjusted p-vale	Significance	Adjusted p-vale
Category	16 h		24 h	
DMSO vs. 0.625 μ M Stattic	n.s.	0.9961	n.s.	0.9882
DMSO vs. 1.25 μ M Stattic	n.s.	0.9591	n.s.	0.8426
DMSO vs. 2.5 μ M Stattic	n.s.	0.8532	n.s.	0.6600
DMSO vs. 5 μ M Stattic	n.s.	0.5999	n.s.	0.1597
DMSO vs. 10 μ M Stattic	n.s.	0.1599	**	0.0061
DMSO vs. 15 μ M Stattic	n.s.	0.2328	**	0.0022
DMSO vs. 20 μ M Stattic	n.s.	0.1430	***	0.0006
0.625 μ M Stattic vs. 1.25 μ M Stattic	n.s.	> 0.9999	n.s.	0.9998
0.625 μ M Stattic vs. 2.5 μ M Stattic	n.s.	0.9990	n.s.	0.9949
0.625 μ M Stattic vs. 5 μ M Stattic	n.s.	0.9751	n.s.	0.7487
0.625 μ M Stattic vs. 10 μ M Stattic	n.s.	0.6524	n.s.	0.1275
0.625 μ M Stattic vs. 15 μ M Stattic	n.s.	0.7621	n.s.	0.0638
0.625 μ M Stattic vs. 20 μ M Stattic	n.s.	0.6201	*	0.0244
1.25 μ M Stattic vs. 2.5 μ M Stattic	n.s.	> 0.9999	n.s.	> 0.9999
1.25 μ M Stattic vs. 5 μ M Stattic	n.s.	0.9983	n.s.	0.9676
1.25 μ M Stattic vs. 10 μ M Stattic	n.s.	0.8640	n.s.	0.4000
1.25 μ M Stattic vs. 15 μ M Stattic	n.s.	0.9278	n.s.	0.2480
1.25 μ M Stattic vs. 20 μ M Stattic	n.s.	0.8419	n.s.	0.1208
2.5 μ M Stattic vs. 5 μ M Stattic	n.s.	> 0.9999	n.s.	0.9957
2.5 μ M Stattic vs. 10 μ M Stattic	n.s.	0.9637	n.s.	0.6112
2.5 μ M Stattic vs. 15 μ M Stattic	n.s.	0.9864	n.s.	0.4301
2.5 μ M Stattic vs. 20 μ M Stattic	n.s.	0.9542	n.s.	0.2430
5 μ M Stattic vs. 10 μ M Stattic	n.s.	0.9980	n.s.	0.9787
5 μ M Stattic vs. 15 μ M Stattic	n.s.	0.9997	n.s.	0.9233
5 μ M Stattic vs. 20 μ M Stattic	n.s.	0.9970	n.s.	0.7811
10 μ M Stattic vs. 15 μ M Stattic	n.s.	> 0.9999	n.s.	> 0.9999
10 μ M Stattic vs. 20 μ M Stattic	n.s.	> 0.9999	n.s.	0.9997
15 μ M Stattic vs. 20 μ M Stattic	n.s.	> 0.9999	n.s.	> 0.9999

proneural TC	Significance	Adjusted p-value	Significance	Adjusted p-value
Category	40 h		48 h	
DMSO vs. 0.625 μ M Stattic	n.s.	0.2124	n.s.	0.2043
DMSO vs. 1.25 μ M Stattic	**	0.0037	**	0.0011
DMSO vs. 2.5 μ M Stattic	**	0.0026	***	0.0003
DMSO vs. 5 μ M Stattic	****	< 0.0001	****	< 0.0001
DMSO vs. 10 μ M Stattic	****	< 0.0001	****	< 0.0001
DMSO vs. 15 μ M Stattic	****	< 0.0001	****	< 0.0001
DMSO vs. 20 μ M Stattic	****	< 0.0001	****	< 0.0001
0.625 μ M Stattic vs. 1.25 μ M Stattic	n.s.	0.9247	n.s.	0.8032
0.625 μ M Stattic vs. 2.5 μ M Stattic	n.s.	0.8934	n.s.	0.6307
0.625 μ M Stattic vs. 5 μ M Stattic	*	0.0440	**	0.0022
0.625 μ M Stattic vs. 10 μ M Stattic	****	< 0.0001	****	< 0.0001
0.625 μ M Stattic vs. 15 μ M Stattic	****	< 0.0001	****	< 0.0001
0.625 μ M Stattic vs. 20 μ M Stattic	****	< 0.0001	****	< 0.0001
1.25 μ M Stattic vs. 2.5 μ M Stattic	n.s.	> 0.9999	n.s.	> 0.9999
1.25 μ M Stattic vs. 5 μ M Stattic	n.s.	0.6636	n.s.	0.2895
1.25 μ M Stattic vs. 10 μ M Stattic	****	< 0.0001	****	< 0.0001
1.25 μ M Stattic vs. 15 μ M Stattic	****	< 0.0001	****	< 0.0001
1.25 μ M Stattic vs. 20 μ M Stattic	****	< 0.0001	****	< 0.0001
2.5 μ M Stattic vs. 5 μ M Stattic	n.s.	0.7226	n.s.	0.4608
2.5 μ M Stattic vs. 10 μ M Stattic	****	< 0.0001	****	< 0.0001
2.5 μ M Stattic vs. 15 μ M Stattic	****	< 0.0001	****	< 0.0001
2.5 μ M Stattic vs. 20 μ M Stattic	****	< 0.0001	****	< 0.0001
5 μ M Stattic vs. 10 μ M Stattic	**	0.0048	****	< 0.0001
5 μ M Stattic vs. 15 μ M Stattic	****	< 0.0001	****	< 0.0001
5 μ M Stattic vs. 20 μ M Stattic	****	< 0.0001	****	< 0.0001
10 μ M Stattic vs. 15 μ M Stattic	n.s.	0.8859	n.s.	0.4525
10 μ M Stattic vs. 20 μ M Stattic	n.s.	0.6122	n.s.	0.1700
15 μ M Stattic vs. 20 μ M Stattic	n.s.	> 0.9999	n.s.	0.9999

RAV21 BTIC	Significance	Adjusted p-vale	Significance	Adjusted p-vale
Category	16 h		24 h	
DMSO vs. 0.625 μ M Stattic	n.s.	> 0.9999	n.s.	0.9275
DMSO vs. 1.25 μ M Stattic	n.s.	> 0.9999	n.s.	0.4116
DMSO vs. 2.5 μ M Stattic	n.s.	0.9548	**	0.0036
DMSO vs. 5 μ M Stattic	n.s.	0.2592	***	0.0002
DMSO vs. 10 μ M Stattic	****	< 0.0001	****	< 0.0001
DMSO vs. 15 μ M Stattic	****	< 0.0001	****	< 0.0001
DMSO vs. 20 μ M Stattic	****	< 0.0001	****	< 0.0001
0.625 μ M Stattic vs. 1.25 μ M Stattic	n.s.	> 0.9999	n.s.	0.9938
0.625 μ M Stattic vs. 2.5 μ M Stattic	n.s.	0.9927	n.s.	0.1949
0.625 μ M Stattic vs. 5 μ M Stattic	n.s.	0.4412	*	0.0302
0.625 μ M Stattic vs. 10 μ M Stattic	****	< 0.0001	****	< 0.0001
0.625 μ M Stattic vs. 15 μ M Stattic	****	< 0.0001	****	< 0.0001
0.625 μ M Stattic vs. 20 μ M Stattic	****	< 0.0001	****	< 0.0001
1.25 μ M Stattic vs. 2.5 μ M Stattic	n.s.	0.9976	n.s.	0.7426
1.25 μ M Stattic vs. 5 μ M Stattic	n.s.	0.5351	n.s.	0.2844
1.25 μ M Stattic vs. 10 μ M Stattic	****	< 0.0001	****	< 0.0001
1.25 μ M Stattic vs. 15 μ M Stattic	****	< 0.0001	****	< 0.0001
1.25 μ M Stattic vs. 20 μ M Stattic	****	< 0.0001	****	< 0.0001
2.5 μ M Stattic vs. 5 μ M Stattic	n.s.	0.9456	n.s.	0.9988
2.5 μ M Stattic vs. 10 μ M Stattic	****	< 0.0001	****	< 0.0001
2.5 μ M Stattic vs. 15 μ M Stattic	****	< 0.0001	****	< 0.0001
2.5 μ M Stattic vs. 20 μ M Stattic	****	< 0.0001	****	< 0.0001
5 μ M Stattic vs. 10 μ M Stattic	****	< 0.0001	****	< 0.0001
5 μ M Stattic vs. 15 μ M Stattic	****	< 0.0001	****	< 0.0001
5 μ M Stattic vs. 20 μ M Stattic	****	< 0.0001	****	< 0.0001
10 μ M Stattic vs. 15 μ M Stattic	n.s.	0.9980	n.s.	0.9197
10 μ M Stattic vs. 20 μ M Stattic	n.s.	0.9979	n.s.	0.6350
15 μ M Stattic vs. 20 μ M Stattic	n.s.	> 0.9999	n.s.	0.9998

RAV21 BTIC	Significance	Adjusted p-vale	Significance	Adjusted p-vale
Category	40 h		48 h	
DMSO vs. 0.625 μ M Stattic	n.s.	0.1696	n.s.	0.0630
DMSO vs. 1.25 μ M Stattic	**	0.0018	***	0.0001
DMSO vs. 2.5 μ M Stattic	****	< 0.0001	**	0.0016
DMSO vs. 5 μ M Stattic	****	< 0.0001	****	< 0.0001
DMSO vs. 10 μ M Stattic	****	< 0.0001	****	< 0.0001
DMSO vs. 15 μ M Stattic	****	< 0.0001	****	< 0.0001
DMSO vs. 20 μ M Stattic	****	< 0.0001	****	< 0.0001
0.625 μ M Stattic vs. 1.25 μ M Stattic	n.s.	0.8848	n.s.	0.7697
0.625 μ M Stattic vs. 2.5 μ M Stattic	n.s.	0.4028	n.s.	0.9787
0.625 μ M Stattic vs. 5 μ M Stattic	***	0.0005	***	0.0002
0.625 μ M Stattic vs. 10 μ M Stattic	****	< 0.0001	****	< 0.0001
0.625 μ M Stattic vs. 15 μ M Stattic	****	< 0.0001	****	< 0.0001
0.625 μ M Stattic vs. 20 μ M Stattic	****	< 0.0001	****	< 0.0001
1.25 μ M Stattic vs. 2.5 μ M Stattic	n.s.	0.9974	n.s.	0.9996
1.25 μ M Stattic vs. 5 μ M Stattic	n.s.	0.0765	n.s.	0.0919
1.25 μ M Stattic vs. 10 μ M Stattic	****	< 0.0001	****	< 0.0001
1.25 μ M Stattic vs. 15 μ M Stattic	****	< 0.0001	****	< 0.0001
1.25 μ M Stattic vs. 20 μ M Stattic	****	< 0.0001	****	< 0.0001
2.5 μ M Stattic vs. 5 μ M Stattic	n.s.	0.4119	*	0.0154
2.5 μ M Stattic vs. 10 μ M Stattic	****	< 0.0001	****	< 0.0001
2.5 μ M Stattic vs. 15 μ M Stattic	****	< 0.0001	****	< 0.0001
2.5 μ M Stattic vs. 20 μ M Stattic	****	< 0.0001	****	< 0.0001
5 μ M Stattic vs. 10 μ M Stattic	****	< 0.0001	****	< 0.0001
5 μ M Stattic vs. 15 μ M Stattic	****	< 0.0001	****	< 0.0001
5 μ M Stattic vs. 20 μ M Stattic	****	< 0.0001	****	< 0.0001
10 μ M Stattic vs. 15 μ M Stattic	n.s.	0.2995	*	0.0157
10 μ M Stattic vs. 20 μ M Stattic	***	0.0007	****	< 0.0001
15 μ M Stattic vs. 20 μ M Stattic	n.s.	0.5891	n.s.	0.0872

RAV26 BTIC	Significance	Adjusted p-vale	Significance	Adjusted p-vale
Category	16 h		24 h	
DMSO vs. 0.625 μ M Stattic	n.s.	0.9965	n.s.	0.0770
DMSO vs. 1.25 μ M Stattic	n.s.	0.8563	****	< 0.0001
DMSO vs. 2.5 μ M Stattic	n.s.	0.2050	****	< 0.0001
DMSO vs. 5 μ M Stattic	**	0.0032	****	< 0.0001
DMSO vs. 10 μ M Stattic	****	< 0.0001	****	< 0.0001
DMSO vs. 15 μ M Stattic	****	< 0.0001	****	< 0.0001
DMSO vs. 20 μ M Stattic	****	< 0.0001	****	< 0.0001
0.625 μ M Stattic vs. 1.25 μ M Stattic	n.s.	0.9989	n.s.	0.1539
0.625 μ M Stattic vs. 2.5 μ M Stattic	n.s.	0.7116	**	0.0018
0.625 μ M Stattic vs. 5 μ M Stattic	*	0.0492	****	< 0.0001
0.625 μ M Stattic vs. 10 μ M Stattic	***	0.0005	****	< 0.0001
0.625 μ M Stattic vs. 15 μ M Stattic	****	< 0.0001	****	< 0.0001
0.625 μ M Stattic vs. 20 μ M Stattic	****	< 0.0001	****	< 0.0001
1.25 μ M Stattic vs. 2.5 μ M Stattic	n.s.	0.9783	n.s.	0.9045
1.25 μ M Stattic vs. 5 μ M Stattic	n.s.	0.2660	n.s.	0.1364
1.25 μ M Stattic vs. 10 μ M Stattic	**	0.0072	***	0.0004
1.25 μ M Stattic vs. 15 μ M Stattic	****	< 0.0001	****	< 0.0001
1.25 μ M Stattic vs. 20 μ M Stattic	****	< 0.0001	****	< 0.0001
2.5 μ M Stattic vs. 5 μ M Stattic	n.s.	0.9080	n.s.	0.9108
2.5 μ M Stattic vs. 10 μ M Stattic	n.s.	0.1718	n.s.	0.0557
2.5 μ M Stattic vs. 15 μ M Stattic	**	0.0058	***	0.0001
2.5 μ M Stattic vs. 20 μ M Stattic	***	0.0008	****	< 0.0001
5 μ M Stattic vs. 10 μ M Stattic	n.s.	0.9382	n.s.	0.7338
5 μ M Stattic vs. 15 μ M Stattic	n.s.	0.2859	*	0.0235
5 μ M Stattic vs. 20 μ M Stattic	n.s.	0.0922	**	0.0028
10 μ M Stattic vs. 15 μ M Stattic	n.s.	0.9697	n.s.	0.7782
10 μ M Stattic vs. 20 μ M Stattic	n.s.	0.7905	n.s.	0.3763
15 μ M Stattic vs. 20 μ M Stattic	n.s.	> 0.9999	n.s.	0.9996

RAV26 BTIC	Significance	Adjusted p-vale	Significance	Adjusted p-vale
Category	40 h		48 h	
DMSO vs. 0.625 μ M Stattic	****	< 0.0001	****	< 0.0001
DMSO vs. 1.25 μ M Stattic	****	< 0.0001	****	< 0.0001
DMSO vs. 2.5 μ M Stattic	****	< 0.0001	****	< 0.0001
DMSO vs. 5 μ M Stattic	****	< 0.0001	****	< 0.0001
DMSO vs. 10 μ M Stattic	****	< 0.0001	****	< 0.0001
DMSO vs. 15 μ M Stattic	****	< 0.0001	****	< 0.0001
DMSO vs. 20 μ M Stattic	****	< 0.0001	****	< 0.0001
0.625 μ M Stattic vs. 1.25 μ M Stattic	****	< 0.0001	***	0.0007
0.625 μ M Stattic vs. 2.5 μ M Stattic	****	< 0.0001	****	< 0.0001
0.625 μ M Stattic vs. 5 μ M Stattic	****	< 0.0001	****	< 0.0001
0.625 μ M Stattic vs. 10 μ M Stattic	****	< 0.0001	****	< 0.0001
0.625 μ M Stattic vs. 15 μ M Stattic	****	< 0.0001	****	< 0.0001
0.625 μ M Stattic vs. 20 μ M Stattic	****	< 0.0001	****	< 0.0001
1.25 μ M Stattic vs. 2.5 μ M Stattic	****	< 0.0001	****	< 0.0001
1.25 μ M Stattic vs. 5 μ M Stattic	****	< 0.0001	****	< 0.0001
1.25 μ M Stattic vs. 10 μ M Stattic	****	< 0.0001	****	< 0.0001
1.25 μ M Stattic vs. 15 μ M Stattic	****	< 0.0001	****	< 0.0001
1.25 μ M Stattic vs. 20 μ M Stattic	****	< 0.0001	****	< 0.0001
2.5 μ M Stattic vs. 5 μ M Stattic	****	< 0.0001	****	< 0.0001
2.5 μ M Stattic vs. 10 μ M Stattic	****	< 0.0001	****	< 0.0001
2.5 μ M Stattic vs. 15 μ M Stattic	****	< 0.0001	****	< 0.0001
2.5 μ M Stattic vs. 20 μ M Stattic	****	< 0.0001	****	< 0.0001
5 μ M Stattic vs. 10 μ M Stattic	**	0.0023	***	0.0007
5 μ M Stattic vs. 15 μ M Stattic	****	< 0.0001	****	< 0.0001
5 μ M Stattic vs. 20 μ M Stattic	****	< 0.0001	****	< 0.0001
10 μ M Stattic vs. 15 μ M Stattic	n.s.	0.3397	n.s.	0.0606
10 μ M Stattic vs. 20 μ M Stattic	*	0.0128	***	0.0002
15 μ M Stattic vs. 20 μ M Stattic	n.s.	0.9467	n.s.	0.8469

RAV27 BTIC	Significance	Adjusted p-vale	Significance	Adjusted p-vale
Category	16 h		24 h	
DMSO vs. 0.625 μ M Stattic	n.s.	0.9453	n.s.	0.6119
DMSO vs. 1.25 μ M Stattic	n.s.	0.7546	n.s.	0.1686
DMSO vs. 2.5 μ M Stattic	*	0.0153	****	< 0.0001
DMSO vs. 5 μ M Stattic	****	< 0.0001	****	< 0.0001
DMSO vs. 10 μ M Stattic	****	< 0.0001	****	< 0.0001
DMSO vs. 15 μ M Stattic	****	< 0.0001	****	< 0.0001
DMSO vs. 20 μ M Stattic	****	< 0.0001	****	< 0.0001
0.625 μ M Stattic vs. 1.25 μ M Stattic	n.s.	> 0.9999	n.s.	0.9980
0.625 μ M Stattic vs. 2.5 μ M Stattic	n.s.	0.3755	**	0.0053
0.625 μ M Stattic vs. 5 μ M Stattic	*	0.0141	****	< 0.0001
0.625 μ M Stattic vs. 10 μ M Stattic	****	< 0.0001	****	< 0.0001
0.625 μ M Stattic vs. 15 μ M Stattic	****	< 0.0001	****	< 0.0001
0.625 μ M Stattic vs. 20 μ M Stattic	****	< 0.0001	****	< 0.0001
1.25 μ M Stattic vs. 2.5 μ M Stattic	n.s.	0.6749	n.s.	0.0612
1.25 μ M Stattic vs. 5 μ M Stattic	n.s.	0.0558	***	0.0002
1.25 μ M Stattic vs. 10 μ M Stattic	****	< 0.0001	****	< 0.0001
1.25 μ M Stattic vs. 15 μ M Stattic	****	< 0.0001	****	< 0.0001
1.25 μ M Stattic vs. 20 μ M Stattic	****	< 0.0001	****	< 0.0001
2.5 μ M Stattic vs. 5 μ M Stattic	n.s.	0.9390	n.s.	0.8321
2.5 μ M Stattic vs. 10 μ M Stattic	***	0.0008	****	< 0.0001
2.5 μ M Stattic vs. 15 μ M Stattic	****	< 0.0001	****	< 0.0001
2.5 μ M Stattic vs. 20 μ M Stattic	****	< 0.0001	****	< 0.0001
5 μ M Stattic vs. 10 μ M Stattic	n.s.	0.0681	***	0.0001
5 μ M Stattic vs. 15 μ M Stattic	****	< 0.0001	****	< 0.0001
5 μ M Stattic vs. 20 μ M Stattic	****	< 0.0001	****	< 0.0001
10 μ M Stattic vs. 15 μ M Stattic	n.s.	0.7099	n.s.	0.1657
10 μ M Stattic vs. 20 μ M Stattic	n.s.	0.6863	n.s.	0.1668
15 μ M Stattic vs. 20 μ M Stattic	n.s.	> 0.9999	n.s.	> 0.9999

RAV27 BTIC	Significance	Adjusted p-vale	Significance	Adjusted p-vale
Category	40 h		48 h	
DMSO vs. 0.625 μ M Stattic	n.s.	0.1362	**	0.0019
DMSO vs. 1.25 μ M Stattic	***	0.0001	****	< 0.0001
DMSO vs. 2.5 μ M Stattic	****	< 0.0001	****	< 0.0001
DMSO vs. 5 μ M Stattic	****	< 0.0001	****	< 0.0001
DMSO vs. 10 μ M Stattic	****	< 0.0001	****	< 0.0001
DMSO vs. 15 μ M Stattic	****	< 0.0001	****	< 0.0001
DMSO vs. 20 μ M Stattic	****	< 0.0001	****	< 0.0001
0.625 μ M Stattic vs. 1.25 μ M Stattic	n.s.	0.5669	n.s.	0.7247
0.625 μ M Stattic vs. 2.5 μ M Stattic	****	< 0.0001	**	0.0002
0.625 μ M Stattic vs. 5 μ M Stattic	****	< 0.0001	****	< 0.0001
0.625 μ M Stattic vs. 10 μ M Stattic	****	< 0.0001	****	< 0.0001
0.625 μ M Stattic vs. 15 μ M Stattic	****	< 0.0001	****	< 0.0001
0.625 μ M Stattic vs. 20 μ M Stattic	****	< 0.0001	****	< 0.0001
1.25 μ M Stattic vs. 2.5 μ M Stattic	**	0.0018	n.s.	0.0977
1.25 μ M Stattic vs. 5 μ M Stattic	****	< 0.0001	****	< 0.0001
1.25 μ M Stattic vs. 10 μ M Stattic	****	< 0.0001	****	< 0.0001
1.25 μ M Stattic vs. 15 μ M Stattic	****	< 0.0001	****	< 0.0001
1.25 μ M Stattic vs. 20 μ M Stattic	****	< 0.0001	****	< 0.0001
2.5 μ M Stattic vs. 5 μ M Stattic	n.s.	0.6238	*	0.0475
2.5 μ M Stattic vs. 10 μ M Stattic	****	< 0.0001	****	< 0.0001
2.5 μ M Stattic vs. 15 μ M Stattic	****	< 0.0001	****	< 0.0001
2.5 μ M Stattic vs. 20 μ M Stattic	****	< 0.0001	****	< 0.0001
5 μ M Stattic vs. 10 μ M Stattic	****	< 0.0001	****	< 0.0001
5 μ M Stattic vs. 15 μ M Stattic	****	< 0.0001	****	< 0.0001
5 μ M Stattic vs. 20 μ M Stattic	****	< 0.0001	****	< 0.0001
10 μ M Stattic vs. 15 μ M Stattic	****	< 0.0001	****	< 0.0001
10 μ M Stattic vs. 20 μ M Stattic	****	< 0.0001	****	< 0.0001
15 μ M Stattic vs. 20 μ M Stattic	n.s.	> 0.9999	n.s.	0.9935

mesenchymal BTIC	Significance	Adjusted p-value	Significance	Adjusted p-value
Category	16 h		24 h	
DMSO vs. 0.625 μ M Stattic	n.s.	0.9995	n.s.	0.8786
DMSO vs. 1.25 μ M Stattic	n.s.	0.9914	n.s.	0.2932
DMSO vs. 2.5 μ M Stattic	n.s.	0.6319	**	0.0024
DMSO vs. 5 μ M Stattic	n.s.	0.1188	****	< 0.0001
DMSO vs. 10 μ M Stattic	****	< 0.0001	****	< 0.0001
DMSO vs. 15 μ M Stattic	****	< 0.0001	****	< 0.0001
DMSO vs. 20 μ M Stattic	****	< 0.0001	****	< 0.0001
0.625 μ M Stattic vs. 1.25 μ M Stattic	n.s.	> 0.9999	n.s.	0.9909
0.625 μ M Stattic vs. 2.5 μ M Stattic	n.s.	0.9450	n.s.	0.2204
0.625 μ M Stattic vs. 5 μ M Stattic	n.s.	0.4276	*	0.0180
0.625 μ M Stattic vs. 10 μ M Stattic	***	0.0006	****	< 0.0001
0.625 μ M Stattic vs. 15 μ M Stattic	****	< 0.0001	****	< 0.0001
0.625 μ M Stattic vs. 20 μ M Stattic	****	< 0.0001	****	< 0.0001
1.25 μ M Stattic vs. 2.5 μ M Stattic	n.s.	0.9902	n.s.	0.8105
1.25 μ M Stattic vs. 5 μ M Stattic	n.s.	0.6387	n.s.	0.2356
1.25 μ M Stattic vs. 10 μ M Stattic	**	0.0022	****	< 0.0001
1.25 μ M Stattic vs. 15 μ M Stattic	****	< 0.0001	****	< 0.0001
1.25 μ M Stattic vs. 20 μ M Stattic	****	< 0.0001	****	< 0.0001
2.5 μ M Stattic vs. 5 μ M Stattic	n.s.	0.9920	n.s.	0.9927
2.5 μ M Stattic vs. 10 μ M Stattic	n.s.	0.0586	***	0.0005
2.5 μ M Stattic vs. 15 μ M Stattic	**	0.0023	****	< 0.0001
2.5 μ M Stattic vs. 20 μ M Stattic	**	0.0015	****	< 0.0001
5 μ M Stattic vs. 10 μ M Stattic	n.s.	0.4497	*	0.0163
5 μ M Stattic vs. 15 μ M Stattic	n.s.	0.0554	****	< 0.0001
5 μ M Stattic vs. 20 μ M Stattic	*	0.0400	****	< 0.0001
10 μ M Stattic vs. 15 μ M Stattic	n.s.	0.9908	n.s.	0.8802
10 μ M Stattic vs. 20 μ M Stattic	n.s.	0.9811	n.s.	0.7702
15 μ M Stattic vs. 20 μ M Stattic	n.s.	> 0.9999	n.s.	> 0.9999

mesenchymal BTIC	Significance	Adjusted p-vale	Significance	Adjusted p-vale
Category	40 h		48 h	
DMSO vs. 0.625 μ M Stattic	n.s.	0.0565	*	0.0119
DMSO vs. 1.25 μ M Stattic	****	< 0.0001	****	< 0.0001
DMSO vs. 2.5 μ M Stattic	****	< 0.0001	****	< 0.0001
DMSO vs. 5 μ M Stattic	****	< 0.0001	****	< 0.0001
DMSO vs. 10 μ M Stattic	****	< 0.0001	****	< 0.0001
DMSO vs. 15 μ M Stattic	****	< 0.0001	****	< 0.0001
DMSO vs. 20 μ M Stattic	****	< 0.0001	****	< 0.0001
0.625 μ M Stattic vs. 1.25 μ M Stattic	n.s.	0.6169	n.s.	0.7328
0.625 μ M Stattic vs. 2.5 μ M Stattic	***	0.0005	**	0.0026
0.625 μ M Stattic vs. 5 μ M Stattic	****	< 0.0001	****	< 0.0001
0.625 μ M Stattic vs. 10 μ M Stattic	****	< 0.0001	****	< 0.0001
0.625 μ M Stattic vs. 15 μ M Stattic	****	< 0.0001	****	< 0.0001
0.625 μ M Stattic vs. 20 μ M Stattic	****	< 0.0001	****	< 0.0001
1.25 μ M Stattic vs. 2.5 μ M Stattic	n.s.	0.2621	n.s.	0.3856
1.25 μ M Stattic vs. 5 μ M Stattic	***	0.0003	****	< 0.0001
1.25 μ M Stattic vs. 10 μ M Stattic	****	< 0.0001	****	< 0.0001
1.25 μ M Stattic vs. 15 μ M Stattic	****	< 0.0001	****	< 0.0001
1.25 μ M Stattic vs. 20 μ M Stattic	****	< 0.0001	****	< 0.0001
2.5 μ M Stattic vs. 5 μ M Stattic	n.s.	0.5468	n.s.	0.0577
2.5 μ M Stattic vs. 10 μ M Stattic	****	< 0.0001	****	< 0.0001
2.5 μ M Stattic vs. 15 μ M Stattic	****	< 0.0001	****	< 0.0001
2.5 μ M Stattic vs. 20 μ M Stattic	****	< 0.0001	****	< 0.0001
5 μ M Stattic vs. 10 μ M Stattic	****	< 0.0001	****	< 0.0001
5 μ M Stattic vs. 15 μ M Stattic	****	< 0.0001	****	< 0.0001
5 μ M Stattic vs. 20 μ M Stattic	****	< 0.0001	****	< 0.0001
10 μ M Stattic vs. 15 μ M Stattic	*	0.0230	***	0.0006
10 μ M Stattic vs. 20 μ M Stattic	**	0.0014	****	< 0.0001
15 μ M Stattic vs. 20 μ M Stattic	n.s.	0.9980	n.s.	0.9690

RAV21 TC	Significance	Adjusted p-vale	Significance	Adjusted p-vale
Category	16 h		24 h	
DMSO vs. 0.625 μ M Stattic	n.s.	0.9996	n.s.	0.9991
DMSO vs. 1.25 μ M Stattic	n.s.	0.9992	n.s.	0.9954
DMSO vs. 2.5 μ M Stattic	n.s.	0.9109	n.s.	0.8501
DMSO vs. 5 μ M Stattic	n.s.	0.1555	n.s.	0.2986
DMSO vs. 10 μ M Stattic	n.s.	0.0746	***	0.0001
DMSO vs. 15 μ M Stattic	**	0.0016	****	< 0.0001
DMSO vs. 20 μ M Stattic	***	0.0005	****	< 0.0001
0.625 μ M Stattic vs. 1.25 μ M Stattic	n.s.	> 0.9999	n.s.	> 0.9999
0.625 μ M Stattic vs. 2.5 μ M Stattic	n.s.	0.9978	n.s.	0.9956
0.625 μ M Stattic vs. 5 μ M Stattic	n.s.	0.4863	n.s.	0.7424
0.625 μ M Stattic vs. 10 μ M Stattic	n.s.	0.3018	**	0.0023
0.625 μ M Stattic vs. 15 μ M Stattic	*	0.0147	****	< 0.0001
0.625 μ M Stattic vs. 20 μ M Stattic	**	0.0060	****	< 0.0001
1.25 μ M Stattic vs. 2.5 μ M Stattic	n.s.	0.9988	n.s.	0.9991
1.25 μ M Stattic vs. 5 μ M Stattic	n.s.	0.5252	n.s.	0.8380
1.25 μ M Stattic vs. 10 μ M Stattic	n.s.	0.3343	**	0.0045
1.25 μ M Stattic vs. 15 μ M Stattic	*	0.0178	****	< 0.0001
1.25 μ M Stattic vs. 20 μ M Stattic	**	0.0074	****	< 0.0001
2.5 μ M Stattic vs. 5 μ M Stattic	n.s.	0.9231	n.s.	0.9944
2.5 μ M Stattic vs. 10 μ M Stattic	n.s.	0.7956	*	0.0425
2.5 μ M Stattic vs. 15 μ M Stattic	n.s.	0.1338	****	< 0.0001
2.5 μ M Stattic vs. 20 μ M Stattic	n.s.	0.0692	****	< 0.0001
5 μ M Stattic vs. 10 μ M Stattic	n.s.	> 0.9999	n.s.	0.3404
5 μ M Stattic vs. 15 μ M Stattic	n.s.	0.8873	**	0.0030
5 μ M Stattic vs. 20 μ M Stattic	n.s.	0.7582	****	< 0.0001
10 μ M Stattic vs. 15 μ M Stattic	n.s.	0.9684	n.s.	0.7786
10 μ M Stattic vs. 20 μ M Stattic	n.s.	0.9011	n.s.	0.1325
15 μ M Stattic vs. 20 μ M Stattic	n.s.	> 0.9999	n.s.	0.9725

RAV21 TC	Significance	Adjusted p-vale	Significance	Adjusted p-vale
Category	40 h		48 h	
DMSO vs. 0.625 μ M Stattic	n.s.	0.9833	n.s.	0.9517
DMSO vs. 1.25 μ M Stattic	n.s.	0.9639	n.s.	0.8992
DMSO vs. 2.5 μ M Stattic	n.s.	0.3873	n.s.	0.4728
DMSO vs. 5 μ M Stattic	*	0.0307	**	0.0089
DMSO vs. 10 μ M Stattic	****	< 0.0001	****	< 0.0001
DMSO vs. 15 μ M Stattic	****	< 0.0001	****	< 0.0001
DMSO vs. 20 μ M Stattic	****	< 0.0001	****	< 0.0001
0.625 μ M Stattic vs. 1.25 μ M Stattic	n.s.	> 0.9999	n.s.	> 0.9999
0.625 μ M Stattic vs. 2.5 μ M Stattic	n.s.	0.9548	n.s.	0.9937
0.625 μ M Stattic vs. 5 μ M Stattic	n.s.	0.3711	n.s.	0.2676
0.625 μ M Stattic vs. 10 μ M Stattic	****	< 0.0001	****	< 0.0001
0.625 μ M Stattic vs. 15 μ M Stattic	****	< 0.0001	****	< 0.0001
0.625 μ M Stattic vs. 20 μ M Stattic	****	< 0.0001	****	< 0.0001
1.25 μ M Stattic vs. 2.5 μ M Stattic	n.s.	0.9780	n.s.	0.9987
1.25 μ M Stattic vs. 5 μ M Stattic	n.s.	0.4603	n.s.	0.3687
1.25 μ M Stattic vs. 10 μ M Stattic	****	< 0.0001	****	< 0.0001
1.25 μ M Stattic vs. 15 μ M Stattic	****	< 0.0001	****	< 0.0001
1.25 μ M Stattic vs. 20 μ M Stattic	****	< 0.0001	****	< 0.0001
2.5 μ M Stattic vs. 5 μ M Stattic	n.s.	0.9805	n.s.	0.8291
2.5 μ M Stattic vs. 10 μ M Stattic	****	< 0.0001	****	< 0.0001
2.5 μ M Stattic vs. 15 μ M Stattic	****	< 0.0001	****	< 0.0001
2.5 μ M Stattic vs. 20 μ M Stattic	****	< 0.0001	****	< 0.0001
5 μ M Stattic vs. 10 μ M Stattic	***	0.0005	****	< 0.0001
5 μ M Stattic vs. 15 μ M Stattic	****	< 0.0001	****	< 0.0001
5 μ M Stattic vs. 20 μ M Stattic	****	< 0.0001	****	< 0.0001
10 μ M Stattic vs. 15 μ M Stattic	****	< 0.0001	****	< 0.0001
10 μ M Stattic vs. 20 μ M Stattic	****	< 0.0001	****	< 0.0001
15 μ M Stattic vs. 20 μ M Stattic	n.s.	0.7486	n.s.	0.6738

RAV26 TC	Significance	Adjusted p-value	Significance	Adjusted p-value
Category	16 h		24 h	
DMSO vs. 0.625 μ M Stattic	n.s.	0.9588	n.s.	0.9993
DMSO vs. 1.25 μ M Stattic	n.s.	0.7927	n.s.	0.4846
DMSO vs. 2.5 μ M Stattic	n.s.	0.4892	n.s.	0.2627
DMSO vs. 5 μ M Stattic	**	0.0021	****	< 0.0001
DMSO vs. 10 μ M Stattic	****	< 0.0001	****	< 0.0001
DMSO vs. 15 μ M Stattic	****	< 0.0001	****	< 0.0001
DMSO vs. 20 μ M Stattic	****	< 0.0001	****	< 0.0001
0.625 μ M Stattic vs. 1.25 μ M Stattic	n.s.	> 0.9999	n.s.	0.8832
0.625 μ M Stattic vs. 2.5 μ M Stattic	n.s.	0.9933	n.s.	0.6849
0.625 μ M Stattic vs. 5 μ M Stattic	n.s.	0.1041	****	< 0.0001
0.625 μ M Stattic vs. 10 μ M Stattic	****	< 0.0001	****	< 0.0001
0.625 μ M Stattic vs. 15 μ M Stattic	****	< 0.0001	****	< 0.0001
0.625 μ M Stattic vs. 20 μ M Stattic	****	< 0.0001	****	< 0.0001
1.25 μ M Stattic vs. 2.5 μ M Stattic	n.s.	> 0.9999	n.s.	> 0.9999
1.25 μ M Stattic vs. 5 μ M Stattic	n.s.	0.2769	*	0.0182
1.25 μ M Stattic vs. 10 μ M Stattic	****	< 0.0001	****	< 0.0001
1.25 μ M Stattic vs. 15 μ M Stattic	****	< 0.0001	****	< 0.0001
1.25 μ M Stattic vs. 20 μ M Stattic	****	< 0.0001	****	< 0.0001
2.5 μ M Stattic vs. 5 μ M Stattic	n.s.	0.5717	n.s.	0.0552
2.5 μ M Stattic vs. 10 μ M Stattic	****	< 0.0001	****	< 0.0001
2.5 μ M Stattic vs. 15 μ M Stattic	****	< 0.0001	****	< 0.0001
2.5 μ M Stattic vs. 20 μ M Stattic	****	< 0.0001	****	< 0.0001
5 μ M Stattic vs. 10 μ M Stattic	n.s.	0.1147	****	< 0.0001
5 μ M Stattic vs. 15 μ M Stattic	**	0.0085	****	< 0.0001
5 μ M Stattic vs. 20 μ M Stattic	**	0.0051	****	< 0.0001
10 μ M Stattic vs. 15 μ M Stattic	n.s.	0.9951	n.s.	0.9811
10 μ M Stattic vs. 20 μ M Stattic	n.s.	0.9861	n.s.	0.8184
15 μ M Stattic vs. 20 μ M Stattic	n.s.	> 0.9999	n.s.	0.9998

RAV26 TC	Significance	Adjusted p-vale	Significance	Adjusted p-vale
Category	40 h		48 h	
DMSO vs. 0.625 μ M Stattic	n.s.	0.9987	**	0.0058
DMSO vs. 1.25 μ M Stattic	n.s.	0.8872	*	0.0345
DMSO vs. 2.5 μ M Stattic	**	0.0032	****	< 0.0001
DMSO vs. 5 μ M Stattic	****	< 0.0001	****	< 0.0001
DMSO vs. 10 μ M Stattic	****	< 0.0001	****	< 0.0001
DMSO vs. 15 μ M Stattic	****	< 0.0001	****	< 0.0001
DMSO vs. 20 μ M Stattic	****	< 0.0001	****	< 0.0001
0.625 μ M Stattic vs. 1.25 μ M Stattic	n.s.	0.9985	n.s.	0.9998
0.625 μ M Stattic vs. 2.5 μ M Stattic	*	0.0362	n.s.	0.7688
0.625 μ M Stattic vs. 5 μ M Stattic	****	< 0.0001	****	< 0.0001
0.625 μ M Stattic vs. 10 μ M Stattic	****	< 0.0001	****	< 0.0001
0.625 μ M Stattic vs. 15 μ M Stattic	****	< 0.0001	****	< 0.0001
0.625 μ M Stattic vs. 20 μ M Stattic	****	< 0.0001	****	< 0.0001
1.25 μ M Stattic vs. 2.5 μ M Stattic	n.s.	0.2309	n.s.	0.4121
1.25 μ M Stattic vs. 5 μ M Stattic	****	< 0.0001	****	< 0.0001
1.25 μ M Stattic vs. 10 μ M Stattic	****	< 0.0001	****	< 0.0001
1.25 μ M Stattic vs. 15 μ M Stattic	****	< 0.0001	****	< 0.0001
1.25 μ M Stattic vs. 20 μ M Stattic	****	< 0.0001	****	< 0.0001
2.5 μ M Stattic vs. 5 μ M Stattic	****	< 0.0001	****	< 0.0001
2.5 μ M Stattic vs. 10 μ M Stattic	****	< 0.0001	****	< 0.0001
2.5 μ M Stattic vs. 15 μ M Stattic	****	< 0.0001	****	< 0.0001
2.5 μ M Stattic vs. 20 μ M Stattic	****	< 0.0001	****	< 0.0001
5 μ M Stattic vs. 10 μ M Stattic	****	< 0.0001	****	< 0.0001
5 μ M Stattic vs. 15 μ M Stattic	****	< 0.0001	****	< 0.0001
5 μ M Stattic vs. 20 μ M Stattic	****	< 0.0001	****	< 0.0001
10 μ M Stattic vs. 15 μ M Stattic	****	< 0.0001	****	< 0.0001
10 μ M Stattic vs. 20 μ M Stattic	****	< 0.0001	****	< 0.0001
15 μ M Stattic vs. 20 μ M Stattic	n.s.	> 0.9999	n.s.	> 0.9999

RAV27 TC	Significance	Adjusted p-value	Significance	Adjusted p-value
Category	16 h		24 h	
DMSO vs. 0.625 μ M Stattic	n.s.	> 0.9999	n.s.	> 0.9999
DMSO vs. 1.25 μ M Stattic	n.s.	> 0.9999	n.s.	> 0.9999
DMSO vs. 2.5 μ M Stattic	n.s.	0.9971	n.s.	0.9863
DMSO vs. 5 μ M Stattic	n.s.	0.7674	n.s.	0.2054
DMSO vs. 10 μ M Stattic	n.s.	0.1035	****	< 0.0001
DMSO vs. 15 μ M Stattic	**	0.0027	****	< 0.0001
DMSO vs. 20 μ M Stattic	**	0.0014	****	< 0.0001
0.625 μ M Stattic vs. 1.25 μ M Stattic	n.s.	> 0.9999	n.s.	> 0.9999
0.625 μ M Stattic vs. 2.5 μ M Stattic	n.s.	> 0.9999	n.s.	0.9999
0.625 μ M Stattic vs. 5 μ M Stattic	n.s.	0.9493	n.s.	0.4878
0.625 μ M Stattic vs. 10 μ M Stattic	n.s.	0.2760	***	0.0003
0.625 μ M Stattic vs. 15 μ M Stattic	*	0.0132	****	< 0.0001
0.625 μ M Stattic vs. 20 μ M Stattic	**	0.0074	****	< 0.0001
1.25 μ M Stattic vs. 2.5 μ M Stattic	n.s.	> 0.9999	n.s.	0.9998
1.25 μ M Stattic vs. 5 μ M Stattic	n.s.	0.9577	n.s.	0.4682
1.25 μ M Stattic vs. 10 μ M Stattic	n.s.	0.2966	***	0.0002
1.25 μ M Stattic vs. 15 μ M Stattic	*	0.0150	****	< 0.0001
1.25 μ M Stattic vs. 20 μ M Stattic	**	0.0084	****	< 0.0001
2.5 μ M Stattic vs. 5 μ M Stattic	n.s.	0.9941	n.s.	0.8198
2.5 μ M Stattic vs. 10 μ M Stattic	n.s.	0.4984	**	0.0022
2.5 μ M Stattic vs. 15 μ M Stattic	*	0.0410	****	< 0.0001
2.5 μ M Stattic vs. 20 μ M Stattic	*	0.0245	****	< 0.0001
5 μ M Stattic vs. 10 μ M Stattic	n.s.	0.9583	n.s.	0.2560
5 μ M Stattic vs. 15 μ M Stattic	n.s.	0.3378	***	0.0004
5 μ M Stattic vs. 20 μ M Stattic	n.s.	0.2463	***	0.0001
10 μ M Stattic vs. 15 μ M Stattic	n.s.	0.9707	n.s.	0.5637
10 μ M Stattic vs. 20 μ M Stattic	n.s.	0.9344	n.s.	0.3498
15 μ M Stattic vs. 20 μ M Stattic	n.s.	> 0.9999	n.s.	> 0.9999

RAV27 TC	Significance	Adjusted p-vale	Significance	Adjusted p-vale
Category	40 h		48 h	
DMSO vs. 0.625 μ M Stattic	n.s.	0.9998	n.s.	0.9858
DMSO vs. 1.25 μ M Stattic	n.s.	0.8055	n.s.	0.1497
DMSO vs. 2.5 μ M Stattic	n.s.	0.5558	*	0.0154
DMSO vs. 5 μ M Stattic	****	< 0.0001	****	< 0.0001
DMSO vs. 10 μ M Stattic	****	< 0.0001	****	< 0.0001
DMSO vs. 15 μ M Stattic	****	< 0.0001	****	< 0.0001
DMSO vs. 20 μ M Stattic	****	< 0.0001	****	< 0.0001
0.625 μ M Stattic vs. 1.25 μ M Stattic	n.s.	0.9822	n.s.	0.7429
0.625 μ M Stattic vs. 2.5 μ M Stattic	n.s.	0.8892	n.s.	0.2367
0.625 μ M Stattic vs. 5 μ M Stattic	***	0.0006	****	< 0.0001
0.625 μ M Stattic vs. 10 μ M Stattic	****	< 0.0001	****	< 0.0001
0.625 μ M Stattic vs. 15 μ M Stattic	****	< 0.0001	****	< 0.0001
0.625 μ M Stattic vs. 20 μ M Stattic	****	< 0.0001	****	< 0.0001
1.25 μ M Stattic vs. 2.5 μ M Stattic	n.s.	> 0.9999	n.s.	0.9970
1.25 μ M Stattic vs. 5 μ M Stattic	*	0.0280	****	< 0.0001
1.25 μ M Stattic vs. 10 μ M Stattic	****	< 0.0001	****	< 0.0001
1.25 μ M Stattic vs. 15 μ M Stattic	****	< 0.0001	****	< 0.0001
1.25 μ M Stattic vs. 20 μ M Stattic	****	< 0.0001	****	< 0.0001
2.5 μ M Stattic vs. 5 μ M Stattic	n.s.	0.0859	**	0.0015
2.5 μ M Stattic vs. 10 μ M Stattic	****	< 0.0001	****	< 0.0001
2.5 μ M Stattic vs. 15 μ M Stattic	****	< 0.0001	****	< 0.0001
2.5 μ M Stattic vs. 20 μ M Stattic	****	< 0.0001	****	< 0.0001
5 μ M Stattic vs. 10 μ M Stattic	***	0.0002	****	< 0.0001
5 μ M Stattic vs. 15 μ M Stattic	****	< 0.0001	****	< 0.0001
5 μ M Stattic vs. 20 μ M Stattic	****	< 0.0001	****	< 0.0001
10 μ M Stattic vs. 15 μ M Stattic	***	0.0002	****	< 0.0001
10 μ M Stattic vs. 20 μ M Stattic	****	< 0.0001	****	< 0.0001
15 μ M Stattic vs. 20 μ M Stattic	n.s.	0.8099	n.s.	0.1191

mesenchymal TC	Significance	Adjusted p-value	Significance	Adjusted p-value
Category	16 h		24 h	
DMSO vs. 0.625 μ M Stattic	n.s.	0.9991	n.s.	0.9998
DMSO vs. 1.25 μ M Stattic	n.s.	0.9959	n.s.	0.9856
DMSO vs. 2.5 μ M Stattic	n.s.	0.9401	n.s.	0.8566
DMSO vs. 5 μ M Stattic	n.s.	0.2177	*	0.0302
DMSO vs. 10 μ M Stattic	**	0.0030	****	< 0.0001
DMSO vs. 15 μ M Stattic	****	< 0.0001	****	< 0.0001
DMSO vs. 20 μ M Stattic	****	< 0.0001	****	< 0.0001
0.625 μ M Stattic vs. 1.25 μ M Stattic	n.s.	> 0.9999	n.s.	> 0.9999
0.625 μ M Stattic vs. 2.5 μ M Stattic	n.s.	0.9996	n.s.	0.9905
0.625 μ M Stattic vs. 5 μ M Stattic	n.s.	0.6444	n.s.	0.1436
0.625 μ M Stattic vs. 10 μ M Stattic	*	0.0325	****	< 0.0001
0.625 μ M Stattic vs. 15 μ M Stattic	***	0.0008	****	< 0.0001
0.625 μ M Stattic vs. 20 μ M Stattic	***	0.0004	****	< 0.0001
1.25 μ M Stattic vs. 2.5 μ M Stattic	n.s.	> 0.9999	n.s.	> 0.9999
1.25 μ M Stattic vs. 5 μ M Stattic	n.s.	0.7465	n.s.	0.3624
1.25 μ M Stattic vs. 10 μ M Stattic	n.s.	0.0522	****	< 0.0001
1.25 μ M Stattic vs. 15 μ M Stattic	**	0.0015	****	< 0.0001
1.25 μ M Stattic vs. 20 μ M Stattic	***	0.0007	****	< 0.0001
2.5 μ M Stattic vs. 5 μ M Stattic	n.s.	0.9418	n.s.	0.6998
2.5 μ M Stattic vs. 10 μ M Stattic	n.s.	0.1653	****	< 0.0001
2.5 μ M Stattic vs. 15 μ M Stattic	**	0.0082	****	< 0.0001
2.5 μ M Stattic vs. 20 μ M Stattic	**	0.0043	****	< 0.0001
5 μ M Stattic vs. 10 μ M Stattic	n.s.	0.9008	*	0.0322
5 μ M Stattic vs. 15 μ M Stattic	n.s.	0.2896	****	< 0.0001
5 μ M Stattic vs. 20 μ M Stattic	n.s.	0.2025	****	< 0.0001
10 μ M Stattic vs. 15 μ M Stattic	n.s.	0.9860	n.s.	0.8369
10 μ M Stattic vs. 20 μ M Stattic	n.s.	0.9621	n.s.	0.4754
15 μ M Stattic vs. 20 μ M Stattic	n.s.	> 0.9999	n.s.	0.9998

mesenchymal TC	Significance	Adjusted p-vale	Significance	Adjusted p-vale
Category	40 h		48 h	
DMSO vs. 0.625 μ M Stattic	n.s.	0.9989	n.s.	0.6710
DMSO vs. 1.25 μ M Stattic	n.s.	0.9077	n.s.	0.2695
DMSO vs. 2.5 μ M Stattic	n.s.	0.2206	*	0.0110
DMSO vs. 5 μ M Stattic	****	< 0.0001	****	< 0.0001
DMSO vs. 10 μ M Stattic	****	< 0.0001	****	< 0.0001
DMSO vs. 15 μ M Stattic	****	< 0.0001	****	< 0.0001
DMSO vs. 20 μ M Stattic	****	< 0.0001	****	< 0.0001
0.625 μ M Stattic vs. 1.25 μ M Stattic	n.s.	0.9990	n.s.	0.9996
0.625 μ M Stattic vs. 2.5 μ M Stattic	n.s.	0.6599	n.s.	0.7112
0.625 μ M Stattic vs. 5 μ M Stattic	****	< 0.0001	****	< 0.0001
0.625 μ M Stattic vs. 10 μ M Stattic	****	< 0.0001	****	< 0.0001
0.625 μ M Stattic vs. 15 μ M Stattic	****	< 0.0001	****	< 0.0001
0.625 μ M Stattic vs. 20 μ M Stattic	****	< 0.0001	****	< 0.0001
1.25 μ M Stattic vs. 2.5 μ M Stattic	n.s.	0.9659	n.s.	0.9672
1.25 μ M Stattic vs. 5 μ M Stattic	***	0.0004	****	< 0.0001
1.25 μ M Stattic vs. 10 μ M Stattic	****	< 0.0001	****	< 0.0001
1.25 μ M Stattic vs. 15 μ M Stattic	****	< 0.0001	****	< 0.0001
1.25 μ M Stattic vs. 20 μ M Stattic	****	< 0.0001	****	< 0.0001
2.5 μ M Stattic vs. 5 μ M Stattic	*	0.0323	***	0.0008
2.5 μ M Stattic vs. 10 μ M Stattic	****	< 0.0001	****	< 0.0001
2.5 μ M Stattic vs. 15 μ M Stattic	****	< 0.0001	****	< 0.0001
2.5 μ M Stattic vs. 20 μ M Stattic	****	< 0.0001	****	< 0.0001
5 μ M Stattic vs. 10 μ M Stattic	****	< 0.0001	****	< 0.0001
5 μ M Stattic vs. 15 μ M Stattic	****	< 0.0001	****	< 0.0001
5 μ M Stattic vs. 20 μ M Stattic	****	< 0.0001	****	< 0.0001
10 μ M Stattic vs. 15 μ M Stattic	***	0.0002	****	< 0.0001
10 μ M Stattic vs. 20 μ M Stattic	****	< 0.0001	****	< 0.0001
15 μ M Stattic vs. 20 μ M Stattic	n.s.	0.9625	n.s.	0.7227